Molecular Views on Mechanisms of Brønsted Acid-Catalyzed Reactions in Zeolites

Céline Chizallet, Christophe Bouchy, Kim Larmier, Gerhard Pirngruber

▶ **To cite this version:**

Céline Chizallet, Christophe Bouchy, Kim Larmier, Gerhard Pirngruber. Molecular Views on Mechanisms of Brønsted Acid-Catalyzed Reactions in Zeolites. Chemical Reviews, 2023, 123 (9), pp.6107-6196. 10.1021/acs.chemrev.2c00896 . hal-04127786

HAL Id: hal-04127786
https://ifp.hal.science/hal-04127786v1

Submitted on 14 Jun 2023

HAL is a multi-disciplinary open access archive for the deposit and dissemination of scientific research documents, whether they are published or not. The documents may come from teaching and research institutions in France or abroad, or from public or private research centers.

L'archive ouverte pluridisciplinaire **HAL**, est destinée au dépôt et à la diffusion de documents scientifiques de niveau recherche, publiés ou non, émanant des établissements d'enseignement et de recherche français ou étrangers, des laboratoires publics ou privés.

Molecular Views on Mechanisms of Brønsted Acid-Catalyzed Reactions in Zeolites

Céline Chizallet,* Christophe Bouchy, Kim Larmier, Gerhard Pirngruber

IFP Energies Nouvelles, Rond-Point de l'Echangeur de Solaize, BP 3, 69360 Solaize, France

Abstract.

The Brønsted acidity of proton-exchanged zeolites has historically led to the most impactful application of these materials in heterogeneous catalysis, mainly in the fields of transformations of hydrocarbons and oxygenates. Unravelling the mechanisms at the atomic scale of these transformations has been the object of tremendous efforts in the last decades. Such investigations have extended our fundamental knowledge about the respective roles of acidity and confinement in the catalytic properties of proton exchanged zeolites. The emerging concepts are of general relevance, at the crossroad of heterogeneous catalysis and molecular chemistry. In the present review, emphasis is given to molecular views on the mechanism of generic transformations catalyzed by Brønsted acid sites of zeolites, combining the information gained from advanced kinetic analysis, in situ and operando spectroscopies, and quantum chemistry calculations. After reviewing the current knowledge on the nature of the Brønsted acid sites themselves, and the key parameters in catalysis by zeolites, a focus is made on reactions undergone by alkenes, alkenes, aromatic molecules, alcohols and polyhydroxy molecules. Elementary events of C-C, C-H and C-O bond breaking and formation are at the core of these reactions. Outlooks are given to take up the future challenges in the field, aiming at getting ever more accurate views on these mechanisms, and as the ultimate goal, to provide rational tools for the design of better zeolite-based Brønsted acid catalysts.

1. Introduction

Zeolites are nanoporous aluminosilicates, described as 3D frameworks of TO_4 tetrahedra (T = Si, Al, etc.). Since their discovery by Cronstedt in 1756, many natural polymorphs were found. The first occurrence of synthetic zeolites was reported by Sainte-Claire Deville in 1862. [1] Their suitability for industrial applications then led to tremendous efforts to obtain new synthetic forms, whose diversity goes far beyond that of natural known solids.[2–4] Zeolites are widely used in refining and chemical industry as catalysts or sorbents.[5–8] The Brønsted acidity of proton exchanged zeolites, defined as their thermodynamic ability to donate protons,[9] catalyzes a large set of chemical reactions.[10–13] Acidity can be tuned by chemical composition, in terms of framework and extra-framework species, as well as synthesis and pre-treatment procedures. Proton exchanged zeolites will be the focus of the present review, given their relevance for past, current, and future practical implementation. Historically, most Brønsted acid-catalyzed reactions in zeolites concerned the transformation of hydrocarbons, driven by the need for high-quality fuels from petroleum feedstocks. [6–8] Gradually, the spectrum of acid-catalyzed reactions for which zeolites are useful is enlarging, now embracing the transformation of biobased compounds,[12,13] and plastic recycling.[14]

A particular feature of zeolite catalysis is the predominant role of the pore structure in the stabilization of reactants, products and intermediates, known as the confinement effect.[15–17] **Table 1** reports the main geometric features of the most important zeolite topologies that will be discussed in the following. The pore structure imposes geometrical constraints which does not allow certain molecules to fit in (or only in very specific configurations). The structural match between the host molecule and the pore structure will determine the extent of van der Waals interactions and the degree of rotational freedom and will, therefore, determine the adsorption enthalpy and entropy. The composition and geometry of the pore wall also determine

the electric field inside the pores,[18] which is very important for the stabilization of charged species or transition states. In contrast to porous solids with a non-organized pore structure, the well-defined crystalline structure of zeolites allows for a precise description of these confinement effects, and the large diversity of pore architectures allows for tuning them very finely, in close analogy to enzymatic catalysis or to the design of the active sites in homogeneous catalysis. An advanced knowledge of the nature of the key chemical intermediates, and of the way they are interacting with the zeolite framework is, therefore, required for developing more efficient industrial catalysts on a rational basis. A large set of techniques has been employed to obtain insights on these intermediates, starting with the detailed analysis of reaction products as a function of time. Careful kinetic investigations have played a tremendous role in drawing conclusions about intermediates, which are not directly observable, in analogy to knowledge obtained in liquid phase organic chemistry.[17,19] Progress is still made continuously in this field, linked to the increase of the temporal resolution of the product detection methods, and to their sensitivity for highly diluted species. In situ and operando spectroscopies[20] have shed new light on the nature of the species present in the pores.[21–25] The temporal and special resolutions, as well as the sensitivity and ability to distinguish intermediates from spectator species and species responsible for the deactivation of the catalysts, is still a challenge.[26,27] Finally, first principles calculations, most often at the density functional theory (DFT) level, provide unprecedented information about the nature and stability of chemical intermediates, but also transition states.[25,28–32] As will be discussed in the following, the quality of the models representing the active sites, as well as the level of theory and methods employed to deal with thermal effects, strongly impact the conclusions made.

Table 1. Characteristics of some of the zeolite frameworks abundantly discussed in this review, according to the IZA database.[33] The channel dimensionality corresponds to pore openings of more than 6MR.

Code	CHA	TON	FER	MFI	MOR	BEA(A)	FAU
Representation	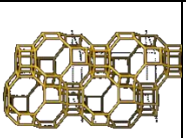	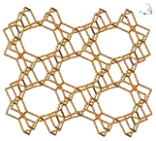	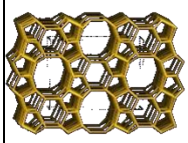	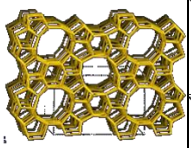	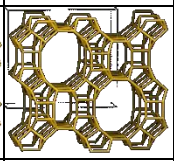	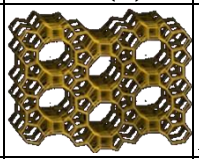	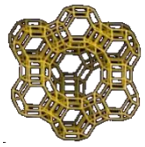
Larger ring size	8MR	10MR	10⊥8MR	10⊥10MR	12⊥8MR	12⊥12MR	12MR
Dimensionality	3D	1D	2D	3D	2D	3D	3D
Dimensions*	7.37 / 3.72	5.71 / 5.11	6.31 / 4.69	6.36 / 4.70	6.70 / 6.45	6.68 / 5.95	11.24 /7.35

* Maximum diameter of sphere that can be included /diffuse along (Å).

Many reviews have been published, embracing the very abundant literature dealing with the determination of the acidity of zeolites,[8,21–23,28–32,34–44] and catalysis by zeolites as investigated in academia and applied in industry.[5,7,10–13,25,45–58] In the present review, we select a complementary molecular point of view, gathering both experimental and computational insights. We analyze the state of art of the knowledge obtained by the aforementioned techniques (detailed kinetic investigations, in situ and operando spectroscopies, first principles calculations) about mechanisms involved in Brønsted acid-catalyzed transformations in zeolites. This includes the identification of the relevant intermediates and transition states, together with the respective kinetics of their formation and transformation into products, when available. In catalysis by zeolites, the question of the structure, location, and accessibility of the active sites arises systematically, even more for non-ideal catalysts, when non-framework species are present, and when diffusion limitations occur. Thus, section 2 introduces the current knowledge on the nature and acidity of the possible active sites in Brønsted acidic zeolites. Section 3 sets the scene by giving the basics of catalysis by zeolites, deconvoluting questions linked to adsorption, diffusion, and reaction kinetics. **Figure 1** sketches most relevant concepts for sections 2 and 3. These tools are important to understand the approaches undertaken, the knowledge obtained so far, and the remaining challenges, for understanding mechanisms catalyzed by proton exchanged zeolites, that are the object of the subsequent sections.

Considering the high importance of carbocation chemistry in the mechanisms of reactions catalyzed by proton exchanged zeolites, we devote section 4 to the current knowledge in terms of carbocation stability in zeolites. Sections 5-10 describe insights on the atomic scale mechanisms of transformations of alkenes (section 5), alkanes (section 6), aromatic molecules (section 7), of alcohol and sugar dehydration reactions (section 8), of carbonylation reactions (section 9) and finally methanol to olefins reactions (section 10). Concerning computational approaches, there are several methods to model a zeolite catalyst, and several relevant levels of theory to be used for the computation of given properties. The reader is referred to refs. [28,30] for a detailed description of these aspects.

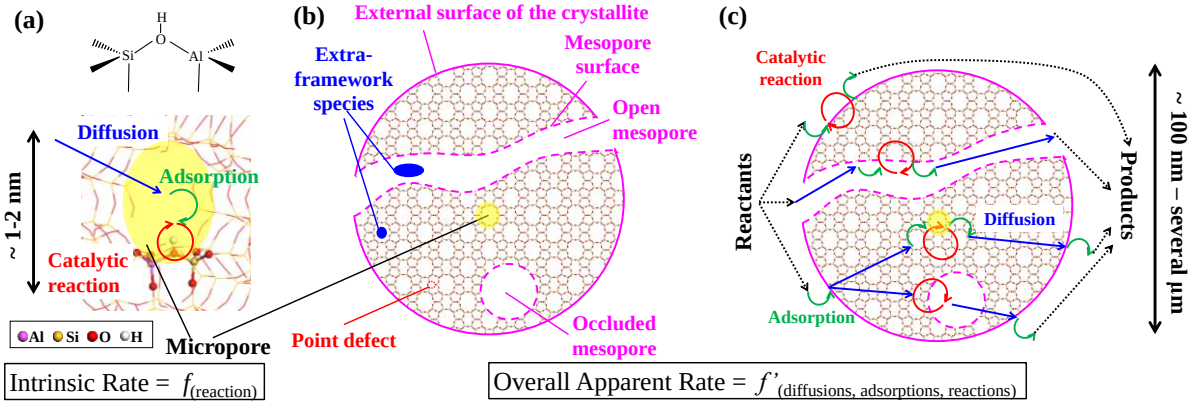

Figure 1. (a) Model of Brønsted acidic zeolite, restricted to the micropore, with consideration of diffusion, adsorption and reactions steps, (b) scheme of default and finite size nature of an intricate zeolite crystallite. A spherical crystallite model is arbitrarily chosen. (c) Integration of the variety of sites and of steps for the definition of the overall reaction rate. Extraframework species are omitted in (c) for the sake of clarity, but the same formalism applies.

As will be illustrated in the following, many analogies shall be made between heterogeneous catalysis by zeolites, and homogeneous catalysis, even biocatalysis.[59] Common concepts are invoked, such as the molecular nature of the active site, high degree of mobility of many intermediates and transition states (in that sense, zeolite active sites behave more like a confined homogeneous catalyst than a merely heterogeneous one) and confinement.

2. Nature and acidity of the active sites of proton exchanged zeolites

2.1. General features

The stability and reactivity of reaction intermediates in acidic zeolites depends strongly on the nature, the location and the acidity (a consequence of the two former parameters) of the active sites under consideration. The advanced characterization and quantification of these features is thus of primary importance before undertaking reactivity investigations. Spectroscopic and titration methods have been key in that respect, together with computational achievements. At this stage, it is useful to recall that a purely siliceous zeolite is hardly reactive, due to the highly covalent nature of the Si-O bond (in comparison to Al-O bonds for example, as shown by bond overlap population computations[60]), and the very stable tetrahedral coordination of framework silicon atoms (Si_V being encountered starting from the most common Si_{IV} state only in situations where very strong nucleophiles and bases are present[60–64]). A noticeable exception is the Beckmann rearrangement of cyclohexanone oxime into ε-caprolactam and related reactions, that was shown to be efficiently catalyzed by highly siliceous ZSM-5 (or silicalite-1) with high external surface area,[65–68] including by nanosheets,[69] leading to the assignment of silanols as active sites in this case, in particular those hosted in silanols nests.[70] The reactivity of silanols and silanol nests in Beckmann rearrangement was confirmed by DFT calculations.[71] However, most of the time, acidity arises thanks to the presence of heteroatoms in the framework.

In the common case where trivalent aluminum atoms replace tetravalent silicon atoms at framework positions, a compensation cation is additionally present to compensate for the positive charge deficit. When it is a proton, it has been known for decades that a bridging Si-(OH)-Al group is formed (**Figure 2-a**),[72–74] that exhibits Brønsted acidity (section 2.2). *A priori,* a perfect bulk of aluminosilicate zeolites is not expected to exhibit Lewis acidity, although this

was recently debated (section 2.3).[75–77] The question of the role of the external surface of the crystallites, of mesopores and extraframework species generated during various post-treatments will be developed in sections 2.4 and 2.5.

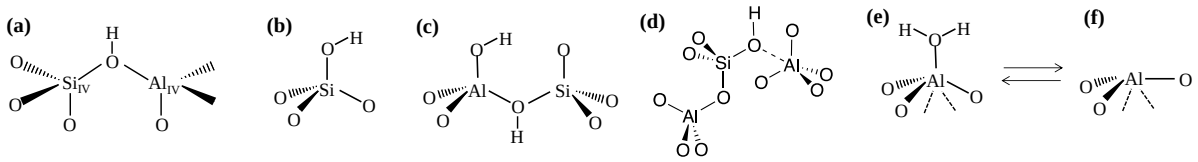

Figure 2. Some of the possible hydroxyl groups present in and on acidic zeolite catalysts: (a) bridging Si_{IV}−(OH)−Al_{IV} groups, (b) silanols at the external surface and at defects, (c) Al−OH groups close to bridging OH groups at the external surface of zeolites, discussed in refs [78–81], (d) Pseudo-Bridging Silanols (PBS) suggested by first principles calculations on amorphous silica−alumina (ASA),[60,82–84] represented as confirmed by NMR,[84] (e) water molecules adsorbed at surface aluminum, suggested by first principles calculations at the external surface of zeolites,[80,81,85] and on amorphous silica−alumina,[82,83] the coordination number of aluminum may vary from IV to VI depending on the location at the surface, the temperature, and the water partial pressure. (f) Lewis acid sites at the external surface of zeolites and on ASA, suggested by first principles calculations, obtained upon dehydration of (e).[80–82]

2.2. Bridging Si-(OH)-Al groups: location, environment, and acidity

The bridging OH groups have a characteristic IR band usually close to 3600 cm^{-1}.[22,86] In the first reports, the bridging OH group was described as a silanol group coordinated to a tricoordinated Al site (i.e. with the Al-O bond broken). [73] However, the much lower frequency within zeolites with respect to silica and silica-alumina, led the authors to conclude about the remanence of a strong interaction between the Si-OH and the aluminum atom. Early quantum chemistry calculations corroborated the assignment of the IR feature to bridging OH groups as shown in **Figure 3-a**.[72,87] Since then, many first principles studies have confirmed this assignment, and have brought an additional level of detail when several bands in this spectral zone are observed.

In particular, in the case of ZSM-5, this band appears close to 3610 cm^{-1}.[85,88–90] A combination of Varying Temperature Infrared spectroscopy, OH-OD exchange, and DFT calculations, led to the proposal of the acid sites are specifically located on given O atoms associated with specific T sites in the MFI structure.[91] Such an assignment, however, remains

debatable, in particular for the MFI framework, considering the number of non-equivalent sites, the very narrow interval of experimental O-H elongation frequencies (generally, less than 10 cm^{-1}), *versus* the large variations of computed frequencies due to hydrogen-bonds, usually over-estimated by DFT calculations. Recently, thanks to DFT calculations, a distinction could be made between the bridging OH groups perturbed/unperturbed by EFAls (Extra-Framework Aluminum species), responsible for higher/lower frequencies in infra-red, observed experimentally thanks to temperature variations combined with a Fourier self-deconvolution of the signal (**Figure 3-b**).[85]

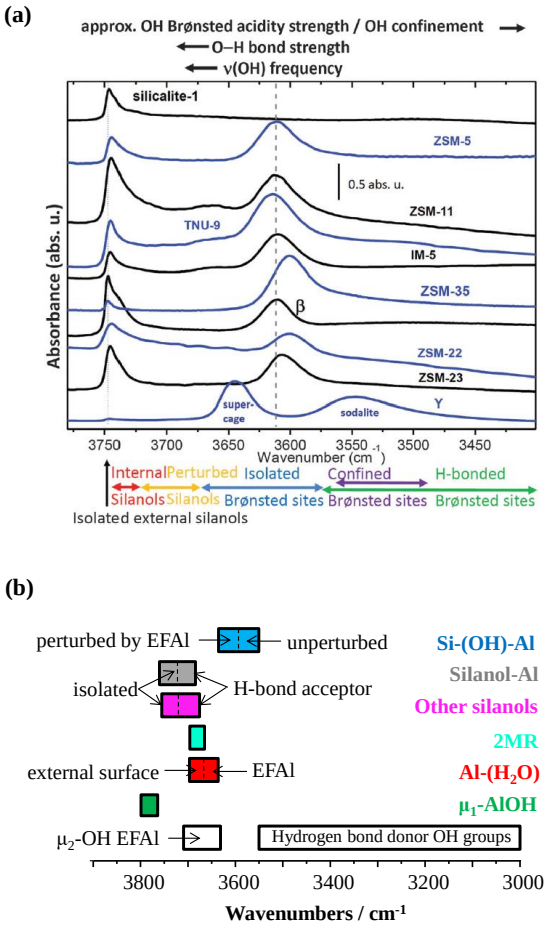

Figure 3. (a) IR spectra of activated protonic zeolites, with assignment of the spectra as proposed in ref. [22]. Reprinted with permission from ref [22]. Copyright 2015 Royal Society of Chemistry (b) Assignment of IR spectra in the O-H stretching zone as found by DFT calculations, for the ZSM-5 zeolite, accounting for external surface sites and EFAls. Reprinted with permission from ref [85]. Copyright 2021 American Chemical Society.

Regarding Mordenite, two components can be deconvoluted within the asymmetric band, qualified as high frequency (HF, 3612 cm^{-1}) and low frequency (LF, 3585 cm^{-1}) components.[22,92] A common assignment follows the location of the acid sites, the HF band being assigned to bridging OH groups hosted in the straight 12MR channel, the LF one being assigned to OH groups pointed to the 8MR pocket. This assignment was proposed on the basis of probe molecules adsorption experiments (pyridine, benzene, cyclohexane, CO, among others), showing a stronger decrease of the HF band with respect to the LF one, in agreement with the respective accessibility of the sites towards the probe molecule.[92–95] However, DFT calculations do not reproduce this distinction so clearly,[18,78,96,97] suggesting a mix within HF and LF bands or sites located at 12MR or 8MR. Sastre et al. found that the electrostatic field around each bridging OH group is the influential parameter, due to the inclusion of rings of variable size at the local level, but not at the channel or pocket level.[18] Isolated sites, found both in 8MR and 12MR, would be responsible for the HF band, whereas H-bonded sites, also found both at 8MR and 12MR, for the LF one. A deconvolution of the O-H stretching signal into three (instead of two) components was proposed by Marie et al.[98] The authors invoked the sites located at the intersection between the 12MR channel and the 8MR pocket to be at the origin of the third component.

For zeolite Y (FAU), the splitting between the high frequency band (HF, close to 3650 cm^{-1}) and the low frequency band (LF, close to 3550 cm^{-1})[73,99,100] is much larger than in the case of Mordenite. Since the LF band does not interact with weakly basic molecules[101] it was assigned to OH groups pointing into the sodalite cage, while the fully accessible HF band was ascribed to OH groups pointing into the supercage (**Figure 3-a**).[99] Jacobs and Mortier rationalized the difference in the OH stretching frequencies by a difference in the electrostatic field strength, which is related to the size of the ring.[102] In this case, the DFT computed frequencies corroborate the empirical assignment.[103]

^{1}H magic angle spinning (MAS) nuclear magnetic resonance (NMR) has also been often used to characterize the bridging OH groups in various zeolites, although it is less routine than infra-red. A certain level of symmetry with respect to the FTIR observations is often reported. In the case of ZSM-5, most bridging OH groups resonate close to 4 ppm.[37,41,85,104] For Faujasite, similar as in infra-red, two signals are distinguished, one close to 3.9 ppm and the other one above 4 ppm (depending on the reports, 4.6 – 4.9 ppm), assigned to protons pointing towards the supercage and sodalite cage respectively,[37,105] in agreement with theoretical calculations.[106] In the presence of excess water, a signal at 9 ppm was observed in ZSM-5 and assigned to hydrated hydronium ion.[107]

We are currently not at the stage where we can easily identify the position of the bridging OH group (including the position of the Al atom) giving rise to a specific spectroscopic feature for any zeolites (either IR, or ^{1}H NMR). DFT calculations have been used to quantify the respective stabilities of the sites as a function of the T site location for Al, and O position for H. However, in most cases, whatever the zeolite topology, the difference in stability between the most and least stable site is around 50 kJ.mol^{-1} at most.[78,80,81,97,108–117] In practice, the Al location is thought to be mainly dictated by the local environment in the synthesis medium, thus in solution, in the presence of alkali cations and/or a structure directing agent.[118,119] Thus, the rather moderate energy difference from one site location to another, does not constitute a dominant driving force for the final location. However, the combination of experiments and DFT calculations may be more conclusive, as discussed above for the interpretation of infra-red spectra of ZSM-5.[91] ^{27}Al MQ MAS NMR was used in this spirit to gain some insight in the location of framework aluminum atoms in terms of T site, comparing the experimental and DFT computed spectroscopic features.[120–123] Not less than 6 and 10 lines could be identified and assigned to specific T sites for ZSM-23[121] and ZSM-5,[120] respectively. In the presence of the tetrapropylammonium cation, Dib et al. proposed an approach combining ^{29}Si-^{27}Al NMR

correlations and DFT calculations to locate preferred T-site positions of Al.[124] The origin of this preferential location was found to be the Coulomb interaction between Al and the alkylammonium cation. Similar reasoning had formally been at the origin of the proposal of the location of Al atoms in the EUO framework either in the 10MR channel and 12MR side pockets (in the EU-1 zeolite) *versus* at the intersection of these (for the ZSM-50 zeolite).[125] Neutron diffraction later confirmed this.[126] Notably, X-Ray standing waves analysis led to a successful determination of the location of Al atoms in scolecite,[127] but, to the best of our knowledge, has never been successfully transposed to other zeolites so far. More recently, resonant X-ray powder diffraction across the Al K edge was successfully employed to identify aluminum siting in several ferrierite samples.[128] A combination of ^{27}Al NMR, EXAFS and DFT molecular dynamics simulations also led to the identification of the most probable Al siting in zeolite Beta samples.[129] These techniques are far from routine, and it can be noted that successful results are reported each time for a different zeolite framework, showing that there are still efforts to be done to solve this question in a universal manner.

Another important factor is the proximity of Al atoms (and hence of acid sites) in the framework, i.e. the presence of Al "pairs" (separated by Si). AlSiAl sequences can be detected by the ^{29}Si NMR spectrum, but some of these pairs may be located in opposite walls of a pore channel, i.e. they would not always be able to cooperate in catalytic reactions.[118] Al pairs in the same channel/cavity can be quantified by the ion exchange capacity of divalent cations, like Co^{2+} or Cu^{2+}, provided that the exchange is carried out under conditions, which avoid hydrolysis (and hence oligomerization) of the hexaaqua complexes of the respective cations. In the case of Co^{2+}, one can potentially go further and determine specific cation sites from the UV-VIS spectra, i.e. identify the rings where the Al pairs are located,[118] but this method has recently been challenged, a) because of the difficulty to avoid formation of Co oxide clusters (or dimers)

and b) because of the insufficient specificity of the UV-VIS bands used for identifying the different sites.[130]

Probe molecules have been extensively used to quantify the Brønsted acidity of bridging OH groups in zeolites. Adsorption/desorption measurements are performed thanks to numerous analytical techniques, including infra-red spectroscopy. It is beyond the scope of the present review to account for all the achievements in that respect. Detailed information can be found in numerous previous reviews.[22,131–133] The Brønsted acidity is defined as the thermodynamic ability of the species under consideration to donate a proton to another species, called the base.[9] It is thus natural to relate this to the deprotonation energy (DPE) of the acid site, which has been done very early by quantum chemistry approaches.[32,72,111] Correlations between the DPE and the T-O-T angles were found based on small cluster calculations,[134] but these trends tend to disappear in more recent reports,[106,135,136] showing that the DPE depends on many local effects that cannot be captured by a single angle. Notably, the DPE value obtained with clusters converges very slowly with cluster size,[137] whereas DPE values extracted from periodic calculations are not truly reliable, due to the problem of the electroneutrality of the cell, compensated after proton removal by a positive background charge.[136,137] Recently, a method associating both formalisms was proposed. It shows that Brønsted acidity decreases when the density of the zeolite increases,[137] which echoes the relation found by Rybicki et al. between the DPE and the dielectric constant of the zeolites.[135,138]

The equilibrium constant of the acid-base equilibrium, however, depends on the properties of the acid site (here, the bridging OH group of the proton exchanged zeolite) and of the base for the reactant side, but also on the stability (in terms of Gibbs free energy) of the reaction products, which are the conjugated base of the acid and the conjugated acid of the base, often in interaction one with the other. This is illustrated in **Figure 4-a** (pyridine playing the role of the base). In the case of zeolites, the interactions in the {conjugated base, conjugated

acid} pair, including framework atoms, are of tremendous importance, and reflect the evolution of confinement effects upon proton transfer. Notably, some probe molecules (such as CO) do not involve a proton transfer, thus here the equilibrium is balanced differently in terms of covalent, electrostatic and van der Waals interactions.[133,139,140] Finally, these acidity characterizations need to be correlated to catalytic properties, for which the molecules to be transformed differ (both in terms of basicity and confinement effect) from usual probe molecules. Thus, it remains a current challenge to select the appropriate probe molecule to infer catalytic properties of bridging OH groups of zeolites.[22,140–142]

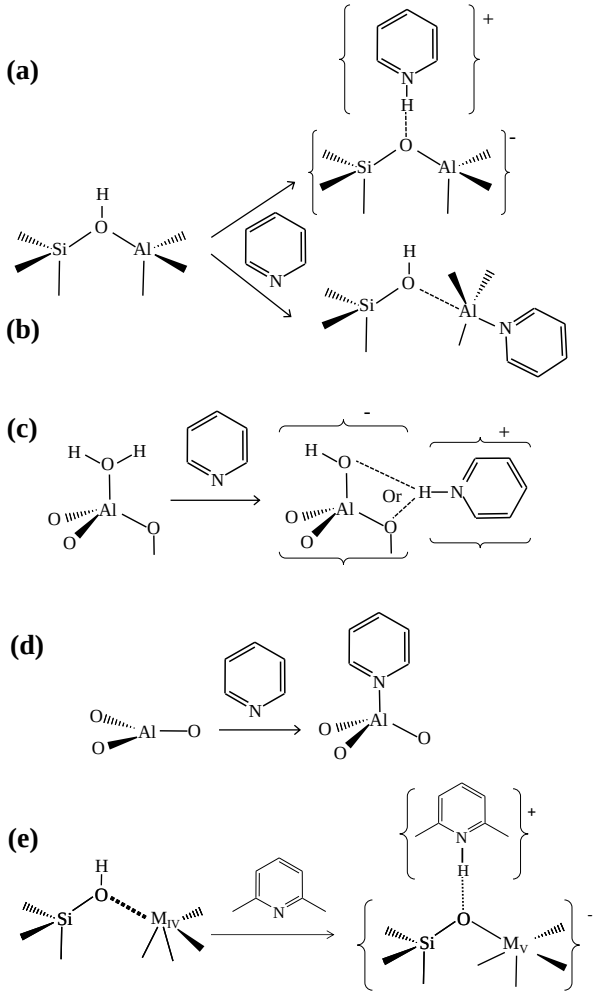

Figure 4. Adsorption of pyridine on acid sites present in the bulk (a) and at the external surface (c)-(e) of zeolites and amorphous silica alumina (ASA), according to DFT calculations. Adsorption on bridging OH groups either playing the role of a Brønsted acid site (a) of Lewis acid site (b), (c) Brønsted acidity of Al-(H_2O) groups at the external surface of zeolites and ASA, (d) Lewis acidity of Al_{III} at the external surface of zeolites, (e) Brønsted acidity of Pseudo-bridging silanol groups on ASA, with M = Al or Si. Adapted from refs. [60,81] Reprinted with permission from refs [60,81]. Copyright 2010 Wiley-VCH and 2020 American Chemical Society.

2.3. Lewis acidity of framework-associated aluminum sites

Aluminum surface cations (for example on aluminas) are well-known to exhibit Lewis acidity, both from experimental and computational investigations.[143,144] Thus, the question of the Lewis acidity of framework Al^{3+} species is open. Probe molecules such as CO or pyridine are well-suited to detect Lewis acid sites, giving rise to specific vibration frequencies when the adsorption is monitored by FTIR.[22] Moreover, ^{27}Al MAS NMR allows the monitoring of the evolution of coordination number of aluminum,[145] that shall also take place when a basic molecule adsorbs on the Lewis acidic Al. However, for protonic zeolites, samples have to be hydrated first, otherwise some aluminum atoms are qualified as "invisible". This is likely due to a strong anisotropy when the proton is bound to a given oxygen atom around the Al,[146] whereas in the presence of water, this position is averaged through fast proton jumps.

Most often, when Lewis acid sites are detected on a protonic zeolite sample, the assignment to EFAl species is proposed. However, some authors propose that framework or framework-associated (not completely dislodged from the framework) Al^{3+} could exhibit Lewis acidity themselves, as extensively reviewed in ref.[147]. Recently, a correlation of the number of framework-associated Al_{VI} sites detected by ^{27}Al MAS NMR spectroscopy on hydrated Mordenite samples, with the number of Lewis acid sites seen by pyridine and CO adsorption followed by FTIR, was observed.[75] The knowledge obtained on various frameworks (Faujasite, Beta, ZSM-5) about the reversible tetrahedral (even trigonal, as monitored by XANES at the Al K-edge[148] or ^{27}Al MAS NMR[149,150]) to octahedral coordination conversion upon hydration/dehydration[146,151–155] led the authors to assign this behavior to framework-associated aluminum ions. The comparison of adsorption features with CO *versus* pyridine led to the identification of a preferred location of the said framework Lewis acid sites in the side pockets of Mordenite.[156] Similarly, Phung and Busca proposed the existence of framework Lewis sites

in a H-Y sample free of extraframework species and assigned this to the coordination extension of aluminum.[77] Their assignment of this acidity to framework Al ions is based on the perturbation by various probe molecules of the low-frequency band, assigned to inaccessible O-H groups. They proposed an approach in anti to the bridging OH group to explain this behavior, like the representation given in **Figure 4-b**.

Density functional calculations show that bulk framework Al sites are indeed able to adsorb water[157,158] and pyridine[81] molecules, provided the molecule approach takes place in anti to the bridging OH group. The latter is thus transformed in a pseudo-bridging silanol group (using the terminology chosen for amorphous silica-alumina surfaces[60,82]), where the anti Al-O bond is more or less elongated. Theoretically however, the maximal coordination number reached is five, instead of six, if the aluminum remains in its framework position. A higher coordination number may be reached if some additional Al-O bonds are broken, with partial disconnection of the Al atom.[159] Moreover, the calculations suggest that the Lewis *versus* Brønsted acid site expression depends on the accessibility and stabilization of the OH group itself (expression of Brønsted acidity) *versus* that of the position in anti (expression of Lewis acidity).[81]

Notably, some earlier experimental works assigned the Lewis acidity of zeolites to threefold-coordinated Si atoms obtained from the dehydroxylation action of probe molecules such as ammonia and pyridine.[73,89] The Lewis acidity of silicon is indeed not zero, as attested by the possible extension of four to five of the coordination number of silicon in zeolites containing fluorine, as seen by ^{29}Si MAS NMR,[62,63] and in amorphous silica-alumina upon basic probe molecule adsorptions, as suggested by DFT calculations.[60,83] However, the threefold coordinated state of silicon was never observed experimentally in zeolites, to the best of our knowledge.

2.4. Extraframework species and internal defects

Aluminosilicate zeolites are often used after post-treatments, typically steaming and acid leaching, leading to dealumination, and leaching in basic media, leading to desilication.[6,52,158,160] These treatments are known to give rise to mesopores and extraframework species (**Figure 1**). On top of affecting the acidic properties, mesopores and extra-framework species also impact mass transfer and confinement effects. Ravi et al. have very recently reviewed the possible EFAl structures and their impact on the Lewis acidity of zeolites.[147] The picture is far from simple. Compiling data from various sources, Ravi et al. indeed show that the amount of EFAl is not correlated to the number of Lewis acid sites, thus questioning the old paradigm that EFAls are at the origin of Lewis acidity of zeolites. Moreover, EFAls are thought to have an impact on the Brønsted acidity of neighboring bridging OH groups. This effect, called the Lewis-Brønsted synergy, was inspired by seminal works dealing with alkane cracking, and will thus be detailed later in section 6.4.

From a computational point of view, two main strategies are found in the literature for the understanding of the structure and the acidity of extra-framework species:[28,158] i) either tentative structures are proposed and a ranking of stability is determined to identify the most likely ones, or ii) the formation mechanism of the defect itself is investigated, so as to deduce which sites of the zeolites are most prone to demetallation, based on a full kinetic analysis. The first approach leads faster to a large variety of structures, whose impact on acidity is then computationally investigated. The second one gives more reliable models, but in a much slower way. To date, these models have been restricted to the simulation of point defects and mononuclear extra-framework species, the propagation/condensation of which and their consequences on acidity need to be complemented.

In the spirit of the first approach, isolated $[Al(OH)_x(H_2O)_{n-x}]^{3-x}$ complexes were first simulated at the MP2 level to reproduce the evolution of the coordination number of aluminum

(from four to six), and the impact of the charge of the EFAl on its stability.[161] The latter parameter, tuned by protonation/deprotonation reactions, appeared to be more influential on the stability than the coordination change promoted by water adsorption/desorption, in the absence of consideration of the effect of the zeolite framework. Periodic models including the description of the mononuclear EFAl/framework interactions were then proposed.[162,163] They demonstrate a significant variation in the mobility of the EFAl in the pores as a function of the hydration level (dehydrated forms keeping anchored on specific sites[163] whereas hydrated forms may be mobile, as shown my ab initio molecular dynamics -AIMD-[162]) and as a function of the local topology. Mobile hydrated species are occluded in some circumstances, when a dense hydrogen bond network forms between the EFAl and cages (illustrated in the case of gmelinite[162]). Similar hydration-dependent stability was found by DFT simulations of the interaction of Al^{3+}, $Al(OH)_2^+$, $Al(OH)_3$ with T_6 clusters aiming at representing Faujasite.[164] Tricoordinated aluminum sites were proposed to be present in dealuminated H-Y zeolite thanks to the combination of MAS NMR and DFT calculations.[165] The evolution of the stability of the EFAls in Faujasite as a function of their nucleation degree (from one to four Al atoms) was also addressed by periodic DFT calculations.[166,167] The species containing three and four Al atoms, in particular $[Al_3O_4H_3]^{4+}$ were shown to be strongly stabilized in the sodalite cage. The acidity of EFAls and the impact of EFAls on the acidity of the neighboring bulk bridging OH groups was also addressed by these computational studies. As expected, dehydrated Al^{3+} cations in Mordenite appeared to be strong Lewis acid sites as shown by the simulation of CO adsorption.[163] Strong Lewis acidity was also found by combining T_{10} cluster DFT calculations and ^{31}P MAS NMR for trimethylphosphine adsorption at Al_{III} species in dealuminated H-Y zeolite.[165] Much more controversial conclusions were obtained regarding a possible synergy effect between EFAls and bridging OH groups, which acidity with respect to probe molecules such as ammonia, pyridine or acetone, was found to be either unaffected,[165] enhanced[166–168] or

reduced.[169,170] The question of this synergy effect between Brønsted and Lewis acid sites in catalysis will be further detailed in section 6.4.

The second computational approach was first proposed by Swang and coworkers,[171] considering the dealumination and desilication of the H-SSZ-13 zeolite by stepwise water dissociative adsorption. While dealumination was found to be less activated than desilication, the energy barriers determined in this work were prohibitive (more than 200 $kJ.mol^{-1}$) due to a very unstable disilanol intermediate, namely a 2MR bonded by one or two pentahedral silicon atoms. Alternative mechanisms were proposed later for dealumination of CHA, MFI, MOR and FAU frameworks, avoiding such intermediates. They are based on an approach of the first water molecule on the aluminum atom, specifically in anti with respect to the bridging OH group, followed a 1,2 dissociation of water.[157,172] The resulting energy barriers are much lower (close to 100 $kJ.mol^{-1}$), and the attack appears to be regioselective for the intersection sites of H-ZSM-5, which was confirmed experimentally more recently.[120] Such low-activated mechanisms were also confirmed computationally for other zeolites, variable Si/Al ratios, in the presence of HCl and for other cations than protons.[173–177] Similar anti mechanisms also appeared to be valid for siloxane bridge breaking.[178] The cooperative role of water was also addressed recently and provide even lower barrier than for a stepwise water adsorption, together with alternative mechanisms.[178–180] Most investigations of this kind make use of a GGA level of theory, within a periodic representation of the framework. PBE-D2 water adsorption energies were compared for specific configurations with a hybrid MP2/DFT scheme, which showed good agreement between both levels of theory.[157] Recently, a more systematic study of the impact of the level of theory on water adsorption energy evidenced non-negligible variations (up to 50 $kJ.mol^{-1}$) depending on the choice made (GGAs versus MP2 versus RPA).[181]

Thus, many questions regarding the structure and acidity of EFAl species still remain open, and, therefore, their role in catalysis raises many question marks too. This area of research deserves further developments.

2.5. External surface sites

Even in the absence of EFAl species, the ideal picture of an aluminosilicate zeolite catalyst exhibiting only bridging OH groups is far from being sufficient. Indeed, the real zeolite catalysts also exhibit external surface sites, at the border of the crystallites, by contrast to the internal surface sites, within the micropores (**Figure 1**). Characterizing and modelling these surface sites is of prime importance, especially as a current trend is to go towards smaller and smaller zeolite particle size, mainly with the aim of reducing mass transfer issues. Objects such as nanocrystals (below 100 nm),[182] embryonic zeolites (below 10 nm),[183] nanosheets,[184] nanoslabs,[185] delaminated and 2D zeolites,[4,186] are attractive in that respect.

Infra-red spectroscopy shows the presence of numerous silanol groups at the external surface,[22] which is expected from an interrupted condensation process (**Figure 3-a**). A detailed assignment of the 3740 cm^{-1} zone was proposed in the case of ZSM-5,[187] making a distinction between terminal and geminal silanols (3747 and 3742 cm^{-1} respectively), expected at the external surface, versus internal silanols (3730-3700 cm^{-1}). From DFT calculations, a distinction is made between isolated *versus* hydrogen-bond acceptor groups,[85] both being expected at the external surface. Hydrogen-bond acceptors are involved in the hydrogen-bond by their oxygen atom (by contrast with donors that are involved in the hydrogen-bond by their H atom). Their signal appears between 1.3 and 2.2 ppm in ^{1}H NMR.[37,41] Here again, DFT calculations suggest a specific ranking between isolated silanols (below 2 ppm) and hydrogen-bond acceptors (above 2 ppm).[85] Their acidity, quantified by deprotonation energy calculations, is significantly lower than that of bridging OH groups.[188] Al-OH groups are also observed

(about 3650 cm^{-1} and 2.6 ppm), and very often assigned to extra-framework species (see section 2.4). DFT calculations extend these spectral zones to other kinds of groups, as will be discussed in the next paragraphs.[85]

Computational studies have been undertaken to elucidate the surface structure of numerous zeolites, mainly with the goal of defining the most stable surface orientations, rather than getting a detailed view on the acidity of the sites.[28] A few DFT studies focused on these aspects, by introducing Brønsted acid sites (substituting a Si^{4+} ion by a $\{Al^{3+},H^{+}\}$ pair) on initially purely siliceous models, for ZSM-5,[79,81,85,110,135,141,189–192] Mordenite,[78,193] Beta,[80] Chabazite,[194] and more recently Faujasite.[195] The symmetry of the framework being broken at the external surface, a largest variety of environments and nature of sites may be invoked. Surface Si-(OH)-Al groups are shown to be as stable as bulk sites. At the outermost surface (**Figure 5-a**), Al-OH close to bridging OH groups are also possible, with a specific spectroscopic signature at 3780 cm^{-1}, observed as a small band experimentally.[85]

DFT calculations performed for several surface orientations of zeolites H-ZSM-5, Beta and Y showed, however, that the most stable surface sites are not bridging OH groups, but Al-$(H_2O)(OH)_n$ species (n=0-2), the proton being harbored by the Al-OH instead of a bridging oxygen (Figure 5-b and c).[80,81,195] The Al-(H_2O) moieties are expected to give rise to an IR frequency between 3700 and 3650 cm^{-1} (**Figure 5-b**, usually assigned to extra-framework species) and a ^{1}H NMR chemical shift of 3.8 ppm (when isolated) or close to 3 ppm (if one H is hydrogen-bond donor).[85] The 3.8 ppm specific signal could be distinguished experimentally from the 4 ppm contribution assigned to bridging OH group, thanks to ^{1}H DQ-SQ NMR spectroscopy.[85]

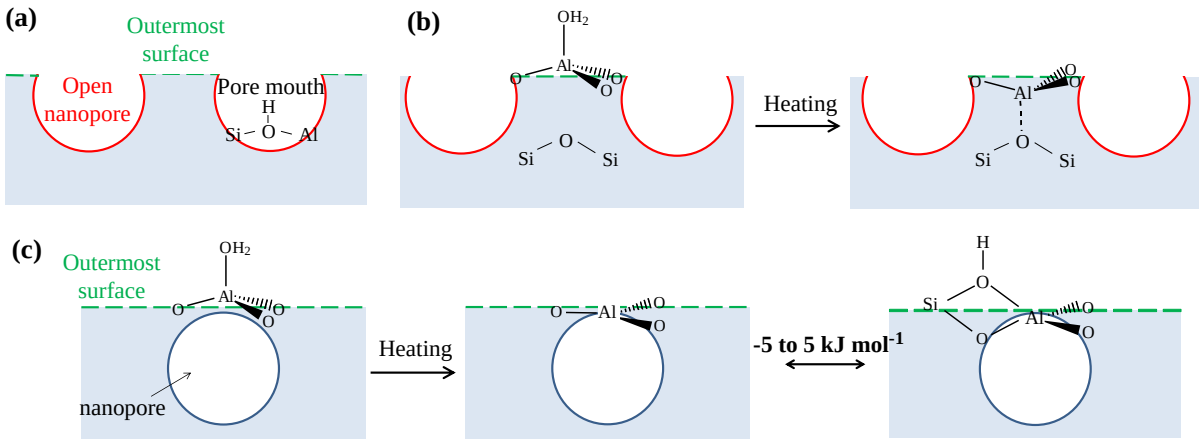

Figure 5. Some OH groups present at the external surface of zeolites, as suggested by DFT, and their behavior upon dehydration. (a) Bridging Si-(OH)-Al group at the pore mouth, stable towards dehydration, (b) Al-$(H_2O)(OH)_n$ (exemplified here for n = 0) with a siloxane bridge close-by, giving rise to a distorted Al_{IV} after dehydration, (c) Al-(H_2O) without any siloxane bridge close-by, giving rise to an Al_{III} species after dehydration, possibly in equilibrium with a 2MR. Adapted and extended from ref. [28]. Reprinted with permission from ref [28]. Copyright 2020 American Chemical Society.

The dehydration temperature of the Al-$(H_2O)(OH)_n$ species depends on the water partial pressure, but also on the local environment of the site (**Figure 5-b** and **c**). In case a siloxane bridge is in the vicinity of the Al atom, an additional Al-O bond forms at the same time the dehydration occurs. This results in a compensation of effects in terms of coordination number, the Al keeping a Al_{IV} coordination state.[80,81] In the case where such a siloxane bridge is not close enough, the aluminum atom remains three-fold coordinated after dehydration.[81] It may be wondered whether some of the Al_{III} species observed on zeolites by XAS could not be due to such environments.[148] DFT calculations also showed in the case of Mordenite and ZSM-5 that when a silanol group is in the vicinity of the Al_{III} site, the energy of the systems remains almost unchanged upon closing of a 2MR ring, generating a new kind of surface bridging OH group.[85,193] By FTIR, these 2MR species are expected to contribute to the same spectral zone as Al-(H_2O), ie between 3700 and 3650 cm^{-1} (**Figure 3-b**), whereas by ^1H NMR, DFT predicts a contribution close to 4.5 ppm, in the same spectral range as other kinds of bridging OH groups.[85] Conversely, upon excess hydration, the aluminum holding the surface Al_{IV}-$(H_2O)(OH)_n$ groups are likely to be transformed into Al_V and Al_{VI},[81] as observed experimentally

by ^{27}Al NMR and XAS.[75,196] Notably, Ravi et al.[75] made such an observation in the case of Mordenite and assigned this to bulk aluminum ions, but one may wonder whether the external surface can also contribute to such a phenomenon, as suggested by DFT.

Computationally, the Brønsted and Lewis acidity of external surface groups was quantified thanks to descriptors such as the deprotonation energy[110,135,138,188,194] and the interaction strength with various probe molecules (CO, [80,192,197] pyridine,[81,194,195,198] ammonia,[194,199] 2,6-dimethylpyridine, [131] trimethylphosphine oxide[141,189]). From these various descriptors, bridging OH groups appear to exhibit similar, if not higher, acidity at the external surface compared to the bulk. Deprotonation energy drops at the surface due to smaller effective dielectric constant,[135,138] an effect that is in some cases compensated by a lower confinement effect.[81] This gives a support to the pore-mouth catalysis concept (see later section 5.3).[200,201] It is confirmed that silanol groups are very weak Brønsted acid sites. Al-$(H_2O)(OH)_n$ are predicted to exhibit intermediate acidity between bridging OH groups and silanols (**Figure 4-c**).[80] The aluminum exposed after dehydration behave as Lewis acid sites, in particular in Al_{III} environments (**Figure 4-d**),[81,195] including at the surface of zeolite Y. This suggest that Lewis acid sites also exist in the absence of EFAl (usually considered as the main source of Lewis acidity).[195] Confinement effect was shown to play a huge role in the stabilization of the conjugated acid of the basic probe molecule. By DFT, adsorption configurations were found that maximize the corresponding interactions, in spite of the external position of the sites.[81,199] The electrostatic field was computed to be as intense in the open nanopores as in the bulk, but depleted at the outermost surface.[80]

3. Basics of catalysis by zeolites

A specific feature of catalysis by microporous materials is that the reactivity is not only governed by the structure of the active sites, but also by the access to and the adsorption on these sites, i.e. by diffusion and confinement effects, as pictured in **Figure 1**. These points will be briefly addressed in the following sections.

3.1. Adsorption/desorption: confinement and specific interactions

Adsorption effects play a major role in catalysis by zeolites. Many differences in reactivity and selectivity of zeolites could be traced back to adsorption effects.[202–205] In the case of bimolecular reactions it is important to tune the acido-basicity of the zeolite so that both reactants can adsorb in the zeolite pores.[206,207] In the simple case of a single reactant in acid catalysis, a predominant role of adsorption is to concentrate the reactant on the active acid sites. This is true for all heterogeneously catalyzed reactions, but the specificity of zeolites is that the adsorption strongly depends on the pore size and pore geometry. The adsorption of apolar molecules, i.e. of hydrocarbons in general, is governed by van der Waals interactions between the adsorbate and the zeolite pore wall. Derouane was the first one to suggest that there should be an optimal fit between the size of the adsorbate molecule and the pore, which allows maximizing the van der Waals interactions.[16] This theory was experimentally confirmed by Eder and Lercher, who showed that there is a good correlation between heat of alkane adsorption and pore size of zeolites (**Figure 6**). Below 0.5 nm a decrease is observed because repulsive interactions start to come into play.[208] The experimental trend was reproduced by molecular simulations, which furthermore yielded important information on the preferred adsorption sites of the alkanes.[209] In small pore zeolite with cage-like structures (RHO and LTA), the alkanes adopted coiled configurations inside the cages, while in other zeolites, the

adsorption was evenly distributed over the pore volume. Note, however, that these simulations were carried out for pure silica structures, i.e. the effect of specific adsorption on the acid sites was not considered. Experimental measurement indicate that the specific interaction with the acid sites increases the heat of adsorption by 7-10 $kJ.mol^{-1}$.[210]

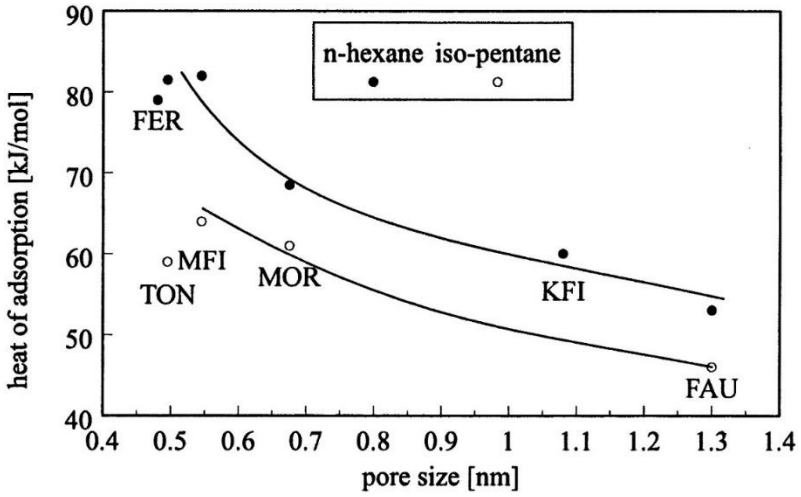

Figure 6. Relation between pore size and heat of adsorption of alkanes. Reprinted with permission from ref [208]. Copyright 1997 American Chemical Society.

The adsorption constants of alkanes generally increase with increasing heat of adsorption (i.e. with a more negative adsorption enthalpy), but the increase is counterbalanced by the concomitant decrease of the adsorption entropy. This phenomenon is called the compensation effect;[211] it is especially pronounced for small pore zeolites where the loss of degrees of freedom upon adsorption is more pronounced.[212] If the hydrocarbon loadings are low (gas phase, low pressure), the selectivity in the adsorption of mixtures can be well predicted by the relative affinity of the single components.[213] Heavier molecules are generally more strongly and therefore selectively adsorbed. However, under conditions where the pores are saturated with adsorbates (i.e. under liquid phase conditions), the adsorption is not any more governed by the affinity of a single adsorbate with the zeolite pore, but by the efficiency of packing of the mixture into the pore volume. For entropic reasons, the molecules which occupy the smallest volume are selectively adsorbed because they allow packing a maximum number

of molecules into the available pore space. This can lead to an inversion of the adsorption selectivity compared to gas phase conditions, i.e. the preferential adsorption of a smaller molecule (size entropy effect)[214] or of the more branched molecule (configurational or length entropy effect).[215,216]

3.2. Diffusion

The acid sites of zeolites are generally located within the micropores. Reactants must diffuse through these micropores to access the acid sites. Especially in the case of medium and small pore zeolites, the micropore diffusion process may be slow and strongly affect the reactivity. Strong differences in the diffusion rate of different reactants or products are, by the way, at the origin of some of the famous shape selectivity effects of zeolites.[217] In the case of ZSM-22, ZSM-23 and SAPO-11 it has been shown that the isomerization of alkanes is actually only taking place at the pore mouth, because the diffusion of alkanes into the bulk of the crystal is extremely slow. [200,201,218] This leads to a very selective branching near to the end of the paraffin chain on these zeolites. Moreover, surface barriers play an important role. Especially for small zeolite crystals, the molecule transfer from an adsorbed state on the external surface of the crystal into the pore entrance is the rate limiting step of molecular transport.[219–221] It is, thus, not surprising that the nature of the external surface and the presence of active acid sites on the latter can have a significant impact on the reactivity of zeolites.

3.3. Intrinsic kinetics *versus* effective kinetics

Measurements of the kinetics of zeolite catalyzed reactions in the gas phase are usually carried out in fixed bed reactors under plug flow conditions. The measured rate constants are effective rate constants, which encompass the contribution of diffusion and adsorption effects to the overall reactivity. Computational studies at the atomic scale, on the other hand, give

information on the activation barriers of a molecule adsorbed on a given acid site, i.e. on the intrinsic rate constants, and usually do not consider diffusional rate limitations. For a proper comparison between measured and calculated rate constants, (i) the absence of diffusional limitations should be ensured, (ii) the rate constant should be normalized by the number of active sites in the catalyst.

Concerning the influence of diffusion, it is important to recall that the relevant criterion is not the absolute rate of diffusion, but the relative rates of reaction vs. mass transport, expressed by the ratio R^2k/D, where k is the rate constant, R the characteristic length of the diffusion path (for a spherical particle the radius) and D the diffusion coefficient. The square root of this ratio is the Thiele modulus; it must be lower than 0.1 to ensure the absence of diffusional limitations. However, estimation of the Thiele modulus may be challenging due to the difficulty of estimating a representative diffusion coefficient. Ideally, non-equilibrium transport diffusion coefficients in zeolites relevant to the reaction conditions should be used, that take into account mixture and pressure effects. Caution must be taken when using diffusion coefficients from Pulse Field Gradient NMR (PFG-NMR) experiments, because it yields autodiffusion coefficients (i.e. in the absence of a concentration gradient), which may be up to three orders of magnitude higher than transport diffusion coefficients.[222,223] Diffusion coefficients obtained from gravimetric uptake experiments or chromatographic methods are generally more suitable for calculating a Thiele modulus, even if they do not take into account mixture or pressure effects (the temperature effect should ideally be extrapolated from an Arrhenius plot), but these approximations may be judged acceptable for a rough estimation of the Thiele modulus, which may be sufficient in many cases. While numerous diffusion data are available for hydrocarbons in the gas phase, few relevant data is available in the presence of a solvent, for instance in the case of the conversion of carbohydrates. In the case of 10MR zeolites like ZSM-5, the diffusion of (di)branched alkanes and aromatics is extremely slow, in the order

of 10^{-16} to 10^{-17} $m^2.s^{-1}$ (these are effective diffusion coefficients obtained by fitting reactivity data or transient experiments).[224,225] For dibranched alkanes the characteristic times of diffusion R^2/D are in the order of 10^3-10^4 s,[226] i.e. it is highly likely that diffusion becomes limiting for reactions involving these molecules. In the case of 12MR zeolites like USY Faujasites, the reported diffusion coefficients for n-paraffins are several orders of magnitude higher, i.e. 10^{-8} to 10^{-10} $m^2.s^{-1}$.[227–229] Diffusion limitations are, therefore, less likely, but cannot be ruled out for fast reactions ($k > 100$ s^{-1}). The usual experimental verification of the absence of diffusional limitation consists in varying the crystal size; in a reaction-controlled regime the crystal size should not have any impact on the reaction rate. In practice, however, it is challenging to vary the size of zeolite crystals without changing at the same time their acidity,[230–233] which makes interpreting kinetics as a function of crystal size extremely difficult.[234]

The normalization of the reaction rate by the number of acid sites is another critical issue. There are numerous methods of measuring the number of acid sites in a zeolite. To cite a few of them:

- Multiplying the Al content of zeolite by the fraction of framework Al, determined by NMR, with possible corrections by the sodium content[235], although some species are not detected by ^{27}Al NMR (called “invisible Al”)
- Using the high temperature desorption peak of the NH_3 temperature programmed desorption (TPD), after proper calibration[236–238]
- Measuring the amount of strongly adsorbed protonated pyridine by IR spectroscopy, applying appropriate extinctions coefficients[239]
- Quantifying the peak of the bridging Si-(OH)-Al groups in the ^{1}H NMR spectrum, after proper deconvolution[85]
- TPD of n-propylamine or iso-propylamine[240]

Each of these methods has some shortcomings and ambiguities. In the ^{27}Al NMR spectrum, the question arises whether the distorted tetrahedral (or pentacoordinated) Al species should be counted as acid sites or not.[241] NH_3 TPD profiles are usually very broad and need to be decomposed to distinguish physisorbed NH_3 and NH_3 adsorbed on "strong" acid sites, the definition of strong being sometimes arbitrary.[236] Moreover, NH_3 TPD generally does not allow for distinguishing Brønsted and Lewis acid sites.[242] IR detection of pyridinium ions selectively probes Brønsted acid sites capable of protonating pyridine.[22] Weakly bonded pyridinium ions are eliminated by evacuation at different temperatures. The evolution of adsorbed amount of pyridinium ions as a function of the desorption temperature is related to an acid strength distribution, but as in the case of NH_3 TPD the concept is ill defined and purely empirical. Moreover, the published extinction coefficients vary significantly.[239] In ^{1}H NMR, the bridging silanol groups are detected directly (not via probe molecules) and quantification is more straightforward, but if H-bonding occurs the chemical shift distribution becomes very broad and a proper decomposition is difficult. Some works have reported good agreement,[243] but in other cases significant discrepancies between the different methods have been observed.[244]

To deduce activation barriers and activation entropies from kinetic measurements, the Eyring formalism is frequently used.[245] In the absence of diffusion limitations, the reaction rate of a heterogeneously catalyzed reaction of first order with respect to the adsorbed reactant is the product of the concentration of acid sites (n), the coverage by reactant (θ) and the intrinsic rate constant (k_{int}).

$$r = n * \theta * k_{int} \qquad \text{Eq. 1}$$

For gas phase reactions at low coverage, the coverage is K_{ads}*p, where K_{ads} is the adsorption equilibrium constant of the reactant, and p its partial pressure. The rate normalized by the number of active sites is, therefore,

$$\frac{r}{n} = K_{ads} * k_{int} * p = k_{app} * p \qquad \text{Eq. 2}$$

K_{ads} can be expressed by the adsorption enthalpy and entropy, while k is expressed via the activation enthalpy and the activation entropy in the Eyring formalism.

$$k_{app} = \exp\left(-\frac{\Delta_r H^0_{ads}}{RT}\right) \exp\left(\frac{\Delta_r S^0_{ads}}{R}\right) * \frac{k_B T}{h} * \exp\left(\frac{\Delta_r S^{\ddagger}}{R}\right) \exp\left(-\frac{\Delta_r H^{\ddagger}}{RT}\right) \qquad \text{Eq. 3}$$

k_{app} is the measured rate constant normalized by the number of active sites. Plotting then $\ln(k_{app}/T)$ vs 1/T. (Eyring plot, Eq. 4), yields the sum of the adsorption and the activation enthalpies as its slope while the sum of the adsorption and activation entropies is determined from the intercept.

$$ln\left(k_{app}\frac{h}{k_B T}\right) = \frac{\Delta_r S^0_{ads} + \Delta_r S^{\ddagger}}{R} - \frac{\Delta_r H^0_{ads} + \Delta_r H^{\ddagger}}{RT} \qquad \text{Eq. 4}$$

Note that some authors use an Arrhenius plot, i.e. $\ln(k_{app})$ vs 1/T. In this case, the slope is the sum of the adsorption enthalpy and the activation energy, the latter differing from the activation enthalpy by the quantity RT. The Eyring approach is more rigorous for the determination of intrinsic kinetic parameters.

The adsorption parameters are usually obtained by separate measurements, which allows for determining the activation parameters ΔH_{act} and ΔS_{act}. Systematic errors in the determination of the rate constant or the number of active sites will affect the entropy term. Additionally, an error in the determination of apparent activation energy (i.e. the slope of the Eyring/Arrhenius plot) of 3 $kJ.mol^{-1}$ (which is quite a conservative estimate) will, at 773 K, translate into an error of ~4 $J.mol^{-1}K^{-1}$ in the entropy term. For calculating the activation entropy, the adsorption entropy must be subtracted, which itself has an uncertainty of several $J.mol^{-1}K^{-1}$. One should, therefore, be very careful in interpreting small differences in the activation entropy as they may fall into the uncertainty of the measurements.

4. Stability of carbocations in zeolites

As it will be shown in the following sections, carbocation chemistry is believed to be at the core of the mechanisms of hydrocarbons transformations in zeolites. Analogy with knowledge obtained in superacid media led to such a proposal.[246] Carbocations may belong to two main families: carbenium ions (classical trivalent cations of carbon compounds, **Figure 7-a**) and carbonium ions (nonclassical penta or tetracoordinated three-center bound cations, **Figure 7-b**).[247] Notably, earlier terminology only made use of the "carbonium" label, for both classes of cations. Some authors currently mix both terminologies to date, which we do not do in the following. Carbenium ions may be formed after proton transfer to an alkene (which, in its non-protonated adsorbed form at the bridging OH group, is called a π-complex), or by cleaving a carbonium ion (see later section 6), whereas carbonium ions may be obtained after protonation of an alkane, or addition of a carbenium ion on a C-C bond.[6]

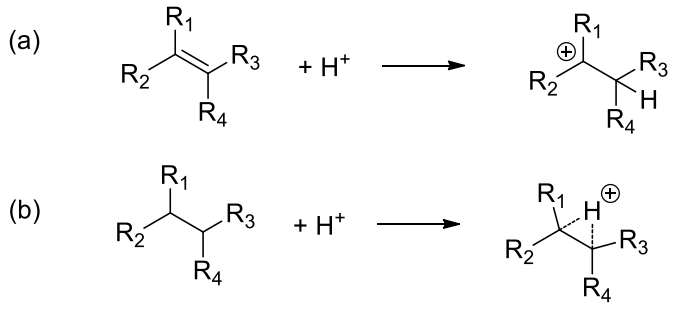

Figure 7. Examples of (a) carbenium (from alkene) and (b) carbonium (from alkane) ions possible structures.

However, isolating carbocation intermediates is challenging due to their usually short lifetime.[246] Highly resonant forms were observed in zeolites.[25,246,248–256] In particular, stable alkylcyclopentenyl ions could be observed directly by ^{13}C CP MAS NMR (**Figure 8-a**)[254,257–262] UV-Visible[263] and infra-red spectroscopy,[263,264] in line with DFT calculations.[265] Conversely, only indirect evidence was given of short-lived carbenium ions.[21,266–268] ^{13}C scrambling was observed after adsorption of butenes in various zeolites, assigned to the

existence of protonated cyclopropanes (PCP), thus to carbocation species, but it was not clear whether such species were only transition states, or true intermediates.[24] The observation of tert-butylammonium by ^{1}H and ^{13}C MAS NMR, assigned thanks to DFT calculations, after reacting ammonia with tert-butanol, was interpreted as a proof of the existence of the tert-butyl ion itself.[269,270] Conversely, oligomerization products (mainly, from alkenes) and alkoxides (mainly, from alcohols) are easily observable in zeolites by ^{13}C MAS NMR and FTIR.[21,24,246,257,266–268,271–276] Alkoxides are formally obtained by formation of a C-O bound between a carbenium ion and a framework oxygen atom, as illustrated in **Figure 9**.

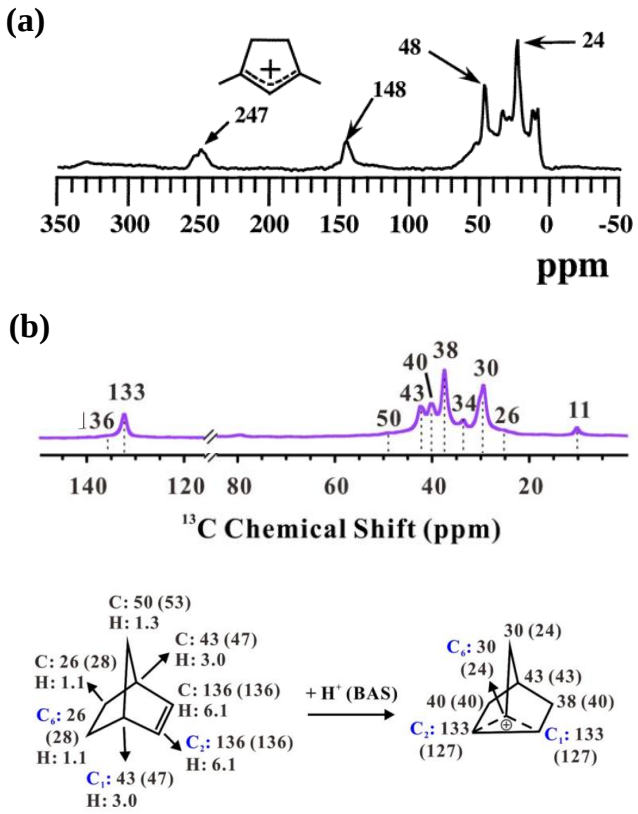

Figure 8. (a) ^{13}CP MAS NMR spectrum of the $C_7H_{11}^+$ cation formed upon ethylene adsorption and reaction on H-ZSM-5. Adapted with permission from ref. [259]. Copyright 2001 American Chemical Society. (b) top: ^{13}CP MAS NMR spectrum of 2-norbornene reacted with H-ZSM-5 at 373 K, bottom: experimental and computed (into brackets) chemical shifts of 2-norbornene and of the non-classical ion obtained upon protonation in H-ZSM-5. Reprinted with permission from ref. [277]. Copyright 2021 John Wiley and Sons.

Earlier quantum chemistry calculations, in the 80's and early 90's, using small cluster models at semi-empirical or Hartree-Fock levels, concluded that carbenium ions were transition

states along the formation pathway of alkoxides, calculated to be local energy minima.[278–285] It was afterwards shown, however, that such a conclusion could be impacted by several factors, beside the nature of the carbenium ion itself - primary *versus* secondary *versus* tertiary, and variation of chain length.[285–289] First, the consideration of confinement effect in the model is crucial. Going from small clusters (with only one to three T sites) to much larger ones (encompassing the description of a complete cavity) or to periodic models, as it was undertaken starting from the second half of the 90's, leads to an enhanced stabilization of charged species such as carbenium ions.[170,290–297] It also reveals steric constraints for the formation of alkoxides, depending on the local topology around each T site, preventing in some cases the formation of the C-O bond.[286,298,299] Second, the level of theory used in the calculation has a strong impact on the respective energies of alkoxides and carbenium ions.[285,286,300–302] In the prototypical case of the tert-butyl ion formation starting from isobutene, hybrid QM/QM approaches at the MP2:PBE level demonstrated that the carbenium ion becomes a local energy minimum at this level of theory within Ferrierite, whereas it was not the case at the GGA level (**Figure 9-a**).[301] Finally, thermal effects were shown to favor carbenium ions with respect to alkoxides. This was first demonstrated by static approaches, accounting for the vibrational degrees of freedom of adsorbed species, possibly with constrained translational and rotational movements of carbenium ions, as the later are disconnected from the framework, contrary to alkoxides.[269,295,297,303,304] More recently, this also appeared from ab initio molecular dynamics, starting from alkenes of various sizes.[305–308] However, due to constraints of computational resources, combining a high level of theory (beyond GGA) and AIMD is highly challenging. A few very recent achievements have been reported, that open the door to more systematic investigation of this question in the near future.[302] At the GGA+dispersion level of theory currently accessible for AIMD of hydrocarbons in zeolites, secondary carbenium ions are not

always deep free energy minima, and easily lead to spontaneous transfer of the proton to the zeolite framework, yielding the corresponding π-complex.[306,309,310]

Notably, most investigations cited so far deal with the stability of carbenium ions in the bulk structure of zeolites, in the vicinity of bridging Si-(OH)-Al groups. The picture is much less detailed at sites located on the external surface of the zeolites, or on amorphous zones. From periodic PBE+D2 calculations, the formation of a tertiary carbenium ion from isobutene appeared to be as favorable at bridging OH groups in open micropores as in the bulk (**Figure 9-b**).[80] This is again a confirmation that pore mouth catalysis may take place. However, the formation of the carbenium ion appeared to be not feasible at Al-(H_2O) acid sites at the outermost surface, confirming the milder acidity of these groups (as mentioned in section 2.5). DFT calculations performed on amorphous silica alumina models moreover demonstrated that the carbenium ion is a local energy minimum only at PBS-Al sites (Pseudo-Bridging silanol groups pointing closing with an aluminum atom), but with a high energy penalty with respect to the alkoxide and π-complex (**Figure 9-b**).[295]

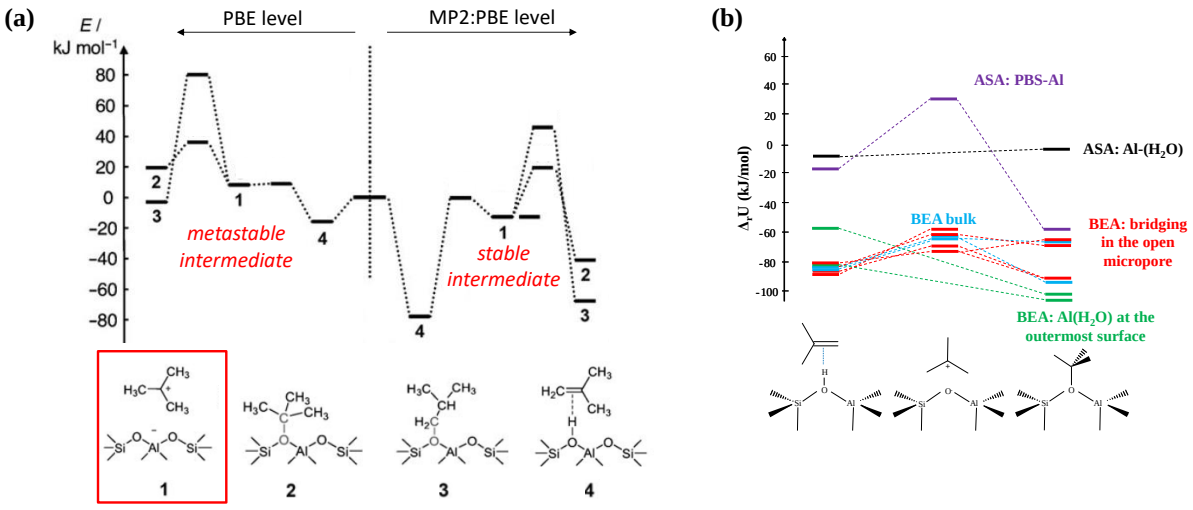

Figure 9. (a) Potential energy surfaces for species formed upon isobutene adsorption in the ferrierite zeolite, computed at the PBE level (left) and with a hybrid MP2/PBE method. Adapted with permission from ref [301]. Copyright 2010 John Wiley and Sons. (b) DFT+D2 energy diagram comparing the stability of various forms of adsorbed isobutene on amorphous silica alumina (ASA) (PBS-Al and Al-(H_2O), values taken from ref.[295]) and

zeolite Beta (bulk and surface sites[80]). $\Delta_r U$ is referenced to gas phase isobutene. Reprinted with permission from ref. [80]. Copyright 2017 John Wiley and Sons.

Protonated aromatic rings are important compounds in acid-catalysis by zeolites, as illustrated in sections 7 and 10. Alkylbenzenes protonated at the aromatic cycle (so-called Wheland-type intermediates) were observed experimentally in Beta and ZSM-5 zeolites thanks to infra-red and UV-visible spectroscopies.[311,312] Heptamethylbenzenium was also characterized in several occasions, in particular by ^{13}C MAS NMR,[313] and its stability in various zeolites confirmed by DFT calculations.[313–316] Computationally, several kinds of other substituted Wheland complexes were found to be local (free) energy minima in zeolites,[299,317–323] including recently by AIMD,[324–326] although the local minimum is shallow, with a poorly activated proton restitution to the zeolite framework, due to the non-aromatic character of the Wheland complex. Moreover, carbenium ions held by lateral alkyl chains when conjugated with the aromatic ring are also local energy minima,[291,320,321] characterized by fluorescence microscopy.[327]

Carbonium ions are basically formed by protonation of an alkane. For a long time, no carbonium ion could ever be observed as a stable species within a zeolite. The H/D exchange reaction of neopentane over D_2O exchanged zeolites was assigned to the participation of carbonium ions.[328] In 2021, Tang and coworkers[277] reported the *in situ* observation of the 2-norbornyl cation in ZSM-5 by ^{13}C MAS NMR combined to DFT ab initio molecular dynamics calculations. Natural density partitioning analyses demonstrated the non-classical nature of the ion, which appeared to be stable along a 25 ps AIMD trajectory at 298 K, and to give rise to a specific signal at 133 ppm in ^{13}C NMR (**Figure 8-b**).

Earlier small cluster calculations found no carbonium as being stable as local energy minima, but found such species as transition states.[32,281,329,330] Later first principles calculations, however, conclude that the ions coming from the protonation of butane[290,298,331] pentane[332] and

hexane[333,334] are shallow local energy minima after protonation of the corresponding alkanes by a bridging OH group. This is also the case for protonation of propane in several zeolites, as found recently by a MP2/DFT+D2 hybrid method (including CCSD(T) corrections).[335] The protonated C-C bond is predicted to be elongated, if not broken after protonation (see intermediate IM in **Figure 28**). Similar observations as for carbenium ions were made for carbonium ions, in terms of electrostatic stabilization when periodic cells are chosen to model the system instead of small clusters,[290,336] of impact of the level of theory that affects the shape of the energy landscape and impacts the intermediate *versus* transition state nature of the carbonium.[290,336]

Protonated cycloalkanes, in particular protonated cyclopropanes (PCP) are another important class of non-classical carbocations. They consist in a hydrocarbon containing a cyclopropane ring, itself holding an extra proton. They have been invoked for a long time as important species in carbenium ion isomerization reactions in superacidic media, and by extension in zeolites, but whether they are intermediate or transition state has remained unclear.[6,337–339] To the best of our knowledge, such species have never been observed experimentally, except for the species obtained upon protonation of 2-norbornene shown in **Figure 8**, that actually belongs to the PCP family. Several kinds of PCPs have been distinguished (**Figure 10**).

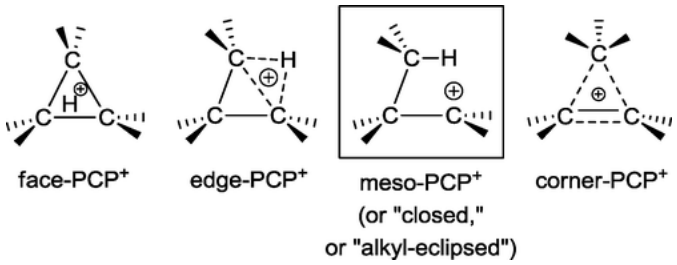

Figure 10. Various kinds of PCP structures (noted PCP$^+$ in ref [340]). Calculations reported in ref. [340] support the preference for the meso-PCP form. Reprinted with permission from ref. [340]. Copyright 2016 American Chemical Society.

Earlier extended Hückel calculations suggest for the simplest PCP $C_3H_7^+$ the possibility of forming the corner-protonated isomer.[341] Semi-empirical calculations on non-optimized structures then suggested that the edge-protonated species is the most stable.[342,343] Geometry optimizations (aiming at identifying local energy minima) were led for isolated species and revealed a "methyl-eclipsed" (**Figure 10**) structure,[344] that was found to be a relevant form of primary carbenium ions.[340] Some more recent ab initio calculations, including AIMD and coupled-cluster calculations, suggest that both edge and corner-protonated PCPs behave as transition states instead of reactions intermediates,[115,310,340,345–350] although a PCP ion of very low lifetime was invoked as an intermediate in alkene methylation mechanism.[351] The corner PCP transition state containing seven carbon atoms in the Chabazite zeolite cage, appeared to be much more stable than the corresponding edge PCP, both for electronic and dynamics reasons.[345] Due to the easy rotation of the CH_3 group of the corner-protonated PCP, averaging of its asymmetry leads to an in average symmetric PCP, contrary to the edge-protonated PCP. Thus, again, the level of theory and the consideration of thermal effects have a dramatic impact on the estimation of the stability.[340]

The existence and stability of these various kinds of charged hydrocarbons within zeolites is at the core of mechanism proposals made for most reactions detailed afterwards in this review. Identifying these species experimentally, or clearly evaluating their stability by computational chemistry, remains a challenge so far.

5. Transformation of alkenes and bifunctional transformation of alkanes

Although the direct conversion of alkenes in zeolites may be carried out, the high coverage of acid sites by alkenes leads to various reactions (bimolecular hydrogen transfer, alkylation, polymerization…) that greatly complexify the kinetic analysis. Thus, the chemistry of the

transformation of alkenes is mainly studied on a fundamental point of view *via* the bifunctional transformation of alkanes, where alkenes are generated in situ by dehydrogenation reactions. This results in lower coverages which largely simplifies the reaction schemes. When bifunctional catalysis is at stake, two catalytic functions are required: a hydro/dehydrogenating function and the acidic (zeolite) function (**Figure 11**). After the dehydrogenation step, alkenes are protonated on the zeolite Brønsted acid sites and their transformation is believed to be linked to carbenium ion chemistry.[352–354] The olefinic products are then hydrogenated on the metallic phase and desorbed from the catalyst. Because of their practical interest, bifunctional catalysts have been vastly studied in the literature. Describing the conditions for a good synergy between the two catalytic functions is beyond the scope of this review, and the reader can read about this topic elsewhere.[355,356] Operating conditions associated with the bifunctional conversion of alkanes are very broad. Temperatures typically range from 473 K to 773 K, the total pressure from 0.1 to 7 MPa, the hydrogen to hydrocarbon molar ratio from 10 to 400.[356,357,350,358] The operating conditions markedly impact the coverage of Brønsted acid sites with carbenium ions, as illustrated by a kinetic modelling study of n-octane hydroconversion on Pt/H-USY catalyst.[354] Increasing the total pressure higher than 1 MPa results in coverage of Brønsted acid sites below 0.05, due to the shift of the dehydrogenation equilibrium disfavoring the formation of olefins. Extremely low coverage values were also reported for n-heptane hydroconversion on Pt/H-Beta catalyst studied by a multiscale kinetic modelling approach.[350] The coverage of Brønsted acid sites is also influenced by the nature of the zeolite which impacts its protonation and physisorption properties.[354] In the following, we describe isomerization, cracking and oligomerization reaction mechanisms catalyzed by the zeolite phase.

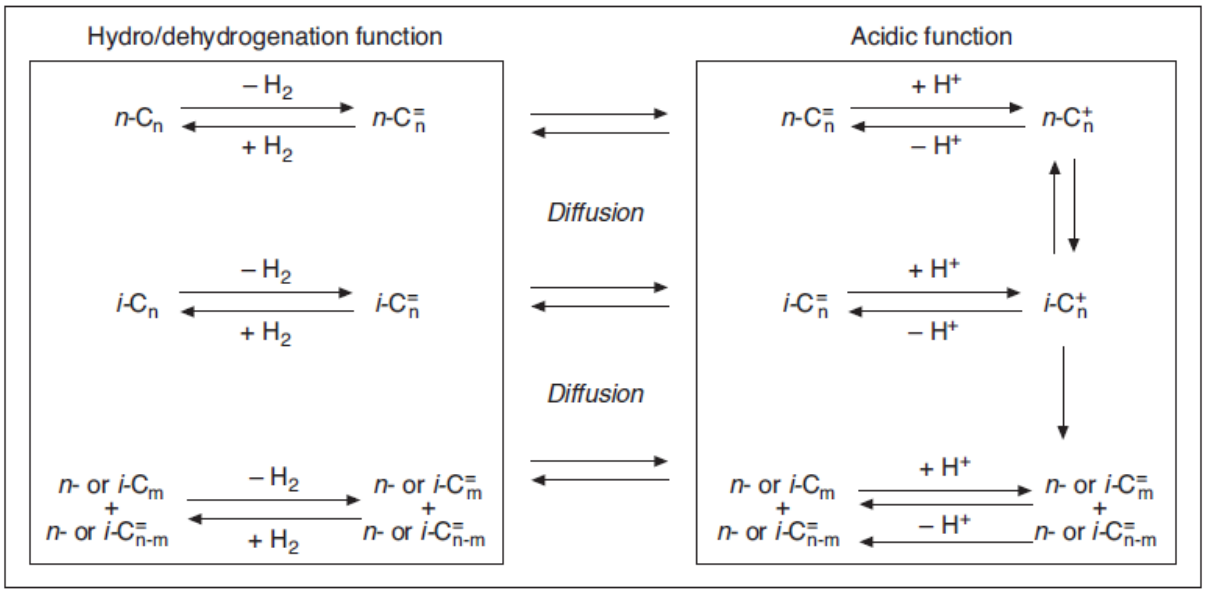

Figure 11. Bifunctional mechanism for hydroisomerisation and hydrocracking, from[357]

5.1. Skeletal isomerization

For acyclic molecules, two kinds of skeletal isomerization can take place, namely type A or type B. In type A isomerization, the branching degree of the carbocation is not modified whereas it increases or decreases for type B isomerization (**Figure 12**). Both reactions mainly occur via a monomolecular mechanism, although a bimolecular mechanism has also been reported for n-heptane isomerization over Pd/H-Beta zeolite catalysts,[359] and for butene isomerization (see section 5.5). Type A isomerization occurs orders of magnitude faster than type B[6,356,357] although both reactions proceed via cyclic carbonium ions like protonated cyclopropane (PCP).[6] The intermediate *versus* transition state nature of the PCP has long been debated, as discussed in section 4. Most recent computational investigations conclude that edge and corner protonated PCPs are not local energy minima but saddle points of isomerization reactions,[115,310,340,345–350] even if some "meso" forms of PCP are actually closed forms of primary carbenium ions intermediates.[340] Type B isomerization was proposed to require a corner-to-corner proton jump of the PCP. This slow step is not required for the type A

isomerization and was suggested to be at the origin of the difference in rate between the two reactions.[360] This intuition was confirmed by recent AIMD results, obtained thanks to the blue moon sampling approach, for the isomerization of tertiary C_7 carbenium in the Chabazite zeolite.[345]

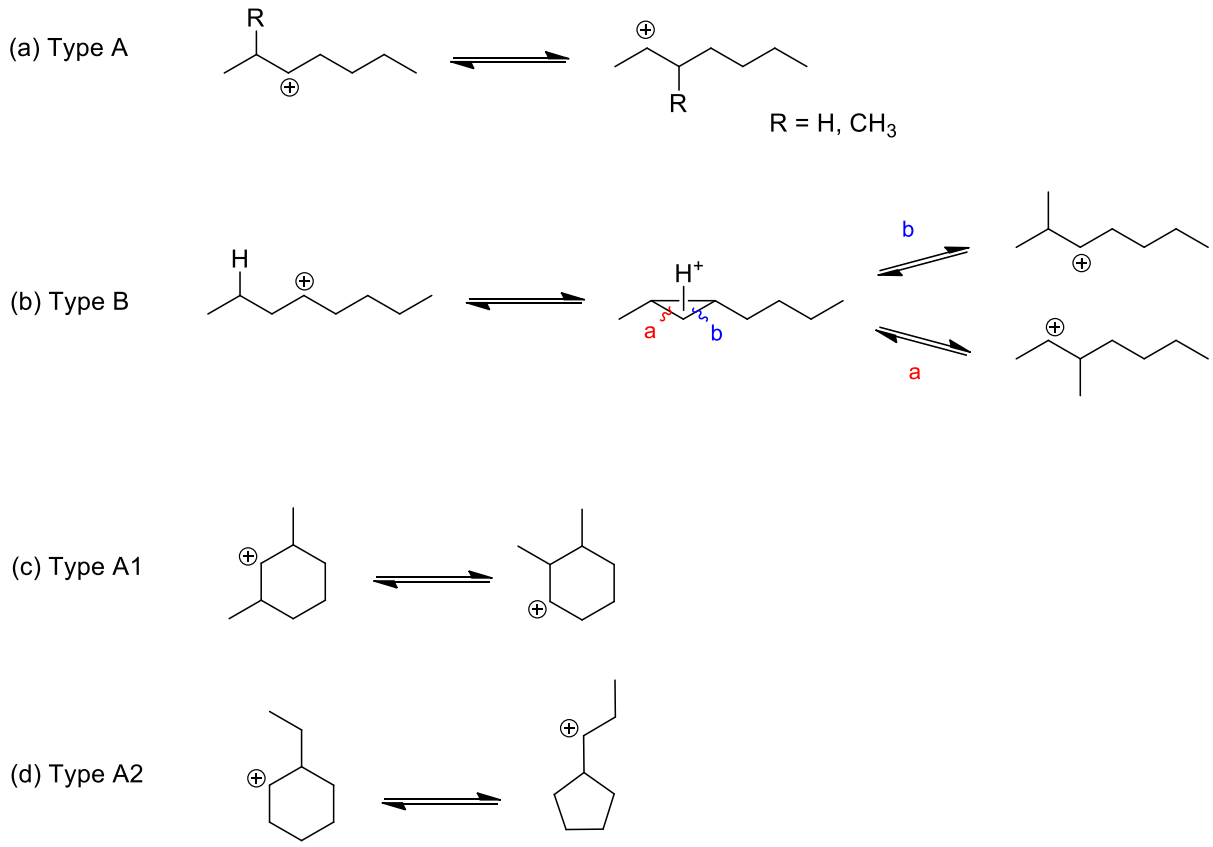

Figure 12. (a) Type A and (b) type B isomerization of carbenium ions (after protonation of the alkene), (c) Type A1 and (d) Type A2 distinctions specific to the cyclic carbenium ions. (a) and (b) adapted from [357].

A much lower free energy barrier was found for type A isomerization compared to type B. This is primarily due to the different protonated cyclopropane at stake for each reaction. The edged-protonated cyclopropane associated with type B isomerization has indeed a lower stability than the corner-protonated cyclopropane associated with type A isomerization (**Figure 13**). This was assigned to enthalpic terms, due to the tighter nature of the edge-PCP with respect to the corner-

PCP, and likely to entropic terms, as AIMD demonstrates a much higher mobility of the protonated CH_3 moiety of the PCP, with an easy rotation of this CH_3 above the C-C bond, which is not the case for the much more constraint edge-PCP. Such simulations moreover show that PCPs are highly mobile in the zeolite cavity, an effect that is not considered by static calculations, thus leading to a large overestimation of the free energy barrier.[345] Hence, AIMD methods are required to properly investigate such mechanisms.

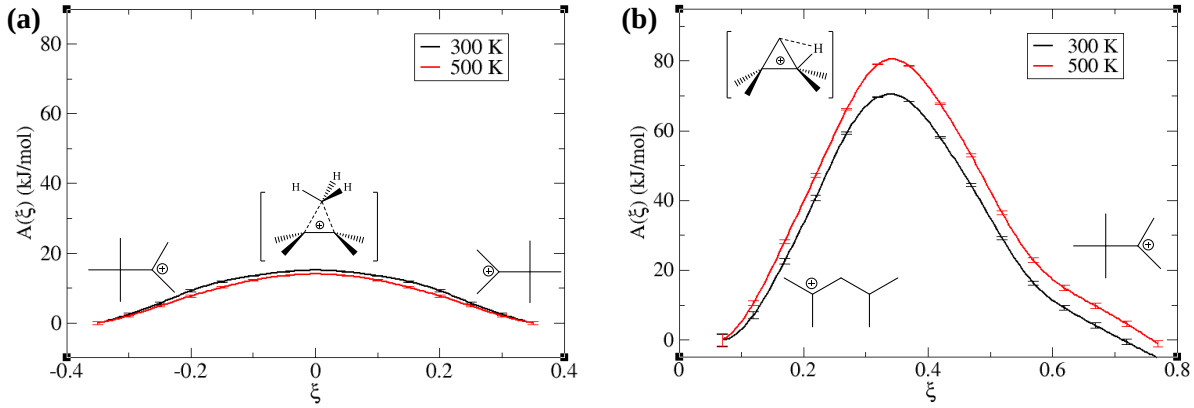

Figure 13. Free energy profiles computed using the blue moon ensemble approach for (a) type A and (b) type B isomerization of C_7 carbocations in chabazite. Reprinted with permission from [345]. Copyright 2019 Elsevier.

Stabilization of the PCP transition state in a local microporous environment is a function of various energetic factors, that could be formally decoupled via thermochemical cycles.[361] Factors related to the properties of the zeolite are the following:

- the deprotonation energy (DPE) of the Brønsted acid site, i.e. the intrinsic strength of the acid site;
- the van der Waals interaction of the framework with the PCP;
- the structural deformation of the framework and the PCP;
- the electronic interaction of the conjugated anion with the PCP.

The ensemble averaged DPE of proton associated with isolated framework aluminum was calculated for different aluminosilicate frameworks of practical interest, namely MFI, *BEA, FER, MOR, CHA and FAU using periodic models.[136] Ensemble averaged DPE were

comparable for every aluminum T-site location within a given framework, and for all the frameworks. It thus appeared that for aluminosilicates the stabilization of the PCP transition state is primarily dictated by the local topology of the micropore surrounding the Brønsted acid site. For a given framework like MFI, the DPE increases markedly by substituting framework aluminum by other elements such as Fe, B or Ga.[362] Concomitantly, the stabilization of the charged PCP by the deprotonated zeolite site decreases as the DPE increases.[361]Experimental results confirmed that the first-order rate constant, per proton, for n-heptane isomerization over Al, Ga, Fe or B-MFI zeolites decreases while the DPE increases.[361] Notably, such a direct link between the DPE, the stabilization of the charged PCP, and the isomerization rate constant only holds true if the other reaction intermediates are not charged, or not as sensitive as the PCP to the stabilization given by the deprotonated zeolite site. In ref. [361], alkoxides are invoked as intermediates in that respect, but computational results tend to show that neutral π-complexes are expected to play a dominant kinetic role with respect to alkoxides.[302,306,310,363]

For cyclic alkenes (in the case of an endocyclic C=C bond), three kinds of skeletal isomerization reactions can take place.[6] Type A isomerization is split in two subcategories (**Figure 12-c and d**). For type A1 isomerization, the number of endocyclic carbons and the branching degree of the cycle is not modified. For type A2 isomerization, the number of endocyclic and exocyclic carbons is modified but the branching degree of the cycle is not modified. For type B isomerization, the branching degree of the cycle is modified. Akin to acyclic molecules, type A1, A2 and B isomerization reactions are also believed to occur via a PCP intermediate, and type A isomerization reactions are expected to occur faster than type B. However, some experimental results suggest that the zeolite topology can significantly impact the relative rates of the two reactions. Weitkamp et al. observed that for ethylcyclohexane and methylcyclohexane, type B isomerization is significantly accelerated compared to type A for MOR zeolite, whereas this is not the case for FAU and MFI zeolites.[364] The authors suggested

that the peculiar behavior of the MOR zeolite is related to a transition state selectivity effect. To the best of our knowledge this hypothesis has not been assessed later by computational studies.

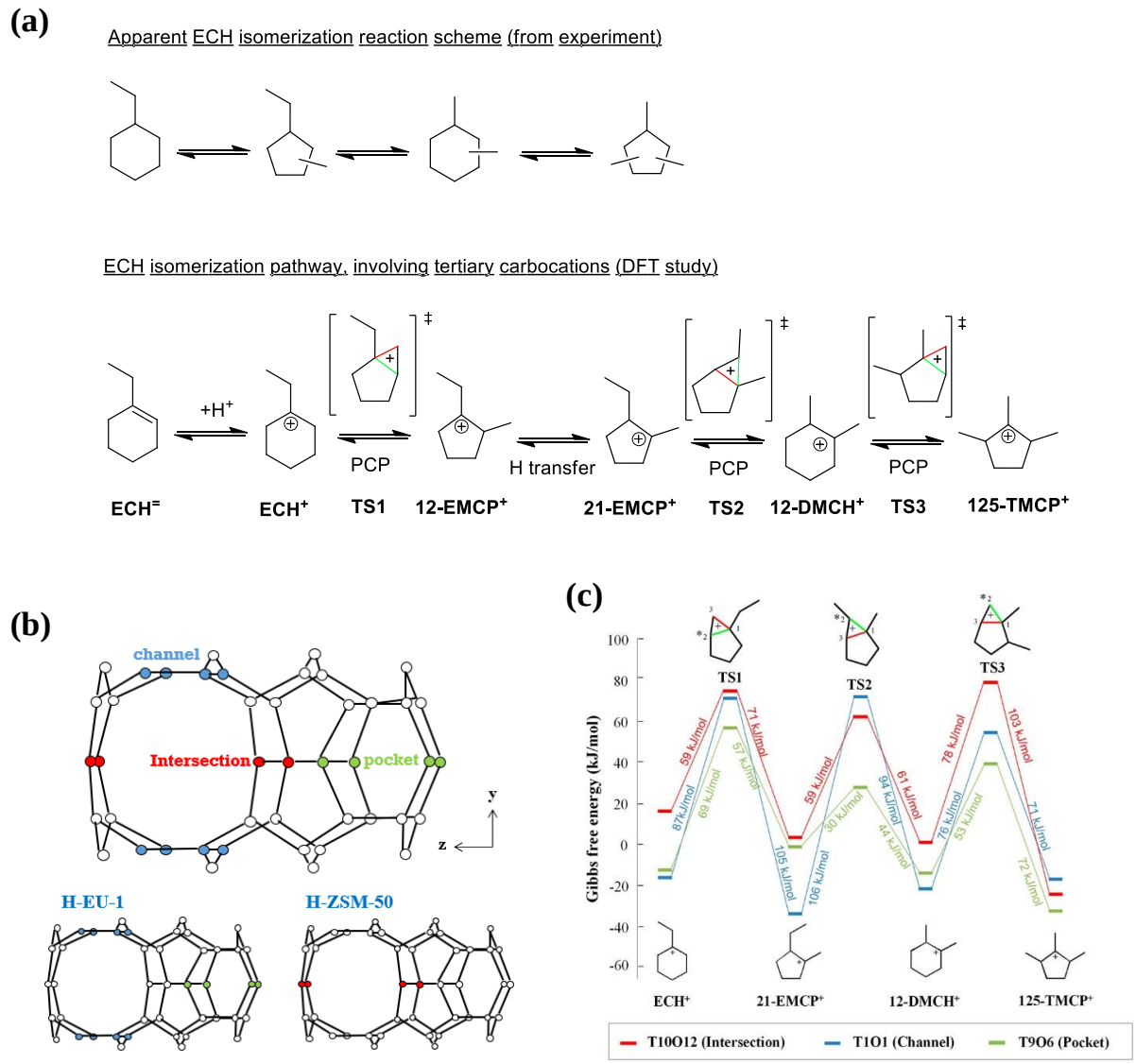

Figure 14. Ethylcyclohexane (ECH) hydroisomerization over Pt/EUO zeolites. (a) ECH apparent isomerization reaction scheme deduced from experiment[235] and corresponding reaction pathway studied by DFT;[115] (b) section of the EUO framework (10MR channel in the x axis) with the possible location of Al sites, and corresponding location of Al sites in H-EU-1 and H-ZSM-50 zeolites; (c) corresponding free Gibbs energy profile at 550 K for sites located at the intersection, in the channel or in the pocket. Reprinted with permission from ref [115]. Copyright 2019 American Chemical Society.

More recently, the impact of the acid site environment (i.e. the acid site localization) within a given zeolite framework (EUO) was investigated for ethylcyclohexane (ECH) hydroisomerization (**Figure 14**). Convergent experimental and ab initio results were obtained.[115,235] EUO zeolites are intermediate pore size zeolites, exhibiting monodimensional 10MR channels (5.8 * 4.1 Å) with 12MR side pockets (6.8 * 5.8 Å). The local environment of the acid site can therefore be significantly different depending on the locus of the site. Proper choice of the synthesis conditions and organic template allows to locate the active site either at the pocket and channel intersection (ZSM-50 zeolite) or in the pocket and the channel (EU-1 zeolite).[125,126] From catalytic experiments, the apparent isomerization scheme of ECH was established, and a corresponding isomerization pathway was studied by DFT. Ab initio calculations suggest that sites located in the pocket (as in EU-1 zeolite) are more reactive than those located at the intersection (as in ZSM-50). The cyclic carbenium ions involved in the reaction are indeed much less stabilized at the intersection than in the pocket. The origin of this difference is mainly due to smaller dispersion contributions to the adsorption energy for sites located at the intersection. Such results were in full accordance with catalytic experiments, as acid sites in EU-1 were found fifteen times more active than those in ZSM-50.

5.2. Cracking

It is generally believed that carbocation cracking occurs via a beta-scission reaction,[365,366] although another mechanism involving protonated cyclopropane has also been proposed.[367,368] Beta-scission corresponds to the breaking of the carbon-carbon bond in beta position of the positively charged carbon. As a result, two smaller molecules are generated: an olefin and another carbocation. According to the branching degree, and thus the relative stability of the carbocations involved, five types of beta-scissions can be distinguished (**Table 2**). The following ranking is reported for the rate of the different beta scissions:[357] A >> B1 ≈

B2 > C >> D. The ranking can be directly related to the relative stability of the initial and final carbocations involved.

Table 2. The five types of beta-scission reactions.[357]

Type	Minimal number of C-atoms in chain	Carbenium ions involved	Example
A	8	tert → tert	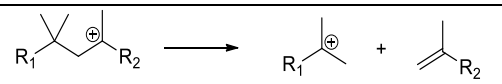
B1	7	sec → tert	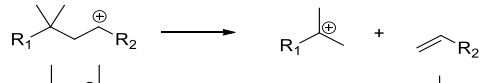
B2	7	tert → sec	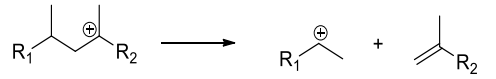
C	6	sec → sec	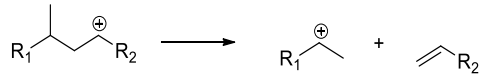
D	5	sec → prim	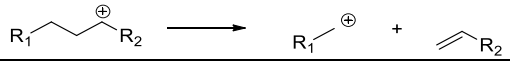

The relative rates of aliphatic carbenium ions isomerization and cracking are reported as follow, according to ref. [6]: type A beta-scission >> type A isomerization > B1 type beta-scission > B2 type beta-scission ≈ type B isomerization > type C beta-scission >> type D beta-scission. For n-alkenes, in the absence of shape selectivity effects, isomerization and cracking are consecutive reactions as type D and even type C beta-scissions are occurring slower than type B isomerization.[369,370] In the case of primary cracking, the observed distribution of cracked product appears comparable for reactants ranging from n-C_8H_{18} to n-$C_{16}H_{34}$ for FAU zeolites.[371] The cracked product distribution is typically symmetrical and centered around half of the carbon number of the reactant C_nH_{2n+2}. Production of methane, ethane and corresponding C_{n-1} and C_{n-2} alkanes is virtually absent (type D beta-scission). Production of propane and C_{n-3} alkanes is also disfavored compared to other fragments as the former cannot be produced by the faster type A scission. This is illustrated in **Figure 15** for n-decane hydroconversion. **Figure 15** also report the cracked product distribution observed when monobranched nonanes,

dibranched octanes and tribranched heptanes are used as reactant. The cracked product distributions obtained from n-decane, monobranched and dibranched C_{10} molecules are remarkably similar. Underlying reasons are that (a) the dibranched C_{10} are more prone to undergo cracking than monobranched and linear C_{10} (type B beta-scissions at stake) and (b) the methyl shift reactions (type A isomerization) are faster than the type B beta-scissions. As a result, when the cracking reaction appears, the dibranched products distribution is the same (i.e. at equilibrium) regardless of the initial reactant. The situation is completely different for tribranched reactants, especially 3,3,5-trimethylheptane. Cracked molecules obtained are almost exclusively C_5 molecules. This is a consequence of the very fast cracking of the 3,3,5 trimethylheptane (type A scission) compared even to methyl shift reactions. Experimental studies about the hydrocracking of branched alkanes with more than ten carbon atoms are scarce. Hydrocracking of 2,6,10,14-tetramethylpentadecane on Pt/USY and Pt/silica-alumina catalyst revealed a specific pattern of the cracked product distribution, especially at low cracking products yields. The pattern of cracked product distribution was related to the positions of the methyl groups in the reactant molecule.[372]

Conceptually, selective isomerization of n-alkane molecules to specific α,α,γ tribranched isomer(s) before the cracking reaction could allow to tune the pattern of cracked products distribution, for example, towards central cracking of the initial molecule. This approach was undertaken by Thybaut and coll.[373] Based on single event microkinetic model (SEMK), hypothetical appropriate zeolites topologies were proposed. Hypothetical zeolite topologies based on a combination of FAU and TON topology were found promising. The supercages of the FAU, with acid site, were associated with the tubular channels of TON topology of proper length, devoid of acid sites. Catalytic reaction could only occur in the supercages occupied by the inner carbon of the alkyl chains whereas the outer carbons are physisorbed in the channel. The TON moiety prevents the mobility of methyl groups along the

carbon chain, thus favoring the α,α,γ tribranched isomer over other isomers where methyl groups would be distributed along the chain.

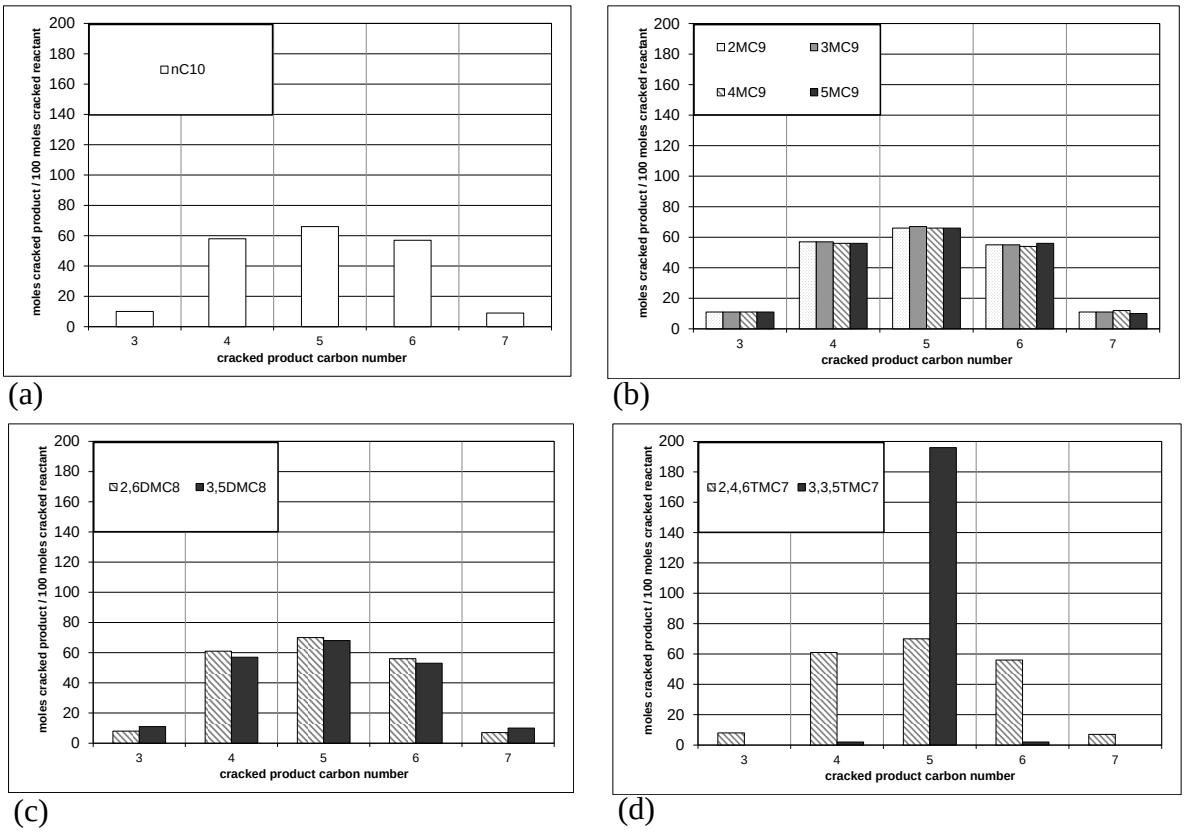

Figure 15. Evolution of the cracked product distribution (mol cracked product / 100 mol of cracked reactant) for $C_{10}H_{22}$ alkanes converted on Pt/USY catalyst: (a) n-decane, (b) methyl nonanes, (d) dimethyl octanes and (d) trimethyl heptanes, data extracted from[374]. Primary cracking, mol cracked products / 100 mol of cracked reactant: 199 – 202.

Mazar and coll. investigated various beta-scission modes associated with C_6 and C_8 olefins in H-ZSM-5 using dispersion-corrected DFT calculations.[375] Depending on the olefinic reactant, different beta-scission mechanisms could be at stake. Despite this diversity, the activation energy of the reaction was found to be primarily related to the amount of positive charge required by carbon atom in beta position of the protonated carbon to achieve full sp^2 hybridization (**Figure 16**). Transition state structure is indeed associated with full sp^2 hybridization of the alpha and beta carbon (the two atoms of the C-C bond that breaks).

However, the nature of the transition state associated with beta-scission reactions is still a matter of discussion. Earlier Hartree-Fock and DFT studies were performed using cluster models, and alkoxy groups covalently bound to the zeolite, rather than carbocations, were considered as stable intermediates.[282,283] Three transition states associated with three reaction paths were found, one-"ring-like" transition state (meaning that the transition structure is connected at the same time to two framework oxygen atoms) and two "hydrogen-bonded" transition states, also implying the formation of cyclopropanes. More recent works of static DFT calculations usually consider alkoxides as intermediates too. Barriers often superior to 100 kJ.mol^{-1} were computed, with large variations from one report to the other.[294,375–379] More recent AIMD studies shed new light on the mechanisms into play.[306,309] For the cracking of 4,4-dimethyl-penten-2-ium (B1 beta-scission) and 2,4-dimethyl-penten-2-ium (B2 beta-scission) in Chabazite, the free energy barrier calculated for B2 was found higher than for B1.[306] This was associated with different types of transition states: for B2, the transition state is not associated with the carbon-carbon bond cleavage of the molecule but with the proton transfer between the resulting secondary propenium cation and the zeolite. For both beta-scissions the energy barriers were found lower than those obtained by static DFT approach.

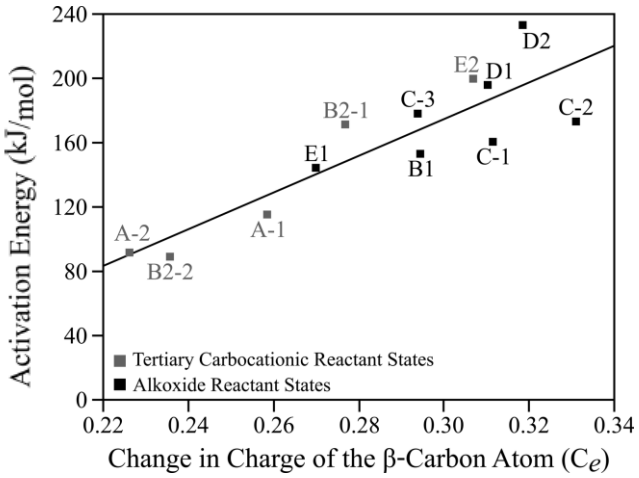

Figure 16. Evolution of the activation energies of beta-scission with the change in the charge of the beta carbon atom from the reactant to the transition state, as computed by DFT. Letters stand for the different beta-scission types. Reprinted with permission from ref [375]. Copyright 2013 American Chemical Society.

Regarding cyclic reactants, it is well known that the beta-scission of endocyclic carbon – carbon bond (i.e. ring opening) is markedly more difficult than for exocyclic ones.[356] A sterical reason is generally invoked to explain this.[380] The beta carbon-carbon σ sp^3 orbital bond that is part of the ring is nearly perpendicular to the π orbital of the sp^2 hybridized charged carbon. Therefore, there is a minimal overlap between the orbitals and the electron transfer is difficult at the transition state. For aliphatic carbenium, the beta carbon-carbon bond can rotate freely, and the overlapping of the orbitals is thus more pronounced. The inherent higher stability of endocyclic carbon – carbon bonds compared to exocyclic ones lead to peculiar hydrocracking pattern of alkyl-substituted rings. For naphtenes with 10 to 12 carbons, it is quoted as the "paring reaction", as the alkyl groups of the cycle rearrange and are eliminated from the cycle as an iso-alkane, while the cycle is largely preserved.[381] This is illustrated **Figure 17** for 1,2,4,5 tetramethylcyclohexane (1,2,4,5 TMCH), cracked on a bifunctional Ni/silica-alumina catalyst. Pattern of the cracked product distribution emphasizes that 1,2,4,5 TMCH is mainly cracked in isobutane and methylcyclopentane. The intrinsic stability of the C_5 and C_6 rings enables alkyl rearrangement via methyl shift and ring contraction to occur, until a configuration favorable to the fast type A beta-scission exocyclic is obtained. The proposed mechanism also explains why the paring reaction is operative for naphthene with at least 10 carbons number. Below ten carbons number, favorable configurations providing exocyclic type A beta-scission are not possible. Similar observations were made for the hydrocracking of octyl-cyclohexane over Pt/USY. Main cracked products families were napthenes and iso-alkanes.[382–384]

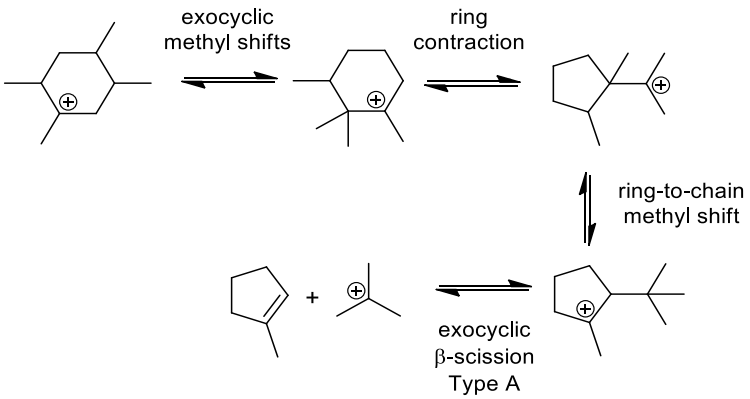

Figure 17. Illustration of the paring reaction: 1,2,4,5 tetramethylcyclohexane hydrocracking over Ni/Silica-alumina catalyst; proposed mechanism for the paring reaction, adapted from[381] . Primary cracking, mol cracked products / 100 mol of cracked reactant: 196. Methylcyclopentane and isobutane account for 74% mol of the total cracked products.

Recently, static DFT calculations were performed to study the ring opening of 1,3-dimethylcyclohexenium and 1,3,3-trimethylcyclopentenium in EUO zeolite.[346] For the former compound, a stable tertiary carbenium ion was identified as a ring opening product, but the associated transition state could not be identified, as it is likely close in structure and energy with respect to the product. For the later compound, all attempts to optimize a ring opening product were unsuccessful, as the resulting secondary carbocation was found to spontaneously re-close upon optimization. Thus, in that case, according to DFT results, no ring opening occurs. This was related to the inaccuracy of static DFT approach to successfully model secondary carbocations in zeolites.[306,308–310] AIMD investigations will be needed in the future to gain more accurate knowledge for these ring opening mechanisms that have only been scarcely considered in the existing literature.

5.3. Isomerization vs cracking selectivity

As mentioned previously the relative rates of aliphatic carbenium ions isomerization and cracking are reported as follow: type A beta-scission >> type A isomerization > B1 type beta-scission > B2 type beta-scission ≈ type B isomerization > type C beta-scission >> type D

beta-scission. In the absence of any shape selectivity effect, selective isomerization of carbenium ions with seven or more atoms of carbon is an issue as some multibranched carbenium ions are more prone to crack than to isomerize, due to the fast type B beta-scission and very fast type A beta-scission (for eight or more atoms of carbon).[385,386]

The situation can even be worsened if diffusional issues are at stake within the microporous network as the diffusion of the more reactive branched isomers is slower than the corresponding less reactive n-alkanes. Diffusion constants were calculated using forcefield molecular dynamic simulation for n-alkanes and monobranched alkanes with seven to thirty carbon numbers.[387] The zeolites studied were TON, EUO and MFI, modeled as pure silica frameworks, hence without explicitly simulating the Si *versus* Al distribution, nor the acid sites. At 600 K, regardless of the carbon number, the n-alkane diffusion was found to be one order of magnitude faster than the corresponding monomethyl isomers for the three zeolites. It is likely that similar differences exist for the corresponding alkenes. Thus, branched isomerization products may be trapped longer than non-branched compounds due to diffusion limitations, leading to overcracking for the former.

Recently a computational screening approach was proposed to identify optimal zeolite structures for the selective hydroisomerization of long chain hydrocarbons.[388] It was considered that selectivity to hydroisomerization is mainly driven by the effect of adsorption, according to the principle that a given catalyst will be selective to hydroisomerization if the adsorption of the linear alkane is favored over that of the corresponding isoalkanes in order for the latter to quickly desorb before overcracking occurs. Configurational-bias Monte Carlo simulations in the grand canonical ensemble were performed to compute molecule adsorption in the micropores. It was found that high affinity for n-alkane adsorption is associated with narrow and smooth channels. Six of the top seven IZA structural code database identified by the computational screening were indeed patented or described in the literature. This suggests that

adsorption effects are indeed of crucial importance. The major importance of adsorption effects was suggested previously for phenantrene hydroconversion over bifunctional catalysts using various zeolites (MFI, FAU and *BEA).[389] The catalytic tests results coupled with force-field and GC-MC simulation indicated that the adsorption energy of the isomerized products is the key parameter governing the isomerization (vs cracking) selectivity. A too strong adsorption of the isomerized products is detrimental to the isomerization selectivity as consecutive cracking reactions are favored. A recent study further emphasizes the impact of adsorption effects for hexadecane hydroconversion over bifunctional catalyst using *BEA zeolite,[390] via the variation of the experimental conditions. It was found experimentally that the isomerization selectivity decreases when the total pressure increases. GC-MC simulations showed that pressure increase favored the adsorption of i-C_{16} compounds compared to n-C_{16} and therefore enhanced their consecutive cracking. The detrimental effect of the total pressure on the isomerization selectivity during hexadecane hydroconversion was also reported over bifunctional catalysts using MTT[391] and AEL materials.[392]

Following the discovery from Miller in the mid-eighties with SAPO-11,[355–357] zeotype materials with one dimensional channels and tubular intermediate pore size were proven to be particularly suitable for the selective isomerization of long chain alkanes in bifunctional catalysis. Zeolites with TON or MTT topology are typical examples.[201,393,394] Such results were rather unexpected as with low dimensionality and medium pore size microporous network, the diffusion of alkanes and corresponding alkenes can be severely impeded. Common features associated with such zeolites are the high selectivity for monomethylbranching versus multibranching up to very high conversions. The methylbranching near the terminal carbon of the chain is favored (i.e. 2-methyl or 3-methyl isomers). Moreover, specific isomers are preferentially formed among the dibranched isomers. Typical spacing between the methyl groups of the dibranched isomers is higher than two carbon atoms.[393,395] The reactivity of the

isomers towards cracking is therefore lowered because these configurations are not favorable for cracking as type C instead of type B beta scissions is at stake (**Table 2**). Little could be said about tribranched isomers because of identification issues. Pore mouth and keylock catalysis occurring in the micropores opening of the zeolite crystals has been proposed to explain the experimental results. According to this, branching at specific positions is primarily driven by adsorption effects. The alkene optimizes van der Waals interaction with the zeolite micropores and then undergoes protonation and skeletal branching. Easy desorption of the branched isomer occurs when the branching is generated at the outside of the first restriction of the pore.[200] Pore mouth catalysis corresponds to the adsorption of one end of the molecule whereas keylock corresponds to the adsorption of the two ends of the molecule. The latter is favored when the alkane length and the temperature of reaction increase.[396] **Figure 18** depicts some favorable adsorption configuration of methyl-uncosanes on ZSM-22. Recent DFT calculations suggest that 3-heptene preferably adsorbs at the pore mouth of the channel of ZSM-23.[397]

Pore mouth and keylock concepts do not meet a consensus in the literature, although recent works substantiate this concept both from a theoretical (see section 2.5) and experimental point of view (as evidenced in the case of etherification of β-citronellene with ethanol on zeolite Beta[398]). Regarding isomerization *versus* cracking selectivity, other explanations have been proposed to account for the peculiar properties of zeotype materials with one dimensional channels and tubular intermediate pore size, which are related to the diffusional behavior of different isomers. Product shape selectivity has been proposed to explain the favored methylbranching near the end of the carbon chain for monobranched isomers as 2-methyl and 3-methyl branched isomers are found to diffuse faster than inner methyl branched isomers, from C_7 to C_{16} molecules.[399–401] For dimethylbranched isomers the situation appears more elusive as experimental measurements as well as simulations are challenging. Raybaud and coll. performed diffusion path simulations to evaluate the energy barrier of dimethylbranched C_7

isomers diffusion in ZSM-22 and ZSM-23.[400] Branching of the two methyls on the same carbon severely impedes the diffusion of the isomers with an energy barrier higher than 90 kJ.mol^{-1}. Energy barriers were found much lower for 2,3 and 2,4-dimethylpentane (29-39 kJ.mol^{-1} and 50-55 kJ.mol^{-1} ranges for ZSM-22 and ZSM-23 respectively). Based on configurational bias Monte Carlo simulations, Schenk et al. calculated the Gibbs free energy profile as a function of the position of 2,n-dimethyl pentadecane isomers (n being the position of the second methyl group) along the channel in the TON structure.[203] The position of the second methyl group impacted markedly the diffusion of the molecule as the shape of the isomer could be commensurate, or not, with the microporous network.

Transition state selectivity inside the microporosity was also suggested to explain the formation of specific (dibranched) C_7 isomers.[400] This hypothesis was proposed based on the calculated enthalpy of adsorption of different cyclopropanes, considered as a proxy of the corresponding protonated cyclopropanes transition states, in the ZSM-22. To the best of our knowledge, advanced simulations using DFT were not performed to revisit this.

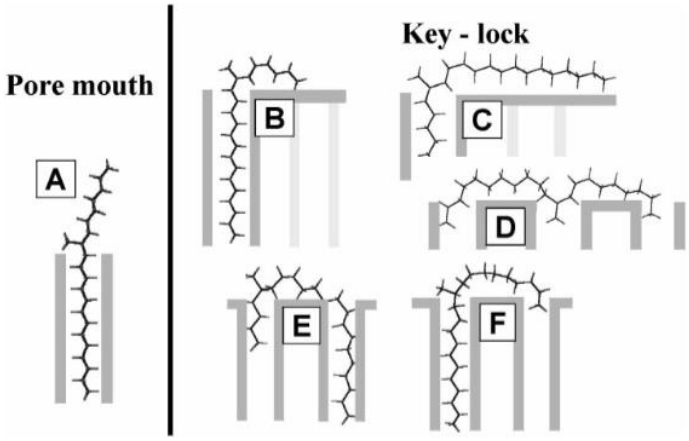

Figure 18. Favorable adsorption configurations of methyl-uncosanes on ZSM-22. Reprinted with permission from ref [200]. Copyright 2001 Elsevier.

Recently Noh and coll. proposed that the strength of the Brønsted acid site, defined as the deprotonation energy, also influences the intrinsic selectivity of cracking versus

isomerization (i.e. without diffusional effect).[361] MFI zeolite with various heteroatoms, i.e. Al, Fe, Ga and B, were evaluated in the hydroconversion of 2,4 dimethylpentane. It was found experimentally that the ratio of rate constants of beta-scission versus isomerization increased when the strength of the acid site diminished. According to DFT calculations, the transition states associated with isomerization were more stabilized with increasing acid strength compared to transition states associated with beta-scission, due to differences in positive charge distributions. This result seems to contradict the commonly accepted hypothesis that acid sites of mild or weak acid strength should be more suitable for selective hydroisomerization catalysts.[357,402] Actually, increasing the acid site strength also enhances the intrinsic kinetics of the reaction. As a result, for a given zeolite structure, acid sites density and crystal size, the Thiele modulus increases (see section 3.3) and intracrystalline diffusion limitations can eventually be at stake. This would favor secondary reactions like cracking if the starting reactant is a linear olefin. Therefore, particular care must be taken when interpreting experimental isomerization selectivities in terms of intrinsic cracking and isomerization rates, as the extent of secondary reactions depends on the entanglement of kinetic and diffusion phenomena within the microporous network, as illustrated in **Figure 19**.

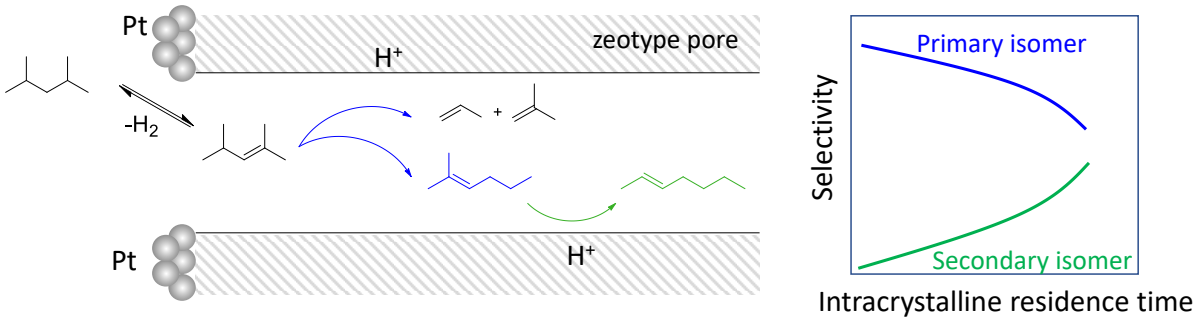

Figure 19. Interplay between kinetic and diffusion phenomena, illustrated for 2,4 dimethyl-pent-2-ene conversion. The primary products correspond to blue lines (isomerization and cracking) and secondary products to green line (secondary isomerization). Adapted with permission from ref [361] . Copyright 2018 American Chemical Society.

5.4. Oligomerization

The oligomerization of alkenes, especially short ones, is of practical interest for the production of liquid hydrocarbon fuels as well as petrochemicals like branched alkylbenzenes, oxo alcohols or alkylated phenols.[403] Short alkenes can be generated from conventional fossil resources but also from dehydration of alcohols produced through biomass fermentation.[404,405] Experimental studies of the oligomerization reaction over zeolites are tedious as side reactions like skeletal and double bond isomerization, cracking, cyclisation, and hydrogen transfer can take place. The formation of heavy oligomers and aromatics induces the deactivation of the catalyst by coking. The occurrence of side reactions expands the spectrum of products well beyond "true oligomers" (i.e. alkenes with a carbon chain number that is a multiple of the alkene reactant carbon chain number). This is illustrated in **Figure 20** for 1-butene oligomerization with the FER zeolite. Noticeably other products than alkenes can be observed, like alkanes, and traces of aromatics and cycloalkanes in this specific example. The term of "conjunct polymerization" has been coined by Pines [406] to describe the reactions at stake for the formation of these products, as opposed to the "true" oligomeric ones.

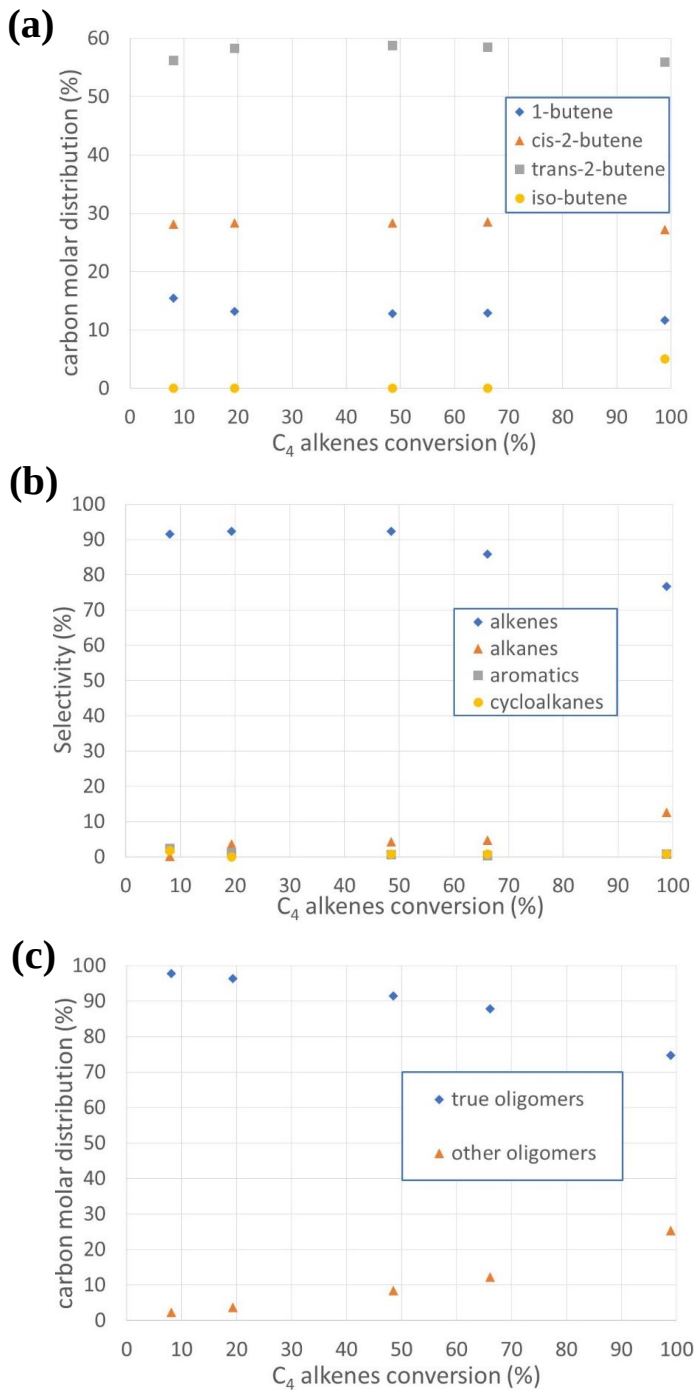

Figure 20. Products obtained during 1-butene oligomerization with FER zeolite, extracted from ref [407] . (a) C_4-alkenes distribution as a function of C_4-alkenes conversion: 1-butene is rapidly isomerized into cis-2 and trans-2 butene via double bond isomerization; (b) selectivity of products lumped according to their family as a function of C_4-alkenes conversion: H transfer reaction becomes apparent at high conversion; (c) oligomers distribution as a function of C_4-alkenes conversion: other oligomers are formed as apparent secondary products via side reaction (true oligomers cracking, oligomerization of cracked alkenes…). Reaction conditions: $P_{tot} = P_{1\text{-butene}} = 6.3$ MPa, T = 423 K, WHSV: 0.18-49.7 h^{-1}.

For a given zeolitic structure, operating conditions, especially temperature, markedly influence the extent of "conjunct polymerization". The latter is favored when the temperature is increased.[408,409] Neglecting the cyclisation and aromatization reactions, a reaction scheme for propene oligomerization is provided in **Figure 21** as an illustrative example.

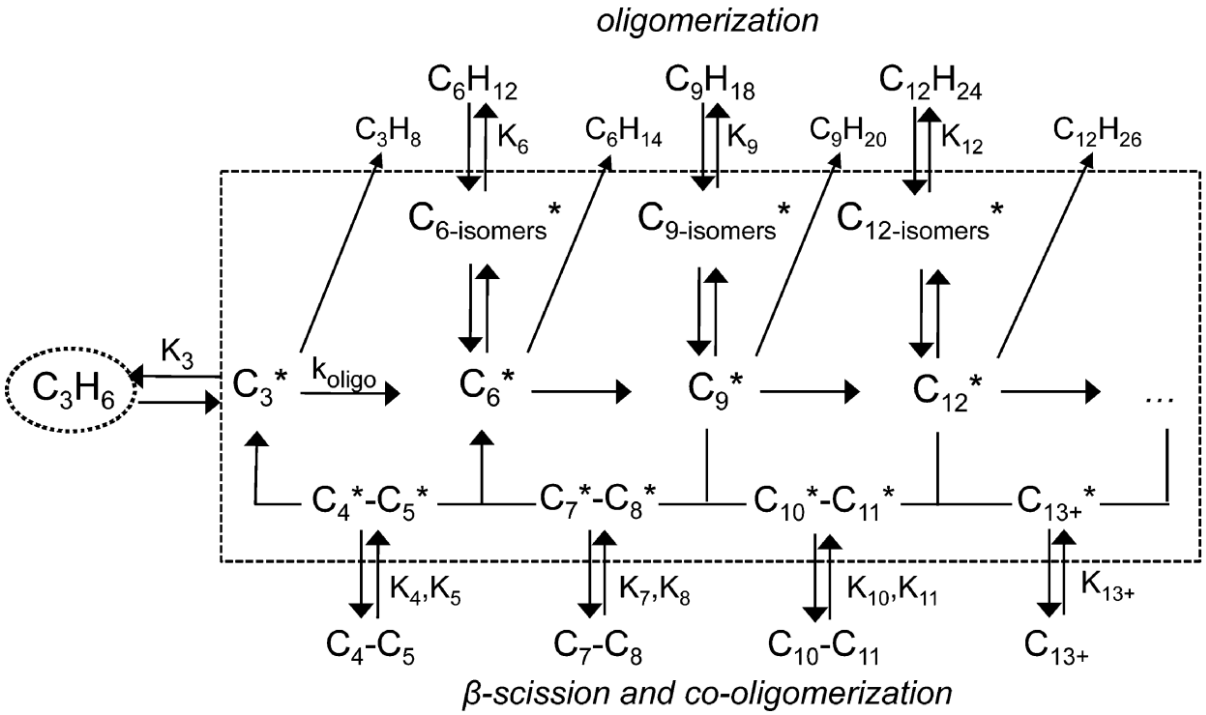

Figure 21. Propene oligomerization on solid acids. True oligomers (C_6H_{12}, C_9H_{18}, $C_{12}H_{24}$…) are formed by successive addition of propylene and other oligomers are formed by beta-scission of true oligomers and co-oligomerization of the cracked alkenes. C_n* stands for the alkoxide of n carbon in equilibrium with corresponding alkene in the gas phase via K_n. Reprinted with permission from ref [410]. Copyright 2016 American Chemical Society.

The products selectivities are markedly impacted by the microporous topology of the zeolite, as reported for example for ethylene,[411] propene[412] or 2-butene oligomerization.[413] The branching degree of the oligomerized products was found to decrease with the micropore diameter of the zeolite structure. Contribution of external surface acid sites can however significantly lower the shape selectivity effect of the microporous structure.[414,415] The true oligomers selectivity is also markedly impacted by the zeolite topology as illustrated in **Figure**

22-a for propene oligomerization. A geometric descriptor, coined as the "undulation parameter" **Ω**,[410] was found of relevance to rationalize the experimental selectivities (**Figure 22-b**). The undulation parameter is defined as follows:

$$\Omega = PLD / LCD \qquad \text{Eq. 5}$$

PLD and LCD are the pore limiting diameter (Å) and the largest cavity diameter (Å) of the zeolite framework, respectively. **Ω** is dimensionless and *not related* to the intrinsic size of the voids or channels of the framework. Frameworks with low **Ω** values exhibit low true oligomers selectivity for propene oligomerization as large oligomers can be formed in the largest cavities and must diffuse through smaller pores to eventually diffuse out of the structure. This imposes a diffusional restriction for such species and favor their consecutive beta-scission in smaller products. For **Ω** values close to unity, such restriction is not operative and higher true oligomers selectivities are obtained.

For a given micropore topology, mass transfer limitations of oligomers inside the microporosity could also be at stake[416] and affect the products selectivities by increasing consecutive reactions. [415,417–419] A diffusion parameter Ψ was introduced by Sarazen et coll.:[410]

$$\Psi = [H^+] * L^2 \qquad \text{Eq. 6}$$

where $[H^+]$ is the volumetric proton density (mol H^+ nm^{-3}) and L the zeolite crystal radius (nm). For a given reaction, micropore topology and Brønsted sites acid strength, Ψ can be considered as a surrogate of the Thiele modulus and can be calculated according to the physicochemical properties of the zeolite. Evolution of the true oligomers selectivity for a set of H-ZSM-5 zeolites with a large range of Ψ values evidenced the occurrence of secondary reactions enhanced by mass transfer limitations of the true oligomers inside the microporous network, i.e. cracking and co-oligomerization (**Figure 22-c**).

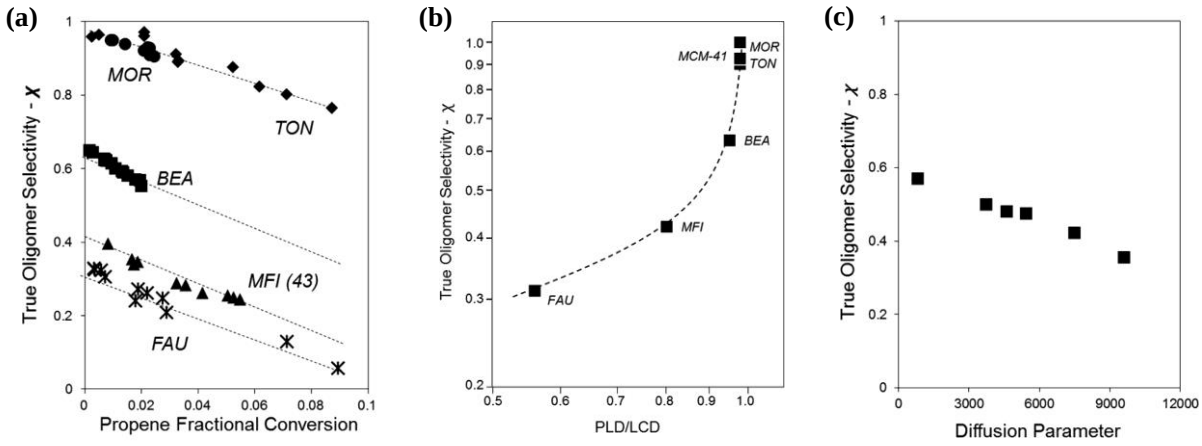

Figure 22. Propene oligomerization: evolution of the true oligomers selectivity as a function (a) of conversion for various zeolites, (b) of the undulating parameter Ω of various zeolites (propene fractional conversion range: 0.003-0.009), (c) of the diffusion parameter Ψ of various Al-MFI zeolites (propene fractional conversion range: 0.005-0.015). Reaction conditions: $P_{propene}$ = 0.058-0.060 MPa, T = 503 K. Reprinted with permission from ref [410]. Copyright 2016 American Chemical Society.

Provided that mass transfer limitations are not at stake, some discrepancies are observed in the literature about the impact of volumetric proton density on the turnover rate per Brønsted acid site. This may be related to the different methods used to evaluate the number of protons in the zeolitic materials (see section 3.3). For propene oligomerization over MFI zeolites it was reported that increasing proton density has no impact on the turnover rate.[420] Other studies reported that increasing proton density has a negative impact on the turnover rate.[421,422] This effect was ascribed to the negative impact of oligomers crowded in the microporous network. In addition to the averaged volumetric proton density, the local proton proximity was also found to have a spectacular impact on the turnover rate.[422] It was suggested that the desorption of the oligomeric species could be enhanced when two protons are at proximity compared to isolated protons.

Oligomerization is linked to carbenium ion chemistry and is the reverse of the beta-scission reaction previously described. Oligomerization reaction is exothermic and lowers the number of moles in the system. The reaction is favored at high reactant pressure and low temperatures (typically below 573 K, except for ethylene). As a result, the coverage of Brønsted

acid site with adsorbed species (π-bonded alkenes, alkoxides and/or carbocations) is close to unity during oligomerization reaction,[420,421,423,424] which is a major difference with the isomerization and cracking conditions discussed in sections 5.1 and 5.2 for bifunctional catalysts. The first step of the oligomerization reaction, i.e. dimerization, was investigated by DFT method for ethylene, propylene, 1-butene and trans-2-butene.[425] A cluster model was used for the zeolite. Two pathways were evaluated. In the "stepwise" pathway, a first alkene is adsorbed as an alkoxide on the cluster, and a second alkene is physisorbed. Then the alkoxide desorbs from the zeolite and a carbon-carbon is formed with the second alkene. Carbenium ion-like transition states are associated with the formation of the alkoxide (TS1) and of the carbon-carbon bond (TS2). Energetic barriers were found significantly higher for the second step whatever the reacting alkene. In the "concerted" pathway, a first alkene molecule is adsorbed on the acidic site via a π-complex and the second alkene molecule physisorbed in the vicinity. The mechanism features also a carbenium ion-like transition state. In a concerted way, the proton is partially transferred to one of the sp^2 carbon of the π-complex whereas the second sp^2 carbon is attacked by the π-electrons of the second alkene. The prevailing mechanism could not easily be determined, due to rather close energy barriers, and to the lack of quantification of free energies. The two mechanisms were also computationally investigated later for ethylene dimerization other FAU zeolite.[377] A hybrid model computed with the ONIOM method was used for the zeolite structure. In this study, for the "stepwise" pathway, the energetic barriers were found similar for TS1 and TS2. The "stepwise" pathway was proposed to prevail over the "concerted" pathway. Most often, with some exceptions,[378] the "stepwise" pathway is considered to prevail in the literature[420,421,426,427] but the chemisorbed intermediate can be an alkoxide or a carbocation, depending on the study (**Figure 23**). The nature of the chemisorbed intermediate (alkoxide or carbocation) should depend on the reactant and the zeolite structure. Recent ab initio and molecular dynamic simulations suggest that branched carbenium ions can

be stable species even at temperatures typical of the oligomerization reactions (i.e. below 570 K) in a CHA or MFI zeolite.[306,308] Notably, the entropic terms have only been scarcely evaluated for computed oligomerization reaction profiles, and never by AIMD, to the best of our knowledge. They are expected to play a significant role as the number of molecules varies along the profile.

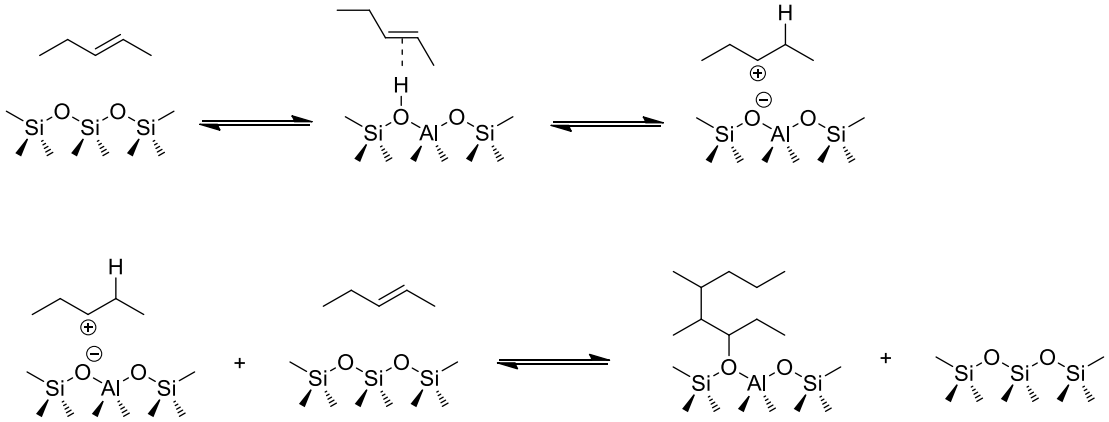

Figure 23. An illustration of the "stepwise" pathway, for 2-pentene dimerization over zeolite Brønsted acid site. Adapted from [426] . In this illustration the chemisorbed intermediate is a 3-pentenium carbocation.

Experimental results on propene dimerization showed the impact of the zeolite topology on the first order rate constant per proton.[420] The rate constant was found to dramatically increase when the void diameter of the structure decreased from 1.1 nm (FAU) to ca 0.6 nm (TON). This was ascribed to a better stabilization of the transition state by confinement thanks to more effective van der Waals interaction with the framework, as shown by the evolution of the dispersion component to the dimerization energy (referenced to an alkoxide plus a gas phase propene molecule) computed for TON, MFI, *BEA, FAU frameworks at the PBE-D3 level. A recent DFT study moreover suggest that the trans-2-butene dimerization is less favorable at the external surface than at the internal surface of zeolite Beta,[427] which is also probably a consequence on the lower confinement effect at the external surface. Increasing the acid strength of the site (expressed as the deprotonation energy) was also found to increase the first order rate constant per proton.[420] This was ascribed to a preferential stabilization of the

transition state compared to the alkoxide precursor as the stability of the conjugated anion increases.

Finally, very recently a new pathway was proposed for the dimerization of linear butenes and pentenes in H-ZSM-5.[428] Based on the comparison between experimental[426] and calculated[428] (by a QM/QM CCSD(T)/GGA approach) thermodynamic dimerization enthalpies at 323 K, alkenes are proposed to dimerize as cyclo-alkanes rather than longer alkenes at low temperature (**Figure 24**). These cycloalkanes would also explain why the infra-red signal of bridging OH groups perturbed by C=C bonds (π-complexes) decreases while increasing temperatures from ranges where the alkene reactant is adsorbed, to ranges where it is converted into dimers.[426,429,430] Formation of cyclic alkanes as primary products has not been reported to the best of our knowledge for butene oligomerization on H-ZSM-5 at higher temperatures, typically 473-523 K.[431–433] Further studies may be done to assess if the "cyclo-alkane" pathway is still favorable compared to the "branched alkene" pathway at 473-523 K, taking also into account the entropic contributions (i.e. calculation of Gibbs free energies) and free energy barriers. If the "cyclo-alkene" pathway is at stake under relevant temperature (473-523 K), the branched alkene dimers experimentally observed as reaction products must be obtained by hydride abstraction followed by ring opening via beta-scission of the cyclo-alkanes. At first sight, this looks unlikely as both the ring opening and the hydride abstraction steps are difficult, as mentioned in sections 5.2, 6.1 and 7.2, respectively.

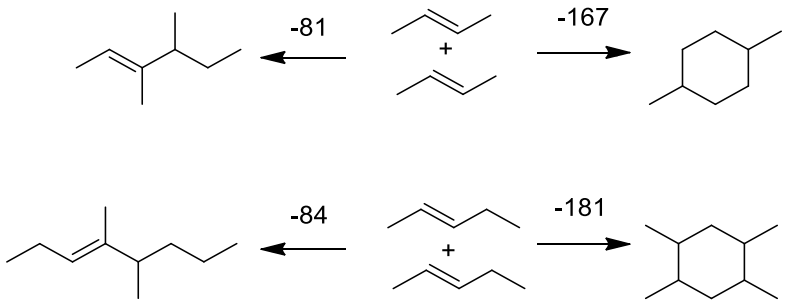

Figure 24. Dimerization of 2-butene and 2-pentene to produce a branched alkene or methyl-substituted cycloalkane, from [428]. The calculated heats of dimerization at 323 K are given in kJ.mol^{-1}.

5.5. The specific case of butene isomerization

Compared with longer alkenes, the skeletal isomerization of butenes is a most debated case,[48,434] as the traditional PCP mechanism would lead to the formation of highly improbable primary carbenium ions (**Figure 25-a**). Several kinds of alternatives have been proposed, some of them making use of all kinds of reactions detailed in the present section 5. Due to high selectivity in the n-butene to isobutene process, the Ferrierite zeolite has been much investigated.[435,436]

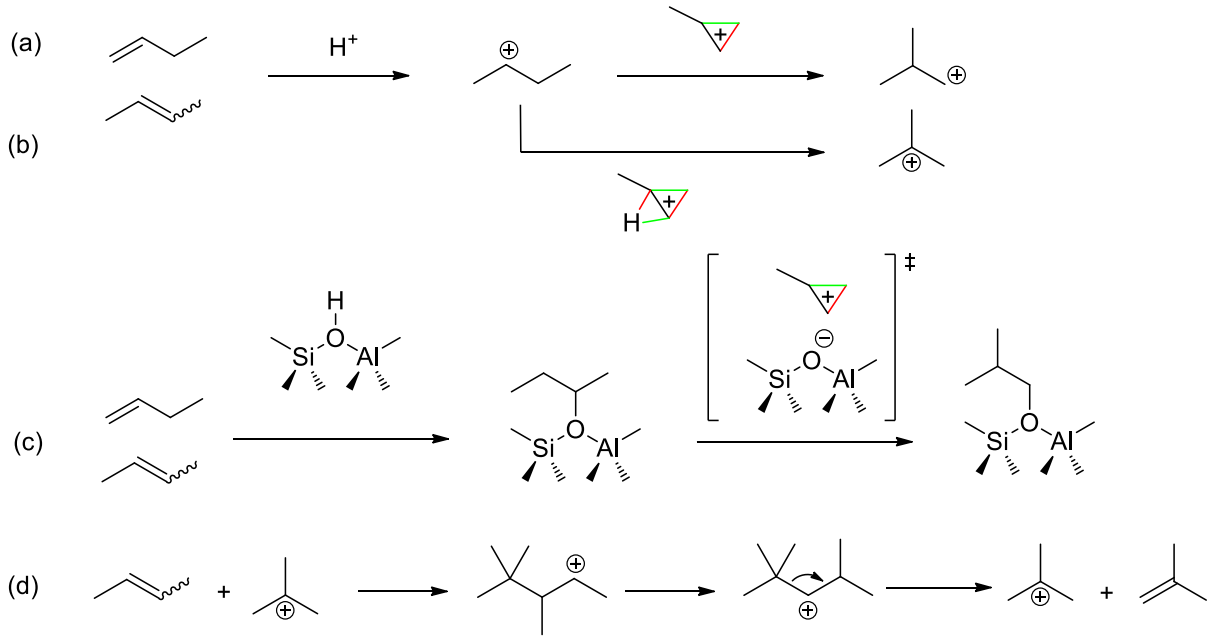

Figure 25. Possible butene isomerization mechanisms. (a) usual mechanism through carbenium and PCP, (b) variant with additional H migration to avoid primary cations, as computed in ref. [437], (c) alkoxide-based mechanism, computed in ref. [438,439], (d) bimolecular pathway, with autocatalytic role of isobutenium, as proposed in ref. [440,441].

A monomolecular reaction has been invoked,[435] that would be limited by isobutene desorption in Ferrierite.[442] Such a mechanism is likely to predominate (over bimolecular mechanisms, see next paragraph) at low pressure and high temperature.[435] Starting from n-butane and making use of a bifunctional Pt/H-Mordenite catalyst, Wulfers and Jentoft showed thanks to isotopic labelling that at low butene partial pressure, the mechanism is indeed

monomolecular.[443] Most DFT mechanistic studies on the topic address alkoxide-mediated mechanisms, that circumvent the problem of primary carbenium ions (**Figure 25-c**).[437–439,444–446] From linear butenes, a secondary 2-butoxide species is formed, before a PCP transition state re-opens into a primary isobutoxide. Gleeson invoked the formation of a secondary carbenium ion as a shallow energy minimum before the formation of 2-butoxide in a model of the Ferrierite zeolite.[437] In the same work, a carbenium-based mechanism was also invoked, that avoids the formation of a primary cation, thanks to a concomitant hydride-shift, yielding a tertiary carbenium (**Figure 25-b**). The transition state of this elementary step, however, is computed to exhibit a much higher free energy with respect to the PCP linking alkoxides. In computational studies, the rate limiting step was found to be either the formation of the PCP transition state (in generic cluster models, or cluster models of the ZSM-22, Ferrierite or ZSM-23 zeolites),[437–439,446] or the transformation of isobutoxide into isobutene (clusters representing Ferrierite and ZSM-48),[444,446] assumed in these two references to involve an energetically costly intramolecular H-shift. Although depending on the computing parameters (in particular, cluster size) and on the framework under considerations, the intrinsic barrier, found to vary between 100 and 150 kJ.mol^{-1}, appears to be roughly compatible with the data of Wulfers and Jentoft.[443]

Bimolecular mechanisms, involving the intermediacy of octenes, have also been proposed,[435,436,447] and substantiated by the use of ^{13}C-labeled butenes, although contradicting observations have been reported in terms of impact of time on stream on scrambling.[443,448–450] In such schemes, the first step is a dimerization reaction (see section 5.4), the octenes isomerize by a PCP mechanism (like mechanisms invoked in section 5.1) and undergo cracking (see section 5.2). An autocatalytic role of the tert-butyl carbenium ion was invoked, making it possible to form tri-branched C_8 dimers likely to crack directly according to a type A β-scission (**Figure 25-d**).[440,441] The obvious consequence of the possible occurrence of bimolecular mechanisms is the concomittant production of C_3 and C_5 compounds, indeed reported in many

works, and used a a tracer of bimolecular mechanisms.[435,447] ZSM-5 was shown to promote this mechanisms with respect to the monomolecular one, more stringly than Ferrierite and HPM-1, presumably to due larger pore size and suitable shape.[449] To the best of our knowledge, a single DFT theoretical work, published by Gleeson, addressed the competition between monomolecular and bimolecular mechanisms.[445] In this study, cis-2-butene is reacted with isobutene in a cluster model of Ferrierite (thus addressing the autocatalytic situation), through a carbenium-based mechanism (in this case, the alkoxide-based mechanism appeared less favourable). According to this study, the rate limiting step is the oligomerisation reaction, but the barrier or this step appears to be lower than the computed barrier of the monomolecular mechanims.

Finally, a pseudo-monomolecular mechanism was proposed, that implies the formation of benzylic carbocations (a kind of "active coke") presumably formed from linear butenes, trapped close to the external surface, holding a butyl chain that isomerizes and releases isobutene.[441,451] Such proposal is likely to be of relevance for aged catalysts, where a large part of the porosity is blocked by carbonaceous deposits. Coupling operando infra-red with gravimetry, it was indeed shown that the 8MR pores of Ferrierite are gradually blocked by carbonaceous deposits, whereas vacant sites are still present at the 10MR pores.[452] Together with STEM-EELS results, this led to propose that the active site of aged catalysts are located at the pore mouth of 10MR.[453] Post-treatment of Ferrierite samples have been proposed, such as desilication, to promote such mechanisms by creating new pore mouths.[454]

This last mechanism is more tentative in terms of nature of elementary steps. This, together with the absence of AIMD and high level of theory investigation of the competition between monomolecular and bimolecular pathways, makes the topic still open to many questions.

6. Monofunctional transformation of alkanes

The success of zeolites in catalysis is in a great part due to the enormous performance breakthrough that the use of zeolites has brought about in the fluid catalytic cracking (FCC) process.[56] It is, therefore, not surprising that a lot of research has been dedicated to understanding the paraffin cracking chemistry on zeolites. These reactions have been used right from the 60's to establish the concept of shape selectivity.[455] Cracking of alkanes can occur via two mechanisms:

- cracking via carbonium ions (Haag-Dessau mechanism),
- cracking via carbenium ions (also called the classical mechanism proceeding by beta-scission)

In spite of being an old topic, the carbenium/carbonium chemistry of cracking is still very relevant for understanding and explaining current research topics, like the production of sustainable aviation fuels from biosourced oils or the recycling of plastics. [456–459]

6.1. Carbonium ion cracking (Haag-Dessau mechanism)

6.1.1. General aspects

Although the carbenium ion cracking is certainly more relevant under practical conditions, the carbonium mechanism is detailed first because it is easier to explain and because it is probably involved in the initiation step of carbenium ion cracking mechanism. Moreover, many fundamental experimental and computational studies have been devoted to the investigation of the monomolecular Haag-Dessau mechanism.[460–463]

The mechanism of cracking of alkanes via carbonium ions was developed for superacids.[247] Haag and Dessau transposed this mechanism to solid acids, i.e. zeolites,[464] despite early contradictions in the favor of radical cation mechanisms,[465] that have not been

substantiated further. The Haag-Dessau mechanism assumes that the alkane is protonated (at the most highly substituted carbon atoms) by a strong Brønsted acid to form a 5-coordinated, positively charged carbon atom, a carbonium ion. Carbonium ions can be represented as three centers-two electrons bonds, with an additional hydrogen bridging a C-H or a C-C bond. Carbonium ions are very unstable and probably only exist as transition states or as shallow local energy minima, as mentioned above (section 4). Because of their instability, they decompose very quickly by breaking a bond involving the five-coordinated carbon atom (α-scission). The transposition of such a mechanism from the superacid media to zeolites was experimentally made based on the analysis of the cracking products of short alkanes at low conversion. Depending on whether a C-C bond or a C-H bond is broken, the carbonium ion leads to cracking or dehydrogenation, respectively.[466] This is illustrated in **Figure 26** for n-hexane cracking.

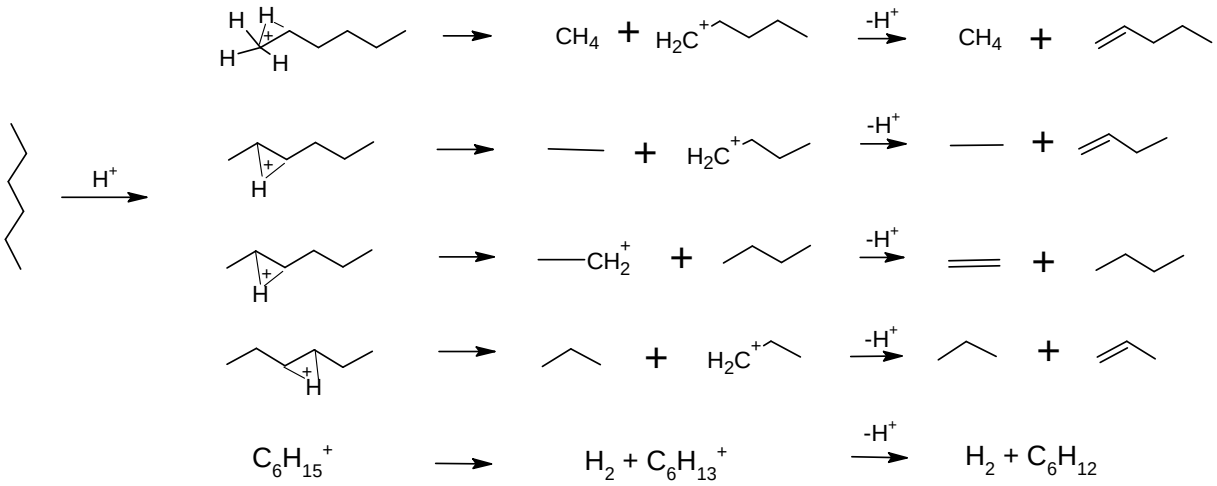

Figure 26. Scheme of carbonium ion cracking of n-hexane. We have chosen a representation where the C-C bond, which is broken, is protonated. The detailed mechanisms of protonation and bond-breaking will be discussed later in this section.

The formation of large amounts of CH_4 and C_2H_6 is a characteristic feature of carbonium ion cracking. [462] In the classical cracking mechanism that will be developed later in section 6.2, CH_4 and C_2H_6 are hardly formed because of the very low stability of the corresponding primary carbenium ions. Another characteristic feature is that equimolar amounts of paraffins and

olefins are produced, as expected from the stoichiometry of the cracking reaction. If long olefins are formed they may crack a second time, thus generating an excess of olefins in the products. Carbonium ion cracking is the dominating mechanism only under very specific conditions, i.e. at high temperatures and low pressures. In the literature it is sometimes called monomolecular cracking or protolytic cracking.

Narbeshuber et al. compared the product selectivities in the cracking of propane, n-butane, n-pentane and n-hexane.[467] **Table 3** shows that for n-alkanes, the breaking of a C-C bond is more probable than the breaking of a C-H bond (leading to dehydrogenation). However, the statement that cracking is preferred over dehydrogenation does not generally hold. Isobutane tends to prefer dehydrogenation to H_2 and isobutene vs. the cracking to CH_4 and propene.[19,468] This is because the dehydrogenation leads to a very stable tertiary tert-butyl carbenium ion.[469] *Vice versa*, in the cracking of neopentane, the formation of CH_4 generates a tert-butyl carbenium ion, which subsequently forms isobutene. Therefore, cracking to CH_4 and isobutene is the main reaction pathway for neopentane, while no dehydrogenation occurs.

Table 3. Selectivity to alkane cracking products in the Haag-Dessau cracking of propane, butane, n-pentane and n-hexane. Reaction rates were normalized to the formation of H_2. Deduced from data reported in ref. [467].

	Relative formation rate of cracking product				
Reactant	CH_4	C_2H_6	C_3H_8	C_4H_{10}	H_2
C_3H_8	1.83	-	-	-	1.00
C_4H_{10}	1.32	1.29	-	-	1.00
C_5H_{12}	0.76	1.70	0.59	-	1.00
C_6H_{14}	0.53	1.69	1.31	0.41	1.00

Concerning the ranking of activation energy (or enthalpy) between cracking and dehydrogenation, the literature reports contradicting results,[467,470–472] probably because the values depend on the properties of the zeolite and maybe also to experimental difficulties in determing precise dehydrogenation kinetics (carbonaceous deposits may be formed).[473–477]

Surprisingly (considering that the previously mentioned experimental difficulties should also impact the determination of activation entropies), a larger consensus however exists regarding a higher measured intrinsic activation entropy for dehydrogenation with respect to cracking.[467,470,472,478]

6.1.2. What theory says about C-C versus C-H breaking

The competition between C-C and C-H bond breaking at bridging OH groups was addressed in several computational studies. QM/MM simulations with the ωB97X-D functional for n-butane conversion in the MFI framework showed that dehydrogenation is more favorable in central positions of the chain, but the intrinsic barriers (at least 190 kJ.mol^{-1} in energy) are slightly higher than those of central C-C cracking (below 180 kJ.mol^{-1}).[479] Qualitatively, this trend is in agreement with previous studies using smaller and non-embedded cluster models, although the latter led to much higher barriers.[480–483] These trends were confirmed more recently for a variety of zeolites.[484] Intrinsic reaction coordinate (IRC) analysis show that dehydrogenation proceeds in a concerted way, involving protonation of the alkane, alkene and dihydrogen formation, and restitution of the proton to the framework.[479] Notably, the concerted nature of such an elementary step questions the initiation mechanism of the carbenium ion cracking mechanisms that will be discussed in section 6.2, that needs carbenium ions to be formed at some stage. Static calculations such as the one discussed in ref. [472] are, however, likely to underestimate the stability of primary and secondary carbenium ions. The transition state for dehydrogenation is a late one, dihydrogen being almost formed (**Figure 27**).[479] This late nature, conferring a loose nature to the transition state, explains why experimentally measured dehydrogenation activation entropies are positive.[470,472,478] This loose nature also explains why static DFT calculations tend to underestimate the positive activation entropy in particular for large pore zeolites.[484]

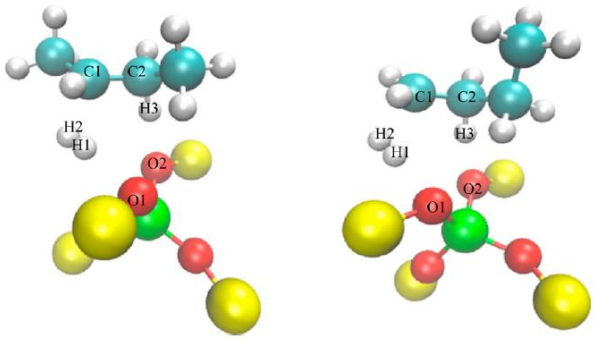

Figure 27. Transition state structure determined by QM/MM calculations for the dehydrogenation of n-butane at the T10 sites in H-ZSM-5 via a methylene group (CH_2, central dehydrogenation, left) or a methyl group (terminal dehydrogenation, right). Green: Al, Yellow: Si, Red: O, Blue: C, White: H. Reprinted with permission from ref. [479]. Copyright 2013 American Chemical Society.

Accounting for dynamic effects thanks to a transition path sampling approach, Bučko et al. also found in the case of n-propane dehydrogenation in Chabazite, that the dehydrogenation of the methylene group (at the center of the chain) is faster than that of the terminal methyl group,[483] which may be linked with the respective stability of the carbenium ions formed. This trend cannot be easily compared to experiments (for alkanes longer than C_3), as in alkane cracking conditions, alkenes very quickly isomerize in terms of C=C bond position. Notably, in the course of some trajectories, cyclopropyl cations were observed before the formation of the dehydrogenation product.[483] This observation could explain the ^{13}C scrambling observed thanks to NMR by Ivanova et al.[485] on H-ZSM-5. However, to the best of our knowledge, the quantification of the intrinsic activation entropy of dehydrogenation by AIMD is still lacking in the literature.

6.1.3. Protonation of C atoms or C-C bond before cracking

A significant amount of computational work has been devoted to elucidating the orientation of the approach of the proton on the alkane, to the definition of the structure of the carbonium ion itself, and to its definition as a transition state or a reaction intermediate. As mentioned in section 4, earlier studies performed on small clusters found carbonium ions as

transition states,[32,281,329,330] but more recent studies find a shallow local energy minimum for these species.[290,298,331–335]

The species found recently by Berger et al. in the case of propane cracking on various zeolites are shown in **Figure 28**.[335] In this work, the two types of protonation (terminal *versus* on the C-C bond) were compared, and an alternative concerted mechanism was also proposed. The energies, enthalpies and free energies of all intermediates and transition states were determined thanks to a hybrid simulation scheme, at the MP2/DFT+D2 level, with CCSD(T) corrections. The C-C bond protonation (via TS_{CC} in **Figure 28**) appears to be the less activated process in terms of energy, with an energy barrier of 184 ± 5 kJ.mol^{-1}, versus 195 ± 5 kJ.mol^{-1} for the terminal protonation (via TS_{term}) and 197 ± 5 kJ.mol^{-1} for the concerted mechanism. This is qualitatively in agreement with previous DFT reports, although energy barriers appeared to vary strongly from one study to another, as a consequence of the chosen active site model and level of theory.[479,481,486] These barriers close to 190 kJ.mol^{-1} are in very good accordance with recent experimental estimates.[474] However, entropy contributions lower the preference for the TS_{CC} pathway, which likely explains why Bučko et al.[487] find a preferred terminal protonation by AIMD (via a Transition Path Sampling approach), in the case of propane cracking in Chabazite. The reverse trend was, however, obtained by the same computational techniques in Mordenite.[96] With AIMD, dynamic effects are taken into account better than in ref. [335], thus entropic components are likely more accurate, but the level of theory (GGA *versus* MP2/DFT+D2+ ΔCCSD(T)) is lower. Thus, combining AIMD with higher levels of theory than GGA will be required in the future to completely solve this question, for which no experimental data exist.

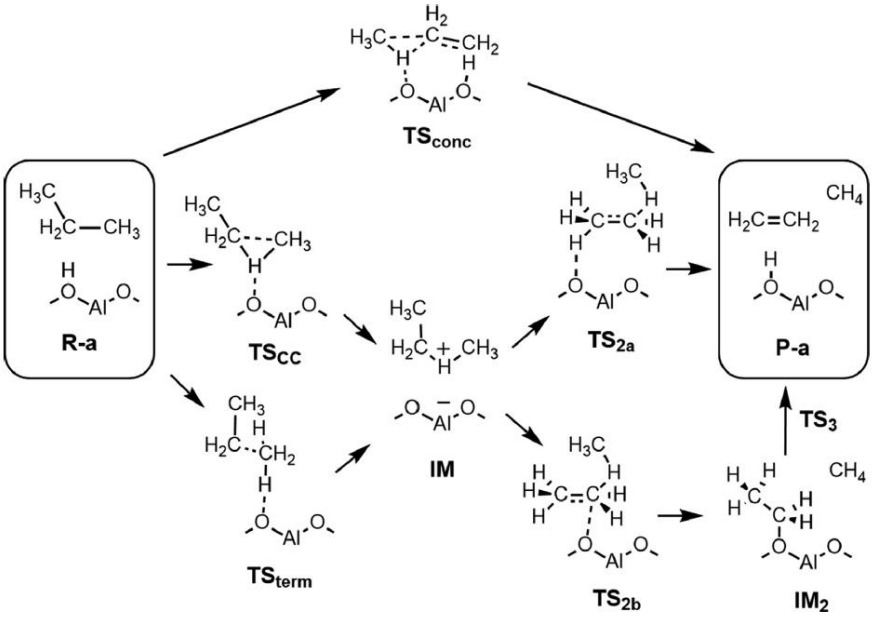

Figure 28. Steps of monomolecular propane cracking over a bridging OH group, following a C-C protonation (TS_{CC}) or protonation of a terminal C atom (TS_{term}), or concerted path (TS_{conc}). Reprinted with permission from ref [335]. Copyright 2021 Elsevier.

6.1.4. Internal versus terminal C-C bond cracking

Concerning the cracking selectivity, the product distribution reported in **Table 3** suggests that the cracking of internal C-C bonds (leading to C_2H_6 or C_3H_8) is favored over the cracking of terminal C-C bonds (leading to CH_4).[467] This is substantiated by lower (by 10 to 30 kJ.mol^{-1}) C-C breaking intrinsic barriers as computed by DFT for various alkanes and zeolites.[332,334,484,486,488] Notably, energy barriers are lower for central cracking but entropic terms compensate a portion of this effect, being in favor of terminal cracking.[19] The terminal cracking transition state indeed exhibits looser nature with respect to the central one, as already revealed by earlier DFT cluster calculations,[488] and confirmed by more recent and refined estimates.[484] However, by static calculations, the entropy loss at the transition state appears to be better estimated for central cracking than for terminal cracking with respect to experiments,[478] due to a more constrained nature of the central cracking TS.[484]

Note also that the fact that central cracking is favored is not completely general: in the case of n-butane cracking by 8MR sites of Mordenite, terminal cracking was suggested to be quicker than central cracking due to a partial access only of 8MR side pockets to the butane reactant.[470] Such rationale, based on the access of central/terminal bonds to the active sites, motivated a recent large scale computational Monte Carlo screening of zeolites and active site locations, to promote a bond-selective adsorption, analyzing both enthalpic and entropic components to the adsorption.[489] Optimal hypothetical zeolite structures could be found, that penalize terminal adsorption due to too small pore sizes, and favor central adsorption due to sufficiently large pore size.

6.1.5. Sizes of alkanes and alkenes products

The breaking of internal C-C bonds preferentially generates a short alkane and a long carbenium ion (which then desorbs as an olefin).[467] Narbeshuber et al. justified this observation with a supposedly higher entropy of the transition state, if a longer carbenium ion is formed. This question has not been deeply analyzed by quantum chemistry calculations, that have been focusing more on the very first steps of the reaction (protonation of the alkane to form the carbonium, known to be the rate determining step from isotope effects measurments[490]). Quasi-classical trajectory (QCT) calculations were undertaken in the case of n-hexane cracking in ZSM-5 and Y, that provides the correct trend with respect to experimental selectivities[491,492] (C_4H_8 and C_2H_6 being more abundant that C_4H_{10} and C_2H_4 at 773 K), but does not elucidate the origin of it.[334] A previous similar approach for pentene cracking in ZSM-5 failed in reproducing the experimental selectivities[467] in ethane versus propene, even if the QCT estimation was found more accurate than the static one.[332]

6.1.6. The role of adsorption and confinement

An important factor that contributes to the specificity of zeolites in the conversion of alkanes is the predominant role of adsorption (as already invoked in section 5.3). The strong adsorption of alkanes in zeolite micropores lowers the apparent activation energy of cracking and contributes to the high activity of zeolites. The seminal works of Narbeshuber et al.[467] and Babitz et al.[491], followed by others,[493–495] suggested that the activity differences of different zeolites (effect of the pore size) *versus* different n-alkanes (effect of the chain length) could be entirely explained by the differences in the adsorption enthalpy of the reactant on the zeolite catalyst: longer alkane chains are more reactive because of their more negative adsorption enthalpy[467] and small pore zeolites have higher TOFs because their stronger confinement leads to more negative adsorption enthalpies[491] (up to the limit where the pore size becomes too small to allow the alkane to fit in). The rationale was extended to amorphous silica-alumina, shown to exhibit similar intrinsic activation energy for propane cracking that ZSM-5, but much lower heat of adsorption.[496] The nature of the active sites on amorphous silica-alumina remains unclear, and the behavior of the surface sites depicted in **Figure 2-b** to **f** in alkane cracking has not been investigated.

However, more recent work has shown that these adsorption enthalpy arguments may not be sufficient to explain reactivity; in some cases, the adsorption entropy may be the decisive factor.[19,468,470,474,497,498] Gounder and Iglesia analyzed the rate of propane cracking (by carbonium ion cracking) on a series of Mordenite catalysts, where they varied the distribution of acid sites in the 12MR main channels and the 8MR side pockets by Na^+ exchange (Na^+ preferentially exchanges the acid sites in the 8MR side pockets, according to FTIR spectroscopy of the bridging OH groups).[470] By linear regression, they were able to determine the rate constants as well as the apparent activation energies of the acid sites in the 8MR side pockets and in the main channels. As expected from a simple pore size argument, the sites in the side

pockets had a higher site-specific activity. Dehydrogenation was not even detected in samples, which contain bridging OH groups only in the 12MR channel. However, propane does not perturb the 8MR OH groups at 323 K,[211] suggesting a low adsorption equilibrium constant with respect to 12MR sites. 8MR pockets also induce a higher apparent activation energy.[470] Thus, the high activity of the side pockets was not due to a more favorable adsorption in the side pockets, but rather to a less negative activation entropy. The authors explained this surprising result by the fact that propane was not fully confined in the side pocket, but protruded into the main channel, thus, leaving the adsorbed molecule with a high degree of freedom.

Later on, Bucko and Hafner offered an alternative explanation for the decrease in TOF, when H-Mordenite is Na-exchanged.[96] From AIMD calculations, they contradict the assignment of the 8MR as the most active sites, due to a free energy cost for propane moving from the main channel to the side pocket. The assignment of Gounder and Iglesia[470] is mainly based on the hypothesis that Na^+ preferentially occupies the side pocket, which is monitored by infra-red. This hypothesis is also contested by Bucko and Hafner, who claim that the assignment of the infra-red bands to OH groups in the 12MR and 8MR sites is not straightforward.[96] They argued that Na^+ cations were rather mobile at the reaction temperatures of cracking and, thus, not specifically located in the side pockets. In their view, the negative effect of Na^+ was not due to a selective removal of highly active sites in the side pockets, but due to the strong adsorption of the reactant on the Na^+ cations, which indirectly led to a lower coverage of the acid sites. We note that this hypothesis might explain the "poisoning" effect of Na^+ cations, which has been frequently observed in acid catalyzed reactions. [499]

Although the DFT results of Bucko and Hafner are not in line with the Gounder's interpretation, they also confirm the idea of a site specific reactivity (in the case of Mordenite in the main channels and the side pockets), which depends on the location of the acid sites in the zeolite pore structure. This contrast with the paradigm that all acid sites in a zeolite would

contribute equally to activity, based on the seminal work of Haag,[74] who showed that the turn over frequency of n-hexane cracking over (EFAl-free) ZSM-5 (probably under conditions where carbenium ion cracking prevails) was constant over a very wide range of Si/Al ratios.[500] Indeed, more recent work has corrected that picture and shown that TOFs of different ZSM-5 samples in alkane cracking can vary up to a factor of 8.[470,472] This was attributed to the fact that increasing Al content also increased the fraction of acid sites in the channel intersections, providing an advantage in terms of activation entropy. DFT calculations undertaken so far do not confirm the preferred activation entropy at intersection sites,[335] but the determination of this term is tricky. Slight differences between channel and intersection sites in activation energies were reported in previous DFT studies,[479] but not systematically confirmed.[335] Recently, the proximity between framework sites was observed as a source of enhancement of protolytic cracking and dehydrogenation activity in CHA and MFI,[501,502] which was assigned to a higher activation entropy at paired sites than at isolated sites, likely due to a later transition state. Finally, recent ^{27}Al NMR works suggest that an Al species partially dislodged from the framework could be related to higher catalytic activity in n-hexane cracking in ZSM-5, with respect to other kinds of Brønsted acid sites.[503] Thus, even if the precise environments are not always understood, and the origins of the effects not clearly known, site specific reactivity is more and more documented.

For a detailed analysis of turn over frequencies in alkane cracking, the rate constants normalized by the number of acid sites are decomposed into the contribution of adsorption enthalpy and entropy as well as of activation energy (or enthalpy) and entropy, as outlined in Eq 3. As mentioned above, differences in the apparent rate constants were often successfully explained by differences in the adsorption enthalpy term. However, one must keep in mind that the adsorption enthalpy describes the temperature dependence of the adsorption constant K_{ads}. An adsorbate/adsorbent system with a strongly negative adsorption enthalpy usually has a very

high adsorption constant at low temperature, but the value of K_{ads} quickly decreases as the temperature rises. As nicely illustrated by **Figure 29** for various n-alkanes adsorbed in ZSM-5, there is a temperature where a cross-over occurs between the adsorption constant of the high enthalpy adsorbent-adsorbate couple and the low enthalpy adsorbent-adsorbate couple.[474] At the temperatures, where carbonium ion cracking is carried out, we are close to this cross-over temperature. Hence, the adsorption constants of the low and the high enthalpy systems become similar[478] and it becomes difficult to establish a reliable ranking of the K_{ads} values under reaction conditions, especially if the K_{ads} values under reaction conditions are extrapolated from room temperature measurements. For reliable interpretations of the role of adsorption, it is, therefore, very important to measure (or calculate) adsorption parameters under or close to reaction conditions, as done in several recent computational Monte Carlo investigations.[478,504,505]

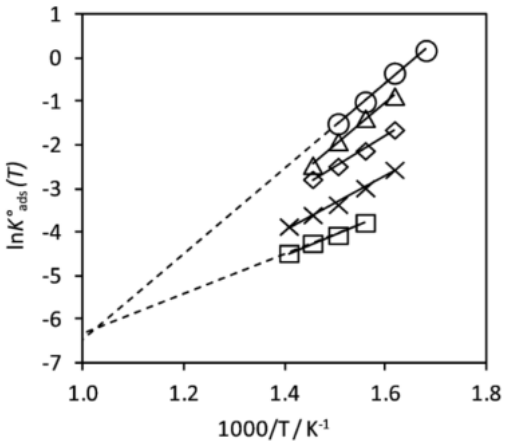

Figure 29. van't Hoff plots of alkane adsorption constants on H-ZSM-5 measured by IR spectroscopy: propane (□), butane (x), pentane (◊), hexane (Δ), heptane (°). Reprinted with permission from ref [474]. Copyright 2016 American Chemical Society.

The decomposition of adsorption/intrinsic reaction contributions and enthalpic/entropic components in the apparent cracking rate equation has motivated a set of works combining experimental and theoretical approaches. Following the rationale presented in ref. [486,504], Janda and coworkers have proposed an evaluation of the adsorption parameters at the Brønsted acid

sites, and at reaction temperatures by Monte Carlo calculations, first for various alkanes (propane to n-hexane) in ZSM-5,[505] then in the case of n-butane cracking for a variety of zeolites.[478] Notably, computing accurate adsorption (free) energies for alkanes in proton-exchanged zeolites is still a current challenge.[506–512] Janda et al. used a forcefield approach, some parameters being fitted by comparison with experiments.[478] The intrinsic reaction parameters were determined in a second step, by subtracting experimental apparent kinetic parameters and computed adsorption parameters. In the end, according to Janda et al.,[478,505] intrinsic kinetic parameters determined by this method depend on the alkane size and on the zeolite framework. Terminal cracking and dehydrogenation of butane behave differently with respect to central cracking in terms of dependency to confinement.[478] In the case of central cracking, both the intrinsic activation enthalpy and entropy decreased when decreasing confinement, which was assigned to a rather early transition state, more constrained than the reactant as confinement decreases. Terminal cracking and dehydrogenation intrinsic activation enthalpy and entropy increase by decreasing confinement, which was assigned to a late transition state, much looser than for terminal cracking (as shown by positive activation entropies), and much looser for large cavities. The dependence of intrinsic activation enthalpy on confinement discussed by the authors is inconsistent with previous reports (see above). Janda et al. assign this inconsistency to the need of considering adsorption parameters at the Brønsted acid sites only, as done in their Monte Carlo approach, and not within the whole zeolite, as done in traditional adsorption measurements. One should note, however, that similar variations in intrinsic activation enthalpy have been qualified as constant or not constant, from one set of work to the other.[513]

More recently, a similar decomposition exercise was undertaken by Travers and co-workers following a fully experimental approach.[474,497] They developed an operando IR system, which allowed them to monitor the alkane coverage of the acid sites at temperatures of around

673 K, while at the same time recording the cracking rates (from propane to n-heptane) on MFI, CHA, FER and TON zeolites. From the temperature dependence of the coverage, they could deduce the adsorption enthalpy and then calculate the adsorption entropy, specifically at the Brønsted acid site, and not in the whole zeolite, which, in line with Janda et al.,[478] appeared to be crucial for a correct decomposition. The temperature dependence of the rate constant yielded the apparent activation energy. They could, thus, evaluate the contribution of all four factors in Eq. 3. The result for various alkanes in MFI is shown in the waterfall plot in **Figure 30**.[474] Similar plots are reported as a function of the zeolite structure in the case of propane and butane cracking in ref. [497]. At the reaction temperatures used in the study, the adsorption constants of n-alkanes still slightly increased with chain length, but this increase could not fully explain the increase in the rate constants. Since the intrinsic activation energy was the same for all alkanes, the increase in the rate constants was attributed to a more favorable activation entropy for the longer alkanes.[474] This may be related to the fact that longer chains offer more possibilities for breaking the carbon chain at central positions, which is preferred in terms of selectivity. Gounder and Iglesia suggest a gain of one-dimensional rotation degree of freedom at the cracking transition state to be at the origin of this chain length dependance of the activation entropy.[19] From one framework to another, the more favorable activation entropy was recorded for smaller pore zeolites (FER, TON)[497] which, according to the adsorption entropy measurements, can be assigned to entropy variations of the reactant (and not of the transition state). The reactant is more constrained in small pores, as constraint (if not more) than the transition state, whereas for larger cavities (MFI and CHA in [497]), the reactant state is much looser than the TS, leading to negative activation entropies. The case of MOR is not included in the series; in that zeolite more subtle effects come into play as previously discussed.

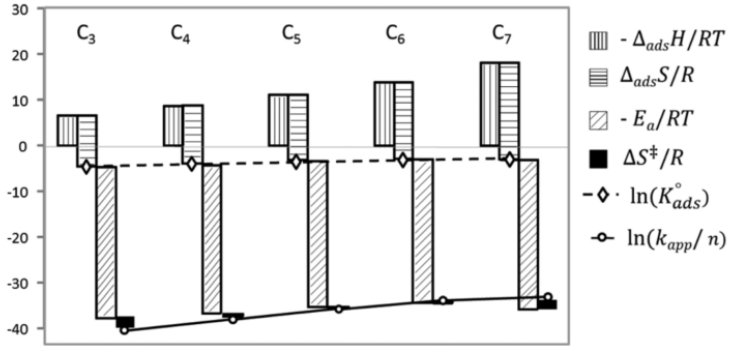

Figure 30. Decomposition of the measured rate constants of alkane cracking over H-ZSM-5 into the contributions of adsorption enthalpy and entropy (and the resulting adsorption constant K_{ads}) and of the intrinsic activation energy and activation entropy. Reprinted with permission from ref [474]. Copyright 2016 American Chemical Society.

Thus, depending on the approach chosen (coupling adsorption measurements at low temperature with apparent kinetics, coupling Monte Carlo adsorption simulations with experiments, or operando measurements of both adsorption and kinetic parameters), different conclusions are obtained with respect to the confinement effect on intrinsic activation enthalpy, showing the high sensitivity of adsorption and kinetic data to the various experimental parameters. In these conditions, from the theory side, using high level approaches is more than ever required. De Moor et al quantified adsorption enthalpies and entropies of ethane to n-octane in FAU, *BEA, MOR and MFI frameworks, using a hybrid MP2/Forcefield QM/MM approach.[511] Getting accurate adsorption free energies required to adopt correction factors for FAU, and to assume given numbers of free rotation and translations of alkanes in the cavities. Within such assumptions however, the identification of the relevant kinetic parameter (activation entropy) impacted by confinement, agrees well with the conclusions of Travert et al.[474,514] Regarding activation enthalpies, Berger et al.[335] recently revisited the case of propane cracking, on the same series of zeolites (FER, MFI, CHA, FAU) as the one considered by Travert et al.[474,497] Computed[335] and experimental enthalpic data compare reasonably well, provided a hybrid simulation scheme, at the MP2/DFT+D2 level, with CCSD(T) corrections is employed (PBE+D2 results in higher differences), as illustrated in **Figure 31**. Over the series

of zeolites considered, the intrinsic activation barrier is observed not to vary much (less than 10 kJ.mol^{-1}). In a more recent study, the hybrid ωB97X-D functional also appeared to perform reasonably well for adsorption and activation enthalpy terms.[515] Regarding activation entropy components, as mentioned previously, much more remains to be done, combining AIMD with high levels of theory. This will be highly useful to fully decipher the respective roles of enthalpy and entropy in protolytic cracking, after decades of continuous efforts.

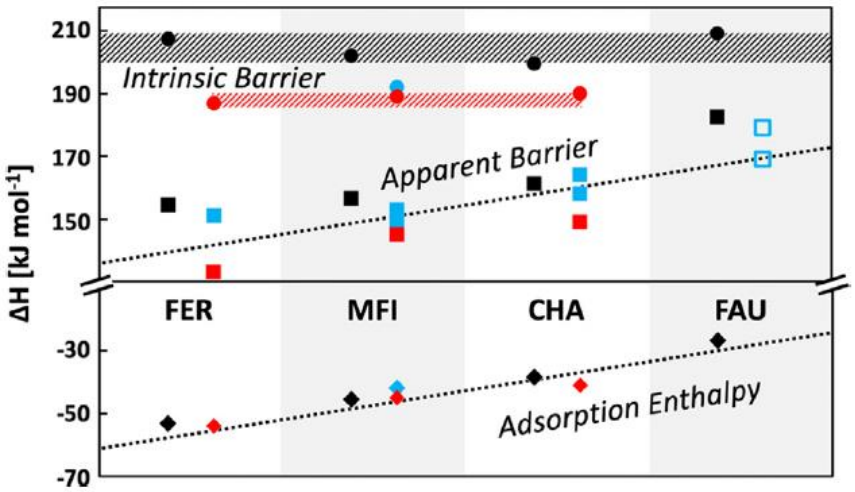

Figure 31. Comparison of propane adsorption enthalpies (diamonds), apparent (squares) and intrinsic (circles) propane cracking enthalpy barriers (black symbols and lines) of computed at 773 K (MP2, corrected at the coupled cluster level, ref. [335]) and experimental results (blue symbols) (refs. [208,211,467,470,507,514,516–520]). Experimental results from the IR operando study of Kadam et al.[497] are shown as red symbols. Reprinted with permission from ref. [335] Copyright 2021 Elsevier.

6.2. Carbenium ion cracking

6.2.1. Deviation from the selectivity pattern predicted by the Haag-Dessau mechanism

The cracking of n-hexane at lower temperatures leads to a very different product pattern than the one illustrated above. **Figure 32** compares the selectivity to cracking products obtained under conditions where carbonium ion cracking is favored (ZSM-5, 773 K[467]) with data obtained with large pore zeolites at lower temperatures.[521] In the latter case, the main cracking

products are propane and iso-butane, while very little propene, n-butene or ethane is formed. The paraffin to olefin ratio is much higher than one, although the stoichiometry of cracking imposes that equal amounts of paraffins and olefins should be formed. Moreover, pentanes (without concomitant formation of methane) and isobutane are produced. As illustrated in **Figure 33**, these products cannot originate from a direct cracking of n-hexane; it must be preceded by isomerization and oligomerization reactions.

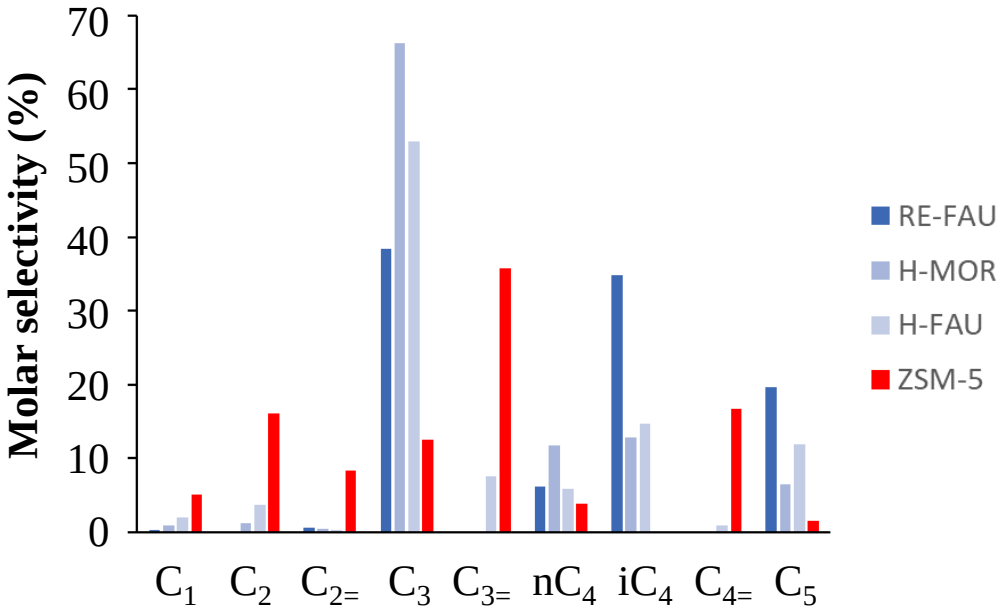

Figure 32. Molar selectivity to cracking products in the cracking of n-hexane. The Figure compares data by Miale et al.,[521] obtained with large pore zeolites at fairly low temperatures (RE FAU = Rare Earth Faujasite and H-MOR at 589 K, H-FAU at 644 K) and by Narbeshuber et al.,[467] obtained at 773 K with H-ZSM-5.

The product distribution can be qualitatively explained by the rules of carbenium ion chemistry, which were established by seminal work in the 1940s.[365] These rules, already mentioned in section 5.2, are based on the simple principle that reactions involving unstable carbenium ions (tertiary carbenium ions being the most stable, primary carbenium ions the least stable) will have a higher activation energy and will, therefore, be slow.

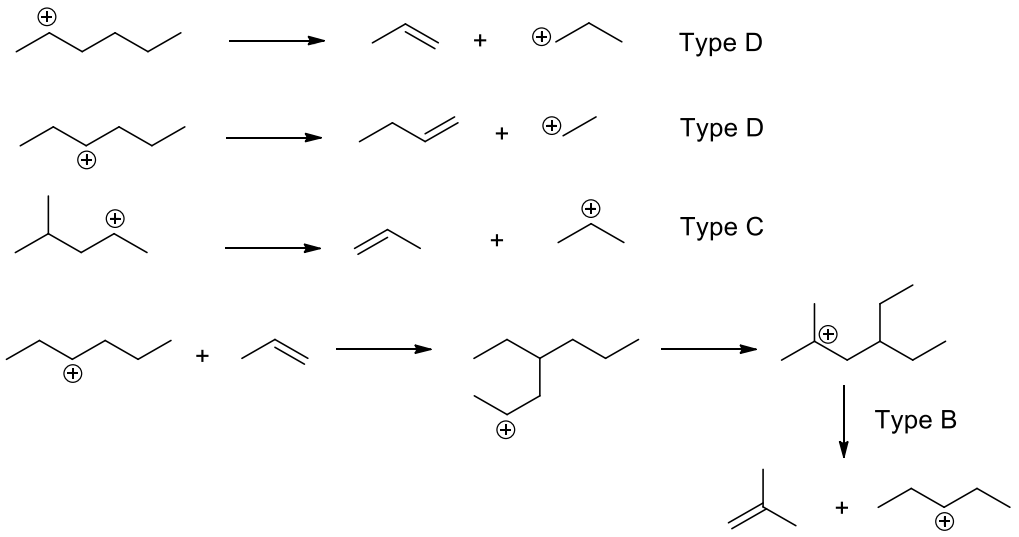

Figure 33. Possible cracking pathways of a C_6 carbenium ion.

For example, a linear alkane like n-hexane can form a secondary carbenium ion (we will discuss this initiation step in section 6.2.2), which can crack into an olefin and a primary carbenium ion. This D-type cracking is possible but occurs very slowly. If the carbenium ion isomerizes to a methyl-branched species, C-type cracking to a secondary C_3 carbenium ion becomes possible, which is a lot more favorable than D-type cracking. This explains the high selectivity to C_3 in the carbenium ion cracking of n-hexane. To explain the formation of isobutane and of C_5 species, alkylation reactions must be invoked. Carbenium ions can react with olefins (produced by initiation steps, vide infra, or from parallel cracking reactions), to produce larger carbenium ions. For example, the C_6 carbenium ion can react with the cracking product $C_3^=$ to form a branched C_9 carbenium ion, which can then readily crack to isobutane and C_5. Alternatively, the C_6 carbenium ion can dimerize by reacting with a $C_6^=$ olefin created by dehydrogenation to a C_{12} carbenium ion, which will also very readily crack into smaller fragments. Abbot and Wojciechowski[522] showed that compounds larger than C_6 are never found in the product of the alkylation/cracking route, because the long carbenium ions very readily crack to C_3, C_4 or C_5. This can be easily understood since from C_7 onwards, the carbenium ions

may isomerize to di-branched species, which can then very favorably crack according to a type B beta-scission (**Table 2**). It is also striking that the products of the alkylation/cracking routes appear as primary products of cracking, although they are secondary products from a mechanistic point of view. At extremely low conversions it is indeed possible to detect the products of the dimerization as the primary reaction products, but they disappear already at 2% conversion. [523] That means that the dimerization/cracking route is extremely fast, compared to the diffusion of the primary cracking products out of the zeolite pores (see the discussion in section 5.3).

6.2.2. The initiation step of carbenium ion cracking

We have not yet discussed the initiation step of carbenium ion cracking, i.e. the question of how carbenium ions are formed from the reactant paraffin. Several initiation mechanisms have been proposed:[524]

- Protonation of the alkane to a carbonium ion followed by cracking or dehydrogenation (**Figure 26**), with mechanisms detailed in section 6.1. ^{13}C NMR scrambling results are indeed compatible with such an initiation route. [485]
- Abstraction of a hydride ion by a Lewis acid site.
- Thermal dehydrogenation or cracking to olefins.

It is now generally accepted that the "Haag-Dessau" pathway via carbonium ions contributes to the initiation step of carbenium ion cracking. However, the hydride abstraction by Lewis acid sites may also play a role. It may notably explain the beneficial role of Lewis acid sites on the TOF of cracking, which was frequently observed.[475,525–527] Section 6.4 is dedicated to the role of EFAls in that respect. The thermal mechanism is of minor importance at moderate temperatures, but probably plays an important role in the industrial FCC process, which operates at very high temperatures. Note that all the above-mentioned initiation mechanisms

formally correspond to a dehydrogenation of the paraffin to an olefin, followed by its protonation on an acid site.

6.2.3. The propagation of the carbenium ion cracking cycle: hydride transfer steps

Cracking of a carbenium ion, formed by one of the initiation mechanisms mentioned above, leads to an olefin and a smaller carbenium ion, which should *in fine* desorb as olefin, thereby regenerating the acid site. [6] However, under the conditions of carbenium ion cracking, the carbenium ion produced by cracking undergoes a hydride transfer reaction with the reactant paraffin. The cracked carbenium ion desorbs as a paraffin and a new carbenium ion of the reactant is created. This closes the catalytic cycle. Since the cycle involves a bimolecular hydride transfer step, it is frequently described as bimolecular cracking, as opposed to monomolecular cracking for the Haag-Dessau mechanism.

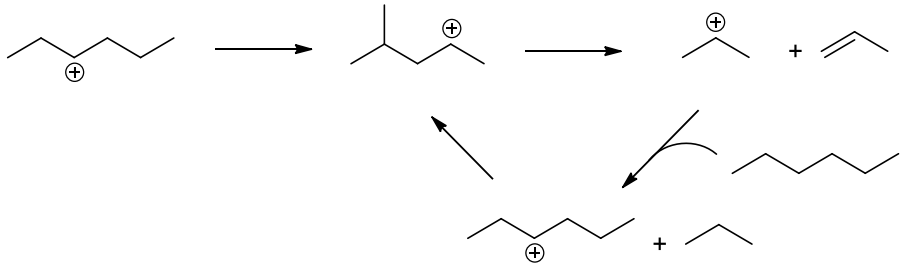

Figure 34. Propagation cycle of carbenium ion cracking.

The net reaction of the cycle in **Figure 34** is $C_6H_{14} \rightarrow C_3H_8 + C_3H_6$.

From computational investigations, hydride transfer between a carbenium ion (or a related alkoxide species) and an alkane molecule was described to proceed via a carbonium shared-hydride intermediate (**Figure 35**),[331,528–531] whose formation is the rate limiting step (non-activated dissociation). The energy barrier from the {alkene, alkane} pair for C_2 and C_3 species has been computed to be between 150 and 170 kJ.mol^{-1} (depending on the level of theory) on the basis of calculations done on small clusters.[331,532] Starting from alkoxides instead

of alkenes, the computed barriers are much higher.[329] More recent computational results show that increasing the degree of branching of the alkene/alkane partners decreases strongly the barriers, and so does the consideration of a periodic model of the zeolite catalyst (Mordenite, in that case), and the inclusion of dispersion corrections, bridging the activation barriers starting from alkoxides below 90 kJ.mol^{-1} when the H-donating species is isobutane for example. [528] This is in line with the experimental observation that isobutene is a much better hydride transfer agents than butene. [533] In Faujasite, considering carbenium ions as the starting point, hydride transfer was computed to be aided by the co-adsorption of an additional olefin molecule, that forms a C-C bond with the carbenium ion formed after hydride transfer.[534] Finally, the formation of the shared-hydride intermediate was computed to be impossible at the external surface of zeolite Beta, even in the neighborhood of bridging OH groups, with was assigned to the lack of confinement effect.[427]

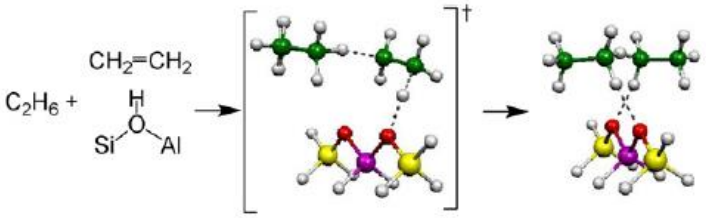

Figure 35. Transition state (center) and shared-hydride intermediate for the hydride transfer reaction between ethane and ethylene. Reprinted with permission from ref. [298] Copyright 2008 Elsevier.

The hydride transfer cycle stops when the cracked carbenium ion desorbs as an olefin instead of undergoing a H-transfer reaction with a feed molecule. In that case, a new initiation step is required to start a new cycle. Shertudke and Hall[535] have tried to estimate the number of propagation cycles before a termination step, by calculating the ratio of the carbenium ion cracking rate to the rate of initiation steps (via the Haag Dessau mechanism). For evaluating the initiation steps, they used the sum of H_2, CH_4 and C_2H_6; for the propagation steps the sum of C_3 to C_5 paraffins (the reactants were isobutane or n-pentane); for the termination steps the

sum of C_2 to C_5 olefins. These hypotheses are questionable, since on the one hand, olefins are also produced in the propagation cycle and on the other hand, they may be consumed by hydrogen transfer reactions forming coke and paraffins (vide infra). Nevertheless, one can assume that the order of magnitude of the estimation should be correct: depending on the system, each initiation step could be followed by up to 15 hydride transfer cycles.[536]

It is a very common feature of carbenium ion cracking that the ratio of paraffins to olefins in the products very often largely exceeds 1,[521,537] i.e. it does not follow the formal stoichiometry of paraffin cracking, which predicts the formation of equal amounts of paraffins and olefins. This is attributed to hydrogen transfer reaction of olefins, which disproportionate into paraffins and aromatics (and in fine coke).[536,538] The importance of these hydrogen transfer reaction, which increase the fraction of paraffins in the products quickly increases with increasing conversion.[539]

6.3. Carbonium *versus* carbenium ion cracking

Carbonium ion cracking and carbenium ion cracking may occur in parallel. At *minima,* carbonium ion cracking (or dehydrogenation) is considered as the initiation step for carbenium ion cracking via a hydride transfer propagation chain. If we assume that each carbonium ion cracking event initiates a carbenium ion cracking cycle, estimating the relative contribution of the two mechanisms comes down to determining the chain length of the propagation cycle by hydride transfer. Pure carbonium ion cracking occurs when the chain length is zero. It is very difficult to estimate the relative contribution of the two mechanisms precisely,[524] since major products like propene may arise from both mechanisms. However, it is possible to describe some qualitative trends, by looking at the yield of products which can only arise from one or the other mechanism. Wielers et al. argued[537] that C_1, C_2 and $C_2^=$ would be exclusively formed by the carbonium ion mechanism; in carbenium ion chemistry, the formation of these products

is very unfavorable. On the other hand, the formation of isobutane from n-paraffins is only possible, if the cracking was preceded by isomerization and/or dimerization steps, i.e. carbenium ion chemistry. Isobutane was, therefore, considered as a marker of the carbenium ion cracking route.

Wielers et al. showed that the C_1 and C_2 selectivities sharply increased with temperature, while that of i-C_4 decreases. In other words, at high temperatures the monomolecular carbonium ion cracking mechanism becomes dominating. This is not surprising, since the carbenium ion chain mechanism must be strongly related to the stability of the carbenium ion on the acid site, which decreases with temperature (increasing temperature favors the desorption as olefins). It was then further showed that the zeolite topology had a major impact of the relative contribution of the two mechanisms. Small pore zeolites like Ferrierite favor the monomolecular cracking route while large pore zeolites like Mordenite of Faujasite mainly favor the bimolecular route.[537,540] Again, this makes sense since the hydride transfer step is sterically demanding and requires larger pore sizes, as confirmed by DFT calculations.[529] Finally, the Si/Al ratio of the zeolite also plays an important role. The (C_1+C_2)/i-C_4 ratio increases with decreasing Al content, suggesting that the bimolecular route needs adjacent Al sites (the order in Al sites is 2 at low temperatures and changes to 1 as the temperature increases, i.e. as the monomolecular mechanism gains in importance).[537,540] It was argued, however, that the 2nd order in Al content is not directly related to the adjacency of sites, but an indirect consequence of the impact of Al on the adsorption properties of the zeolite.[541]

Miyaji et al. [500] went further than the qualitative analysis of Wielers and established a detailed reaction scheme of the cracking of n-pentane, which takes the contributions of carbonium ion cracking and of carbenium ion cracking (after hydride transfer) into account. For ZSM-5 the distribution of reaction products was in accordance with this reaction scheme up to a conversion of 30%; above that conversion a significant amount of aromatics was formed by

hydrogen transfer reactions, which had not been considered in the reaction scheme. The authors were, thus, able to precisely calculate the contribution of monomolecular and bimolecular cracking to the overall conversion. At the conditions used by the authors (high temperature and low pressure), monomolecular cracking was largely dominating, but when increasing the pressure, the bimolecular mechanism strongly gained in importance.

A kinetic analysis of a reaction scheme comprising direct protolytic cracking as well as a hydride transfer propagation cycle [500] shows that the reactant (nP) conversion is the sum of two terms mentioned in Eq. 7.

$$-\frac{d[nP]}{dt} = k_1[nP][H^+] + \frac{k_2 k_1}{k_3}[nP]^2[H^+] \qquad \text{Eq. 7}$$

k_1 is the rate constant of the carbonium ion cracking (or dehydrogenation) step, which is at the same time the initiation step of the hydride transfer propagation cycle, k_2 is the rate constant of the hydride transfer step and k_3 the rate of the termination step (i.e. the desorption of the carbenium ion as an olefin). The first term in Eq. 7 corresponds to the carbonium ion cracking and is first order in the reactant, while the second one represents the hydride transfer cycle and is second order in reactant.[466] Both are first order in the acid site concentration (but as mentioned above, one can envision that the acid site concentration has an indirect effect on the paraffin concentration in the pores by increasing its adsorption)

Regarding confinement effects, under conditions where both monomolecular and bimolecular cracking are possible, significant differences in the product selectivities of small and large pore zeolites are observed.[500,537,542] In small pore zeolites, formation of dimerization products is impossible, so the cracking proceeds mainly via the monomolecular Haag-Dessau mechanism. The selectivity to products issued from a hydride transfer propagation cycle or from dimerization/cracking is generally higher for large pore zeolites. The competition between monomolecular cracking and dimerization/cracking also exists in the cracking of short alkenes.

Again, small pore zeolites favor monomolecular cracking, while large pore zeolites favor dimerization/cracking, thus leading to different product distributions. Baba and co-workers tried to rationalize these activity and selectivity trends by considering the cavity volume of the pore systems and its fit with respect to the volume of the key carbenium ion intermediates.[523,543]

6.4. Roles of EFAls, synergy between Brønsted and Lewis acid sites

The seminal work of Lago et al.[526] showed that mildly steamed ZSM-5 zeolites had a higher turn-over frequency in n-hexane cracking than unsteamed zeolites. This activity increase was attributed to the presence of EFAl species in the zeolite. Such observation has been confirmed many times afterwards, for a variety of zeolites and of alkanes. As already mentioned above, in a hydride transfer cracking cycle, the role of EFAl species can be explained by their contribution to initiation steps. Guisnet et al. moreover suggested that EFAl enhanced hydrogen transfer mechanisms more strongly than cracking.[527] However, the EFAl also affect protolytic cracking rates.[527] A specific role of the EFAl species has been discussed, either in terms of direct implication of the EFAl in the cracking and/or dehydrogenation reaction steps, [475,476,525–527] or in terms of confinement effect tuned by the presence of EFAl,[544] or increase of the initial heat of adsorption of alkanes resulting in higher coverages thanks to the EFAl,[493–495] or by a synergy between EFAl and Brønsted acid sites (BAS), the later corresponding to an increase in the reactivity of BAS close to EFAls.[476,527,545–550] In recent work, a perfectly linear correlation was observed between the TOF of pentane cracking in ZSM-5 and the fraction of BAS species in proximity to EFAl.[551] Since the adsorption properties were not affected by the presence of EFAl, the increase of the TOF was attributed to a more favorable transition state entropy, which is probably related to a "later" transition state in the presence of the EFAl.[551,552]

The origin of the synergy between EFAl species (seen as Lewis acid sites) and BAS has been the subject of debate. DFT calculations were undertaken to understand this. Some of these

studies suggest that the intrinsic Brønsted acidity of bridging OH groups is reduced upon proximity with an EFAl but that the conjugated base is stabilized by hydrogen bonds thanks to the EFAl.[169,170] Other DFT studies suggest an increase in Brønsted acidity of bridging OH groups close to an EFAl.[168,546] More recently, the presence of oligomeric EFAls in the sodalite cage of Faujasite was computed to enhance the acidity of bridging OH groups in the supercages.[166,167] It was assigned to an additional compensation of the negative charge of the deprotonated lattice sites by the multiply charged cationic EFAl cluster. Liu et al. moreover showed that this enhanced relaxation has a direct impact on the intrinsic energy barrier of the cracking of propane,[166,167] lowered by up to 65 $kJ.mol^{-1}$ in the case of trimeric EFAl. The mechanism invoked was, however, unchanged, no direct participation of the EFAl was simulated (being inaccessible in the sodalite cage), and no direct confinement effect of the EFAl being thought (also because the reaction takes place in the supercage, that is EFAl free in these models). To the best of our knowledge, the effect of EFAl on the cracking (and dehydrogenation) activation entropy has not been analyzed computationally so far. Considering the already strongly debated effect of the zeolite framework (without EFAl) on the activation entropy, and the difficulties in simulating relevant configurations for EFAl in zeolites, there is for sure a long way to go before this goal can be reached.

7. Transformation of aromatic molecules

7.1. Isomerization of alkylaromatics

Transformations of aromatic molecules, especially monoaromatics, are of great industrial importance to produce petrochemicals.[46,553] Since different positional isomers of substituted benzene rings have different properties, one must be able to produce the targeted isomer selectively, by using appropriate catalysts. Different types of isomerization can be

distinguished (**Figure 36**). The isomerization of the alkyl chain will not be detailed here as it involves similar mechanisms as those reported for the bifunctional isomerization of alkanes in section 5.1. Type A isomerization does not change the number of alkyl group of the aromatic cycle but either their position or the distribution of numbers of carbons of the alkyl chains. To the best of our knowledge the second one (**Figure 36-c**) has been scarcely studied and will not be detailed here.

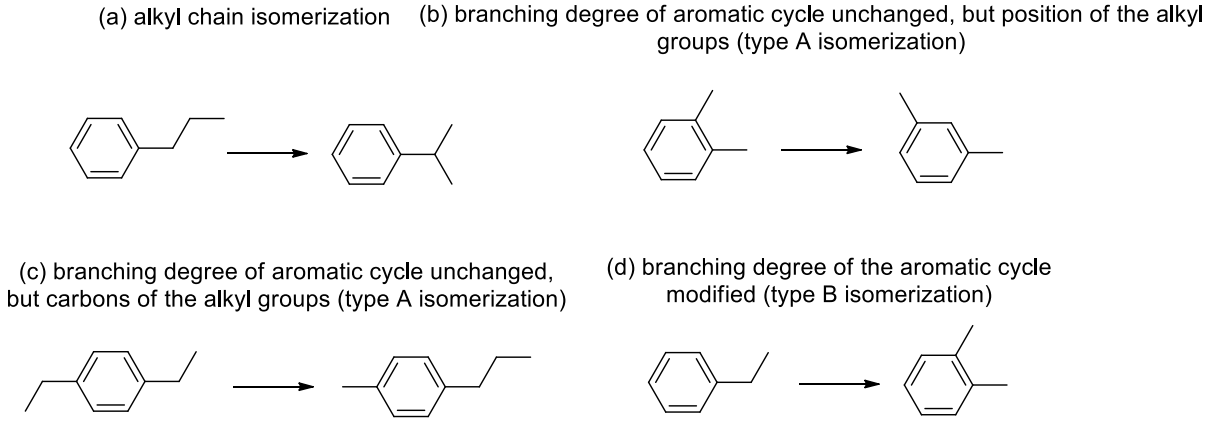

Figure 36. The various types of alkylaromatics isomerization.

Type B isomerization corresponds to the modification of the branching degree of the aromatic cycle. A well-studied example is the isomerization of ethylbenzene to xylenes. This reaction is bifunctional[554–556] and occurs via the contraction and expansion of the corresponding cyclo-olefin intermediate obtained by hydrogenation of the aromatic cycle. In this respect the isomerization mechanism is like the one depicted for cyclo-alkane with bifunctional catalyst in section 5.1. However, because of the reactivity of the aromatic molecule with acid sites, several other reactions occur in parallel:[557,558] (a) the dealkylation of ethylbenzene (monofunctional acid) and the hydrogenation of the ethene produced (monofunctional metallic), see section 7.3, (b) the disproportionation of ethylbenzene (monofunctional acid), see section 7.2, (c) the transalkylation between ethylbenzene and xylenes (monofunctional acid), see section 7.2, (d) the hydrogenation of ethylbenzene (monofunctional metallic), (e) the isomerization of

corresponding ethylcyclohexane to other naphtenes (bifunctional), see section 5.1., (f) the cracking of the naphtenes (bifunctional[559]), see section 5.2..

Different types of zeolites have been studied for this reaction.[560,561] Among them, results obtained with EUO zeolites are noteworthy. EUO zeolites are intermediate pore size zeolites, as described previously (**Figure 14**). During the early stage of the reaction, bifunctional catalyst based on EUO zeolites experienced fast initial deactivation associated with a pronounced increase of the selectivity towards isomerization.[562] The deactivation was caused by coking of the zeolite which resulted in a complete blocking of the microporosity.[561] It was considered that on coked catalyst only the active sites located on the outer surface of the zeolite were operating and that pore mouth catalysis was at stake. Comparison of the fresh and coked catalyst selectivity was used to estimate the internal sites' and outer surface sites' selectivities (**Table 4**). Active site located at the outer surface were found more selective towards isomerization than those located in the microporosity. The high selectivity of the outer surface active sites was proposed to result from an optimal access to these sites for the ethylcyclohexene olefinic intermediates.[562] Later, Marques et al. confirmed that the activity of stabilized (i.e. coked) EU-1 zeolites was markedly impacted by the amount and accessibility of external acid sites of the zeolite.[563]

Table 4. Comparison of the selectivities of internal and outer surface sites of EUO zeolites, at 7-8% EB conversion, adapted from[559].

Zeolite	Si/Al (mol/mol)	Active site localisation	Isom. (%)	Dispropor. (%)	Dealk. (%)	Crack. (%)	Transalk. (%)
EU-1	15	Inside micropores	26	30	23	19	2
		Outer surface	65	23	6	5	0
EU-1	70	Inside micropores	21	36	26	13	3
		Outer surface	37	20	38	4	2
ZSM-50	62	Inside micropores	39	18	32	7	4
		Outer surface	74	12	12	2	1

Many experimental works dealing with the isomerization of xylenes have been published. It is the prototypical example of type A isomerization. The reaction can be performed on acidic solids like zeolites, either via a monomolecular or a bimolecular mechanism[564] as depicted in **Figure 37.** The monomolecular mechanism involves the formation of Wheland complexes by protonation of the aromatic cycle. Methyl shifts are reported to be the limiting step of this mechanism. In the absence of diffusional limitation, direct isomerization of ortho-xylene into para-xylene is not possible according to the intramolecular mechanism, as reported for silica-alumina catalysts.[565] Indeed, ortho-xylene produces meta-xylene as a primary product, while as para-xylene production requires two slow methyl shifts, para-xylene appears as a secondary product. In the presence of intracrystalline diffusion limitations, meta-xylene may isomerize quicker that it desorbs, making para-xylene be formed as apparent primary product. The bimolecular mechanism is a two-step mechanism. It was demonstrated to occur in large pore zeolites like FAU using catalytic experiments with deuterated paraxylene as reactant.[566] The first step of the mechanism involves xylene disproportionation to produce toluene and trimethylbenzenes. The second step of the mechanism involves the transalkylation of trimethylbenzene with xylene reactant to produce another trimethylbenzene and a xylene isomer. The detailed features of the bimolecular mechanism will be discussed section 7.2. as such mechanism involves disproportionation and consecutive transalkylation reactions.

The effect of branched alkanes on the xylene isomerization rate is another way to assess experimentally if a bimolecular mechanism is at stake.[567] Indeed, it was shown that isoalkanes inhibit xylene disproportionation (the first step of the bimolecular mechanism) but not the monomolecular isomerization of xylene.[568] The inhibiting effect was ascribed to an hydride transfer between isoalkanes and the benzylic carbocations that are intermediate species in the disproportionation mechanism, (see later step A of the diphenylmethane mechanism, **Figure**

39-b), decreasing the concentration of the latter's. Estimation of the relative contribution of each mechanism to overall isomerization is not an easy task. It was performed by Morin et al. for meta-xylene isomerization on FAU zeolites.[569] Estimation was based on the fact that monomolecular and bimolecular pathways led to different para to ortho-xylene ratios.[569] Later, an attempt to quantify the relative contribution of each mechanism was performed for the same reaction by Min and coll.[570] Catalytic tests using deuterated experiments were performed, and sixteen zeolites with different structural codes evaluated. The pore topology of the zeolite markedly impacts the contribution of the bimolecular mechanism. The highest contributions (i.e. > 40%) are observed for three dimensional, 12MR materials such as the FAU and *BEA zeolites. Indeed, the bimolecular mechanism is more space demanding as it involves bulkier trimethylbenzenes[571] as reactant and potentially diphenylmethane (DPM) cations as intermediates or transition state (see section 7.2.). For materials with lower dimensionality and/or pore size the bimolecular mechanism contribution was found to be marginal (i.e. less than 20%). It must be emphasized that the contribution of the bimolecular mechanism can be enhanced by the presence of acid sites at the external surface (unrestricted spatial environment). Passivation of such sites can be achieved by suitable treatments, as described for example for ZSM-5 nanocrystals[572] or commercial Mordenite.[573]

As the bimolecular mechanism inherently involves disproportionation and transalkylation reactions, maximal isomerization selectivity (versus disproportionation and transalkylation) should be obtained for materials favoring the monomolecular isomerization pathway, i.e. with restricted spatial environment. This is indeed well reported experimentally for the meta-xylene conversion.[574,575]

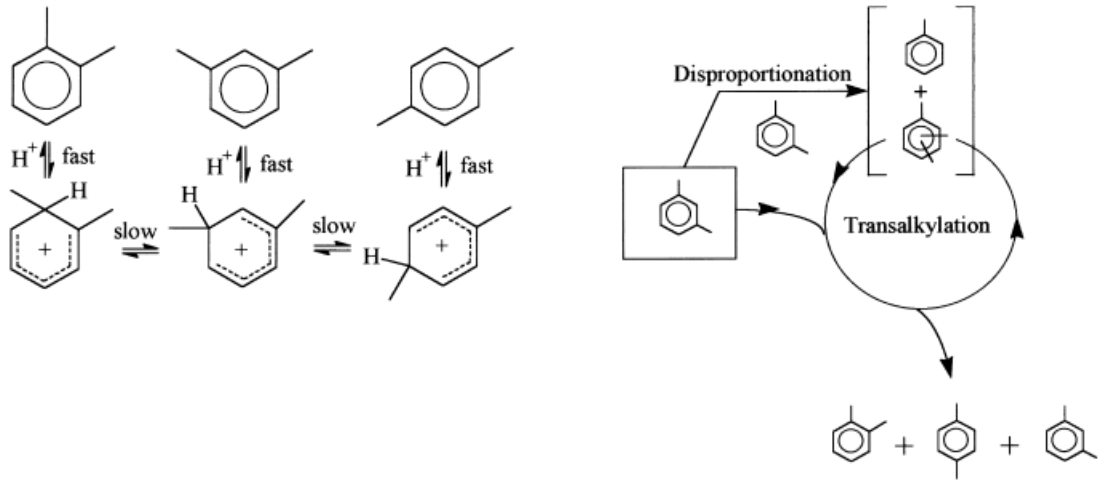

(a) (b)

Figure 37. Xylenes isomerization via (a) monomolecular or (b) bimolecular mechanism. Reprinted with permission from ref. [564]. Copyright 2000 Elsevier.

To the best of our knowledge, the monomolecular isomerization pathway over zeolite has been scarcely studied by DFT simulation methods. Rozanska et al.[291] investigated the monomolecular isomerization of xylenes and toluene catalyzed by Mordenite with periodic DFT. Two competing monomolecular pathways were considered (**Figure 38**). The first pathway involves one transition state associated to the direct shift of the methyl group after the protonation of the aromatic cycle. The shifting methenium ion is stabilized by oxygen atoms of the zeolite framework other than those neighboring the Brønsted acid site involved in the reaction. The second pathway involves demethylation of the protonated aromatic cycle to form an adsorbed aromatic cycle and a methoxy group bound to the zeolite, rotation of the aromatic cycle and methylation of the cycle by the methoxy group. The two transition states associated with the demethylation and methylation steps are similar. They are viewed as a methenium ion sandwiched between the aromatic cycle and the deprotonated acid site.

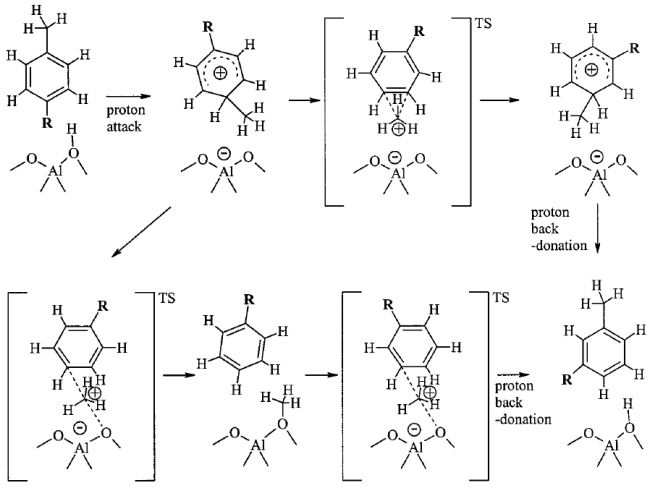

Figure 38. Isomerization of aromatic via monomolecular reaction mechanism catalyzed by zeolite. Two competing reaction pathways are considered. Reprinted with permission from ref. [291]. Copyright 2001 American Chemical Society.

The position of the non-shifting methyl group result in steric constraints that can destabilize the transition states and favor one reaction pathway. For ortho-xylene isomerization both pathways are found competitive with comparable activation energies. For meta and para-xylene isomerization the direct shift pathway is preferred.

7.2. Disproportionation and transalkylation of alkylaromatics

Alkyl group transfer between two aromatics molecules is usually proposed to occur via two possible mechanisms on zeolite (**Figure 39**, illustrated for toluene disproportionation). The first one, the "alkyl-transfer" mechanism, is monomolecular. It involves the formation of alkylbenzenium cation and the alkyl transfer from one aromatic molecule to another via the formation of an alkoxy group on the zeolite. It is very similar to the one proposed for the monomolecular isomerization (**Figure 38**). The only difference is that for the "alkyl-transfer" mechanism the dealkylated and alkylated molecules are not the same. The second one, the "diphenylmethane" (DPM) mechanism, is bimolecular. It involves the formation of

alkylbenzylic cations and the formation of alkyldiphenylmethane cation as key species, DFT calculations suggesting that it is a local energy minimum, thus a reaction intermediates.[318,319,576]

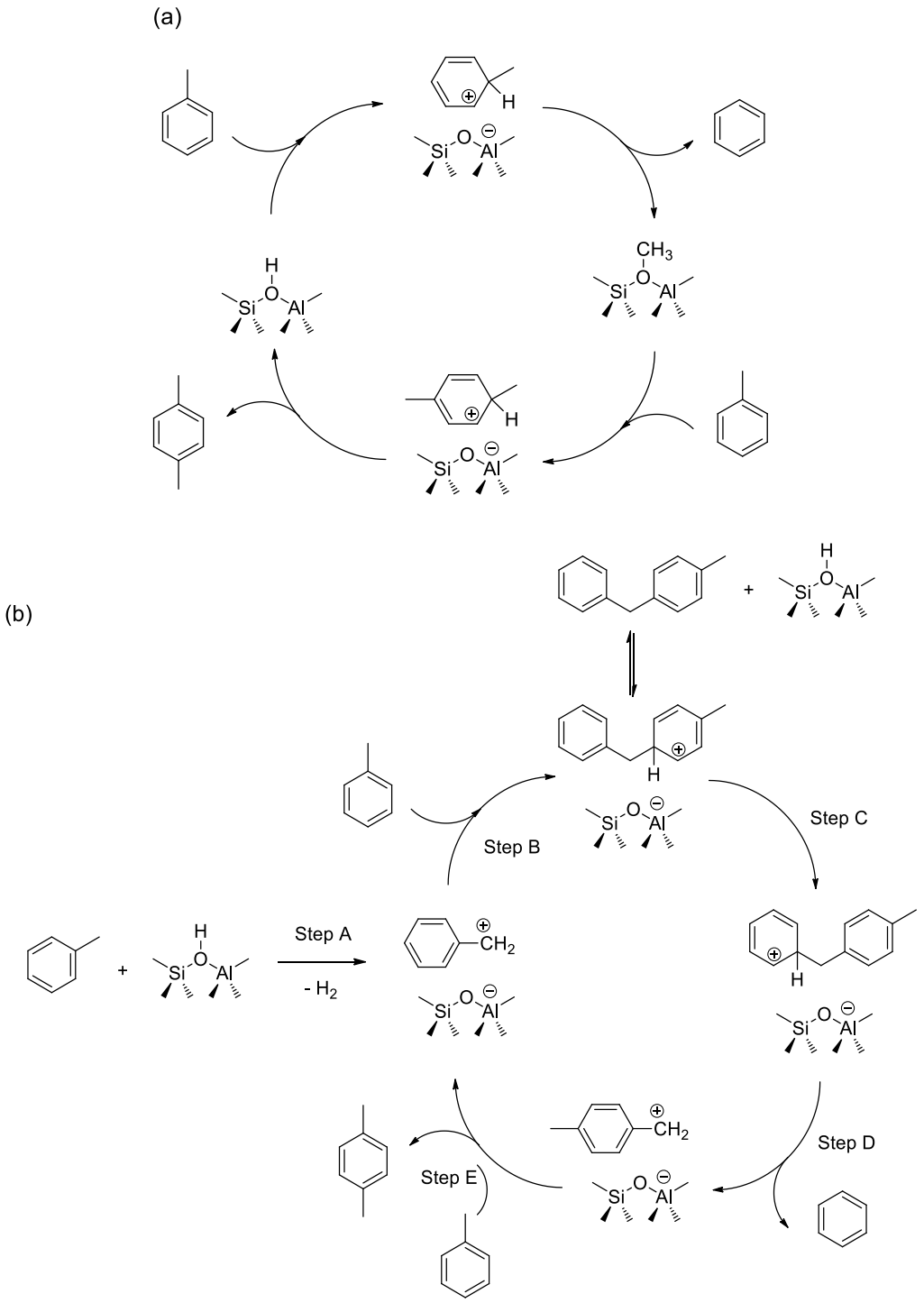

Figure 39. Toluene disproportionation via (a) "alkyl-transfer" or (b) "diphenylmethane" (DPM) mechanism, from ref. [577].

Variants of the DPM mechanism, involving two or even three catalytic cycles with alkyldiphenylmethane species, have also been proposed, for ethylbenzene disproportionation[578,579] and 1,2,4 trimethylbenzene transalkylation with toluene[580] respectively. Initiation of the DPM mechanism, i.e. the hydride abstraction step (step A) is expected to be the most difficult step. According to quantum chemical calculations, m-xylene could react with the Brønsted acid site of a FAU zeolite to form a benzenium cation and hydrogen.[318] Energy barrier can be as high as 175-220 $kJ.mol^{-1}$ according to simulations on various aromatic molecules and zeolites.[318,319,576] It was suggested that Lewis acid sites, or defect sites could play a critical role for this hydride abstraction step for ethylbenzene,[319,581] which is like the discussion taking place for the activation of alkanes, see sections 6.2-6.4. A third mechanism, i.e. the direct methyl transfer from one aromatic molecule to another, has also been studied by DFT, for MOR and TON zeolite.[319,582] Transition state associated with this mechanism is pictured as the methyl carbocation sandwiched between the two aromatic molecules.

Experimental evidence for the DPM mechanism were provided by Xiong et al. for the toluene disproportionation reaction in a ZSM-5 zeolite.[583] Introduction of small amount of diphenylmethane increased the rate of reaction as expected with the DPM mechanism. A kinetic isotope effect was observed comparing the kinetic of toluene-d0 and toluene-d8 disproportionation. This is also in accordance with the DPM mechanism which involves two breaking of sigma C-H bonds (in step A and step E, **Figure 39-b**). The build-up of DPM compounds in the microporosity of ZSM-5 zeolite after exposure to toluene was also directly evidenced by Svelle and coll.[584] To do so, the exposed ZSM-5 were dissolved in hydrofluoric acid and the CCl_4 extract analyzed by GC-MS.

The framework topology of the zeolite is expected to favor the disproportionation (or transalkylation) reaction via the alkyl transfer or DPM pathway according to transition state

selectivity. The DPM pathway involves bulkier transition states and is expected to be favored on large pore zeolites. Huang et all.[585] studied the mechanisms of ethylbenzene disproportionation on large (i.e. FAU) and medium (i.e. MFI) pore zeolites. ^{13}C MAS NMR were performed on the zeolites after exposure to ethyl [α-^{13}C]benzene at various temperatures and duration. On large pore zeolites, the formation of diphenyl ethane species was observed. By contrast, signals associated with ethoxy and oligomeric alkoxy groups were observed on medium pore zeolite. Demuth and coll.[319] performed a DFT study to assess the effect of zeolite pores topology on the relative stability of various trimethyldiphenylmethane species (3mDPMs) inside the micropores. MOR (2D 12MR * 8MR pores) and TON (1D 10MR pores) were chosen for the study. One outcome was that the 3mDPMs were strongly destabilized in the 10MR structure compared to the 12MR. However, even in the 10MR structure, specific 3mDPMs could be stabilized, namely those leading to the formation of 1,2,4 trimethylbenzene and toluene as final products. In the 12MR * 8MR structure, all the studied 3mDPMs could be stabilized. Later on, in the context of m-xylene conversion, Byun and coll. investigated the stability of trimethyl and tetramethyldiphenylmethanes (4mDPM) species in nine zeolites (FAU and eight zeolites containing 10MR) with different framework topology using computational methods based on clusters models.[576] Adsorption energies of the species were found to be correlated with their strain energies (**Figure 40**). Strain energy can be viewed as the energetic penalty cost associated with the deformation that the DPM requires to be accommodated in the void of the zeolite structure. Penalty cost is largely correlated to the deviation of the bond angles of the central sp^3 carbon of the molecule. The strain energy and bond angles deviation were correlated with the maximum sphere diameter (D_i) that could be included in the zeolite network,[586,587] considered as a quantitative descriptor of void of the zeolite structure (**Figure 40**). The DPM's adsorption is strongly disfavored for D_i values below 7 Å.

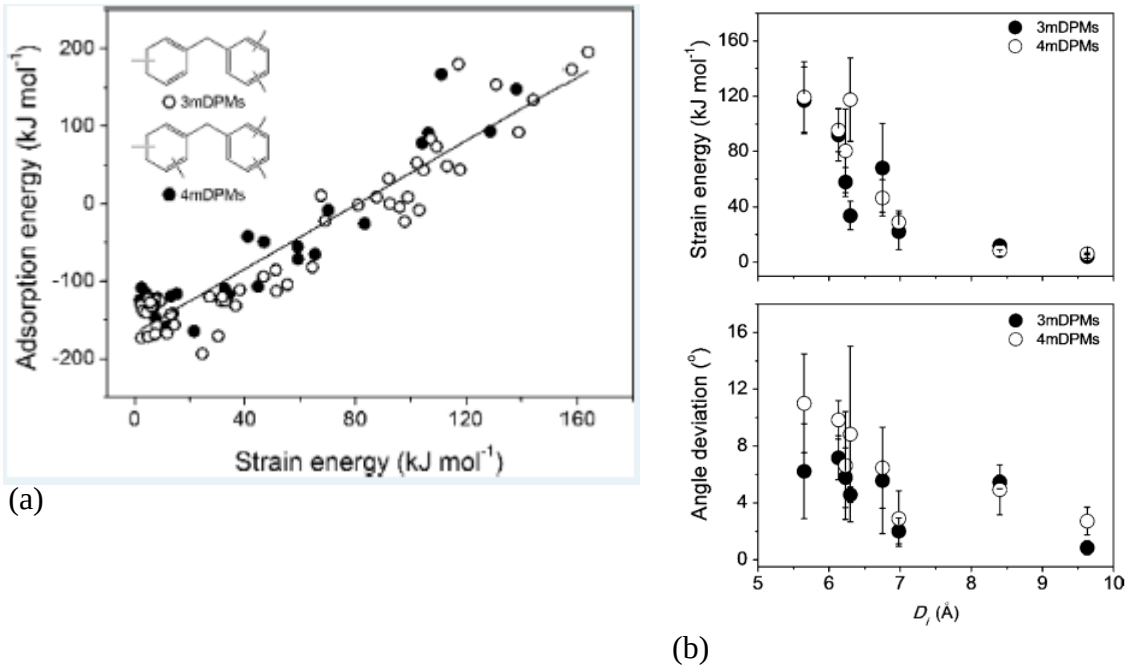

Figure 40. (a) Evolution of the adsorption energy of 3m and 4mDMPs with their corresponding strain energy in nine zeolites, and (b) evolution of the strain energy and the deviation of the central sp^3 carbon bonds angle with the maximum included sphere diameter D_i in the eight zeolites containing 10MR. Reprinted with permission from ref [576]. Copyright 2014 American Chemical Society.

Provided that dismutation and transalkylation reactions are occurring mainly via the DPM mechanism, the inability of a zeolite to stabilize 3 and 4mDPM species should be reflected by a lower contribution of the bimolecular isomerization pathway with respect to the monomolecular one for xylene isomerization. **Figure 41** reports the evolution of the percentage of para-xylene bimolecular isomerization with the D_i of the eight zeolites containing 10MR from **Figure 40**. The bimolecular mechanism is not the dominant one for all the zeolites of the panel. Its contribution decreases with the D_i value, and indeed becomes marginal (i.e. less than 5%) for D_i values below 7 Å, in accordance with the strong increase of the strain energy of the 3 and 4mDMP species. The high percentage of bimolecular isomerization reported for the H-NU-87 zeolite was proposed to result from the significant contribution of external acid sites on this solid.[570]

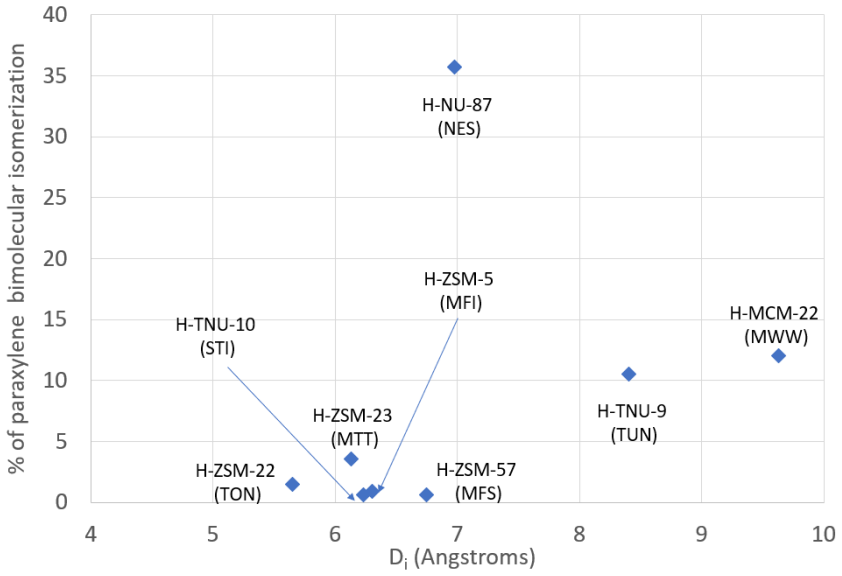

Figure 41. Evolution of the percentage of bimolecular pathway for paraxylene isomerization with the maximum sphere diameter D_i for eight zeolites containing 10MR. Data extracted from[570,586,587].

Stabilization of specific DPM species or associated transition states can result in the formation of specific disproportionation or transalkylation products.[319,574] Reactant shape selectivity can also play a crucial role to obtain specific disproportionation or transalkylation products, and even mask actual transition states selectivity effects.[588] A classic example of reactant shape selectivity, at the industrial scale, is the selective disproportionation of toluene to para-xylene and benzene using modified ZSM-5 zeolite.[589,590] Research about zeolites with micropore channels of different dimensions is an active topic as such structures could favor specific reactants or products shape selectivities for reactions of interest.[591] Recently, aiming at selectively transalkylating toluene with trimethylbenzenes to para-xylene, the diffusion of toluene and trimethylbenzenes in zeolites with intersecting dual pores system (10MR and 12MR) was computed by molecular dynamics study to identify potential candidates.[592,593] The UWY framework was proposed as a promising candidate as the 12MR channel of the structure can accommodate the DPM species whereas the 10MR channels favor the preferential diffusion of para-xylene.

Recent work investigated the impact of the zeolite pore structure on the preferential pathway at stake (i.e. “alkyl transfer” or DPM) for the ethylbenzene (EB) disproportionation reaction by combining DFT calculations and experimental catalytic tests.[320] Four zeolites with three different structural codes were investigated. These include two MWW structures: MCM-22 with 10MR pores, 12MR cavities and external 12MR hemicavities and DS-ITQ-2 with no 12MR cavities and a higher proportion of 12MR hemicavities than MCM-22. 10MR ZSM-5 (MFI) and 12MR Mordenite (MOR) were also studied. The crucial role of van der Waals interactions in the stabilization of the carbocationic intermediates, in addition to electrostatic interactions and spatial requirements was evidenced. Striking simulation results were obtained for the MWW structure. The “alkyl transfer” and the DPM mechanisms were investigated in the large hemicavities cups (7.1 * 7.1 * 7.1 Å) and within the more constrained 10MR channels (4.1 * 5.1 Å) of the structure. The counter-intuitive result is that the space-demanding DPM mechanism is favored inside the constrained 10MR channel, whereas the alkyl transfer one is favored in the voluminous hemicavities cup. Adsorbed EB is more stabilized in the 10MR channel than in the hemicavity because of a higher dispersion contribution (-168 $kJ.mol^{-1}$ vs -120 $kJ.mol^{-1}$). But inside the 10MR channel, for the protonated EB the dispersion contribution changes less (-25 $kJ.mol^{-1}$) whereas it becomes much stronger in the hemicavity (-76 $kJ.mol^{-1}$). Indeed, the protonated EB is located deeper in the hemicavity and maximize its interaction with the zeolite framework (**Figure 42-a**). As a result, for the alkyl transfer mechanism, the free energy required for the EB protonation (first step of the mechanism) was found much higher in the 10MR channels (122 $kJ.mol^{-1}$) than in the hemicavities (40 $kJ.mol^{-1}$). Conversely, hemicavities cup were found less favorable for the DPM mechanism as the ethylbenzene molecule reacting with the ethylbenzenium cation (to form the first intermediate, see step b in **Figure 39-b**) is not sufficiently stabilized by the MWW hemicavity (**Figure 42-b**). Note that, as at several other occurrences mentioned in this review, considering the dispersion contribution

is crucial, otherwise the formation of the EB^+ - EB complex is found to be unfavorable in the 10MR channels.

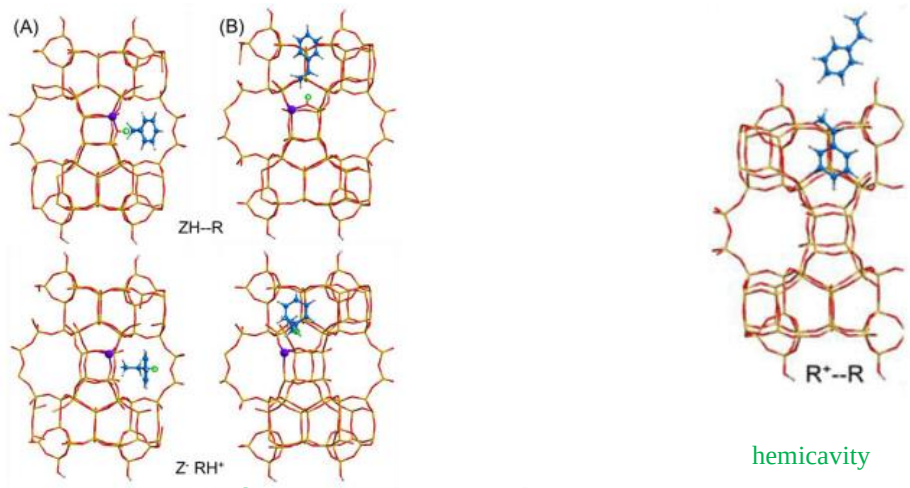

Figure 42. (a) optimized structures of adsorbed ethylbenzene (ZH-R) and protonated ethylbenzene (Z^-RH^+) in the 10 MR channel and hemicavity of MWW and (b) optimized structure of adsorbed ethylbenzenium ion and adsorbed ethylbenzene in the hemicavity of MWW - adsorbed ethylbenzene interacts weakly with the MWW framework. Si and O atoms depicted as yellow and red sticks, Al, C and H atoms as purple, blue and white balls. The proton is highlighted with the green circle. Reprinted with permission from ref [320]. Copyright 2019 American Chemical Society.

The proper local environment of the active site can therefore favor one pathway by specifically stabilizing the associated key intermediates or transition states. The optimal zeolite structure (new or already existing) in accordance with the targeted mechanistic pathway may be synthesized by proper selection of the organic structure directing agent (OSDA). The OSDA should mimic the key intermediates or transition states of the reaction to have a subsequent optimal stabilization of such species in the zeolitic framework during the catalytic reaction.[15] Such an approach was recently illustrated for the transalkylation of diethylbenzene (DEB) with benzene to produce ethylbenzene.[321] Transalkylation can occur via the alkyl-transfer or the DPM mechanism. The alkyl transfer pathway should be minimized as it is more favorable for side reactions like dealkylation or overethylation of DEB (see section 7.3). Diphenyldimethylphosphonium ($DPDMP^+$) was viewed as a good mimic of the DPM intermediates and transition states associated with the DPM mechanism (**Figure 43**).

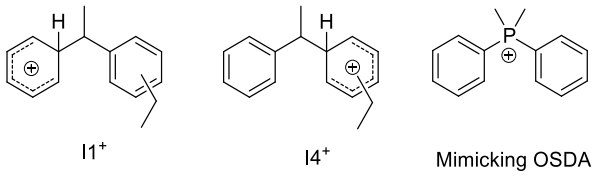

Figure 43. Zeolite synthesis using diphenyldimethylphosphonium, as mimicking OSDA of the DPM intermediates, to favor the DPM mechanism during diethylbenzene transalkylation with benzene, from[321].

$DPDMP^+$ was previously used as OSDA for the synthesis of a new aluminosilicate zeolite, called ITQ-27, with a two-dimensional 12MR channel system[594] (IWV structural code). ITQ-27 indeed exhibited superior DEB conversion and EB selectivity compared to benchmark zeolites (FAU, *BEA and MOR). DFT calculations were performed to compare the energetic profiles for the alkyl transfer and DPM mechanisms for IWV and MOR structures. Results suggested that the DPM pathway is favored in the IWV structure whereas both pathways are competitive in MOR. Experimentally, a higher production of ethene (a hint of the occurrence of the alkyl transfer mechanism) was indeed observed for the MOR zeolite compared to IWV for a given DEB conversion. The lower experimental activity (per Al) observed of the MOR was also in agreement with the higher calculated activation barriers (superior to 80 $kJ.mol^{-1}$ versus 40-70 $kJ.mol^{-1}$ for the IWV structure), **Figure 44**.

The operating conditions also impact the relative contribution of both mechanisms at stake in a zeolite. Increasing the temperature favors the alkyl transfer mechanism as its activation energy is generally higher compared to the DPM mechanism. This was for instance experimentally reported for the n-propylbenzene disproportionation reaction over zeolites Beta, USY, Mordenite and ZSM-5.[595]

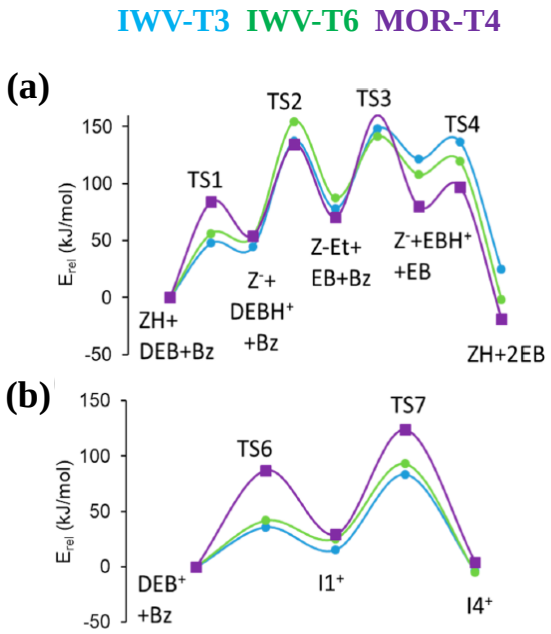

Figure 44. DEB transalkylation with benzene: DFT energetic profiles for (a) alkyl transfer and (b) DPM mechanism (direct proton transfer) pathways for MOR and IWV zeolites. IWV-T3 and IWV-T6 stand for the two most stable Al location in IWV structure, MOR-T4 for the Al location accessible from the 12MR channel in MOR structure. Reproduced from ref [321]. Licensed under CC BY 4.0.

7.3. Dealkylation of alkylaromatics

When the alkyl chain is an ethyl or (iso)propyl group, dealkylation occurs by cleavage of the sp^2 carbon sp^3 carbon bond; i.e. the molecule is de-ethylated or de-propylated. When the alkyl chain is a methyl group dealkylation (demethylation) is not occurring.[596,597] The essential features of the dealkylation mechanism are the same than for the "alkyl transfer" mechanism, except that the alkyl group adsorbed on the zeolite as an alkoxide desorbs as an olefin (after proton back donation). This is illustrated in **Figure 45** for ethylbenzene. However, the olefin can readsorb and undergo secondary reactions like realkylation of an aromatic molecule, oligomerization and coke formation. In the presence of hydrogen, adding a hydrogenating function allows to quickly hydrogenate the olefin and avoid secondary reactions. Such a mechanism does not allow demethylation as the methoxy cannot desorb (no proton available for back donation to restore the acid site). Increasing the temperature is found to favor the

dealkylation mechanism as reported experimentally for ethylbenzene conversion over fourteen zeolites.[579,598] A single event microkinetic model was developed for the ethylbenzene (EB) and xylenes hydroconversion over Pt/ZSM-5 and the activation energy was also found higher for EB dealkylation (194 kJ.mol^{-1}) compared to xylenes' methyl-shift (134 kJ.mol^{-1}) and transmethylation (125 kJ.mol^{-1}).[599]

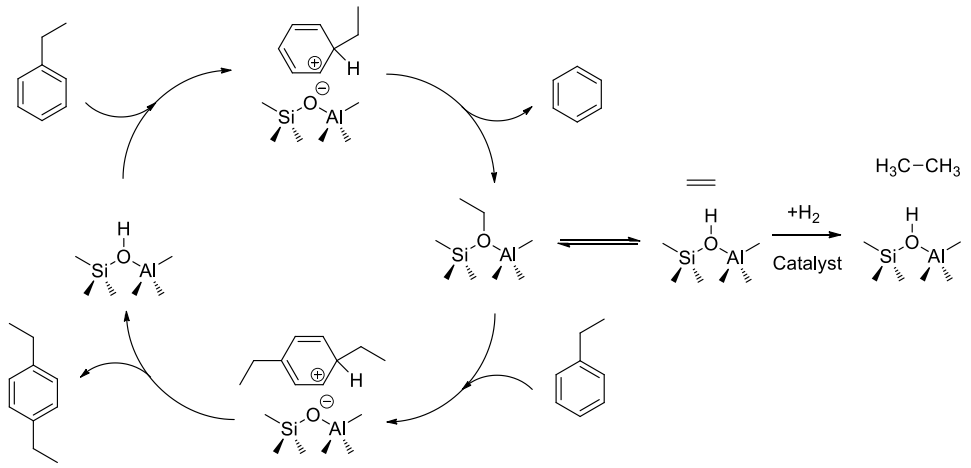

Figure 45. Ethylbenzene transformation via disproportionation ("alkyl transfer" mechanism) or dealkylation. Reprinted with permission from ref. [600] . Copyright 2019 Elsevier.

According to **Figure 45**, the selectivity of a zeolite towards disproportionation (or transalkylation) compared to dealkylation should be profoundly affected by the presence of the hydrogenating function, if the disproportionation (or transalkylation) mainly occurs via the "alkyl transfer" mechanism, as hydrogenation of the olefin avoids consecutive readsorption and realkylation. Conversely, the impact of the hydrogenating function is expected to be less pronounced if the disproportionation (or transalkylation) mainly occurs via the DPM mechanism. This was elegantly demonstrated by Amelse[601] and later confirmed by Silva et al.[602,603] for the ethylbenzene (EB) hydroconversion over MFI and MOR zeolites. Under typical operating conditions of the studies, ^{14}C labelled EB experiments demonstrated that disproportionation occurred mainly via the "alkyl transfer" mechanism with MFI and via the

DPM mechanism with MOR.[601] Adding (by mechanical mixture) a hydrogenating catalyst improved consistently the (EB converted by dealkylation) / (EB converted by disproportionation-transalkylation) ratio by an order of magnitude for the MFI zeolites whereas the effect was much less pronounced for the MOR zeolites (**Table 5**).

Table 5. Conversion of ethylbenzene (EB) on MFI or MOR zeolites – impact of a hydrogenating catalyst on the EB converted by dealkylation to EB converted by disproportionation-transalkylation ratio.

Zeolite type	**Hydrogenating catalyst**	**Feedstock composition**	**EB converted by dealkylation / EB converted by disproportionation-transalkylation* at 40-50% EB conversion**	**Datas extracted from**
MFI (borosilicate)**	Yes (catalyst not specified)	15% EB, 12% PX, 49% MX, 24% OX	1.7	Ref [601]
MFI (borosilicate)**	No	15% EB, 12% PX, 49% MX, 24% OX	0.1	Ref[601]
MFI (aluminosilicate)	Yes (Pt/Al_2O_3)	Pure EB	11.5	Ref[602]
MFI (aluminosilicate)	No	Pure EB	0.6	Ref[602]
MFI (aluminosilicate)	Yes (Pt/Al_2O_3)	20% EB, 80% OX	15.3	Ref[602]
MFI (aluminosilicate)	No	20% EB, 80% OX	0.5	Ref[602]
MOR (aluminosilicate)	Yes (catalyst not specified)	15% EB, 12% PX, 49% mX, 24% OX	0.1	Ref[601]
MOR (aluminosilicate)	No	15% EB, 12% PX, 49% mX, 24% OX	0.04	Ref[601]
MOR (aluminosilicate)	Yes (Pt/Al_2O_3)	Pure EB	0.8	Ref[603]
MOR (aluminosilicate)	No	Pure EB	0.2	Ref[603]
MOR (aluminosilicate)	Yes (Pt/Al_2O_3)	20% EB, 80% OX	0.4	Ref [603]
MOR (aluminosilicate)	No	20% EB, 80% OX	0.2	Ref[603]

* Transmethylation and transethylation between EB and xylenes (if present in the feed)
** AMS-1B[604]

Impact of the channel pore architecture for the selective EB conversion by the dealkylation route was also evidenced later by Serra and coll.[605] Seven zeolites loaded with Rhenium as hydrogenating function were evaluated and major differences in the dealkylation selectivities and activities per acid site were observed (**Figure 46**). Zeolites with 10MR pores exhibited the highest dealkylation selectivities and activities whereas the presence of 12MR pores was found to decrease the dealkylation selectivities and activities. The high dealkylation selectivity was attributed to the low contribution of the DPM mechanism in the 10MR pores zeolites under the operating conditions of the study. Similarly, the high activities of the acid sites were proposed to be linked to a higher confinement of EB in the 10MR pores zeolites.

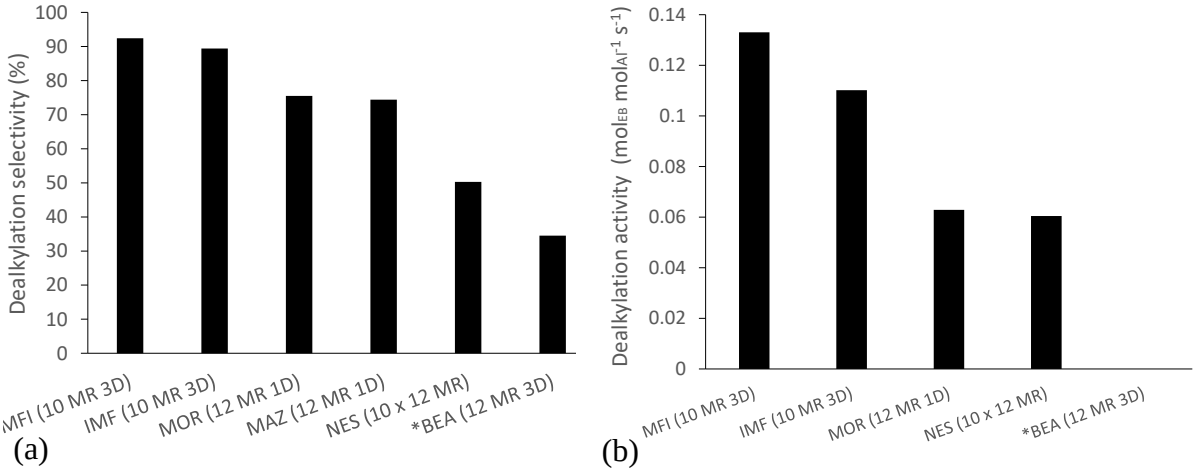

Figure 46. Dealkylation (a) selectivity and (b) activity for ethylbenzene conversion with various zeolites loaded with ruthenium, extracted from[605]. EB conversion range: 68%-93%; Zeolites Si/Al range: 13-18 mol/mol. EB conversion below 7%; acid site considered as Al site.

The impact of the channel pore architecture and crystal size was later studied by Marques Mota et coll.,[606] for three different types of zeolites: *MRE (10MR 1D), MFI (10MR 3D) and MTW (12MR 1D). The results obtained with the bulk materials confirmed the ability of the MFI zeolite to significantly dealkylate EB. This was not observed for *MRE and MTW like zeolites (**Figure 47**). The very low dealkylation selectivity of bulk *MRE compared to MFI looks

puzzling at first sight as the pores diameters of the two zeolites are similar (5.3 * 5.6 Å in *MRE and 5.1 * 5.5 Å; 5.3 * 5.6 Å in MFI). This can tentatively be ascribed to an optimal geometric environment of the active sites in MFI, for instance at the intersection of the channels. Evaluation of MFI with controlled location of the active sites in the framework should be of interest to explore this concept further.[112] Downsizing of the MFI crystals (nanosponge) also results in a huge loss in the dealkylation ability of the zeolite, which can be associated with the loss of the optimal geometric environment required for the reaction. Typically with nanosponge MFI 30% of the Brønsted sites are located at the external surface and the total acid strength distribution assessed by ^{13}P NMR of adsorbed phosphine is shifted to lower values.[607]

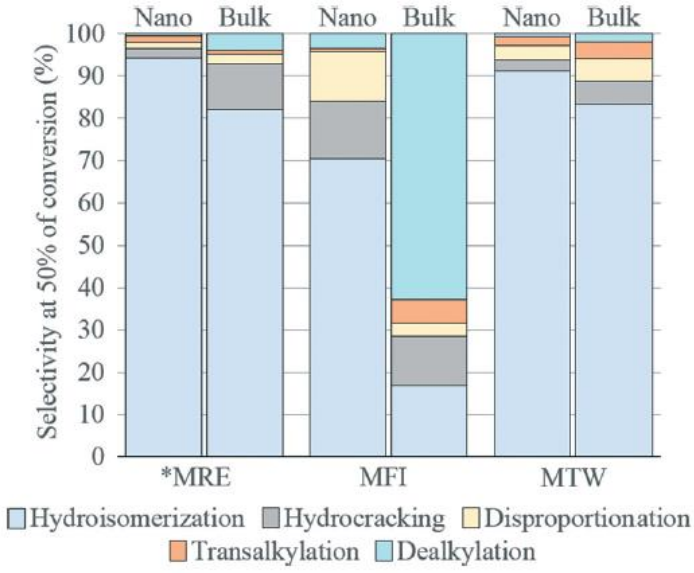

Figure 47. Dealkylation, disproportionation, transalkylation, hydroisomerization and hydrocracking selectivities at ca. EB hydroconversion over *MRE, MFI and MTW zeolites (bulk and nanosponge form). Zeolites Si/Al range: 70-110 mol/mol. Zeolites in mechanical mixture with Pt/Al_2O_3 hydrogenating catalyst. Reprinted with permission from ref [606]. Copyright 2016 Royal Society of Chemistry.

Note that for polymethylsubstituted aromatics, like hexamethylbenzene, dealkylation can also occur via the paring reaction,[608] as will be discussed in more details in section 10.4.

8. Dehydration of alcohols and polyhydroxy molecules

8.1. General aspects

Following the precursor works of Knözinger dealing with alcohol dehydration on alumina,[609,610] this set of reactions was investigated on many kinds of oxides, including proton-exchanged zeolites.[36] The dehydration of alcohols produces two main kinds of products: (i) ethers, upon intermolecular dehydration, (ii) alkenes, obtained by intramolecular dehydration or by the decomposition of ethers, as shown in **Figure 48** in the case of isobutanol. Depending on the structure of the alcohol reactant, the reaction network may also encompass double-bond isomerization reactions and skeletal rearrangement, which are also catalyzed by Brønsted acidity. Notably, in the present section, we focus on mechanisms that do not involve the formation of C-C bond between alcohol molecules. The latter family of mechanisms refers to alcohol to hydrocarbon reactions, which are discussed later in section 10 in the case of methanol.

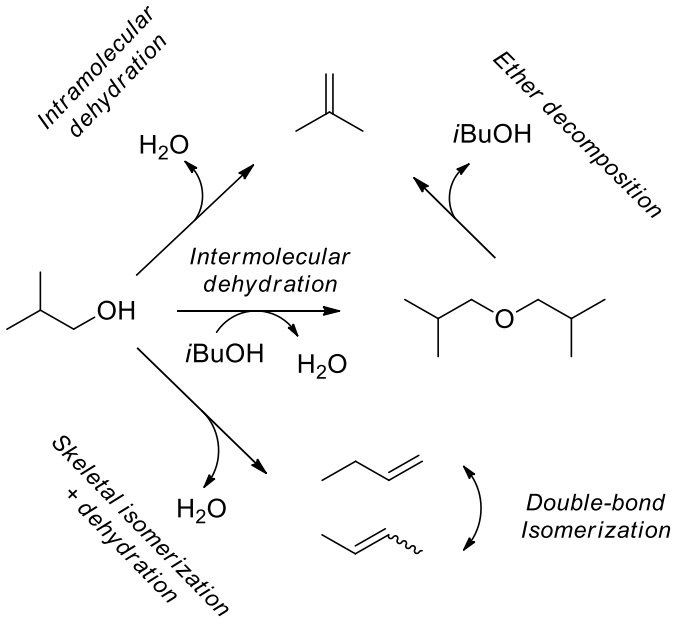

Figure 48. Schematic reaction scheme for isobutanol dehydration.

Several families of solids can catalyze these reactions, with various selectivities. Most of the time, they exhibit either Lewis or Brønsted acid sites. Protonic zeolites are highly efficient for these reactions.[611,612] Beside industrial attractivity,[613,614] the dehydration of alcohols is also widely used as a model reaction for the characterization of the acidity of catalysts.[36,615] In particular, the dehydration of 1-butanol *versus* isobutanol reactions in zeolites was used as a basis of the shape selectivity concept in the 60's.[455,616] Most investigations consider the major catalytic feature of protonic zeolites to be their Brønsted acidity, through the bridging OH groups. The rate of isobutanol dehydration was indeed shown to be correlated to the concentration of Brønsted acid sites determined by pyridine adsorption, for a series of ZSM-5 zeolite samples.[617] For ethanol dehydration in H-ZSM-5, it was suggested that weak acid sites are more selective to the direct formation of ethylene,[618] whereas the stronger ones would be responsible for di-ethylether formation and decomposition.[619] Lewis acidic sites are less often invoked in dehydration reactions, and for instance in ref. [620], the absence of role of Lewis acid sites was shown by co-feeding acetonitrile, believed to poison mainly Lewis acid sites, although acetonitrile is also a popular probe molecule for the quantification of Brønsted acid sites.[22] However, a synergetic role of Brønsted and Lewis acid sites was recently proposed for the production of ethylene from ethanol[621] and butene from tert-butanol[622] in H-ZSM-5 (from the comparison of the performance of samples exhibiting various amounts of EFAls such as Al_{III} characterized by TMPO adsorption), and of propylene from isopropanol on amorphous silica-alumina (from DFT calculations compared with experimental measurements of activation enthalpies).[623] In the proposed mechanisms of such a synergy, the low-coordinated aluminum atoms assist the dissociation of the C-O bond. Finally, the role of the external surface sites is still debated. In the case of butanol dehydration in Ferrierite, which will be developed in section 8.6, a specific role of the external surface of the crystallites is invoked,[624,625] while in the case of the formation of dimethylether from methanol at the external surface of SSZ-13, no

evidence of a specific role of the external Brønsted and Lewis surface sites is provided by computational studies.[626]

8.2. Adsorption state of the alcohol molecule

The first reaction step to be considered is the protonation of the hydroxyl group of the alcohol molecule. The stability of this protonated state, called oxonium (and sometimes a Eigen-like configuration, see **Figure 49**) has been strongly debated, in particular by quantum chemistry calculations. Cluster investigations, up to the MP2 level, conclude that methoxonium does not constitute the local energy minimum for methanol,[627] consistently with NMR spectra recorded for the H-Rho zeolite.[628] However, the shape of the potential energy surface was shown to depend on the level of theory, on the type of zeolite model, on the zeolite framework, on the position of the Brønsted acid site, and on the alcohol under consideration.[629–640] The proton affinity of the alcohol, itself a function of the degree of substitution of the alcohol, was shown to be a relevant parameter to quantify its propensity towards protonation by the zeolite.[635] Methanol in Ferrierite at 300 K,[641] ethanol[642] and 1-propanol in H-ZSM-5 [643] close to 500 K, were show by AIMD to be easily protonated. Below 400 K, ethanol was shown to form a Zundel-like structure at low loading, where the proton is equally shared between the oxygen of the zeolite and the oxygen of the alcohol (**Figure 49**).[618,642] The protonation of the hydroxyl group of the alcohol elongates the C-O bond, making it more prone to undergo elimination. At higher loadings in ethanol, AIMD shows that a second alcohol molecule stabilizes the protonated ethanol (**Figure 49**).[618,642] Similar propensity of the dimer (or higher clusters) for protonation with respect to the monomer was also observed by static DFT calculations in the case of methanol[644] and butanols,[632] and by molecular dynamics in the case of methanol in ZSM-5.[645] This is in agreement with the experimental observation at room temperature by infra-red spectroscopy of protonated methanol and ethanol dimers at high

loadings in H-Y, H-Mordenite and H-ZSM-5, while at low loading the dominant features are that of non-protonated alcohol monomer.[646] Similarly, at 398 K, isobutanol in Ferrierite leads to the appearance of a typical ABC spectral structure in infra-red, showing that the alcohol is hydrogen bonded to the OH group of the zeolite.[624] However, most bridging OH groups of Ferrierite appeared to be unaffected by adsorption, showing that the interaction of isobutanol is restricted to the external surface of Ferrierite crystallites. In conditions where the dehydration reaction takes place, the internal bridging OH groups interact with reaction products only (in particular, water).[624]

Comparing the properties of 3D and 2D (nanosheets) H-ZSM-5 samples and relying on operando infra-red analyses, Kadam et al.[647] concluded that the ethanol dimer could be formed with a larger equilibrium constant at the external surface than in the bulk of the zeolite. The authors assigned this effect to a higher acid strength of the external surface sites with respect to the bulk, but one may wonder whether this could also be explained by a confinement effect that would be more suitable at the external surface considering the size of the ethanol dimer.

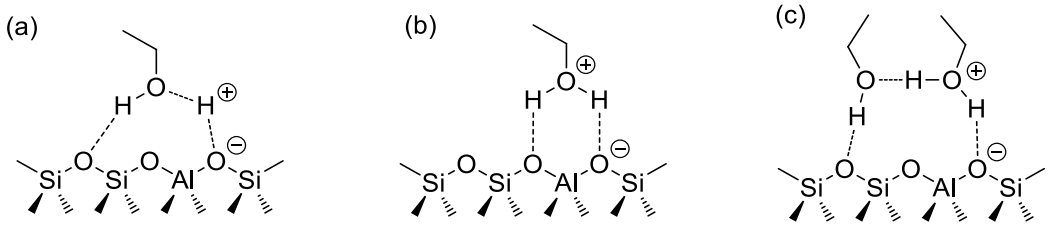

Figure 49. Most stable structures (at 0 K) of the adsorbed ethanol monomer of (a) a Zundel-like configuration, (b) a Eigen-like configuration, and (c) dimer on the Brønsted acid site of H-ZSM-5.

8.3. Monomolecular mechanisms: direct formation of alkenes

After protonation of alcohol molecules, water elimination and proton restitution to the framework are expected. Referring to the traditional textbook terminology, this may proceed by a E1 (with a carbenium ion intermediate, or to its alkoxide equivalent), E2 (synchronous – often called concerted- water and proton release, with participation of the base site that catches

the proton back, hence the name “bimolecular” and the E2 terminology) or E1cb mechanism (with a carbanion intermediate).[648] E1 or E2 are more likely than E1cb on Brønsted acidic catalysts such as zeolites. For the E2 mechanism, an anti-periplanar conformation of the breaking C-H and C-O bounds is in principle preferable, so as to align the corresponding σ orbitals.[648] However, as will be discussed later, such a conformation is not always possible, in the case of cyclic alcohols, or in the case where the protonation site (of the HO^- moiety) and the deprotonation site (hosting the H^+ moiety from the breaking C-H bound) are constrained to be located on the same side of the molecule. The latter situation is likely in catalysis by proton-exchanged zeolites.

Such a mechanism is not possible from methanol. Thus, ethanol is the smallest alcohol to be considered in this case. To the best of our knowledge, in the case of protonic zeolites as catalysts, the E1cb mechanism was never found to be relevant. Among E1 and E2, the most likely mechanism depends strongly on the nature of the alcohol, and on its ability to generate stable carbenium ions. The stability of the latter with respect to alkoxides is also a key question in such mechanisms, as mentioned in section 4.

Infra-red and ^{13}C MAS NMR spectroscopies show that alkoxide species are formed by contacting various alcohols with a variety of zeolites.[24,266,267,271,274–276,611,649–652] Such experimental observation is not trivial, as in analysis conditions, oligomerization products are often formed.[258,275] Alkoxides were proposed to play a key role in the formation of alkenes, thus being in favor of the E1 mechanism.[275,611,652–654] However, one may wonder whether such a mechanism could not coexist with the E2 one, as in the latter case no intermediate is expected to be experimentally observed.

Whereas some computational studies consider the E1 mechanism only, passing through alkoxide intermediates and carbenium-like transition states,[618,655,656] other DFT comparative investigations suggest that the E2 mechanism is favored in the case of 2-propanol dehydration

into propene in H-ZSM-5.[657,658] A E2 mechanism was also computed on pseudo-bridging silanols of amorphous silica-alumina, depicting an activation enthalpy fully compatible with experiments.[623] In this case, however, both the Brønsted and Lewis acidity of the sites were shown to play a role, at variance with zeolites. The case of ethanol in H-ZSM-5[659,660] is less clear. Some studies[659] conclude to a preferred E2 (synchronous) mechanism (called E1-like in ref. [660]), while others find lower free energy profiles for the E1 mechanism (alkoxy-mediated).[660] The case of 1-propanol[643,661] is also ambiguous, with highly competitive calculated enthalpy profiles for E1 and E2 pathways in ZSM-5. The computed activation enthalpy for E1 and E2 mechanisms are, moreover, both compatible with experiments.[643] More recent studies performed with ONIOM models concludes to the preference for the synchronous mechanism for ethene production from ethanol[658,662] and propene from isopropanol[658] (generalized for alumino-, gallo- and borosilicate forms of H-ZSM-5 in ref.[662]). In H-Mordenite, the mechanistic preference is suggested to depend on the acid site location (12MR *versus* 8MR).[663] As a simpler case, the bulkier tert-amyl alcohol was shown to induce a preference for a E1 mechanism without involving alkoxide, but a stable tertiary carbenium ion.[658]

A series of synchronous dehydration mechanism were considered for 1-butanol in 1-butene in various zeolites by John et al.,[632,664–666] thanks to periodic DFT at the PBE+D2 level, in several zeolite frameworks (MFI, FAU, MOR, TON, FER). Focusing on mechanisms leading directly to butene (ether-mediated ones being also considered in this series of work, that will be detailed in sections 8.4 and 8.5), several options were compared. A first mechanism, called "E1-like", takes place in a single step, without carbenium nor alkoxide intermediate. The "E1-like" terminology was chosen, considering the cationic nature of the transition state. Following standard organic chemistry terminology, it may be rather qualified as an intramolecular E2, with a syn elimination of the H^+ of the butanol molecule by the water molecule formed upon protonation of the HO^- moieties (all synchronously). It is compared to a syn-E2 and trans-E2

mechanisms, where the proton of the molecule is abstracted by an oxygen atom from the framework, synchronously with the breaking of the C-O bond of the protonated OH moiety. Alkoxide-mediated mechanisms are also considered. Finally, a bimolecular mechanism, assisted by a second butanol molecule, but without ether intermediate, was investigated. At 400 K, the latter offers the lowest apparent free energy barrier, but the lowest intrinsic barrier is provided by the anti-E2 pathway, which renders well the experimental activation energy measured in ZSM-5.[653] More recent studies taking into account systematically the effect of temperature on the stability of intermediates and transition states have discarded alkoxide-based mechanisms, in favor of synchronous E2 mechanisms, starting from isobutanol, tert-butanol, and 2-butanol.[667]

Considering bridging OH groups at the external surface sites of ZSM-5 for isopropanol dehydration, Prestianni et al. concluded to a similar preferred reaction pathway with respect to framework sites in ZSM-5 and Faujasite, namely a E2 synchronous dehydration mechanism.[191] The computed activation barriers are significantly higher at the external surface sites with respect to internal bridging OH groups. The catalytic sites were simulated thanks to a cluster approach, at the DFT and MP2 levels.

The specific case of the dehydration of substituted cyclohexanols into cyclohexenes in water was the object of intensive experimental and theoretical work, pointing out effects of the substitution level, cycle conformation, and confinement effects on the preferred mechanisms and intermediates.[668–672] E1 *versus* E2 mechanisms were discriminated **Figure 50-a**) on the basis of the following arguments: i) the observation of kinetic isotope effects thanks to the use of deuterium labelled reactant, the reincorporation rate with ^{18}O labelled water,[670,672,673] and the monitoring of ^{13}C scrambling starting from 1-^{13}C-cyclohexanol monitored by NMR and fitted with a microkinetic model,[671] ii) in the case of a E1 mechanism, no significant reactivity differences should be observed when starting from isomers of the same substituted

cyclohexanol (for example, cis versus trans 2-methylcyclohexanol), thus when such differences are observed, a E2 mechanism likely takes place;[669] iii) higher values of activation entropies are expected to correspond to a late transition state and could be an indication of E1 mechanism, at reverse E2 transition states are expected to be more constrained and earlier, so have lower enthalpies of activation,[668,669] these trends correspond to the compensation effect depicted in **Figure 50-a**; iv) the observation of ethylcyclopentene from methylcyclohexanols suggests the existence of carbenium intermediates undergoing cycle contraction reactions.[669] The existence of such cyclic carbenium species was indeed confirmed by DFT calculations (in the absence of water, however) in the EU-1 zeolite,[115] although stabilizing some secondary carbenium ions appeared to be difficult.[346] It may, moreover, be questioned whether this cycle contraction step could not take place once cyclohexene is formed, independently of the existence of a carbenium intermediate. In the presence of water as a solvent, the reaction is considered to be catalyzed by hydronium ions obtained by protonation of water by protons of the zeolite,[107] and not necessarily by the proton bounded to the zeolite itself (as it will be discussed in more details in section 8.7). Thus, for E2 mechanisms in such conditions, the zeolite framework is not expected to restrict the elimination to the syn periplanar conformation, and the more favorable antiperiplanar elimination may be allowed. The observed differences in reactivity observed for trans and cis 2-methylcyclohexanols were thus assigned to the existence (in the case of the cis isomer) of absence (in the case of the trans isomer) of the antiperiplanar configuration leading to the Saytzeff (more substituted) *versus* Hofman (less substituted) products.[669] The impact of the zeolite on the reaction mechanism was found to be low compared to a H_3PO_4 solution with respect to the mechanism involved, but confinement effects were found to play a role on the intrinsic enthalpy barrier for ZSM-5 catalyst (111 $kJ.mol^{-1}$ versus 129 $kJ.mol^{-1}$ in H_3PO_4 for the dehydration of cis-2-methylcyclohexanol).[669,672] The FAU and *BEA frameworks usually leads to higher intrinsic activation enthalpies with respect to MFI, but to more positive activation

entropies, assigned to the larger pore size, smaller confinement effect, and much less constrained transition state, itself of larger size with respect to the reactant.[669,672] In all cases, zeolites are much more active than a H_3PO_4 solution. Static DFT simulations of the E1 *versus* E2 dehydration paths of cyclohexanol were performed in zeolite Beta, and in the presence of water. They confirm the experimental deduction according to which the E1 mechanism is most probable in this case, the transition state for the deprotonation of the intermediate secondary carbenium ion being the limiting one (**Figure 50-b**).[670] More recently, strong framework-dependent solvent effects were reported both on the mechanisms and on the reaction kinetics for cyclohexanol dehydration.[673] In apolar solvent (decalin) and in ZSM-5, the mechanism is likely an E2 elimination, with negative activation entropy, whereas it seems to remain E1 in *BEA and FAU. The reaction rates are much higher in decalin than in water for *BEA and FAU, which is tentatively assigned to a shift from carbenium-base mechanisms in water to alkoxide-based mechanisms in decalin. The lower rate measured for MFI, and the shift to a E2 mechanism, is interpreted as the impossibility of decalin to co-adsorb with cyclohexanol in the MFI framework, due to the smaller pore-size, inducing a reduced stabilization of the alkoxide intermediates by van der Waals interactions with decalin compared to the situation in *BEA and FAU where decalin can co-adsorb.

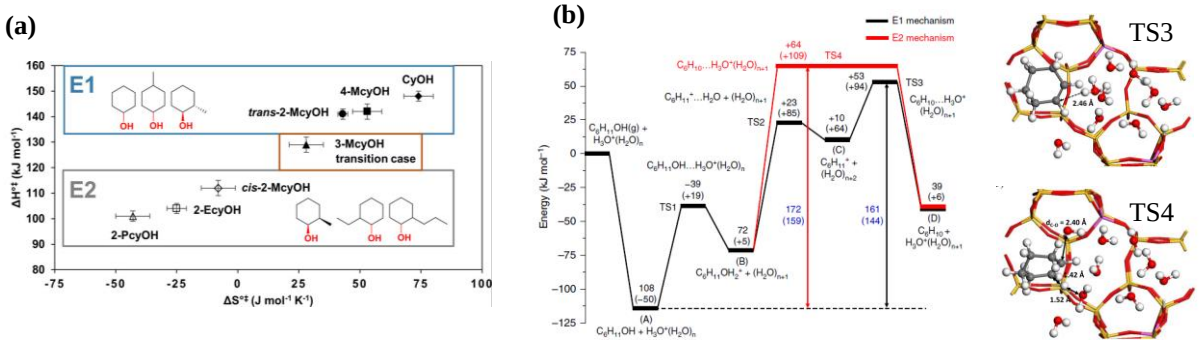

Figure 50. Dehydration of (substituted) cyclohexanol in water, catalyzed by zeolites: (a) compensation effect observed from various substrate, with H-ZSM-5 as a catalyst, and proposed mechanisms (E1 *versus* E2). Reprinted with permission from ref [669]. Copyright 2017 American Chemical Society. (b) Energy diagram computed by periodic static DFT of cyclohexanol dehydration in zeolite Beta, in the presence of a $H_3O^+(H_2O)_7$ acid species.

The structure of TS3 (limiting in the case of the E1 mechanism) and TS4 (E2) are shown. Reprinted from ref. [670]. Licensed under CC BY 4.0.

Thus, from most recent experimental and theoretical works, the co-existence of E1 and E2 mechanisms appears to depend on the alcohol, zeolite, and location of active site under consideration. From the computational point of view, to the best of our knowledge, so far only static investigations have been reported. Further insight from AIMD will be welcome to conclude more firmly about the preferred reaction paths in the cases where this remains ambiguous from experimental considerations. Regarding the external surface sites, a wider investigation accounting for the variety of structures and confinement effects would also be useful.

8.4. Bimolecular mechanisms: formation of ethers and their decomposition

As two alcohol molecules are required, intermolecular dehydration of alcohols into ethers takes place in higher reactant concentration ranges with respect to the intramolecular mechanism, tuned by the operating conditions (pressure, temperature, conversion levels).[611,653,660] A strong impact of the nature of the alcohol with respect to the pore size of the zeolite is observed. For example, the 8MR pocket of Mordenite was found to be unsuitable for the formation of ethers, contrary to the 12MR channel.[674] The ether formation route is strongly inhibited in zeolites exhibiting 8MR pores (eg. Mordenite) for ethanol,[674,675] 1-butanol and isobutanol,[676] where only the corresponding alkene is formed. In zeolites with larger pores, such as ZSM-5 and Faujasite, the intermolecular route is favored, and the ether is the major product in some cases, in particular with ethanol below 550 K.[611,674]

Intermolecular dehydration is expected to take place by nucleophilic substitution. It may proceed through a S_N1 mechanism, which, like the E1 mechanism mentioned in the previous

section, exhibits a carbenium intermediate (or its alkoxide equivalent) that then undergoes a nucleophilic addition by a second alcohol molecule. This kind of proposal has also been called the "dissociative" pathway (**Figure 51**). Alternatively, a S_N2 mechanism may take place, where the addition and the departure of the leaving group (here, water) take place synchronously. This has also been called the "associative" pathway. It is proposed to start from the protonated alcohol dimer depicted in **Figure 49-c** and **Figure 51**.

It was often suggested, from IR and NMR considerations, that ethers are formed by condensation of alcohol with alkoxy species,[611,650,653] meaning that a S_N1 mechanism would take place. Earliest cluster theoretical studies considered the formation of dimethylether from methanol, and compared the dissociative and associative mechanisms.[677,678] The methoxonium ion ($CH_3OH_2^+$) was found to be a transition state before formation of the alkoxide in the case of the dissociative mechanism, but this was contradicted later by periodic DFT calculations, which conclude to its reaction intermediate nature.[679] However, in many studies, the associative mechanism appeared to be the most favorable from computed energy and free energy profiles.[677,678,680] One exception is a periodic investigation performed for DME formation in the TON framework at the RPBE level, that favored a S_N1 mechanism over S_N2.[681] Preference of the dimer mediated mechanism was also computed in the case of diethylether formation from ethanol,[618,660] both by cluster and periodic DFT calculations, and in the case of 1-butanol transformation into butyl-ether.[632]

Experimentally, the role of dimeric ethanol species in the production of di-ethylether, was addressed by Chiang et al.[674] An ethoxy-mediated mechanism was excluded in MFI and MOR on the basis of co-feeding experiments with ethylene, the latter increasing the concentration in ethoxy species, but having no effect on the di-ethylether formation rate. Observing a zero-order in ethanol for the formation of the ether for MFI, MOR and FER, the authors again excluded the participation of an ethoxy mediated mechanism and concluded in

favor of an ethanol dimer mediated mechanism. Zero order indeed reflects the transformation of a dimer into a dimerized transition state, whereas first order would characterize the transition from a {methoxy, gaseous methanol} or {adsorbed methanol, gaseous methanol} pair into a similar dimerized transition state. Similar conclusions were made afterwards, for ethanol,[647] and methanol[682,683] in various zeolites. Notably, one could imagine a zero order in the case where the kinetically relevant intermediate would be a {methoxy, adsorbed methanol} pair, but DFT calculations reported in **Figure 51** show that such a species is less relevant than {methoxy, gaseous methanol} and {adsorbed methanol, gaseous methanol} pairs.

Thus, theoretical and experimental findings generally concur in the associative mechanisms. Several factors appear to moderate such a clear conclusion. First, in the case of dimethylether formation from methanol, the preference for the associative *versus* dissociative mechanism in MFI and CHA was shown to depend on temperature[680,683] and methanol pressure,[644,680,683] thanks to periodic DFT calculations coupled with kinetic analysis relying on the free energy profiles. The dissociative mechanism dominates at low methanol pressure and high temperatures but the associative one becomes quicker at higher methanol pressures/low temperature (typically, 0.004 MPa at 415 K in CHA[644]). This shift indicates higher activation enthalpy but also entropy for the dissociative mechanism.

In ZSM-5, the dependence of the transition temperature with respect to the location of the active site (straight *versus* sinusoidal channel, or their intersection) induces a temperature interval where both kind of mechanisms may co-exist in the same catalyst.[680] Kinetic modelling fitted on temporal analysis of products (TAP) results indicate that the ethoxy-mediated formation of di-ethylether is dominant over the ethanol dimer one.[684] The dissociative pathway was also shown experimentally to become quicker in the presence of paired aluminum sites *versus* isolated sites (tuned by the zeolite synthesis procedure).[685] Similarly, the preferred mechanism was suggested by operando infra-red spectroscopy to differ depending on the Al

distribution in H-ZSM-5 samples (estimated by the Co^{2+} titration method mentioned in section 2.2). The ethanol dimer mediated mechanism would be favored in case of isolated Al atoms, whereas ethoxy-based mechanisms (also producing ethylene) would prevail in the case where two aluminum atoms co-exist in a ring of the framework.[686] This was assigned by the authors to the enhancement of hydrogen-bonds thanks to Al-O-(Si-O)-Al units, stabilizing the second ethanol molecule, although it is unclear why this should not stabilize the protonated dimer too.

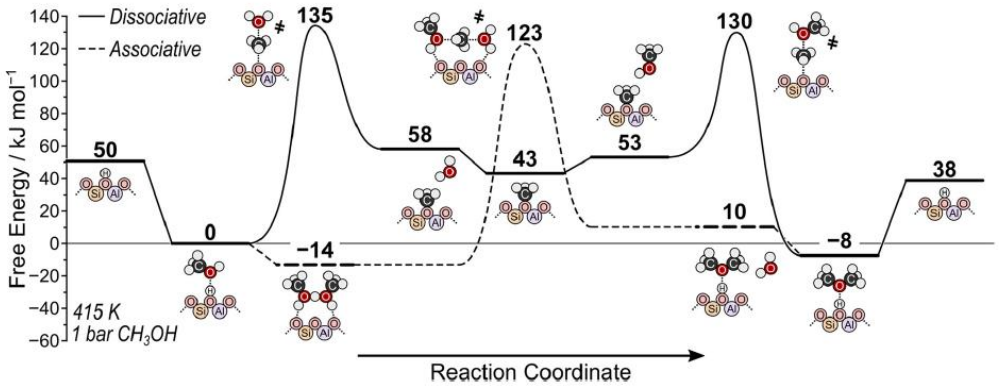

Figure 51. Free energy profile computed by periodic DFT for methanol dehydration into di-methylether in CHA at 415 K and 0.1 MPa of methanol. Reprinted with permission from ref. [644]. Copyright 2019 Elsevier.

Changing the zeolite framework tunes confinement effect, that appears to be influential for first order rate constants for DME formation (at low methanol pressure), but not at high methanol pressure, when the rate is zero order in methanol.[687] At high pressures, the most abundant species is the dimer, and confinement effects indeed compensate between the dimerized reactant and dimerized transition state for the associative mechanism. Conversely, at low pressures, the monomer is the most abundant resting state, that is less sensitive to confinement effects than the transition state (involving the second methanol molecule), which makes the first-order rate constant increase as the van der Waals interaction energy with DME (used as a proxy for the transition state) increases, as probed on FAU, *BEA, SFH, MTW, MOR, MTT and MFI frameworks. Confinement effect changes were also believed to be at the

origin of variations in the local equilibrium constants in the pores for DME formation from a monomer of adsorbed methanol and gas phase methanol, comparing USY zeolites obtained by steaming or further treated by hexafluorosilicate: residual EFAls in the former sample were thought to re-inforce confinement, thus explain higher equilibrium constants in the pores.[544] One may, however, wonder whether a similar synergetic effect as that invoked for alkane cracking (section 6.4) could not play a role.

At the external surface of the CHA framework, Lewis acid sites are expected, and were recently modeled by periodic DFT calculations corrected by a cluster CCSD(T) approach, as well as their reactivity in methanol dehydration into DME.[626] The alcohol is adsorbed by coordination of the hydroxyl group to a surface tricoordinated aluminum atom (Al_{III}), and a an "associative" pathway is found for the formation of DME. However, the free energy barrier of this pathway is computed to be higher than that of a dissociative pathway catalyzed by the external surface bridging OH groups, and bulk bridging OH groups. Considering that lower dehydration rates are measured on 2D nanosheets compared to the 3D catalysts on H-ZSM-5 samples in conditions where di-ethylether is formed from ethanol through the associative mechanism, Kadam et al.[647] suggested that the transition state is less stabilized at the external surface than in the bulk, likely due to a decreased electrostatic confinement effect.[80]

Finally, the effect of the acid strength was systematically addressed in the case of the MFI framework, along the (Al, Ga, Fe, B) framework atom series,[362] revealing a significant dependence of DME formation first-order rate constant with the deprotonation energy, in line with a strong stabilization of the ion pair transition state as the acidity of the site increases (and consequently, the stability of its conjugated base also increases). This dependence is attenuated for the zero-order rate constant as the reactant state itself (the protonated methanol dimer) is similarly stabilized as the transition state. Such dependence of DME formation rate constants with acid strength was also demonstrated computationally for the TON framework substituted

by Al, Ga or In, with a linear dependence of the activation energy with respect to ammonia protonation energy, in the case of the dissociative pathway.[681]

Notably, ether species themselves are likely reactive towards further addition of alcohol molecules. The triethyloxonium ion was indeed observed in ZSM-5 in the course of the dehydration of ethanol at 493 K, with a characteristic signal at 85 ppm (**Figure 52**) assigned thanks to the combination of 2D ^{13}C-^{13}C INADEQUATE MAS NMR and periodic DFT calculations.[688] It was attributed to the ethylation of diethylether. It was also suggested that the decomposition of the triethyloxonium ion above 473 K gives rise to a diethylether molecule plus an ethoxy species, the latter being considered as the precursor of ethene (see section 8.3) in this study. Notably, similar trimers were observed in the case of methanol before.[689]

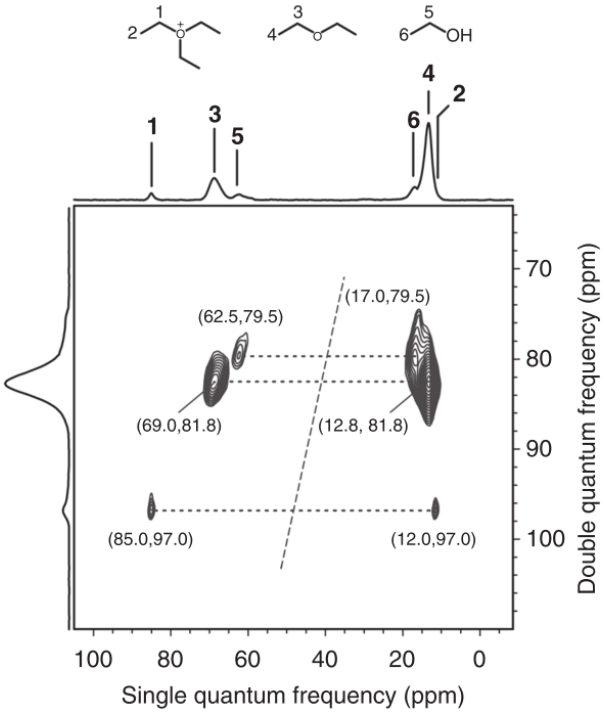

Figure 52. 2D ^{13}C-^{13}C INADEQUATE MAS NMR spectrum of H-ZSM-5 reacted with ^{13}C labeled ethanol at 493 K for 4 seconds, revealing the presence of the triethyloxonium ion. Reprinted from ref [688]. Licensed under CC BY 4.0.

8.5. Ether decomposition versus direct alcohol dehydration

Ethers other than DME can be decomposed into one alkene molecule plus one alcohol molecule. DFT calculations shows that this proceeds by protonation of the ether, followed by elimination of the alkene and alcohol desorption.[632,660] When such a mechanism takes place, the alkene may thus be produced by two competitive routes: direct dehydration or ether decomposition.[611,619]

Thanks to the combination of periodic DFT calculations and of microkinetic modelling based on the findings and data of the DFT calculations, Alexopoulos et al.[660] showed that in the case of ethanol dehydration in H-ZSM-5, ethylene is produced mainly by monomolecular dehydration above 500 K, whereas below 500 K the decomposition of di-ethylether contributes significantly to the formation of ethylene. 5 kinetic parameters over the 40 determined from *ab initio* in ref. [660] were adjusted to improve the fit with experimental data obtained by TAP.[684] These adjustements lead to a predominance of the di-ethylether-mediated ethylene formation over a large temperature range (473-573 K), in line with cofeeding experiments with diethyl ether and ^{13}C labeled ethanol, in the TAP operating conditions.

A similar approach coupling DFT calculations and microkinetic modelling was undertaken in the case of dibutylether decomposition *versus* direct 1-butanol decomposition into butene in ZSM-5.[632] It reveals that in the 400-460 K interval, the ether mediated mechanism prevails. Comparison with experimental selectivities[653] indicates an accurate prediction of the ether formation rate, but an underestimation of the rate of formation of butene by one order of magnitude. A clear effect of the zeolite topology was later computed in terms of balance between direct dehydration of 1-butanol and the ether mediated one, comparing the FAU, MFI, TON and FER frameworks.[664] Over the series, FAU and FER were found to induce larger butene/ether selectivity, but for very different reasons. FAU induces a too low confinement effect for the stabilization of the butanol dimer required for the formation of the ether, making

the direct dehydration of 1-butanol competitive. In FER, steric constraints within the 8MR channel destabilizes the ether that quickly decomposes into butene and butanol. MFI and TON offer the best stabilization of the ether, together with higher ether decomposition barriers, thus explaing their higher ether selectivity.

Thus, reaction conditions, bulkiness of the starting alcohols and of the ether products, as well as framework topology, are key in controling the alkene/ether selectivity, itself a consequence of the prefered route for alkene formation (direct of via the ether). DFT coupled with microkinetics appeared to be a very powerful tool to unravel these questions. Together with the impact of the operating conditions, deviations with findings from experiments raise again the question of the impact of the level of theory and of the sampling method (static *versus* AIMD) on the values of free energy barriers. Small deviations may have a strong effect on selectivity predictions.

8.6. Dehydration combined to skeletal isomerization

Starting from alcohols containing four carbon atoms, the question of the alkene isomers obtained can be raised. Indeed, the propensity of skeletal rearrangements in dehydration conditions are commonly observed from bulky alcohols.[690]

On catalysts such as alumina, isobutanol dehydration produces exclusively the expected isobutene isomer.[609,624,691] However, variable yields of linear butenes are obtained with zeolite catalysts, that depend on the zeolite topology, and on operating conditions.[676] The behavior of the Ferrierite zeolite was experimentally investigated in details in that respect, as a high selectivity (> 80%, higher than the equilibrium distribution) for linear butenes starting from isobutanol was measured.[624,625] Conversely, it is known that Ferrierite is a very efficient catalyst for the skeletal isomerization of linear butenes to isobutene (section 5.5),[436,442,692,693] which seems contradictory with the results obtained for isobutanol dehydration. It was moreover

shown that in similar reaction conditions, butene isomerization is much slower than isopropanol dehydration.[624,694] For all these reasons, the *a posteriori* isomerization of isobutene into linear butenes cannot explain the formation of linear butenes from isobutanol. Notably, starting from butan-1-ol, isobutene can be obtained in other zeolites, such as Theta-1 and ZSM-23, in conditions where the isomerization of butenes is not expected.[695] The isomerization was proposed to proceed right after the formation of primary carbenium ions from isobutanol, without the formation of isobutene as a primary product.[624,625,694] It remains, however, unclear why this primary carbenium ion should be formed easier from the alcohol rather than from the alkene (section 5.5).

In the periodic DFT calculations study of the dehydration of 1-butanol by John et al.[665,666] monomolecular 1-butene isomerization steps, producing 2-butenes and isobutene, were also considered. The formation of isobutene in particular, was investigated through mechanisms involving alkoxides. This appeared to be a minor reaction route thanks to *ab initio* microkinetic modelling. Isobutanol dehydration was also addressed by the same research group in ZSM-5, but the formation of isobutene only was considered.[696] Recently, new monomolecular dehydration routes of butanols were found by periodic DFT calculations performed on the model CHA framework, that are likely to explain the formation of linear alkenes from isobutanol, without relying on *a posteriori* isomerization of alkenes.[667] The most likely ones consist either in first, isomerization of isobutanol into butan-2-ol, then dehydration of the latter into linear but-1-ene and but-2-enes (**Figure 53-a**). Following the energy span concept, this mechanism is more likely than alkoxide-mediated routes, whereas butene isomerization is shown to have a much larger activation barrier than the two latter options. A synchronous dehydration and skeletal isomerization mechanism was also discovered (**Figure 53-b**).

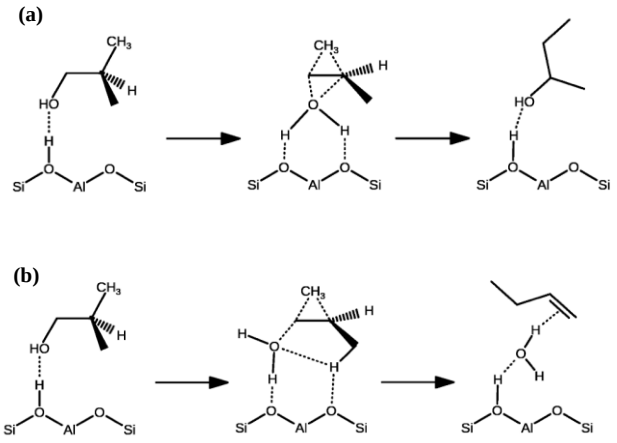

Figure 53. Mechanisms found by periodic DFT explaining the formation of linear butenes from isobutanol: a) isomerization of isobutanol into buta-2-ol, b) synchronous dehydration and isomerization. At the center, the structure of the transition state is depicted. Reprinted with permission from ref. [667] Copyright 2022 Elsevier.

8.7. Effect of water in the dehydration of alcohols

The effect of the presence of water in the reactions of dehydration of alcohols is of a large interest since a) water is one product of the reaction, and thus is inevitably present once the conversion reaches a significant level ; b) in many applications, alcohols originate from biomass, and more specifically from the fermentation of sugars that is carried out in water, i.e. water is always present in such alcohol streams unless a costly drying step is performed;[697] c) from a process point of view, co-feeding water as a thermal buffer is a potential way to mitigate the endothermicity of the reaction. Additionally, the dehydration of some alcohols could advantageously be carried out in liquid water as a solvent, where specific behaviors are expected. Thus, several studies are devoted to deciphering the effect of water during alcohol dehydration in the porosity of zeolites.

In most reports in the literature, water is found to have an inhibitory effect on the alcohol dehydration,[698] which is typically demonstrated experimentally by co-feeding increasing quantities of water to the alcohol stream and monitoring a decrease in the reaction rate. This was observed for both intra- and intermolecular dehydration routes. However, the inhibition is less severe with zeolitic catalysts such as H-ZSM-5 with Si/Al ratio of 50 than it is for Lewis

acidic catalysts, such as γ-alumina, and it becomes almost negligible with a Si/Al ratio of 150.[699] The authors assign this observation to the fact that purely Brønsted acidic sites in H-ZMS-5 are actually not inhibited by water to a large extent, contrary to residual Lewis acidic sites that contribute to the reaction. It should also be noted that in some cases, especially when the alcohol partial pressure and the reaction temperature are relatively high, an increase in the activity, selectivity and/or stability in dehydration are observed upon co-feeding water.[625,700,701] A proposed explanation lies in the moderation of the strong acidic sites of the zeolite by water, which limits the deactivation mechanisms such as the formation of coke. This partly explains why despite the intrinsic inhibitory effect, from a process point of view, the addition of water in the stream may still be beneficial.[625,701]

Two main hypotheses are invoked to explain the inhibition effect : i) a competitive adsorption of water and the alcohols on the active sites and ii) an inhibition caused by the interactions between the alcohol and co-adsorbed water at the active site.[643,661] Although the former would be compatible with the -1 partial order with respect to water observed in the frame of a Langmuir-Hinshelwood kinetic model,[632,666,674,702] several reports have convincingly shown that water is essentially unable to displace alcohol molecules adsorbed on the acidic sites of the zeolites, at least when alcohol and water are present in the same range of partial pressures. This was proven by successive adsorption of water and alcohol (or reverse) monitored by IR-spectroscopy,[643,703,704] and is supported by the significantly more negative adsorption enthalpies of alcohols vs. water (typically -115 $kJ.mol^{-1}$ for methanol, -130 $kJ.mol^{-1}$ for ethanol, -120 $kJ.mol^{-1}$ to -140 $kJ.mol^{-1}$ for 1- propanol vs. -55 $kJ.mol^{-1}$ for water, from molecular modeling or calorimetry data).[643,655] This is all the more true when the alcohol is heavy since the adsorption enthalpies typically decrease with alkyl chain.[655,703]

An inhibition through the interactions between alcohol and co-adsorbed water was studied in details by Lercher and coworkers.[643,661] Through a combination of kinetic analysis

and calorimetry,[643] they demonstrated that the co-feeding of water causes the increase of the enthalpy of activation of both intra- and inter-molecular dehydration of 1-propanol in H-ZSM-5 (to propene and dipropylether, respectively). This could be assigned to a strong energetic stabilization of propanol by co-adsorbed water in the porosity of the zeolite, while the transition state is little-to-no stabilized. The effect holds true whether considering a propanol monomer dehydrating to propene or a dimer dehydrating to the ether (**Figure 54**), and they tentatively assign this inhibition effect to the formation of water-alcohol dimers, or water-alcohol-alcohol trimers.

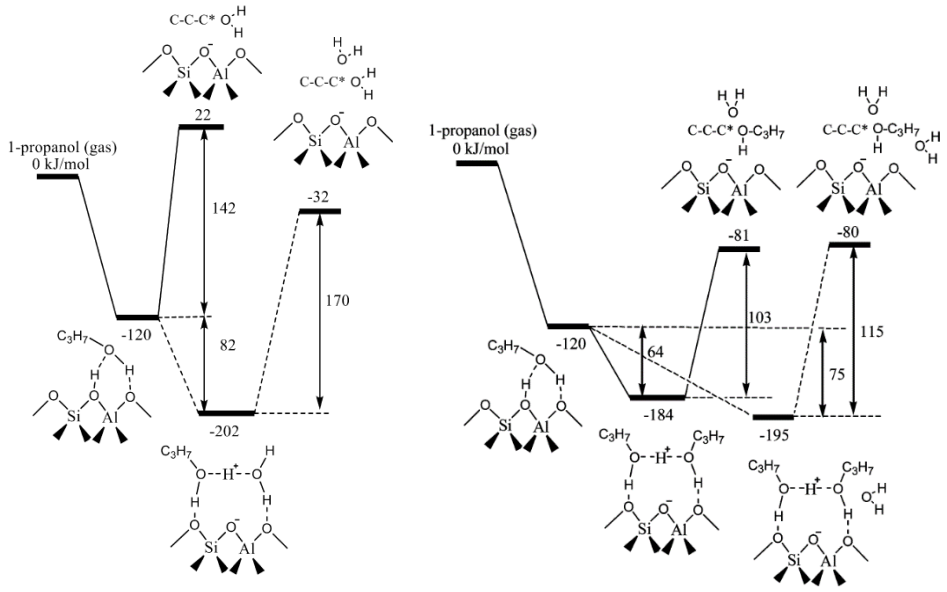

Figure 54. Schematic energy diagrams for the intra-molecular dehydration (left) and inter-molecular dehydration (right) on H-ZSM-5 in the presence (solid lines) and absence of water (dotted lines). Reprinted with permission from ref [643]. Copyright 2015 American Chemical Society.

A later DFT study considered the effect of two to four water molecules in the vicinity of a Brønsted acid site on propanol dehydration.[661] With two water molecules, they could confirm their previous experimental conclusions, and provide molecular models to substantiate the strong interaction through hydrogen bonding between water and alcohol co-adsorbates. The

presence of water stabilizes the alcohol adsorption (from -151 kJ.mol^{-1} to 188.kJ.mol^{-1} without and with co-adsorbed molecules) which causes an activation barrier increase from 135 kJ.mol^{-1} to 172 kJ.mol^{-1}. Further, using AIMD simulations and static calculations, they show that from three water molecules on, the proton from the zeolitic acid site is more easily transferred to the water cluster than to the alcohol, making of the protonated cluster $H^+ \cdot (H_2O)_n$ the active catalyst. The existence of protonated water cluster as active sites in zeolites when the presence of water increases was debated in a number of instances,[107,669,670,705–709] and reports concur to show that they form from 3 or 4 water molecules on in the porosity. In the case of the dehydration of propanol, it was shown that this further stabilizes the system and yields even higher energy barriers (209 kJ.mol^{-1}).[661]

Water inhibition in gas-phase dehydration of alcohols is found to be of -1 order with respect to water on a large range of water partial pressures, however, increasing the water pressure (P_{H2O} = 0.01-0.1 MPa) causes more severe inhibition.[710] A molecular-level explanation for this phenomenon was proposed considering the formation of protonated water clusters. Increasing water pressure increases the size of these clusters, which eventually induce stabilizing interactions between neighboring clusters. Such interactions further stabilize the adsorbed state of alcohols with respect to transition states for their dehydration, which further increase the activation barriers and thus reduces the rates. The characteristics of the zeolite pore structures (pore diameter, undulation parameter) has a large effect in this regard, as in larger pore zeolites the interactions between clusters will occur at higher water partial pressures, and so does the severization of water inhibition.[710] Likewise, acid site density is also expected to play a role, as increasing site density will shorten the distances between the clusters and hence favor their interactions.

When the reaction is performed in liquid water, such as in the case study of cyclohexanol dehydration mentioned in section 8.3, water forms hydronium clusters with up to 8 water

molecules $H^+ \cdot (H_2O)_8$ in H-ZSM-5.[669,670] These clusters form hydrophilic domains that restrict adsorption of cyclohexanol to the water-free (nonpolar) domains (see **Figure 55-A**),[711] hence reducing both adsorption capacity and affinity (adsorption strength). The effect is even more pronounced when the mean distance between BAS, hence between the clusters, is shorter. This was shown by measuring adsorption capacities for H-ZSM-5 of different Si/Al ratios (**Figure 55-B**). Nevertheless, as mentioned above, the presence of coadsorbed water and the formation of such protonated clusters may have a positive effect on dehydration of cyclohexanol (and possibly other alcohols) by facilitating proton transfer and allowing antiperiplanar eliminations, which are typically kinetically more favorable compared to the water-free situation where the elimination is restricted to be synperiplanar.[712]

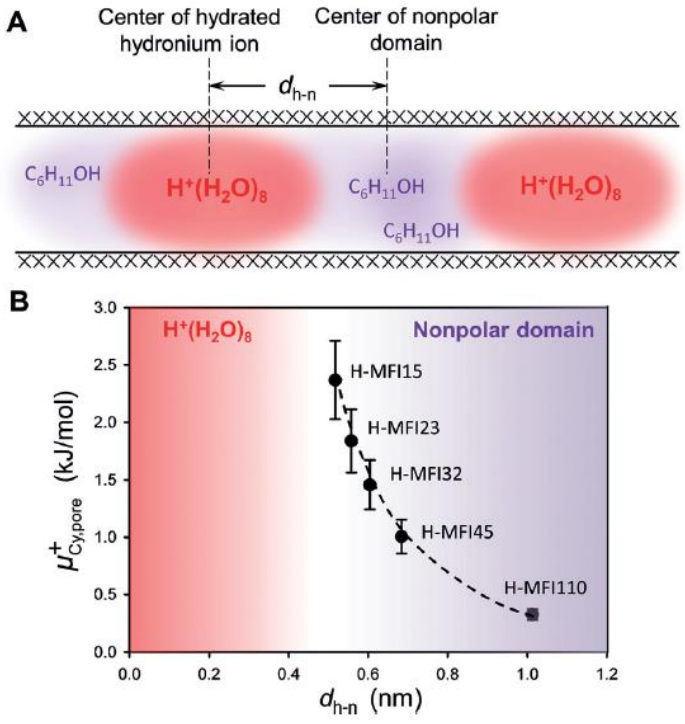

Figure 55. A- Schematic representation of the polar (protonated water clusters) and nonpolar domains within the H-ZSM-5 channels; $d_{h\text{-}n}$ is the average distance between the two types of domains B- Chemical potential of adsorbed cyclohexane as a function of $d_{h\text{-}n}$ evolution with Si/Al ratio of H-ZSM-5. Reprinted with permission from ref [711]. Copyright 2019 John Wiley and Sons.

8.8. Dehydration of polyols – the case of glycerol

Polyols are molecules of increasing interest as they are typical products of biomass conversion, in particular hydrogenolysis of sugars or transesterification of vegetable oils. They can also undergo dehydration reactions, which may lead to various partially deoxygenated products of interest. In that case, the selectivity toward a given product depends on the first hydroxyl group that will undergo the dehydration, hence raises the question of the regioselectivity of the dehydration.

Glycerol is a prototypical polyol originating from the transesterification of vegetal oils to form fatty esters. Converting glycerol with a dehydration catalyst yields several products, including acrolein which is very valuable for its application in the preparation of acrylic acid or DL-methionine.[713–716] Zeolites have been considered as possible Brønsted acidic catalysts able to promote this reaction, typically in gas-phase dehydration carried out in the range 573-673 K, *i.e.* relatively high temperatures.[717–720] **Figure 56** shows the different possible products from acid-catalyzed dehydration of glycerol. Depending on whether the primary or secondary hydroxyl group undergo the first dehydration, different intermediates are obtained. A first dehydration of the primary hydroxyl group yields 2-propene-1,2-diol, which tautomerizes into 1-hydroxy-2-propanone (acetol or hydroxyacetone). This compound is not reactive towards dehydration (no hydrogen atom in β position), hence is found as a byproduct, usually less valuable than acrolein. If the first dehydration takes place on either of the secondary hydroxyl groups instead, propene-1,3-diol is obtained, which tautomerizes into 3-hydroxy-1-propanal (HPA). The latter product is susceptible to undergo a second dehydration that yields acrolein. It may also undergo a retro-aldolization reaction that yields acetaldehyde and formaldehyde. The former is also often observed as an undesired byproduct. Formaldehyde on the contrary is scarcely monitored, but it may decompose to H_2 and CO under such reaction conditions. Alternatively, in liquid-phase reaction, the formation of ethanol is observed, which is proposed

to stem from the hydration of 3-hydroxypropanal followed by C-C bond scission. Other side reactions include the formation of polyaromatic products (within the zeolitic pores) or polyglycols (on the external surface) that generate catalyst deactivation.[721–724]

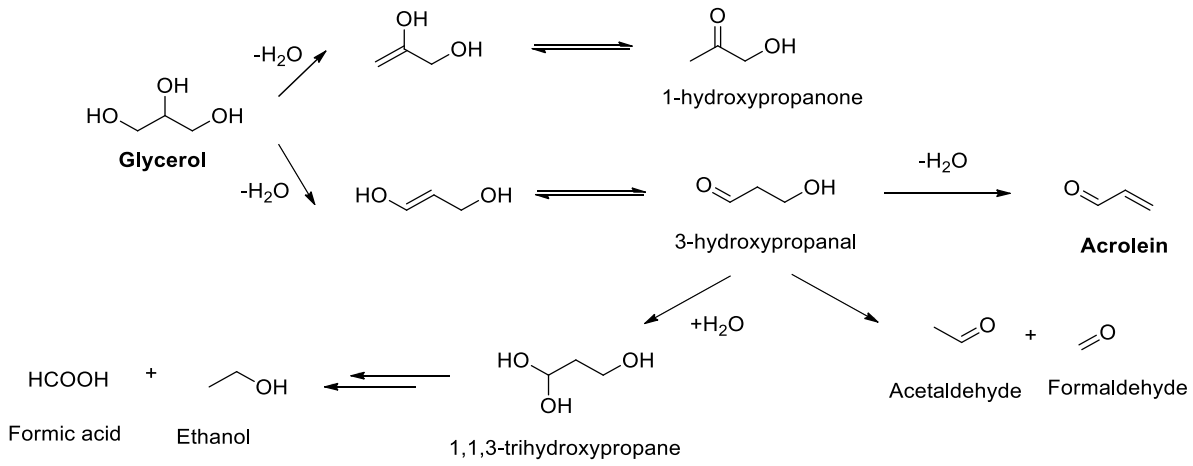

Figure 56. Reaction scheme for acid-catalyzed dehydration of glycerol.

In zeolites, like with many Brønsted acidic catalysts, acrolein is usually found as the major product, with only small quantities of 1-hydroxypropanone (acetol). Using FTIR spectroscopy, Yoda et al. observed the interactions of glycerol adsorbed from gas-phase on H-ZSM-5.[725] They conclude from their experiments that adsorption of glycerol on the BAS is favored on the secondary OH group and detected only acrolein as a product at low temperature (353 K). This observation was confirmed by DFT calculations using rather large cluster models (128 T sites), showing that adsorption on the secondary hydroxyl group is (slightly) more favorable than on the primary (see **Figure 57**, adsorption energies of -177 kJ.mol^{-1} and -164 kJ.mol^{-1}, respectively).[726] Note that this is contradiction with the periodic DFT modeling results obtained by Yun et al.[727] on an amorphous silica-alumina model based on the β-cristobalite model (adsorption energies of -152 kJ.mol^{-1} and -191 kJ.mol^{-1} for adsorption on the secondary and primary OH group, respectively). This might be due to the effect of the structure of the zeolite, particularly a more pronounced steric hindrance between the zeolite

walls and the glycerol in case of adsorption on the primary hydroxyl group. Regarding the first dehydration, the E1 mechanism with an alkoxide intermediate is found more favorable over the E2,[726] concerted elimination. Surprisingly, the activation barrier for the formation of the alkoxide from either of the possible adsorbate (primary of secondary OH group) is competitive, and little difference of stability between the primary and secondary alkoxide is calculated, thus this step is not discriminating. However, the hydrogen abstraction from the alkoxide intermediate is kinetically more favorable from the secondary alkoxide than from the primary (**Figure 57-c**).

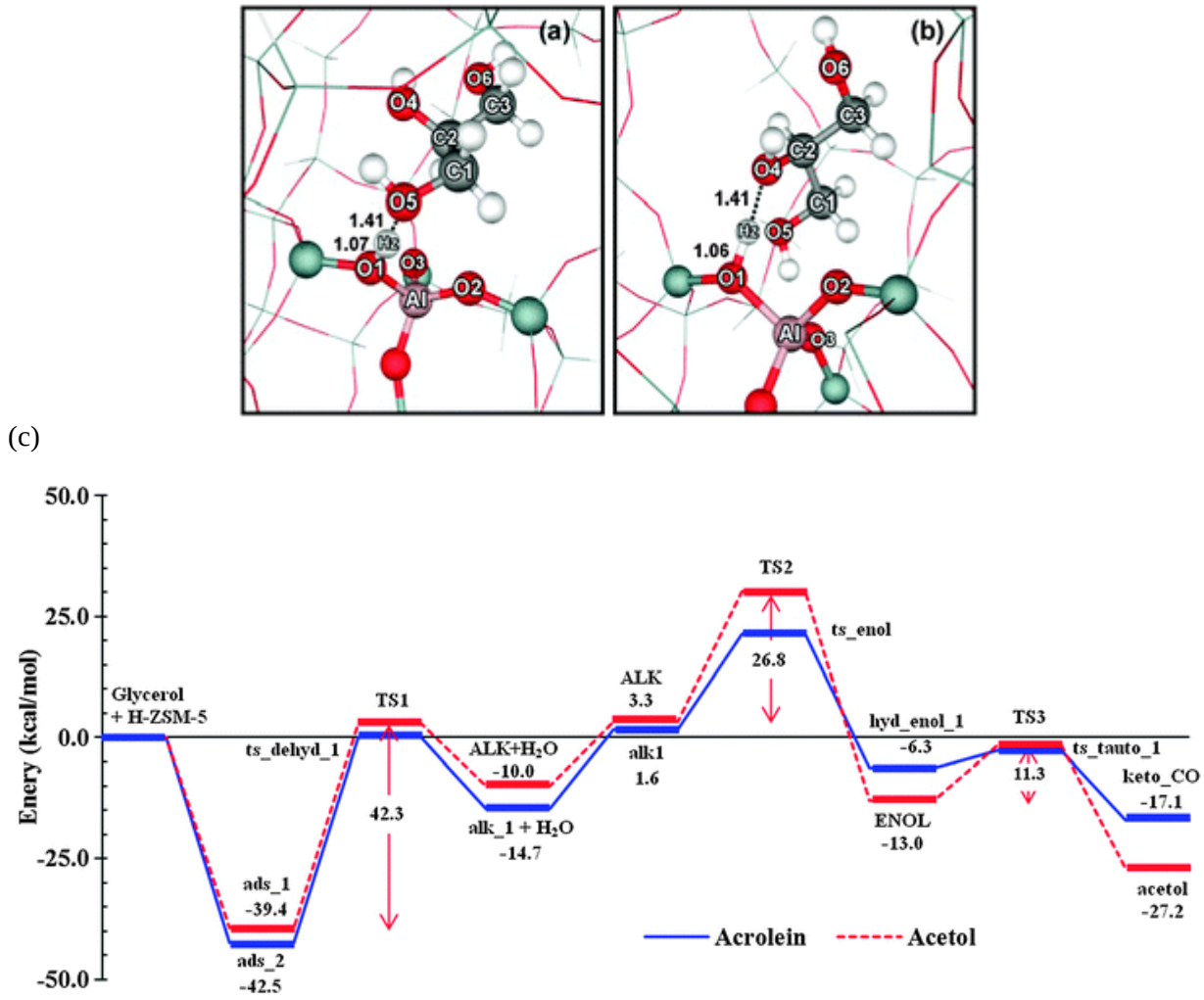

Figure 57. DFT modeling of glycerol adsorption and reactivity on H-ZMS-5 (cluster model). (a) and (b): adsorption of glycerol on the primary (ads_1) and secondary hydroxyl groups (ads_2), respectively. (c) Energy diagram for acetol and acrolein formation pathways (first dehydration only is shown). In the case of the acrolein route, the pathway ends at the intermediate 3-hydroxypropanal, herein noted "keto_CO". Reproduced with permission from Kongpatpanich et al.[726] Copyright 2011 Royal Society of Chemistry.

Thus, overall, the energetic span for this first dehydration is in favor of the formation of the 3-hydroxypropanal intermediate of the acrolein route. In fact, according to a number of reports,[728,729] dehydration on the primary hydroxyl group, and thus acetol formation, exclusively occurs on residual Lewis acidic sites in zeolites. Additionally, Wang et al. showed an existing synergy between Lewis and Brønsted acidic sites in the production of acrolein in ZSM-5 zeolites, by showing an increased catalytic activity in zeolites with purposely added EFAl species (Al/H-ZSM-5) compared to the parent H-ZSM-5 catalyst.[730] The authors proposed that the additional EFAl species act as Lewis acidic sites and promote the second dehydration on the primary hydroxyl group of 3-hydroxypropanal.

The side routes involving the cleavage of C-C bond, including the formation of acetaldehyde or ethanol, are currently poorly understood, as very few works address their formation on a mechanistic point of view, although these products may account for a significant part of the conversion. Noticeably, Lin et al. proposed and calculated several possible C-C cleavage mechanisms, including direct retro-aldolisation like mechanism or rehydration to 1,1,3-trihydroxypropane (THP) followed by elimination of formic acid and ethylene, the latter compound yielding ethanol upon rehydration.[731] However, they surprisingly considered that the retro-aldol condensation as well as the rehydration to THP should occur in homogeneous phase, *ie* that they do not involve the participation of the zeolite catalysts, although one may argue that both reactions can be catalyzed by solid Brønsted acidity. Under this assumption, they conclude from their calculations that C-C cleavage occurs more favorably through THP as an intermediate rather than through direct retro-aldol condensation, which explains the formation of ethanol in their experiments. This pathway is competitive with direct dehydration of hydroxypropanal, or alternatively to dehydration of THP, both leading eventually to acrolein. Corma and coll.[719] discarded the retro-aldolisation mechanism as the origin of fragmentation

species such as acetaldehyde from their experimental observation that very little quantities of formaldehyde or methanol are observed. Besides, the measured H_2/CO molar ratio is much lower than unity, which is expected form decomposition of formaldehyde. They proposed that acetaldehyde is generated by a decarbonylation of a propanedione (1,3-propanedione or 1,2-propanedione, although neither was observed experimentally) generated upon an unspecified hydrogen-transfer reaction (Meerwein-Ponndorf-Verley-like, supposedly) on either hydroxypropanal or acetol. No detailed, molecular-level mechanism is proposed, though.

8.9. Dehydration of sugars

8.9.1. General mechanistic aspects

Moving further in complexity regarding Brønsted-catalyzed transformation of polyfunctional molecules is the field of the conversion of bio-based carbohydrates, and more specifically the dehydration of sugars into platform molecules.[732–736] The most widely targeted molecules from sugars are the furanic compounds, furfural (FF) or 5-hydroxymethylfurfural (5-HMF), usually (but not exclusively) obtained from a straight dehydration of pentoses (xylose being the most abundant in the lignocellulosic biomass) and hexoses (with glucose and to a lesser extent fructose being the most abundant in biomass), and levulinic acid stemming from the acid-catalyzed rehydration of 5-HMF, formic acid being the byproduct (**Figure 58**). The latter reaction occurs in the same conditions as the dehydration of hexoses to 5-HMF provided that enough water is present in the reaction medium (usually when water is used as the solvent of the reaction), so that levulinic acid is often observed as a secondary product in hexoses dehydration. Additionally, the reactions are accompanied with the formation of undesired oligomeric sugars or higher, more dehydrated compounds referred to in the literature as "humins",[737–739] which can possibly cause deactivation of a heterogeneous catalyst.

The interest of the molecules mentioned (5-HMF, FF, and levulinic acid) for a wide range of applications is well explained in a number of recent reviews,[733,740–743] and their production can also be catalyzed by Brønsted acidic zeolites, which may present many practical interests. Herein, we will discuss the data available in the literature regarding the specificity of the reaction mechanisms in zeolites compared to the more widely studied homogeneous catalysis.

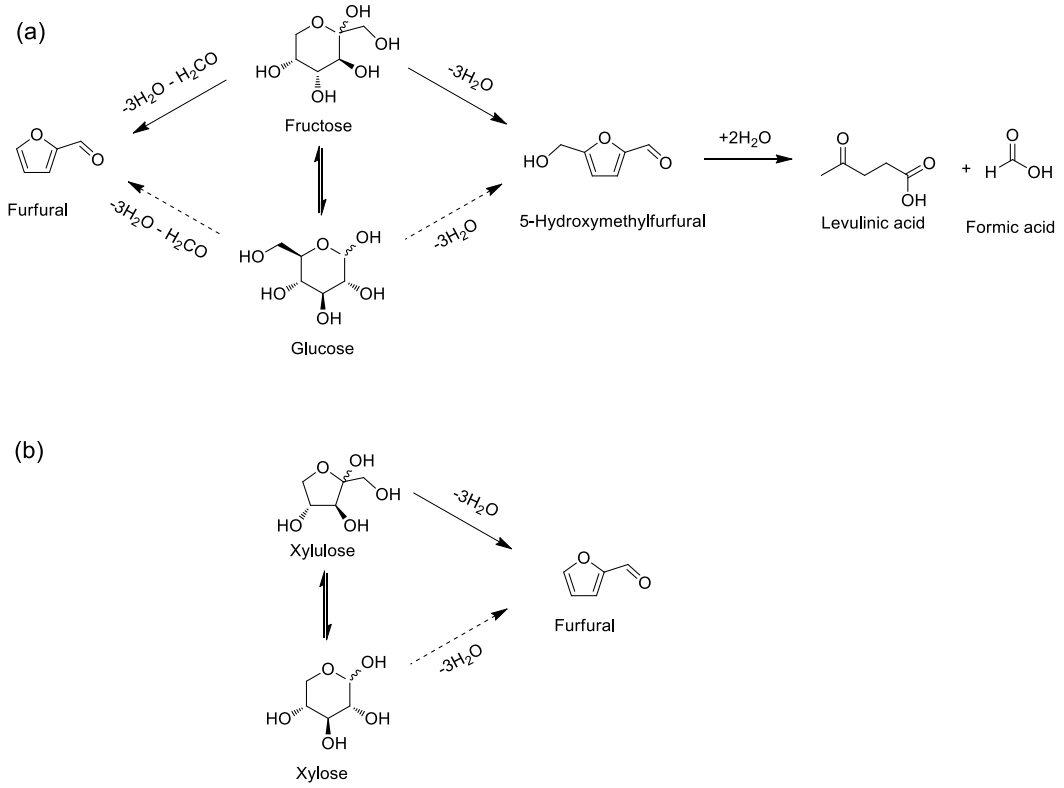

Figure 58. General reaction schemes of (a) fructose/glucose and (b) xylose dehydration catalyzed by Brønsted acids. The representation of the sugars is in their most abundant tautomers in aqueous solutions and holds no mechanistic meaning. Dotted arrows indicate that the corresponding pathways are debated in the literature.

The mechanisms of the dehydration of hexoses to 5-HMF by homogeneous catalysis has been studied extensively in the second half of the XXth century, complemented with more recent molecular modeling studies.[744–748] Detailing these works falls outside of the scope of the

present article and has been summarized in dedicated reviews. [740,749,750]. Only key features and conclusions are provided in the present paper.

The dehydration proceeds faster with fructose than with glucose, hence most studies are devoted to this hexose. Two main mechanisms have been proposed and debated:

1- The "cyclic" mechanism (**Figure 59**),[751,752] in which the reactive intermediate is one of the fructofuranose tautomers of fructose. These species, although not the most abundant ones in solutions (which is the β-fructopyranose), indeed already holds the proper 5-member cycle. It undergoes a first dehydration on the anomeric hydroxyl group, which yields the enol **X** that can tautomerize to the aldehyde **Y**. This intermediate then undergoes two successive dehydration yielding successively intermediate **Z** and 5-HMF.

2- The "acyclic" mechanism (**Figure 60**),[753–756] in which the reactive intermediate is the linear, ketone tautomer of fructose. The key intermediate here is the 1,2-enediol form **A**, which is also an intermediate to the isomerization of fructose into glucose (and reverse) according to the Lobry-de Bruin-van Ekenstein mechanism, usually valid in basic medium. This intermediate can undergo the first dehydration, yielding another key intermediate which is a dione **B** called 3-deoxyglucosone. This intermediate can then undergo a second dehydration on this open form, which can lead, depending on the regioselectivity, to either an intermediate **C** that cyclizes (**D**) and finally undergoes the third dehydration to 5-HMF, or to another intermediate **E** called 2,5-dioxo-6-hydroxyhexanal (DHH) that is suspected to be a precursor of humins in a number of studies.[737,757] Alternatively, intermediate **B** can cyclize and undergo two successive dehydrations (intermediates **F** and **Z**) further to 5-HMF.

Note that in none of these mechanisms the reactive tautomer is the most abundant one; however, the Brønsted acidic conditions required for the dehydration to proceed also catalyze

the tautomeric equilibria between tautomers of carbohydrates, hence these equilibria may be displaced continuously as the extent of the dehydration evolves.

It is generally accepted that the cyclic mechanism is the most favorable pathway based among others on a number of experimental observations that (i) the reactivity of fructose is significantly higher than that of glucose,[758,759] which should not be the case in the acyclic mechanism since the first dehydration involves an intermediate accessible from both sugars (ii) when the reaction is performed in heavy water (D_2O) instead of standard water, no deuterium incorporation in 5-HMF is observed, although the acyclic mechanism features a series of ceto-enolic tautomeric equilibria that should lead to isotopic scrambling on the third carbon atom that should transfer to 5-HMF[751,760] and (iii) the observation on several instances by NMR spectroscopy of the main intermediates of the cyclic pathway, namely **Y** (although rather under its hydrate form than its aldehyde form) and **Z**.[761–763]

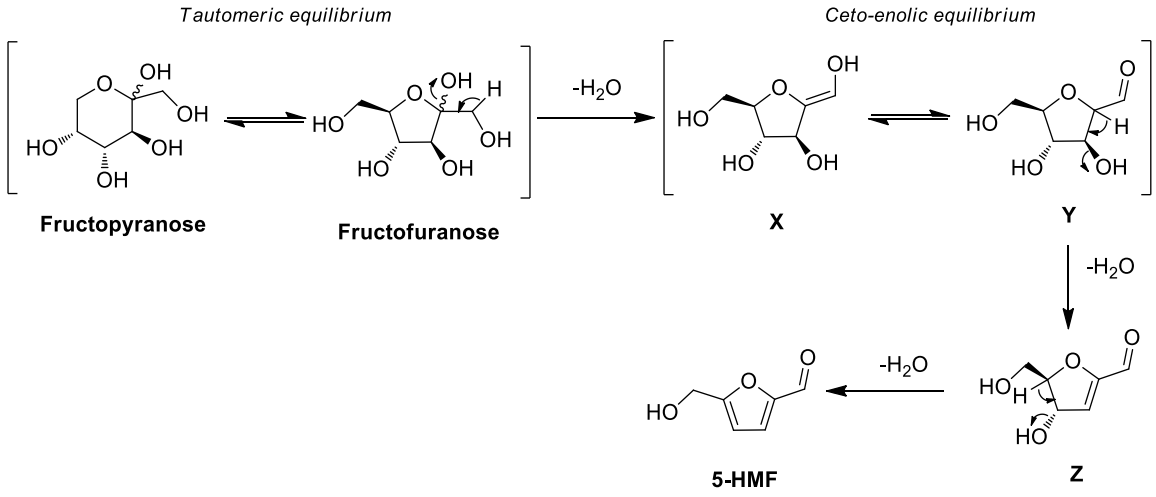

Figure 59. Cyclic reaction mechanism proposed for the dehydration of fructose by Brønsted acidic catalysis.

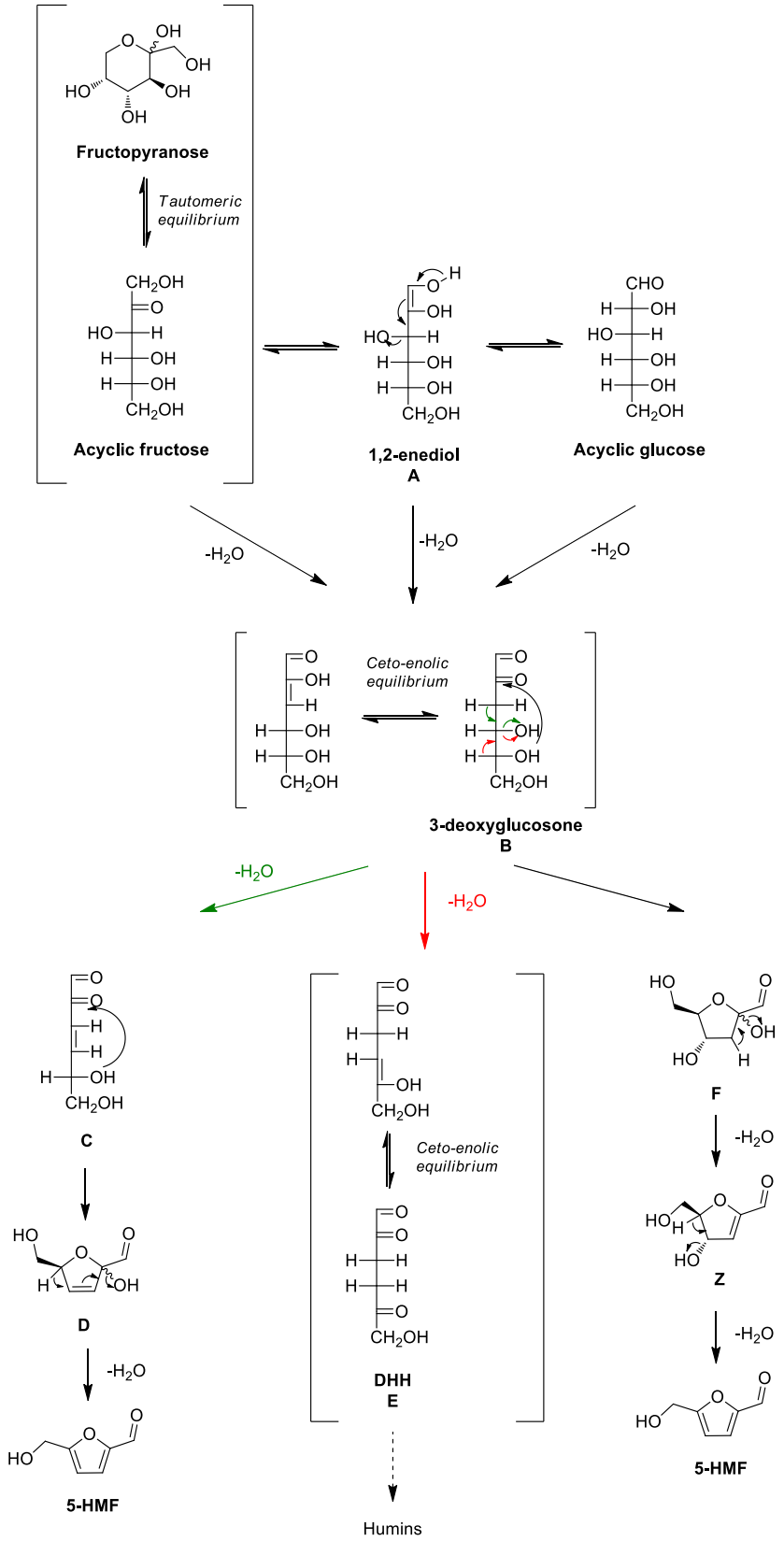

Figure 60. Acyclic reaction mechanism proposed for the dehydration of fructose by Brønsted acidic catalysis.

In the case of the dehydration of glucose, a direct dehydration mechanism on one of the cyclic tautomeric forms is irrelevant since none of these structures are suitable for direct dehydration of 5-HMF. Thus the discussion regarding the mechanism comes down to either a primary isomerization to fructose, directly through a 1,2-hydride shift mechanism or through the 1,2-enediol intermediate mentioned above, or a dehydration of the open form of glucose, leading after tautomerization to the same 3-deoxyglucosone **B** as in the acyclic mechanism of the dehydration of fructose.[753,756] Pathways involving the most abundant pyranose forms of glucose as intermediates and involving carbocation rearrangements towards the formation of the 5-membered ring are also proposed, but recent DFT modeling studies find them less favorable.[744,747,764] Here the consensus on the favored pathway is not as broad as in the case of fructose, and still under debate despite the help of computational studies.

Finally, let us note that the discussion regarding the reaction mechanisms of the transformation of glucose or fructose to 5-HMF can essentially be transposed to the conversion of xylose or its isomer xylulose, respectively, to furfural.[765–768] We will mainly discuss the conversion of hexoses in the following.

8.9.2. State-of-the art in zeolite catalyzed dehydration of sugars

Although a large number of studies aimed at showing the feasibility of using zeolites to catalyze the dehydration of carbohydrates,[769–773] or at optimizing the reaction conditions towards better yields, relatively little amount of work was dedicated to the elucidation of the reaction mechanisms specifically in zeolites, and thus how the mechanistic proposals mentioned above translate to zeolitic catalysts remains unclear. Potentially different mechanisms in the confinement of zeolites pores than in homogeneous phase might arise from either differences in protonation sites on the carbohydrate molecule, akin to the discussion

regarding the dehydration of glycerol (see section 8.8), order of dehydration steps, or reactant shape selectivity of the various tautomers of sugars.

Overall, the general observation that fructose is converted much faster than glucose to 5-HMF is still valid in the case of zeolites as catalysts, which would plead in favor of the cyclic mechanism.[759] Besides, the activation energies measured in the range 120-140 kJ.mol^{-1} in homogeneous phase for fructose conversion[758,774] are comparable with those measured with zeolites : 141 kJ.mol^{-1} in H-Mordenite,[775] 132 kJ.mol^{-1} in H-ZSM-5,[776] which would tend to support similar mechanisms – although the latter value increases significantly to 190-200 kJ.mol^{-1} at high Si/Al ratio, which the authors interpret as an effect of cooperative effects between neighboring Brønsted acidic sites, with no further mechanistic detail. However, several authors claim that the acyclic mechanism should be favored in zeolites by comparing the pore opening diameter of Y zeolites (0.75 nm) to the diameter of the cyclic tautomers (of either glucose or fructose, around 0.9 nm) and conclude that diffusion in the zeolitic pores of the cyclic forms should be limited while the open forms or 1,2-enediol linear intermediate should be able to diffuse more easily.[775,777–779] They ultimately conclude to the reactivity of one of the open forms. However, this argument is debatable, as exclusively cyclic tautomers of glucose in the adsorbed state are observed by ^{13}C MAS NMR in NaY zeolites at 298 and 343 K, showing that their presence in the micropores is possible despite their size being larger than the pore opening, although still shorter than the FAU supercage diameter itself of 1.2 nm, confirming that they do fit as cyclic forms in the microporosity.[780] The explanation to this apparent inconsistency may be explained by the tautomeric equilibria that could be achieved within the micropores (e.g. in the large pore of a zeolite) due to the Brønsted acidity of the zeolite. In fact, Sauer and coll. proposed that the diffusion mechanism of sugars through a zeolite could be a succession of tautomeric equilibria between the linear form (for travelling through the micropore openings) and the more stable cyclic forms within the micropores.[781] Thus, this observation is not

conclusive with respect to the reaction mechanism (cyclic vs. acyclic). Jow et al. observed an enhanced formation of levulinic acid with respect to 5-HMF while reacting fructose on a Y zeolite.[779] They interpreted this observation on the basis of the molecular size of 5-HMF (0.82 nm) that may be too large to diffuse outside of the micropores, which induces an increased contact time in the microporosity. This facilitates its rehydration to levulinic and formic acid. Here again, this argument is debated by Vlachos and coworkers that rather show, by measuring the experimental adsorption isotherms, a significantly stronger thermodynamic adsorption of 5-HMF on the acidic sites compared to glucose or fructose.[782,783] This also increases in principle the likelihood of rehydration using such a heterogeneous catalyst.

Like in the case of glycerol conversion, the synergistic effect of Brønsted and Lewis acidity is discussed in several instances. In general, Lewis acidity, either in homogeneous phase[784,785] or within the porosity of zeolites such as with Sn-Beta zeotype,[786,787] is able to promote the isomerization of glucose into fructose (or xylose into xylulose) as well as fragmentation reactions (retro-aldolisations).[788,789] Using a combination of Brønsted acidity from a zeolite and the Lewis acidity induced by Sn^{4+} moiety grafted in the zeolites significantly improves the yields of 5-HMF from glucose conversion, as well as the formation of C_3 fragments (mainly lactic acid) originating from retro-aldolisation of fructose.[790] This incidentally pleads in favor of the cyclic mechanism since the authors propose that the Lewis moiety promotes the isomerization of glucose into fructose for which the dehydration is easier. In the absence of other elements such as tin, the synergy was also demonstrated in several cases. Vlachos and coll. convincingly showed that the presence of octahedral aluminum species present in the reaction medium using H-Beta zeolite as a catalyst is responsible for an increased activity towards isomerization and side-reactions.[782] They could show by NMR spectroscopy using isotopic labelling strategies that the mechanism for this isomerization follows a 1,2-hydride shift akin to what is observed with Sn-Beta zeolites.[786] These observations are in line

with other results from Sels and coll. regarding the conversion of trioses (glyceraldehyde or dihydroxyacetone).[791] They show that an increased presence of EFAl promotes the Lewis-acid pathways, in this case the conversion of pyruvaldehyde to lactic acid through an apparent intramolecular Cannizzaro-like rearrangement. The exact nature of the active Lewis acidic species is still unclear. While some authors incriminate the EFAl species,[767,782] other reports show that non negligible dissolution of the zeolite occurs during the reaction, possibly due to the formation of homogeneous acidic species such as formic and levulinic acids, and the aluminum ions play the role of homogeneous Lewis acid catalysts.[792,793] Note that Vlachos and coll. could not relate this leaching phenomenon to a loss in activity at reuse of the catalyst. [782]

The formation of undesired polymeric side-products (humins) is unavoidable in the conversion of sugars towards platform molecules, and zeolitic catalysts are no exceptions. The extent of their formation varies a lot depending on the reaction conditions (solvent, temperature, acid concentration…).[737,738] Akin to the formation of coke in hydrocarbon processing using zeolites, the formation of humins may translate into deposition of these products on the surface of the catalysts, inducing active site covering, pore blocking and similar phenomena leading to the deactivation of the catalyst. While such phenomena are undesired, their existence usually does not prevent reaching reasonable dehydration products yields, comparable to those achieved by homogeneous catalysis, at least in batch reaction. The deactivation may be efficiently overcome by thermal treatment such as calcination, to which the zeolitic materials are resilient.[794,795] Although some authors assign the mechanism of the formation of humins to degradation reactions of the furanic compounds,[796,797] these species appear to be relatively stable in acidic conditions towards the formation of humins,[798] and intermediates in the dehydration process should be incriminated instead.[758,799] These intermediates may in principle form on every active sites of the zeolites, the formation of large oligomeric and polymeric species seems to occur rather on the external surface sites,[800] as demonstrated for instance by

selective passivation of the external surface sites by silication.[801] On such materials, the yield in 5-HMF is higher than on the unmodified catalysts. However other results show little effect of surface passivation, putting into question the exact role of the external surface.[782]

Zeolites show a particular behavior in the conversion of glucose and fructose by promoting under some circumstances their transformation into furfural.[759,765,798,802–804] This reaction is favored at relatively high reaction temperatures of 423-473 K and using solvents such as γ-valerolactone (GVL), γ-butyrolactone (GBL), tetrahydrofuran (THF), sulfolane, or 1,4-dioxane, but much less in water and very little in dimethyl sulfoxide (DMSO) for instance. Although this reaction is of little practical/economic use, since furfural can be obtained more readily from the C_5 sugars of the lignocellulosic biomass and in fact is often generated during the initial fractionation, it still presents an academic interest worth considering herein. Furfural is normally observed as a very minor side-product in dehydration of hexoses (typically less than 5 % of selectivity) under catalysis by homogeneous Brønsted acids (HCl, H_2SO_4) or by non-microporous heterogeneous catalysts such as sulfonic resins. Dumesic and coll. obtained however significant yields of furfural when using zeolites as catalysts. H-Mordenite, H-Beta, and H-ZSM-5 proved indeed able to achieve up to 37 % of furfural yield at 448 K in GVL containing 10 %wt of water.[759] The same reaction performed in pure water achieved lower though still significant yields of furfural (up to 14 %). This reaction was further studied by Wang et al., who examined this reaction in more detail.[798,803] They show a strong dependence on the zeolite topology employed, suggesting marked shape-induced selectivity. While the large-pore zeolite H-USY (7.5 Å) afforded a yield of 2.9 % of furfural only (57.1 % of 5-HMF) at 423 K in GBL containing 5 %wt of water, H-Beta (6.6 Å) allowed for reaching an impressive yield of 63.5 % of furfural (12.6 % 5-HMF). The smaller H-ZSM-5 (5.5 Å) afforded 17 % of furfural yield (26.7 % of 5-HMF). Not only the pore opening size matters, since H-Mordenite, that displays pore opening roughly similar to that of H-Beta (6.7 Å) afforded 18.7 % yield of

FF in this study (which is in disagreement with the results from Dumesic showing similar yields of FF in H-Mordenite and H-Beta, although in a different solvent GVL[759]). At higher temperature (443 K), the yields to FF increase but the results are qualitatively similar. The authors make several interesting observations regarding the mechanisms.[798] (i) Furfural is not a product of 5-HMF decomposition since said 5-HMF conversion is low when treated under the same conditions (about 5 %) and no furfural is detected. (ii) The conversion of fructose labelled on the C_1 position yields C_1-labelled 5-HMF (akin to the homogeneous reaction) as well as C_1-labelled furfural, as determined by NMR spectroscopy and mass spectrometry. This shows that the C-C cleavage required for the formation of furfural occurs between the C_5 and C_6 carbon atoms. (iii) A band at 1768 cm^{-1} is observed by contacting a fructose solution in water (the same observation is made in 1,4-dioxane with 5 %wt water) with H-Beta.[805] The authors assign it to the ketone linear form of fructose present in the micropores of the zeolites. This band is not observed upon performing the same experiment with a H-Faujasite zeolite instead of H-Beta. The authors propose a mechanism for the generation of furfural from these observations (**Figure 61**). The acyclic form of fructose undergoes first a dehydration of the HO3 hydroxyl group (intermediate **G**) followed by a retro-aldol condensation yielding a formaldehyde molecule and a C_5 intermediate **H** (although it is dubious how such an intermediate may eventually lead to furfural given the positions of the double bonds). The shape selectivity observed would thus be related to the ability of a given zeolite structure to accommodate, stabilize and convert the linear form of fructose. In H-Faujasite, the pores are large enough to accommodate the more stable cyclic tautomers hence no open form of fructose is observed, and lower yields of furfural are obtained. In the case of the H-ZSM-5 zeolite, the authors propose that the linear intermediates towards the formation of the furfural are generated within the channels of the zeolitic structure, while the cyclization to furfural, as well as the dehydration of the cyclic fructofuranose tautomers to 5-HMF occur either at the intersections

of the channels, which are larger than the channels, or on the external surface of the catalysts (**Figure 61**). The particular role of the solvent in the increase of the selectivity towards furfural is not very clearly understood, although some authors have shown the role of GVL as a solvent to increase the loadings of sugars in zeolites while still affording a decent solubility of the sugars in the liquid phase.[780] Finally, the authors examine the role of Brønsted and Lewis acidity, and conclude that a higher density of Lewis acidic sites favors the C-C cleavage and formation of furfural, which is in line with the general observations regarding the role of Lewis acidity in fragmentation reactions such as the retro-aldolisation invoked here.[798]

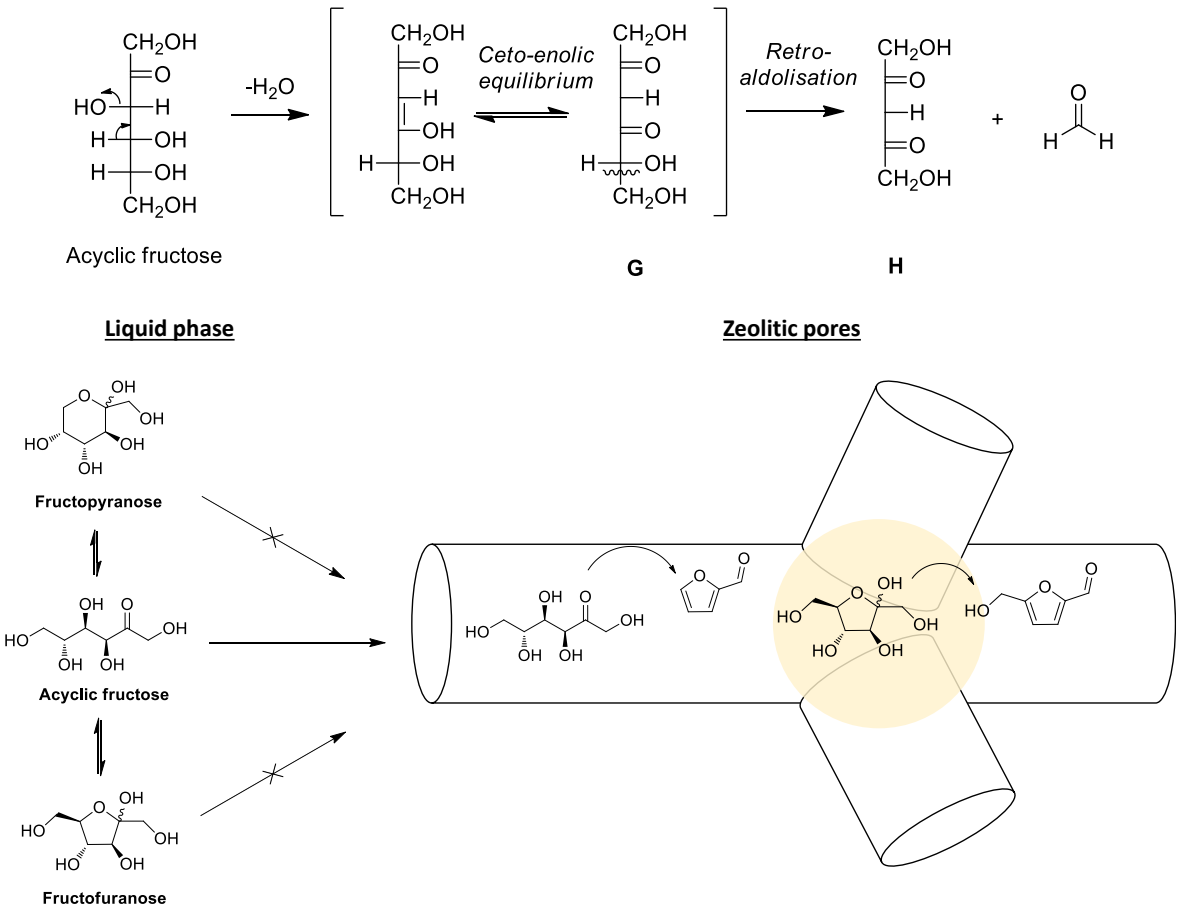

Figure 61. Proposed mechanism for the conversion of fructose to furfural in the porosity of zeolites (H-ZSM-5 here), according to Wang et al.[798,803]

Remarkably, and to the best of our knowledge, little to no molecular modeling study address the dehydration of sugars in the porosity of zeolites while considering the problematic of the confinement effects. A study by Lin et al.[746] does examine several reaction pathways for the dehydration of glucose on solid acid catalysts, but they consider as a model for the zeolite a 12T cluster. Although they could infer some elements of discussion regarding the role of the surface oxygen atoms that seem to participate actively as Brønsted bases in some of the elementary steps, the effect of the confinement could not be discussed in this study. The reaction pathways leading to furfural from hexose, although quite intriguing, also did not trigger modelling studies so far, akin to the rehydration of 5-HMF into levulinic and formic acids, for which little to no mechanistic insight exist in the literature. Finally, the state of the zeolitic proton in the presence of water and the formation of protonated water cluster, as discussed in section 8.7, and its probable influence in aqueous-phase transformation of sugars, was never examined by computational chemistry. Although the task seems very challenging, significant insight can be expected from such studies.

8.10. Concluding remarks

The catalytic transformations of alcohols in zeolites have been the topic of a very large body of studies in throughout the course of the XXth century, up until these days. In the case of "simple" alcohols, i.e. monohydroxy species, numerous fundamental works have been carried out, experimental and theoretical. Quite precise knowledge has been achieved, regarding both the molecular level mechanisms for the various transformation routes (E1 vs. E2 mechanisms, intramolecular or intermolecular dehydration, skeletal isomerization…) and the entanglement of these various routes with the construction of *ab initio*-driven microkinetic models able to describe quite precisely the experimental kinetics. E1 or E2 intramolecular mechanisms are both likely, the dominant one depends on the zeolite topology, on the nature of the alcohol, and

on possible solvent effects. Operating conditions were shown to influence drastically the preferred alkene formation mechanism, ether-mediated (intermolecular) mechanisms being favored at high alcohol pressures and low temperatures over intramolecular mechanisms. Ether formation mechanisms themselves were shown to be strongly related to operating conditions, alkoxide-mediated mechanisms being the most likely at low alcohol pressure, whereas dimer-mediated mechanisms are favored at high alcohol pressure. The effects of pore topology in regard of the nature of the alcohol molecule substrate are also quite well documented, in particular for what regards ether formation pathways, first order (alkoxy-mediated) mechanisms being more sensitive to confinement effects. Nevertheless, open questions remain on the location of acid sites able to transform alcohols longer than propanol, and on the origin of the topology-dependent selectivity in terms of linear versus branched alkenes. The most recent breakthroughs concern the influence of the accumulation of water within the zeolites micropores on the reaction. The findings show an actual change in the nature of the active sites as the water content increases, from the protonic site of the zeolite towards protonated water clusters. This may prove very relevant for further studies regarding the transformation of biomass-based substrates with high water content or even performed in water medium.

The conversion of polyhydroxy molecules, such as glycerol or carbohydrates discussed in this review, was on the contrary far less examined on a fundamental point of view, despite a large body of experimental work in search of performance of catalytic activities. The experimental kinetics and mechanistic studies available in the literature so far do not allow, in our opinion, to obtain a complete description of the mechanisms at stake, especially considering the complexity introduced by the presence of several hydroxyl groups, and hence regio- and chemioselectivity issues more complex than in the case of mono-alcohols. Computational works are almost inexistent, and in no case consider the influence of water and protonated clusters as active site mentioned above. Hence numerous perspectives remain in this field.

9. Carbonylation reactions of alcohols, ethers and alkenes

9.1. General aspects

Carbonylation of methanol is one of the most attractive routes to produce acetic acid. The Monsanto[806] (developed in the 60's) and Cativa[807] (developed in the 90's) processes, making use of transition metal complexes, have been key players in that respect. Carbonylation reactions may also be performed in Brønsted acidic media, which is known as the Koch-type reactions.[808] Since then, many works have dealt with the transposition of this reaction, reporting the formation of various acetyls thanks to the carbonylation of methanol, higher alcohols, DME or alkenes in proton-exchanged zeolites (**Figure 62**).[809–815] The requirement for Brønsted acid sites was demonstrated by a stochiometric poisoning of the acid sites by 2,6-dimethyl-pyridine introduction in the feed, in the case of a H-Mordenite catalyst,[812] even if a role of Lewis acid sites on the adsorption of CO was not excluded.[812,816] Typically, isobutene conversion into trimethyl-acetic acid was reached in H-ZSM-5 at 296 K,[809] whereas methyl-acetate formation from DME was performed at 423-463 K on Mordenite.[812] Beside the intrinsic value of such a reaction for practical applications, it was recently found that it is one of the possible very first C-C bond formation steps in the Methanol-to-Hydrocarbon reactions,[817–822] thanks to kinetic analysis, ^{13}C-^{1}H NMR and DFT calculations, as will be discussed later in section 10.

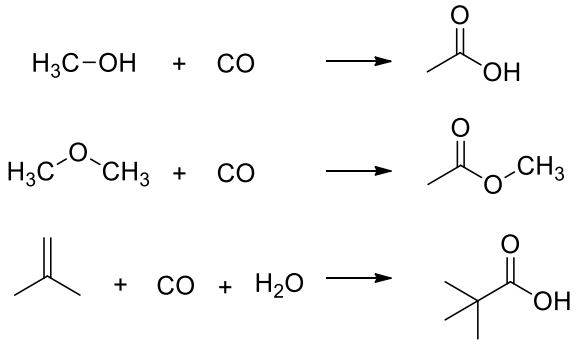

Figure 62. Possible carbonylation reactions of typical substrates (alcohol, ether, alkene).

The generally admitted mechanism invokes the addition of the CO molecule on a carbenium ion or alkoxide obtained from the alcohol, ether or alkene, leading to an acylium ion.[823] In the case of zeolite-catalyzed reactions, the latter then reacts with water to release carboxylic acid and regenerate the bridging OH group of the zeolite. Starting from DME instead of methanol reduces the inhibiting effect of water and makes reaction rates higher, after an induction period where the reaction rate growths upon progressive saturation of the acid sites with methoxides.[812] Inhibiting effect of water was assumed to be linked to adsorption competition with CO, and to the decrease of the rate of formation of methoxy groups.[813] In the case of methanol and DME carbonylation, a direct participation of methoxides was indeed suggested[810] and demonstrated by *in situ* FTIR[813,824] and ^{13}C MAS NMR.[825] Their formation is, however, not the rate determining step.[812] From CO pressure effects, the rate determining step was shown to involve CO insertion in H-Mordenite,[812,813] which is confirmed theoretically.[826–828] Computational studies report a transition state with a planar CH_3 group (in the case of methanol carbonylation, see **Figure 63**) linking to CO and disconnecting from the zeolite in a single step.[821,826–831] The computed free energy barriers for this step are higher than 100 kJ.mol^{-1} and depend on the zeolite and active site under consideration.

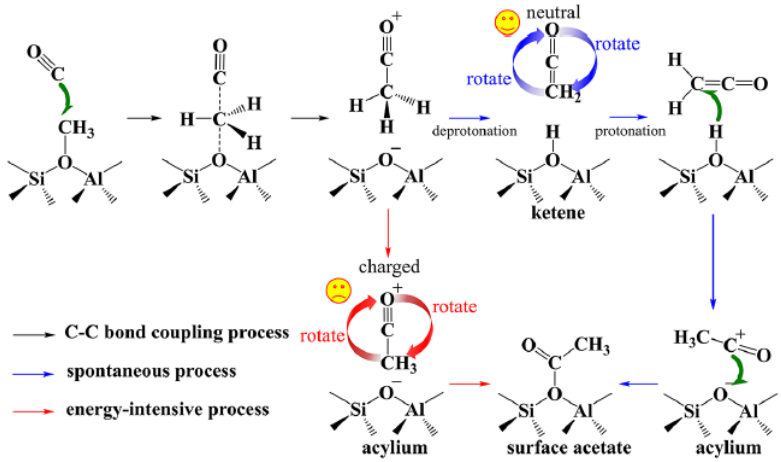

Figure 63. Reaction steps involved during methoxide (obtained from methanol or DME) carbonylation on protonic zeolites, though acylium, ketene and acetyl intermediates. Blue arrows depict the pathway followed by sites located in the 12MR channel of Mordenite and in SSZ-13, whereas red arrows depict the route followed by 8MR sites of Mordenite, according to metadynamics calculations. Reprinted from ref. [832]. Licensed under CC BY 4.0.

Although appearing in computational studies as a reaction intermediate,[826,829] the acylium species was not observed directly in carbonylation conditions on protonic zeolites (whereas it was on metal-exchanged zeolites[833]), although reaction with ammonia led to the expected acetamide.[825] The poor stability of acylium in practice can be explained by its very quick bonding to the zeolite, leading to acetyl groups, as shown by a very low computed transition barrier.[827,829,830,834] Notably, a CH_2=C=O ketene intermediate was also invoked, on the basis of DFT calculations in the case of Mordenite (**Figure 63**).[832,834] This intermediate is expected to be formed from deprotonation of the acylium ion, and subsequently leads to adsorbed acetyls also with low barriers. Experimentally, the observation of CH_2DCOOD after D_2O introduction in the medium was interpreted as the proof of the existence of ketene, because the reaction of D_2O with the surface acetate should only lead to a deuterated carboxylic group (but not deuterate the methyl group).[834] A recent metadynamics study suggests that ketene is formed as a local free energy minimum along the CO carbonylation path at 12MR sites, but not at the 8MR site, before formation of the acetyl.[832] From the structure of the acylium and acetyl species, one may expect that the direct C-$O_{framework}$ formation should be faster than the formation of ketene, that requires deprotonation of the acylium (to transform the CH_3 moieties into CH_2), then re-protonation of the ketene (to transform CH_2 into CH_3). In ref. [832], this counterintuitive observation of ketene is explained by the rotation required to transform the acylium into the acetyl, which is costly due to electrostatic interactions between the reactant and the negatively charged zeolite framework. This cost for the rotation is significantly lowered when passing through a neutral ketene intermediate. From the AIMD study, ketene very quickly reprotonates at 8MR sites of Mordenite due to spatial constraints.

Acetyls connected to the zeolite framework, observed by *in situ* FTIR[824] and ^{13}C MAS NMR assigned thanks to DFT calculations,[835,836] were shown to react with DME to form methyl

acetate and methoxides, giving a substance to the mechanisms proposed in **Figure 64**.[813] The direct reaction of DME with acetates was computationally investigated, with contradictory conclusions depending on the functional. It is computed to be very unlikely in the 8MR pocket of Mordenite with a QM/MM approach with the B97D functional, suggesting that such a reaction mechanism may only take place in larger pores,[826,827] or involve first the decomposition of DME into methanol. But the same barrier was computed to be low in all cases (8MR and 12MR of Mordenite) with the BEEF-vdW functional.[830]

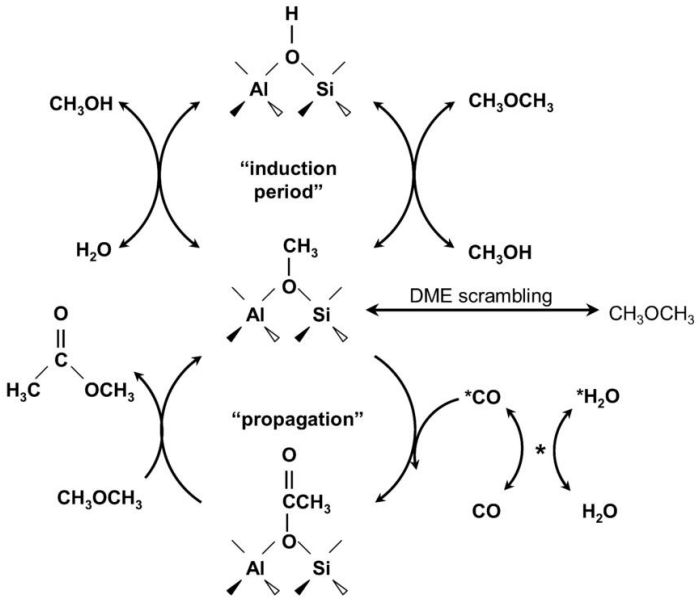

Figure 64. Proposed reaction steps for the carbonylation of DME in protonic zeolites. Reprinted with permission from ref. [813]. Copyright 2007 Elsevier.

9.2. Consequences on confinement effect, specific role of 8MR sites for methanol and DME carbonylation

A very strong effect of confinement was observed in the case of DME carbonylation. H-Mordenite appeared as the most active catalyst, whereas large pore zeolites such as USY or Beta were inactive.[812] Based on the quantification of OH groups in 8MR of Mordenite and Ferrierite by FTIR and titration with alkanes and pyridines, Bhan et al. concluded that solely bridging OH groups located within 8MR are active for DME carbonylation,[837] which was

assigned to a stronger electrostatic stabilization of the charged transition state thanks to electron density difference calculations.[828] Since then, other zeolites exhibiting 8MR structures (H-EU-12, H-ZSM-35, H-ZSM-57, H-SUZ-4, H-SSZ-13, Al-RUB-41 for instance) appeared as attractive for such reactions.[816,838–841] The methyl acetate synthesis rate was even shown to be a relevant tool to monitor the increase in 8MR population of acid sites along a series of Ferrierite samples.[842]

Several computational works were reported to confirm and better understand the specific reactivity of sites located in 8MR of Mordenite, starting from methoxides. Taking into account dispersion interactions (more stabilizing in the 8MR) appeared to be crucial to obtain a significantly lower barrier in 8MR versus 12MR.[826] When not included, or with the BEEF-vdW functional, activation barriers are only slightly different.[826,827,830] A recent AIMD study, coupled to the machine learning perturbation theory (MLPT) approach, showed the importance of taking into account dynamic effects combined to dispersion forces to reproduce the preferential reaction in the 8MR side pocket (**Figure 65**).[829] Indeed, the free energy of activation in the main channel increases by about 15 kJ.mol^{-1} (up to about 130 kJ.mol^{-1}) with respect to a static approach, which is assigned to the poor description of translational and rotational modes in large cavities by static methods. Computational studies are scarcer for other 8MR zeolites, but the ones available confirm the lower activation barriers at sites of the 8MR, although some very subtle local effects make that specific sites in the 8MR are much more active than others (for example, those also shared by a 6MR in Ferrierite[831]).[831,838,841] DFT calculations also reveal a higher carbonylation rate in the straight 10MR channel of ZSM-5, with respect to the sinusoidal channel, and their intersection. The latter was found to promote the formation of coke precursors.[843]

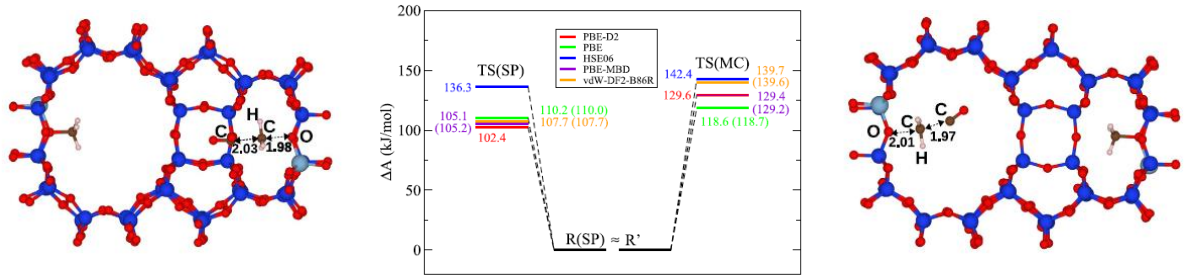

Figure 65. Free energy of activation of methoxide carbonylation in the 8MR side pocket (noted SP) and at 12MR main channel sites (noted MC) of Mordenite at 440 K, computed by AIMD at the PBE-D2 level, and with the MLPT approach for other levels of theory. The transition state structures at the 8MR (left) and 12MR sites (right) computed using a static approach at the PBE-D2 level are also shown. Reprinted with permission from ref. [829]. Copyright 2021 Elsevier.

The competition of methanol and DME carbonylation with other reactions, such as DME formation from methanol and hydrocarbon formation was computed in Mordenite by Boronat et al.,[826,827] suggesting a much higher selectivity of 8MR side pockets towards carbonylation than the 12MR main channel, due to steric constraints. This is an additional argument in favor of the 8MR sites in terms of carbonylation selectivity, even if the experimental picture is not that clear.[844] On top of intrinsic kinetics considerations, Monte Carlo and force-field molecular dynamics calculations have shown that adsorption and diffusion factors are also in favor of a higher reactivity of sites located in 8MR side pockets.[845] Accumulation of CO was found to occur close to methoxide species in 8MR pockets, whereas the methyl-acetate product diffuses rapidly from these zones once formed. Indeed, an inhibition effect by the methyl-acetate reaction products was observed experimentally for high pressures of product only,[830] likely in a regime where it interacts strongly with active sites. All in all, several factors make the 8MR structure desirable for carbonylation reactions, that currently lead to synthesis and post-treatment efforts to remove 12MR sites (in Mordenite) and locate most Brønsted acid sites at relevant positions to improve DME conversion.[842,846–851] Recently, surface barrier effects were invoked to explain the enhanced reactivity of Mordenite after surface etching,[852] even if an effect of the possible variation in distribution of surface OH groups

cannot be excluded. Unfortunately, ^{1}H NMR and FTIR spectra of the etched samples were not compared to that of the initial sample.

9.3. Transformation of longer alcohols, alkenes or alkanes

Carbonylation is faster than the dehydration of alcohols and than skeletal isomerization that may take place concomitantly when starting from butanols (see section 8.6). CO was shown to inhibit ^{13}C scrambling (observed in the absence of CO[258,274]) by ^{13}C MAS NMR in ZSM-5.[809,853] The observation of a fast carbonylation reaction of tert-butanol was interpreted as a proof of the existence of the tert-butyl cation, although the existence and participation of alkoxide groups could not be strictly excluded.[853] The strong similarity of the ^{13}C NMR spectra, starting from isobutene and tert-butanol in the presence of CO, suggests that the carbonylation reactions of alkenes and alcohols indeed have similar intermediates. Starting from isobutanol, trimethylacetic acid (similar as when starting from tert-butanol) forms preferentially over isovaleric acid (the expected product), meaning that intramolecular hydrogen transfer takes place faster than CO addition.[853] Similarly, 2-methyl-butyric acid was mainly formed from butan-1-ol.[853] To the best of our knowledge, possible synchronous carbonylation reactions, that would have neither alkoxides nor carbenium ions as intermediate, have never been invoked. Such a scenario is, however, not to be *a priori* excluded, by analogy with mechanisms computed for alcohol dehydration (see section 8).

Finally, carbonylation was also observed in H-ZSM-5 from alkanes (propane, isobutane) between 373 and 473 K in the presence of CO and water, leading to carboxylic acids.[854] This was assigned to the propensity of alkanes to generate carbenium ions in such conditions by protolysis, as developed in section 6, which also explains why CO inhibits H/D exchange of alkanes.[855] At higher temperature, carbonylation of the alkane cracking products (eventually followed by decarboxylation of the carboxylic acids at 573 K) was also reported.[854]

10. Methanol to olefins reactions

The process for converting methanol to hydrocarbons (MTH), for producing gasoline, was invented by researchers from Mobil in the 1970s.[856] The ZSM-5 catalyst produced a mixture of C_2-C_5 olefins and paraffins and aromatics. However, due to the restrictions of the aromatics content of gasoline and the high demand for olefins, the focus is now on making olefins (MTO). The MTO process has met a major commercial success since it allows circumventing the use of petroleum. While methanol is produced at present mainly from natural gas and coal, the sources might shift to biomass or waste products soon, thereby offering the possibility of a sustainable production of plastics or fuels. The MTO process is also a potential route for CO_2 valorization. CO_2 can be converted to syngas by the Reverse Water Gas Shift (RWGS) reaction, then be transformed to methanol and finally to olefins via the MTO process.[857] There are also many on-going research works concerning the one-pot conversion of syngas to light olefins (or other products),[858] the so-called OXZEO process. It employs a mixture of a (mixed) oxide catalyst (Zn, Ga, Mn, Cr, Zr, etc.) for RWGS and a zeolite catalyst. Its chemistry strongly resembles that of the MTO process.

The chemistry of MTO is very complex and implies almost all the reactions described in the earlier sections of this review: carbonylation, dehydration, oligomerization of alkenes, cracking of alkenes as well as the transformation of aromatics. MTO chemistry has been extensively reviewed in recent years.[29,859–863] We will, therefore, not try to provide an exhaustive account of all mechanistic aspects (especially concerning the first C-C bond formation, which is the focus of the current debate), but only point out some important principles and sum up the most recent discoveries.

The MTO reaction comprises a sequence of different phases:[864]

1. The first step consists in an equilibration between methanol and dimethylether (whose mechanisms are discussed in section 8.4). This intermolecular dehydration reaction is very fast and usually reaches thermodynamic equilibrium.
2. One systematically observes an induction period during which the activity for olefin formation is low. This induction has been associated with the time necessary to build up a "hydrocarbon pool" in the zeolite pores, consisting of a mixture of aromatic compounds trapped in the microporosity of the zeolite, which is source for the olefin production in steady state regime.
3. The steady state period follows, during which methanol conversion is usually complete and olefins are produced via the hydrocarbon pool.
4. Finally, a deactivation period where catalyst activity goes down due to plugging of the pores by carbonaceous deposits is observed.

We will start by summing up the evidence which led to establishing the hydrocarbon pool mechanism, because it is a very instructive lesson of science. After that we will briefly turn to the question of the initial C-C bond formation, which is at the heart of the current scientific debate, but we will not go into detail concerning this point, since it has been exhaustively covered in a recent review.[862] We will then cover recent insights into the induction period where the hydrocarbon pool is generated from the first olefins. Finally, we will discuss some recent results concerning the mechanism of olefin formation from the hydrocarbon pool and address the question of olefin selectivity.

10.1. Direct vs indirect mechanisms: the hydrocarbon pool theory

Initially, Dessau and LaPierre proposed that olefins were produced by the successive methylation (with methyl carbenium ions formed from methanol) of ethylene to higher olefins,

which then cracked to lighter olefins, i.e. $C_2^=$ to $C_4^=$.[865,866] Aromatics were thought to be formed by cyclisation of higher olefins, but did not participate in the olefin formation in this proposal (**Figure 66-a**).

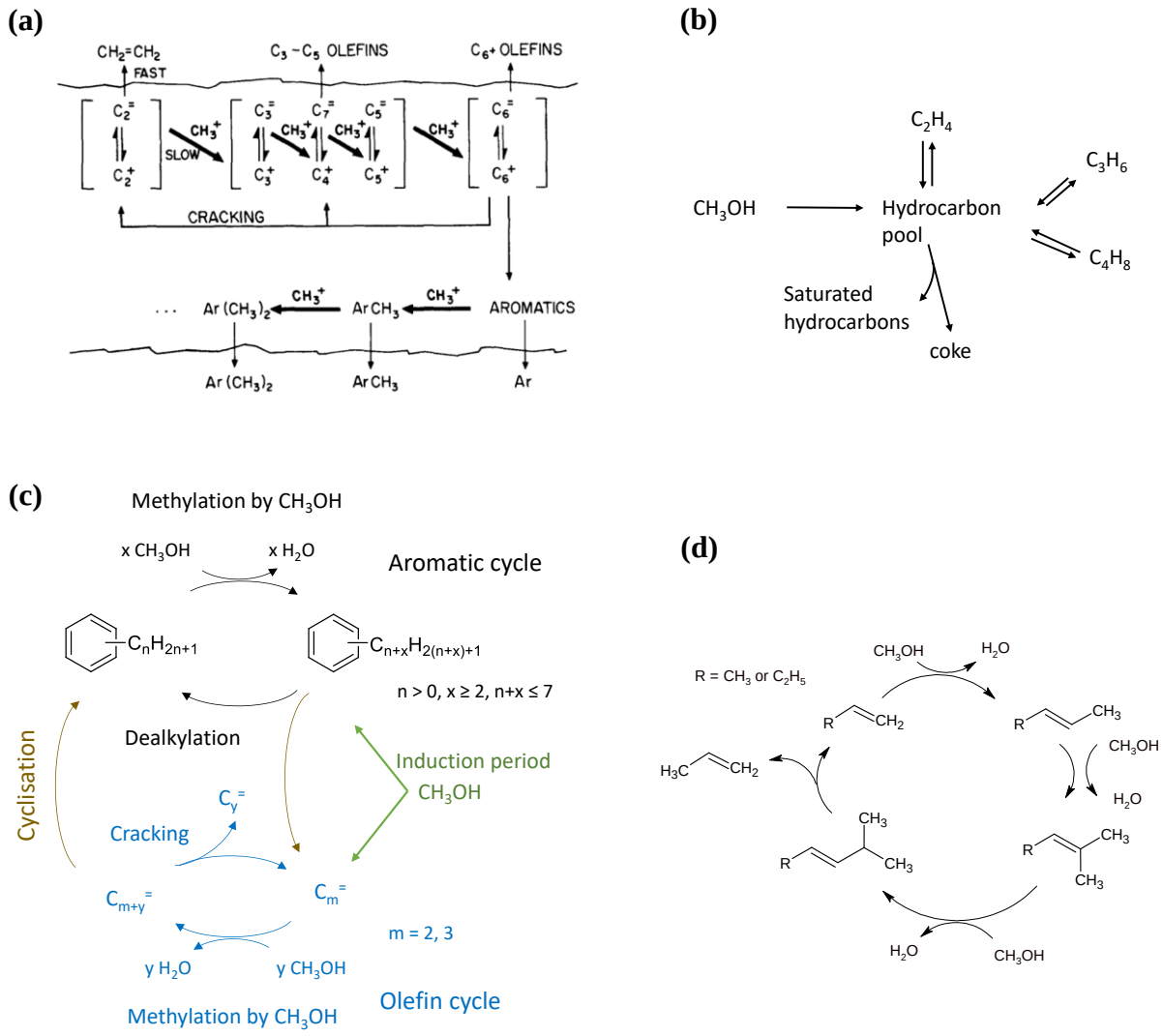

Figure 66. a) MTO mechanism proposed by Dessau and LaPierre for a ZSM-5 catalyst. Reprinted with permission from ref [865]. Copyright 1982 Elsevier. b) Formation of olefins via the hydrocarbon pool, according to ref.[867] c) Schematic illustration of the dual cycle mechanism. d) Scheme of the olefin cycle: short alkenes are methylated to longer alkenes (C_6 or longer), which then crack. The choice of the olefin isomers and of propene as cracking product is an arbitrary example, for the purpose of illustration.

They conceded that this mechanism did not explain the formation of the first ethene molecule, which would trigger the methylation/cracking cycle, but considered the question to be

irrelevant, since the process would be autocatalytic once initiated (the cracking of a higher olefin generated by methylation generates two olefins, which can again be methylated, etc.).

A mechanism based on the methylation of ethene by methanol was, however, invalidated by Dahl and Kolboe[867] who showed by carbon labelling experiments that ethene was virtually inert under steady state MTO reaction conditions (using a SAPO-34 catalyst). They further demonstrated that the carbon labelling distribution of propene and butene products was close to random, which supported the idea that these products were indirectly formed via a "hydrocarbon pool" intermediate (**Figure 66-b**). The hydrocarbon pool consists mainly of multi-methylated benzenes (cyclopentenyl carbenium ions were also detected in NMR studies[864]). The first hint to the role of aromatics was given by the observation that co-feeding aromatics had a positive effect on the MTO reaction.[868] Isotope labeling experiments showed that the aromatics undergo alkylation and dealkylation reactions under MTO conditions and the olefin products contain carbon atoms from the aromatic rings.[869] In small-pore (8MR) zeolites, co-feeding experiments are not possible because aromatics do not diffuse into the pore system, but an analysis of the products trapped in the pores of SAPO-34 showed that the CHA cages contain mainly multi-methyl-benzene molecules.[870] Isotope labeling proved that they are not simple spectators, but actively participate in the reaction, albeit the reactivity differs strongly depending on the degree of methylation as will be discussed below.[871,872] In the case of SAPO-34, hexamethylbenzene molecules are the most reactive species in the hydrocarbon pool.[871]

However, Svelle et al. demonstrated that the mechanism needed to be complexified, at least for the case of ZSM-5.[873] They measured the rate of isotope incorporation of labelled carbon into the products as well as into the products trapped in the pores upon a $^{12}C/^{13}C$ methanol switch. The ^{13}C incorporation into C_3-C_6 olefins was much faster compared to the ^{13}C penetration into ethene and the aromatic molecules. This result suggests that ethene has mechanistically a different origin than the higher olefins. Moreover, the highly methylated

benzene molecules were the least reactive ones, in stark contrast to the behavior of SAPO-34. A detailed analysis of the results led the authors to propose a new dual-cycle mechanism valid for ZSM-5 (at least).[874] In this mechanism, ethene is predominantly formed from the dealkylation of xylenes or trimethylbenzenes (in the case of ZSM-5), as schematically illustrated in **Figure 66-c**. Part of the propene is possibly also formed from aromatics. The formation of higher olefins (C_3-C_6) is mainly attributed to a mechanism similar to the initial proposal of Dessau, namely the successive methylation of olefins by methanol, followed by cracking of the longer olefins. Since the methylation of ethene is very slow compared to that of propene or butene,[875,876] it was supposed that the methylation cycle starts from propene as illustrated in **Figure 66-d**. The net reaction equation of this cycle is $3\ CH_3OH \rightarrow C_3H_6 + 3\ H_2O$. Methylation to a C_7 olefin, followed by cracking to C_3 and C_4 olefins is also possible, but the generation of higher olefins is unlikely since C_7 olefins crack very quickly (see section 5.3).[522]

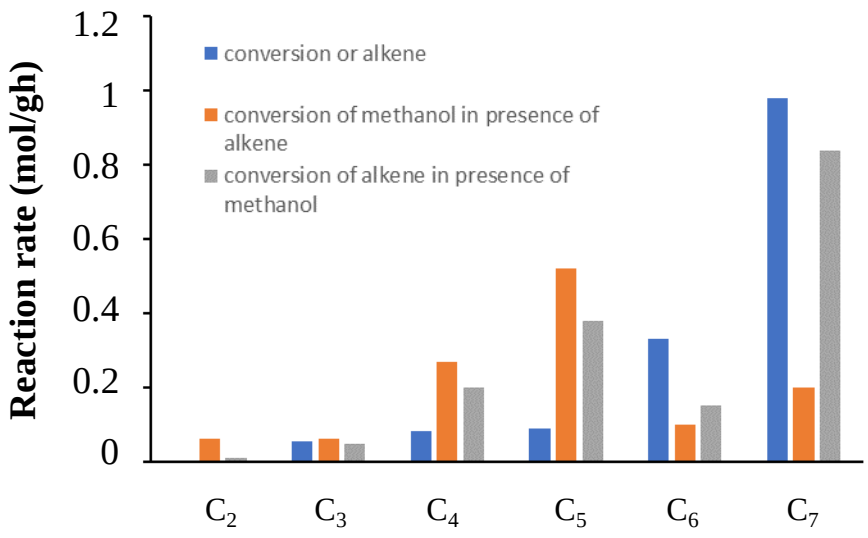

Figure 67. Reaction rate of alkene conversion (by oligomerization or cracking) in the absence of methanol, of the conversion of methanol in the presence of alkene and of the conversion of alkene in the presence of methanol. ZSM-5 (Si/Al = 200 mol/mol), 733 K. Data extracted from ref [877].

The information concerning the olefin cycle was complemented by Wu et al. who compared the rates of alkene oligomerization and alkene methylation by methanol under MTO conditions (**Figure 67**).[877] They found that the fastest methylation reactions occur with C_4 and C_5, while that of C_2 is very slow and higher olefins tend to undergo preferentially cracking. On this basis, they proposed a revised olefin cycle, which relies on the methylation of C_4 and C_5 olefins.

Since the longer olefins (with at least 6 carbon atoms) can also cyclize (by hydrogen transfer reactions, which generate paraffins) to aromatics, the olefin cycle, leading to propene and higher alkenes, and the aromatics cycle, leading to ethene and aromatics, are interconnected. This so-called dual cycle mechanism[874] is now generally accepted. Bhan and co-workers extensively studied the relative importance of the two cycles and the impact on product selectivity (for ZSM-5 catalysts). They showed that co-feeding toluene increases the selectivity to ethene and aromatics, by favoring the aromatic cycle over the olefin cycle.[878] Co-feeding propene had the opposite effect.

10.2. The first C-C bond formation

The hydrocarbon pool theory explains how olefins are formed under steady state conditions, i.e. once the hydrocarbon pool has been built up. However, it does not say anything about how the first aromatics or the first long olefins, which could then initiate the dual cycle, are formed. From an industrial perspective, the question may be considered as irrelevant since most industrial processes include a recycle of C_4^+ olefins,[863] which can be readily alkylated and initiate the hydrocarbon pool. However, the question is of fundamental interest and may also have a consequence on the deactivation process.[819,879]

Most of the early mechanistic proposals for the first C-C bond formation seem energetically unrealistic, i.e. they have very high activation barriers. For examples, (i) alkoxy

chain growth by reaction of methanol with surface methyl groups, (ii) a pathway involving carbene species formed by decomposition of surface methyl groups,[271] (iii) a pathway involving trimethyloxonium cation $O(CH_3)_3^+$, formed by reaction of DME with methanol (see also section 8.4).[880] This led Haw and co-workers to suspect that even for lab experiments the hydrocarbon pool was probably initiated by impurities in the feed and not by a catalytic C-C bond formation.[864] This hypothesis was challenged by Hunger and co-workers who showed that the ethanol and acetone impurities in methanol were largely insufficient to explain the formation of the hydrocarbon pool.[881]

Recent studies have provided much new spectroscopic evidence concerning the question of the first C-C bond formation. We will not treat these results in detail because they have been reviewed very recently.[862] Interestingly, many of the new proposals involve an oxidized form of methanol, i.e. formaldehyde or CO. Certain amounts of CO and H_2 have always been observed in MTO (i.e. reverting methanol synthesis to its initial reactants). They are very easily formed, also in the absence of acid sites,[819] but were until recently considered as irrelevant side products. For example, Munson et al. showed that CO did not accelerate the MTO rate and that labelled CO was not incorporated into the products.[882] However, the experiments were carried out in a NMR reactor at high conversion, i.e. under conditions relevant for the steady state of MTO, but not for the induction period. Still, Hutchings et al. later confirmed that CO had a negligible influence on the induction period of MTO.[883]

Results of the Lercher group suggested that this paradigm should be changed.[819] In TPD experiments where methanol was preadsorbed on the catalyst and then heated either in He or CO, the presence of CO clearly enhanced the formation of olefins. It should be noted, however, that these conditions differ from the continuous reaction, mainly with respect to the water concentration, which is much lower. Considering that zeolites are good carbonylation catalysts (section 9), the authors proposed an involvement of CO in the first C-C bond formation via a

nucleophilic addition of CO on the (electrophilic) surface methoxy group, forming a surface acetyl group. Surface acetyl groups were indeed identified on the surface of SAPO-34 catalysts under MTO conditions; methyl acetate molecules (formed by reaction of methanol with the surface acetyl) were simultaneously detected.[818] Notably, the surface acetyl group can also be viewed as a protonated ketene (CH_2=CO + H^+ → CH_3-CO^+), see section 9.1.

Wang et al. gave support to the role of oxidized forms of methanol in the initiation of the MTO reaction.[884] They carried out the MTO reaction over ZSM-5 under mild conditions (573 K). At very short reaction times, they could detect formaldehyde (and methane) in the products. The formation of formaldehyde was enhanced by EFAl species in the zeolite; a ZSM-5 catalyst without EFAl generated much less formaldehyde. Co-feeding of formaldehyde enhanced the reaction rate, with a high selectivity to ethene. EFAl are known to promote hydrogen transfer reactions (as already illustrated in section 6) and formate species were observed in the conversion of DME over γ-Al_2O_3.[885] The hypothesis is that EFAl species favor the decomposition of CH_3OH into H_2 and formaldehyde and subsequently into CO (although this decomposition is observed to a certain extent on almost any material[819]). CO subsequently reacts with CH_3OH as suggested in **Figure 68**.

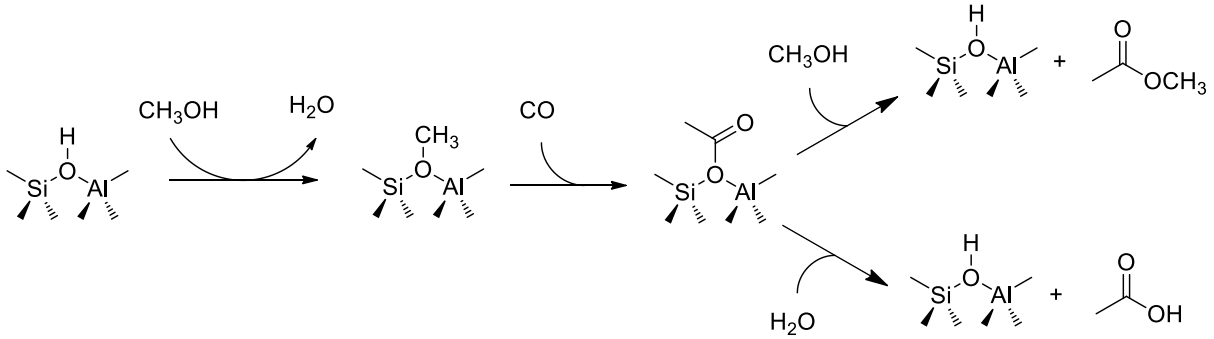

Figure 68. Formation of a surface acetyl group (also called acetate in some papers) by carbonylation of the surface methoxy group, adapted from [819].

Proposals for a direct reaction of formaldehyde with the surface methyl groups have also been made.[884] Irrespective of the detailed reaction mechanism, the idea that either CO or

formaldehyde are involved in the formation of the first C-C bond was reinforced by recent work, which investigated the MTO process with a very sophisticated operando analysis technique, called photoelectron photoion coincidence (PEPICO) spectroscopy.[886] Its high sensitivity for the isomer-selective detection of intermediates provided convincing experimental proof for the involvement of formaldehyde as well as of ketene in the initiation of the MTO reaction.

Other studies reported on the role of aldehydes in MTO chemistry.[887,888] Temperature programmed reaction data shows that acetaldehyde and methylacetate are formed concomitantly with the apparition of the first olefins (**Figure 69**). Surface acetate species and acetaldehyde were also detected on the catalyst surface. Acetaldehyde might be formed from the comproportionation of ketene with methanol, yielding CH_3CHO and CH_2O.[886] In any case, acetaldehyde is already a C_2 species. Therefore, its role in MTO chemistry is related to the question of how the hydrocarbon pool is formed from the first C_2 species, which we will treat in the next section.

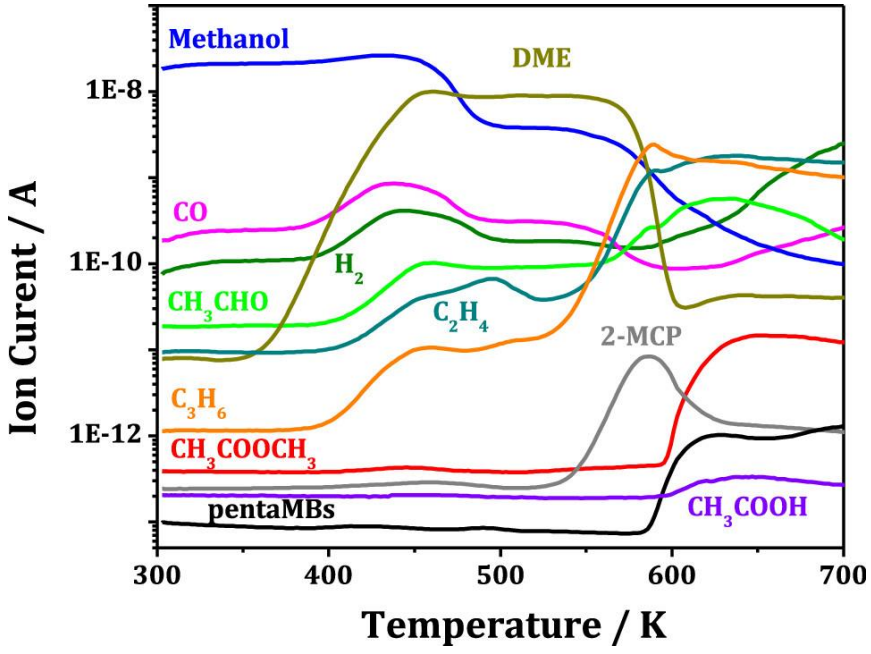

Figure 69. Temperature programmed reaction profiles of methanol conversion over a ZSM-5 catalyst. WHSV = 1 h^{-1}.Reprinted with permission from ref [888]. Copyright 2019 American Chemical Society.

10.3. From the first C_2 species to the hydrocarbon pool

In essence, the question is whether the hydrocarbon pool is generated by oligomerization and cyclisation reactions of oxygenates (formed, for example, by the carbonylation reactions mentioned above) or of olefins. According to some mechanistic proposals, olefins could be the product of the initial C-C bond formation,[862] but they could also result from a reduction of oxygenates, by hydrogen transfer reactions, followed by intramolecular dehydration.[889]

Theoretical work by Plessow and Studt proposed a mechanism where the surface acetyl group is successively methylated to form a dimethylketene, which would then decarbonylate to CO and propene (**Figure 70**).[821,822] Propene then initiates the formation of the hydrocarbon pool. The ketene methylation reactions have very high energy barriers (above 200 $kJ.mol^{-1}$), but the proposal recently found some experimental support: the PEPICO technique managed to detect methylketene (expected product in equilibrium with a surface propionyl species, see **Figure 70**) as an intermediate.[890]

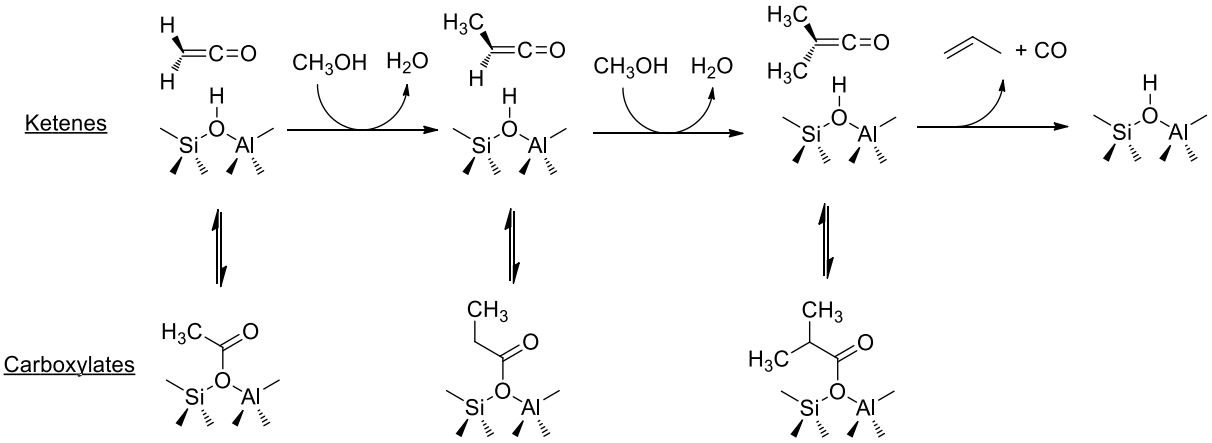

Figure 70. Formation of the first olefin by methylation of CO, followed by methylation of the formed ketene, based on ref[822]

Aldol condensation is another possibility for forming the hydrocarbon pool from the first C_2 species, via acetaldehyde, as mentioned above. The high propensity of aldehydes to cyclize to aromatic species was nicely demonstrated by Hoang et al. They compared the

reactivity of propanal and propene in cyclisation to aromatics.[891] With propanal, cyclization reactions occurred under much milder conditions than with propene. With a propene feed, significant amounts of aromatics were only formed at 773 K, while the aldehyde generated aromatics below 673 K. Moreover, propene mainly led to benzene and toluene, while propanal produced preferentially C_9 aromatics (trimethylbenzenes). The authors proposed that the C_9 aromatics were formed by aldol condensation, followed by cyclization (**Figure 71-a**). In the light of these results, it seems plausible that the hydrocarbon pool in the MTO reaction is (also) formed by aldol condensation of aldehydes and not (only) by oligomerization of alkenes.[892]

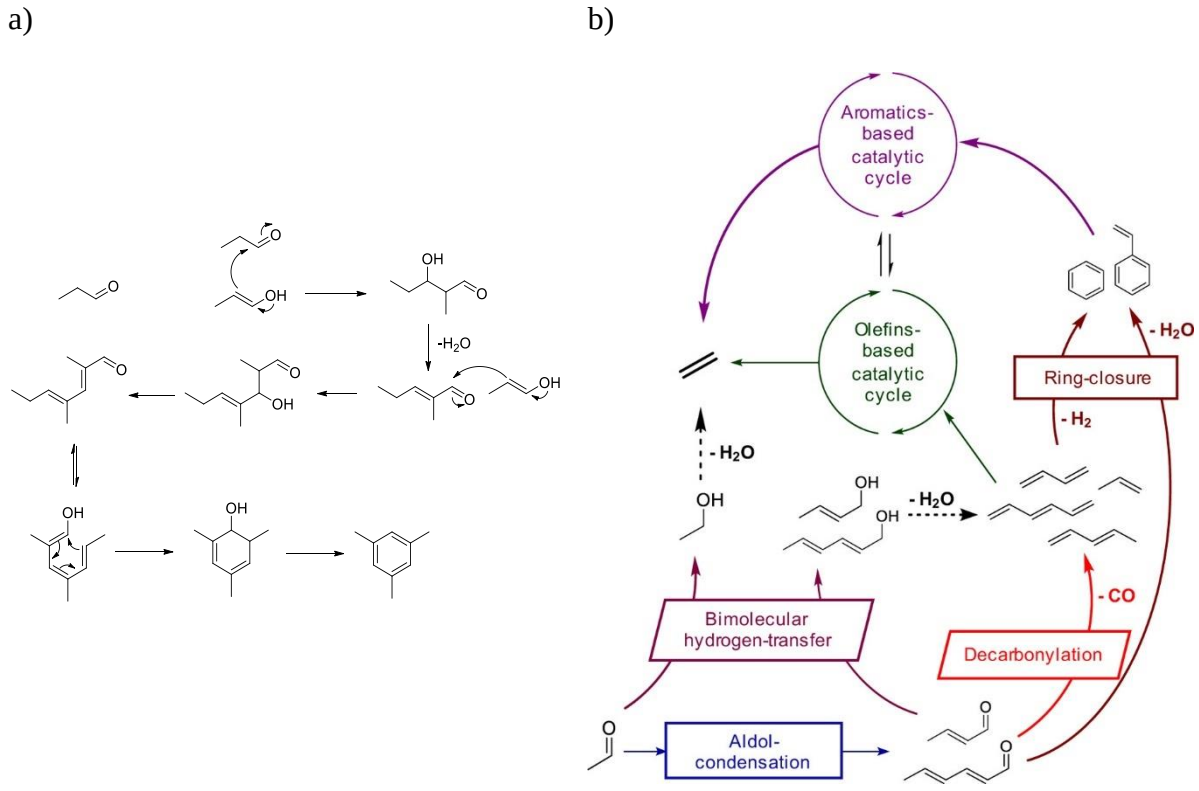

Figure 71. a) Mechanism of formation of aromatics from propanal by aldol condensation and cyclisation, adapted from[891]. b) Transformation of aldehydes under MTO conditions. Reprinted with permission from ref [889]. Copyright 2016 American Chemical Society.

Khare et al. studied the effect of co-feeding of acetaldehyde in the MTO reaction.[889] The aldehyde influenced the MTO reaction in multiple ways. (i) It enhanced the formation of aromatics, via aldol condensation and cyclisation. The increased propagation of the aromatic

cycle increased the selectivity to ethene (see also ref. [887]). (ii) Some ethene was directly produced by hydrogen transfer reactions of acetaldehyde, i.e. its reduction to ethanol, followed by ethanol dehydration. (iii) Decarbonylation products of aldehydes formed by aldol condensation were also detected. They would yield dienes and trienes, which can either undergo ring-closure to aromatics or contribute to the olefin cycle. However, since the overall effect was an enhancement of the aromatics cycle, the cyclisation reactions should be dominating (either via the direct pathway or indirectly, after decarbonylation). All possible reactions of aldehydes under MTO conditions are summed up in **Figure 71-b**.

10.4. Dealkylation mechanisms in the aromatics cycle

In a previous section we have discussed the contributions of the aromatic and the olefin cycle to the product distribution. The aromatic cycle produces olefins by dealkylation reactions. Two mechanisms have been proposed for these dealkylation reactions: (i) the paring mechanism, in analogy to seminal work of Sullivan et al.[608] who proposed a mechanism for the dealkylation of aromatics under hydrocracking conditions, and the (ii) side-chain mechanism. In the side chain mechanism, a methyl substituent of the aromatic ring is alkylated with methanol to form an ethyl group, which can then split off ethene or be further alkylated to isopropyl and split off propene (**Figure 72**). The paring mechanism involves a ring contraction of the aromatic 6-membered ring to a 5-membered ring, creating a $>C_2$ side chain, which can then be split off (**Figure 73**). Note, however, that in the original work of Sullivan the main product was i-C_4, which can form a stable tertiary carbenium ion. The formation of smaller olefins by a paring route is, therefore, quite intriguing. Experimental evidence for the involvement of the paring route comes from isotope labelling studies. When aromatics, labelled on ring atoms, are co-fed with methanol or DME, the labelled atoms end up in the light olefin products[864], i.e. ethene and propene, in SAPO-5[893] and ZSM-5.[894] This is compatible with a

ring-contraction/ring-expansion process, which leads to a scrambling of the carbon atoms in the ring and in the alkyl side chains. However, Haw et al. already pointed out that such ring contraction and expansion reactions, leading to scrambling of labels, could precede the dealkylation process (which might still happen via the side chains).[864]

A recent study from Bhan's group pushed the isotope analysis very far and could thereby quantify the importance of side chain and paring routes for a SAPO-34 catalyst.[895] They compared the measured isotope distributions in the olefins to the theoretically expected results for either the side chain or the paring mechanism (according to **Figure 73**). In the case of ethene, the by far best match was achieved for the scenario of a side-chain mechanism starting from tetramethylbenzene. In the case of propene, the best matching mechanism was the paring route starting from penta- and hexamethylbenzene. This suggests that both mechanisms are operating in parallel, but their importance depends on the degree of methylation of the aromatic hydrocarbon pool. Moreover, the side-chain route would favor ethene and the paring route would favor propene.

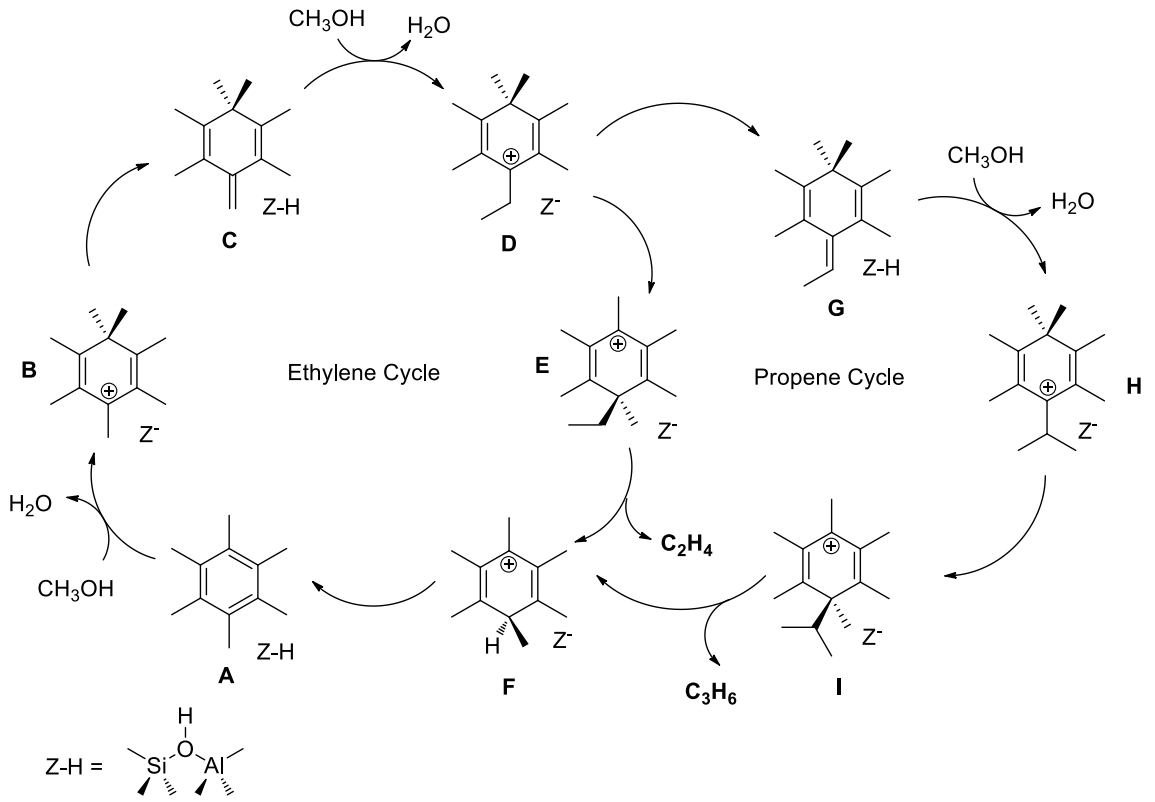

Figure 72. Elementary steps of the side chain dealkylation leading either to ethene or propene, adapted from ref [896].

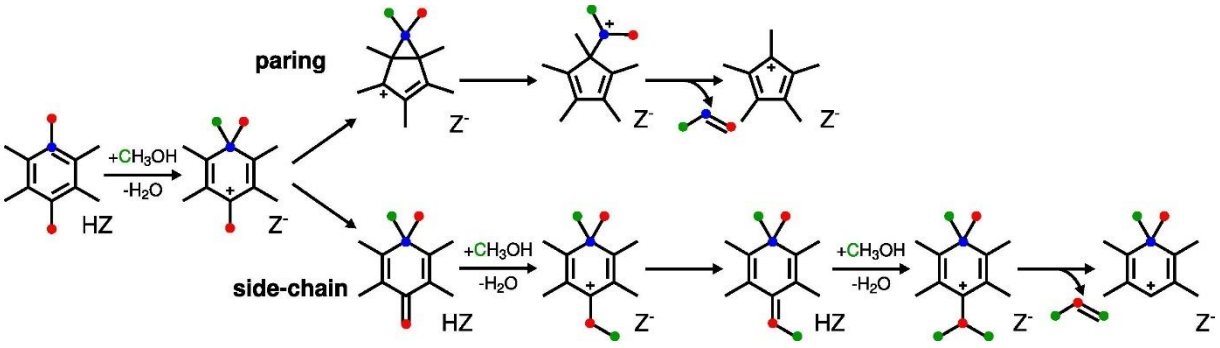

Figure 73. Side chain or the paring route for the dealkylation of hexamethylbenzene to propene: impact on the origin of the carbon atoms in the propene and aromatic product. Reprinted with permission from ref [895]. Copyright 2019 Elsevier.

The detailed mechanisms of the side chain route and of the paring route have been investigated by DFT, including by AIMD. According to the current state of the art,[29,896] the elementary steps of the side chain route towards ethene are (**Figure 72**):

- a geminal methylation of (n)-methyl-benzene (**A**) to a gem-(n+1)-methyl-benzenium cation (**B**). Except for fully methylated benzene, this step obviously competes with ring-methylation on a "free" position of the cycle (**Figure 74**). Ferri et al. recently calculated the Gibbs free energies of geminal *versus* ring methylation and found that the former was generally less favorable.[315]
- The deprotonation to a (n+1)-methyl-methylene-cyclohexadiene (**C**). Note that only a gem-methylated benzene ring will deprotonate to form an exocyclic double bond, the ring methylation more favorably deprotonates to yield (n+1)-methyl-benzene (**Figure 74**).[897]
- Methylation of the methylene group to an ethyl side chain, forming a (n)-methyl-ethyl-benzenium cation (**D**).
- Migration of one of the gem-methyl groups to the ethyl side chain. The presence of geminal methyl and ethyl groups facilitates the splitting off of ethene because it weakens the C-C bond to the ring.[896]
- Simultaneous elimination of ethene and deprotonation, which closes the catalytic cycle.

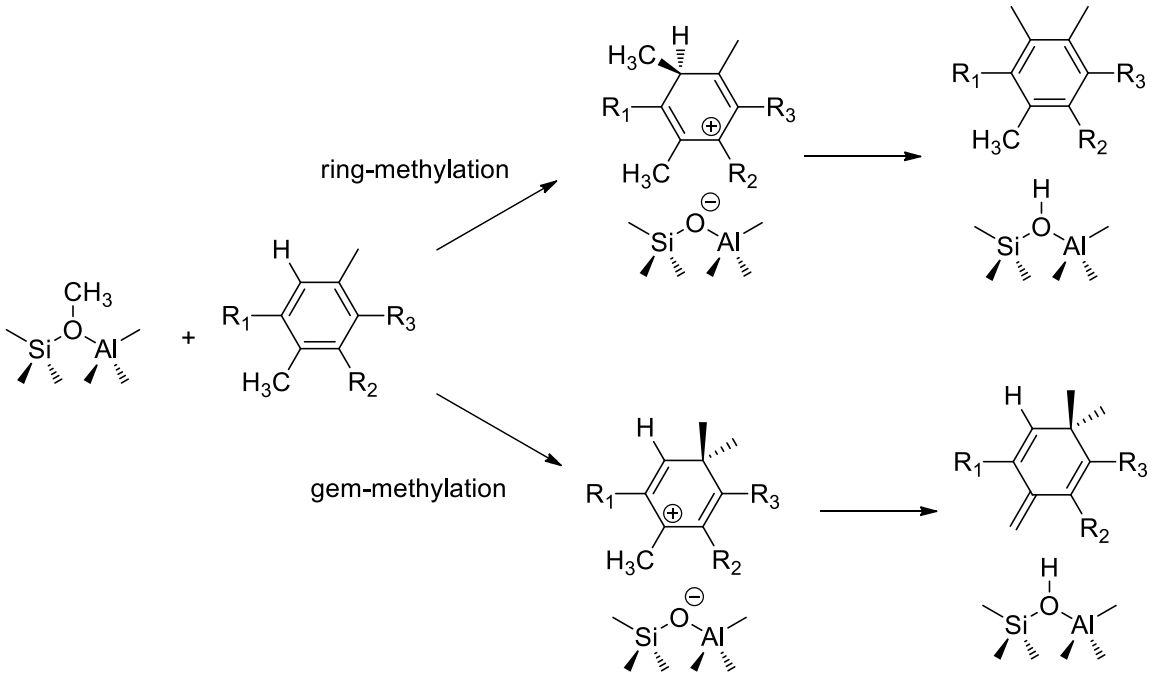

Figure 74. Illustration of geminal vs ring methylation of a substituted benzene ring. R_1, R_2, R_3 = H or CH_3. Only in the case of the gem-methylation, the final deprotonation step leads to an exocyclic methylene group.

For the formation of propene, the ethyl side chain is methylated once more, forming an isopropyl side chain, which then splits off (after migration of a methyl group to form a geminal methyl-isopropyl configuration).

Wang et al. compared the energy barriers leading to ethene and propene (via the side chain route) for SAPO-34 and concluded (in agreement with Bhan et al.[894]) that the side chain route should be selective for ethene.[898] The rate determining step is the reaction of the methylene-cyclohexadiene species with methanol. A DFT study on ZSM-5 found that the formation rates of ethene and propene via the side chain mechanism should be comparable.[899]

There is much less consensus on the elementary steps of the paring route. According to the seminal work of McCann et al., the ring contraction proceeds through a bicyclo-intermediate, which then undergoes ring opening to a substituted cyclopentadienyl cation (as illustrated in **Figure 73**; this transformation also corresponds to the step from **B** to **N** in **Figure 75**).[900] Both steps are uphill in energy and have, on top of that, high activation barriers (Gibbs

free energy barrier for the formation of the bicyclic intermediate of ~220 kJ.mol^{-1}).[901] High energy barriers were also calculated for the subsequent step, i.e. the elimination of propene (in the order of 160 kJ.mol^{-1}).[899,902] The elimination transition state usually corresponds to the highest transition state on the potential energy surface of this mechanism. Overall, until recently, all DFT studies calculated barriers of at least 200 kJ.mol^{-1} were computed for the paring route[899,901,902], suggesting that it would not take a significant part in the reaction.

Plessow and Studt pointed out that the "traditional" paring mechanism involved the formation of an antiaromatic cyclopentadienyl cation (species **N** in **Figure 75**), which is energetically very unfavorable.[903] They, therefore, proposed a different mechanistic route for the paring mechanism (for the case of the CHA structure). In their revised mechanism, they start from methylenecyclohexadiene (which is also the key intermediate in the side chain route), which is protonated and then undergoes ring-contraction (from **C** to **J** in **Figure 75**). This species can crack off propene without forming a primary cation (or a very energetic bicyclic) intermediate (**Figure 75-b**). The transition state of the new cracking mechanism has a Gibbs free energy of only 142 kJ.mol^{-1} (relative to protonated heptamethylbenzene), i.e. significantly lower than in all previous studies and close to the energy barriers commonly found for the methylation of aromatics. Interestingly, they also considered a pathway where a ring expansion back to a 6-membered ring occurred before cracking. In that case, the ring-expansion had the highest energy barrier (127 kJ.mol^{-1}, i.e. of the same order of magnitude). Note that this would also be the barrier for a scrambling of carbon atoms by ring-contraction/ring-expansion.

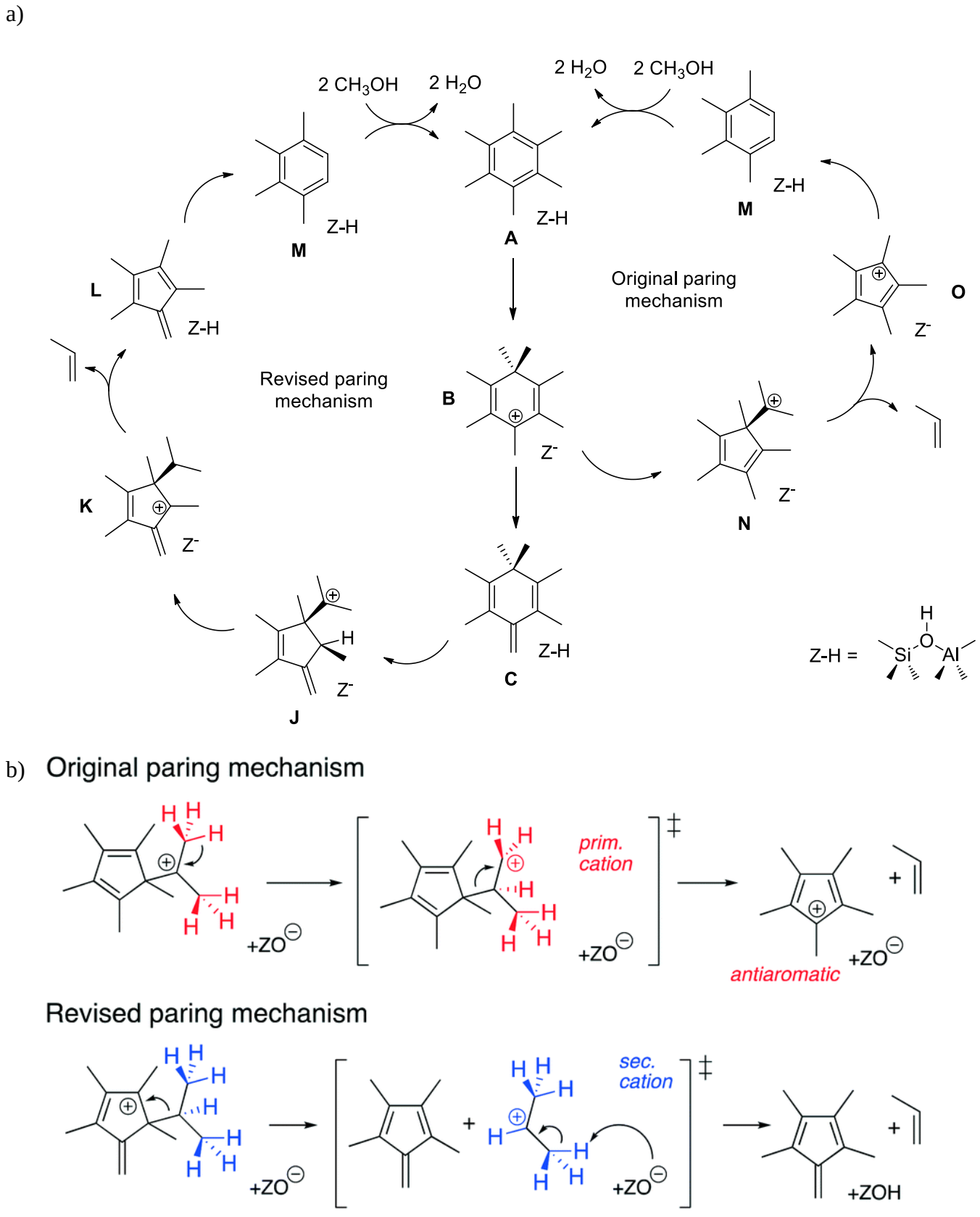

Figure 75. a) Comparison of the revised and the classical paring cycle. b) Comparison of the transition states of the propene cracking step (which usually corresponds to the highest Gibbs free energy) in the original paring mechanism and the revised mechanism.[903] Licensed under CC BY 3.0.

10.5. Shape selectivity effects

Very early on it was recognized that shape selectivity effects play a major role in governing the MTO product distribution.[864] While zeolites like ZSM-5 and Beta produce significant amounts of aromatics, other small pore zeolites like SAPO-34 (or SSZ-13), ZSM-22 or ZSM-23[904] are fully selective to olefins. Aromatics still constitute the hydrocarbon pool inside the pores of these structures, but the bulky aromatic molecules cannot diffuse out of the pore system and are, therefore, not found in the products. Zeolites with very small cages (MCM-35, ERS-7) have no MTO activity at all because they cannot accommodate aromatic hydrocarbon pool intermediates.[905] The size of the cage governs the type of aromatic intermediates that can be stabilized and, thereby, influences the product selectivity.[906] Current research on MTO catalysts strongly focuses on olefin selective 8MR cage-type structures, with the goal of controlling the selectivity towards ethene *versus* propene.

The Davis group examined the selectivity of a large number of small-pore cage-type topologies and found that the olefin selectivity was quite well correlated with the cage-defining ring size, which is the critical diameter of the ellipse that can be inscribed in the cage (**Figure 76**).[907] The zeolites with the smallest cage-defining ring size had the highest selectivity to ethene *versus* propene, while very large cages produced longer olefins.[908]

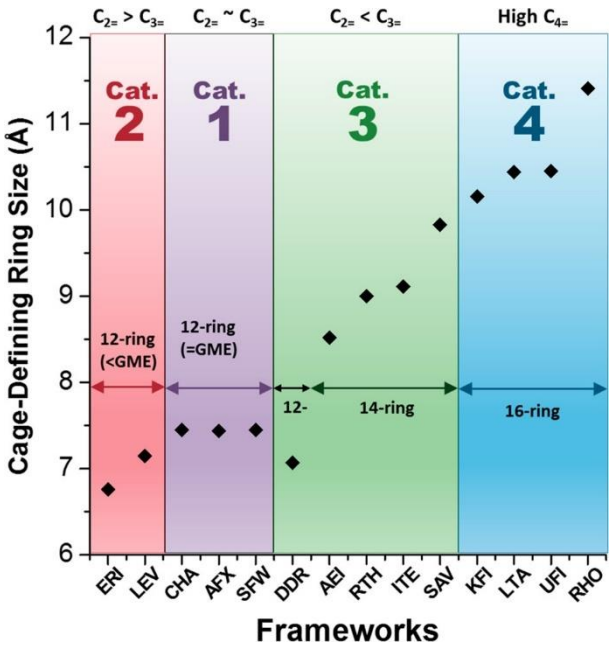

Figure 76. Relation between the cage-defining ring size of the zeolite topology and the selectivity to $C_2/C_3/C_4$ olefins. Reprinted with permission from ref [907]. Copyright 2019 American Chemical Society.

Zhang et al. studied in more detail the small pore zeolite RUB-50 (LEV topology), a cage-type zeolite with a 8MR pore opening, having a very high ethene/propene selectivity.[313] In order to rationalize the high ethene selectivity, the authors calculated with DFT the energy barriers for the side chain mechanism (the paring mechanism was excluded because of very high barriers) leading either to propene or ethene. They found that the additional side chain methylation step required for propene formation had a very high energy barrier, related to the steric constraints in the small levionite cavity. In CHA, much less selective for ethene, both ethene and propene formation had similar energy barriers (the CHA cage is larger than the LEV cage, see **Figure 76**). The authors conclude that the host-guest interactions of the key intermediates in the catalytic cycle govern the product selectivity.

In the same vein, Ferri et al.[315] addressed the selectivity question by calculating the stability of key intermediates of the aromatic cycle in different zeolite topologies: CHA/AEI and RTH/ITE (these pairs are structurally related), all of which have cage structure with 8MR openings. In contrast to Zhang et al., who only looked at the propene/ethene selectivity within

the side chain route, they started from the paradigm that the selectivity towards propene/butene *versus* ethene is related to the relative importance of the paring and the side chain route: the side-chain mechanism favors the formation of ethene, while paring mechanism favors the formation of propene/butene. Their DFT calculations show that the ring-contraction step in the paring route, which leads to a bicyclic intermediate, is only energetically affordable for a fully methylated gem-heptamethyl species. In order words, only fully methylated benzene rings can initiate the paring cycle and yield propene, while a gem-methylation on a partially methylated benzene would favor the side-chain mechanism and formation of ethene. Thus, it all comes down to the probability of ring-methylation *versus* gem-methylation to occur (see **Figure 74**), that was found to depend on the zeolite topology and cage structure. In order to quantify this, the authors propose a descriptor which can predict the relative importance of the two pathways, which is the ratio of the energetic stabilities of the gem-pentamethylbenzenium cation (partially methylated) and of the gem-heptamethylbenzenium cation (fully methylated) as calculated by DFT (called $E_{int(7/5)}$ **in Figure 77**). Indeed, this descriptor very nicely correlates to the propene/ethene selectivity experimentally observed for several small pore zeolites (**Figure 77**). Typically, ITE and RTH types favor the most the fully methylated species and hence are more selective to propene while CHA and to a lesser extent AEI favor the partially methylated species and thus are more selective to ethene.

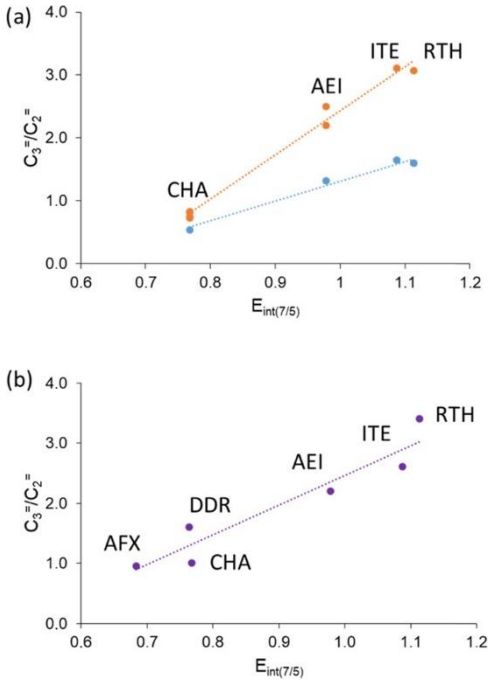

Figure 77. Correlation between the ratio of the stability of gem-heptamethylbenzenium and gem-pentamethylbenzenium cation with the zeolite cage (calculated by DFT) and the experimental propene/ethene ratio. Reprinted with permission from ref [315]. Copyright 2019 American Chemical Society.

However, a follow-up paper showed that this correlation has some limits.[909] The LEV topology has a very low $E_{int(7/5)}$ parameter, reflecting the very low stability of the hepta-methylated benzene ring in the small levionite cage, but experimentally significant amounts of propene, butene and even larger olefins were detected, which were produced by the olefin cycle (not accounted for in the theoretical model). On the other end of the confinement spectrum, the behavior of zeolites with very large cages is also not perfectly described because hydrogen transfer reactions (to alkenes and aromatics) consume part of the olefins.

10.6. Concluding remarks

The MTO chemistry is still a very hot topic of research, because of the industrial importance of the process, which offers a route for making olefins from many raw materials (not necessarily fossil). It is now generally agreed that short olefins are produced indirectly, via a hydrocarbon pool, either from the olefin cycle (cracking of longer olefins to propene, butene,

etc.) or from the aromatic cycle. According to the rules of carbenium ion cracking, the olefin cycle does not produce ethene, but only olefins with at least three carbon atoms. The aromatic cycle generates mainly ethene or propene, by dealkylation of multi-methylbenzene intermediates. Two mechanisms may be operating in the aromatic cycle: the paring mechanism and the side chain mechanism. The side chain route seems to favor ethene, while the paring route mainly makes propene. According to the current state of the art in DFT, both mechanisms rely on the formation of gem-methylated benzene. Theoretical calculations further indicate that the paring route is only energetically affordable for fully methylated benzene rings (which are the dominating intermediates in SAPO-34, but not in ZSM-5). By using zeolites with small cages, it is possible to block the paring route and drive the selectivity towards the side chain mechanism, resulting in a high ethene selectivity. However, this reasoning only works if the contribution of the olefin cycle (selective for propene and butene) is negligible, which is not the case for many zeolites, in particular for ZSM-5. The relative importance of the olefin cycle, the paring route and the side chain route in different zeolites has not been totally clarified and certainly requires further investigations.

Concerning the induction period, which generates the hydrocarbon pool, the current consensus is that CO or CH_2O are involved in the first C-C bond formation, by reaction of the latter with a surface methyl group. Acetaldehyde was detected as an intermediate, and probably contributes to the formation of first aromatic molecules via aldol condensation and cyclisation reactions.

The research on MTO chemistry is a very nice example of how the combined used of intelligent kinetic experiments, spectroscopy and theory allows making sense of a very complex system and is also a very timely example of the fascinating shape selectivity of zeolites.

11. Summary and future orientations

In this review we have highlighted some of the key molecular aspects of Brønsted acid catalyzed reactions in zeolites. The main particularities of these catalysts over other heterogeneous or homogeneous catalysts, that transpire throughout the whole review, lie in (i) their ability to allow for a peculiar carbocation chemistry, (ii) the effect of the confinement within the zeolite pores that greatly affects the activity and the selectivity of the reactions.

In many reactions catalyzed by proton-exchanged zeolites reported in the present review, the impact of carbocation chemistry has been discussed, i.e. it remains highly relevant for rationalizing the catalytic chemistry.[25] Quite often, reactions involving C-C or C-O bond breaking or making are kinetically more limiting than protonation steps, although the intrinsic rate constants of some of the reactions discussed are not sufficiently well quantified to draw a completely general conclusion. A clear exception to this trend is the Haag-Dessau alkane cracking, for which the formation of the carbonium ion upon protonation of the alkane is limiting. This is due both to the very high stability of the reactant molecule (the highest of all reactants) and the poor stability of the carbonium ion. The stability of the carbocation itself in the porosity of the zeolite is a key question for all reactions, which is often addressed by means of ab initio calculations. It essentially depends on the substrate and nature of carbocation (carbenium vs. carbonium, primary, secondary or tertiary cation etc.) although we highlighted that care must be taken since the answer may diverge depending on the calculation methods used. State-of-the art methods should be employed when addressing such issues.

The other recurrent feature that emerges from this review is the predominant role of adsorption and confinement in zeolite catalysis. It has been known for a long time that confinement effects have major influence on activity and selectivity, but the recent advances in molecular modeling have allowed to describe these concepts more precisely, sometimes in a

quantitative manner. With respect to activity, the role of confinement in the zeolite pores had formerly been mainly attributed to the adsorptive stabilization of the reactant on the acid sites. However, several examples in this review show that considering the adsorption of the reactant is not sufficient. It is essential to consider the stabilization of the transition states and/or the key intermediates. A particular feature of Brønsted acid zeolite catalysis is that after the first protonation step, the intermediate molecule is likely to evolve into species that are poorly covalently bond to the catalysts while still exhibiting high adsorption enthalpies due to the interaction in the pore through van der Waals and electrostatic interactions. These species additionally have significantly increased entropy in comparison with intermediates or transition states covalently bound at the surface of other types of catalysts (metals, oxides, etc.). Accounting for these entropy effects is a key requirement for rationalizing reactivity trends. Moreover, confinement effects depend on the local environment of the active sites. This is the basis of the site-specific reactivity of zeolites. A very prominent example is Mordenite where the acid sites in the main channels (12MR) and in the side pockets (8MR) have very different reactivity in alkane cracking, ethanol dehydration and methanol (or DME) carbonylation for example.

In many cases, confinement effects also govern the selectivity of zeolite catalyzed reactions, i.e. they explain many unique features of zeolite catalysis, which are not found with other catalytic materials. Such effects have been known under the term “shape selectivity”. In particular, the term “transition state shape selectivity” was used to describe the fact that some zeolite pore system did not offer sufficient space to form some bulky transition states or intermediates but allowed the formation of others, thereby orienting the selectivity towards these products. Quantum chemical calculations now allow for a precise quantification of the stabilization of different transition states or of critical intermediates as a function of pore topology, thus, pushing the notion of transition state selectivity further.[321,410,576]

Overall, these particularities open in principle the way for tuning zeolite reactivity and/or selectivity by using synthetic methods in order to place the Al atoms (which generate the Brønsted acid sites) in the most adequate T-sites of the zeolite structure.[112,115,842,910–912] Modern methods of zeolite synthesis go even further and try to design the local environment of the acid sites, so as the maximize the stabilization of the targeted intermediates or transition states. This can be done by preparing zeolites with organic structure directing agents that resemble the transition state of the target reactions.[15,59]

We also see that the degree of knowledge that was achieved so far in the understanding of reaction mechanisms strongly depends on the reaction under consideration. This can be explained, in part, by the amount of work devoted to some of the reactions rather than to others, partly for historical reasons. Cracking of alkanes, isomerization of aromatics and conversion of alkenes for instance, are typically involved in petroleum refining processes, hence many studies are available in literature. However, there are also more technical reasons. In several cases, it is possible, and relevant, to examine the behavior of the catalysts at low loading of the zeolite pores. This is the case of reactions in gas phase, where conversion can be maintained as low, thereby also hindering the occurrence of multi-molecular side reactions. For short alkane cracking reactions, in some instances, a full decomposition of the adsorption/reaction and enthalpic/entropic parameters has been provided. Also, the connection with computational studies is rather direct in these cases, as intrinsic kinetics is experimentally determined, and as theoretical studies are made affordable by the limited number of reactive molecules to be considered. Still, considering the dynamics of the intermediates and transition states in the porosity appears to be crucial for most of these reactions. In other examples, though, the reaction intrinsically must occur in conditions where the zeolite pore is highly filled, either by reactive molecules or because of the presence of the solvent. Examples of this kind can be found for the transformation of alkanes and aromatic molecules (depending on the operating

conditions), in the dehydration of sugars and polyalcohols, and in some of the MTO reactions. In such conditions, additional difficulties to get detailed information about the intrinsic kinetics arise. The definition of the Brønsted acid site changes in the presence of water as a solvent for example, with the intervention of protonated water clusters. Solvent or co-adsorbed reactant molecules moreover affect the adsorption strength, and diffusion barriers. From the computational point of view, the simulation of such reactions requires to consider many molecules per simulation unit cell, and their complex dynamic interplay. This makes AIMD studies required in first instances, which is much trickier than with a single reactant molecule.

Despite recent progress made in all fields of research, experimentally and theoretically, the quest for deciphering reaction mechanisms, confinement effects and selectivity of zeolite catalyzed reactions still encounters numerous difficulties that are general to all the reactions mentioned in the present review.

We have seen that a full rationalization of the selectivity of zeolites remains challenging. Many reactions discussed in this review can proceed via different pathways (monomolecular versus bimolecular isomerization of aromatics, direct dehydration of alcohols to olefins versus the indirect pathway via ethers, the aromatic versus the olefin cycle in MTO, and so on). Each pathway has its own transition state selectivity, i.e. it is strongly influence by the zeolite topology. However, the zeolite topology also changes the relative importance of one pathway versus the other. Both from an experimental and from a computational point of view, it is a paramount task to determine the contribution of different pathways as well as their selectivity pattern for a large number of zeolite topologies. Hence, it remains difficult to get the full picture.

Also, the determination of the number and location of the acid sites that are playing a role in catalysis is still a challenge, despite the well-defined nature of zeolite catalysts with respect to other kinds of heterogeneous catalysts. Regarding spectroscopic approaches, difficulties are related to the short lifetime of key intermediates such as carbocations, and to the

occurrence of many side-reactions, which also complexify kinetic analysis. Distinguishing relevant intermediates from spectator species and poisons is generally not trivial and requires coupling operando spectroscopy with transient kinetics, but instrumental progress in IR and NMR spectroscopy as well as in other emerging techniques (like PEPICO) open new possibilities. Second, care must be taken when interpreting differences in turnover frequencies of different samples of the same zeolite structure in terms of T-site specific reactivity, because other factors can influence the intrinsic reactivity of an acid site, such as the presence of Al pairs or the synergy with extra framework aluminum species. The crucial role of extra-framework species has been demonstrated for several reactions, but the effects are not yet fully understood, mainly due to the lack of knowledge on the structure and location of extra-framework species themselves. Third, the stabilization of intermediates or transition states does not explain all the selectivity trends in zeolite catalysis. In many cases, diffusion must be invoked to rationalize the observed rate constants and product distribution.[226,410,589,913] These phenomena are known as reactant or product shape selectivity. Experimentally, possible intraparticle diffusion limitations are also only scarcely quantified,[913,914] due to the difficulty to synthesize a given zeolite at various particle size, while keeping all other influential parameters (such as crystallinity, Si/Al ratio, location of acid sites) unchanged. Hence, significant progress remains to be made in unraveling precisely the role of diffusion in zeolite catalysis.

Regarding the transformation of hydrocarbons, the most advanced achievements are reported for alkane cracking mechanisms according to the Haag-Dessau schemes. The approach undertaken to decompose enthalpy/entropy and adsorption/intrinsic kinetics component is worth being transposed to other transformations, although difficulties will emerge in the case of more reactive substrates to obtain relevant adsorption data at conversion temperature. Regarding the transformation of oxygenates, the main perspectives deal with the transformation of multi-functional molecules, such as polyols and sugars. In the latter case, the possible

conversion from linear to cyclic forms of the reactant within the zeolite further complexifies the analysis, as well as the practical impossibility of carrying out gas-phase reaction and thus the unavoidable implication of a solvent (generally water, but not exclusively so). More generally, the transformation of biosourced molecules usually involves mixtures with water, and/or the implication of solvents. Thus, a key-point will be the understanding of the effect of these additional molecules on the transformation mechanisms.

Regarding first principles calculations, as illustrated by the evolution of the findings with respect to accessible computational resources, the models of the active site, the level of theory, and the methodology chosen for the reactivity investigations strongly influence the conclusions made. Whereas most simple small cluster models often failed in catching the chemistry of these systems, more reliable results have been provided by periodic and hybrid approaches. Still, efforts are needed to account for the role of defects and extra-framework species, the structure of which is not well known. For some of the reactions under consideration, high levels of theory (beyond DFT) and *ab initio* molecular dynamics techniques have been shown to be required for a proper quantification of intrinsic kinetics. Combining both is one of the most important challenges currently faced by the community. Recent developments making use of perturbation theory and machine learning open to door to such achievements.[915,916] Examples have been recently reported for catalysis by Brønsted acid zeolites.[829,917] Another related axis of progress consists in the development of accurate interatomic potential that would make it much cheaper to acquire long molecular dynamics trajectories. Regarding the accuracy of such approaches, active learning schemes proposed recently are promising,[918,919] but, to the best of our knowledge, have never been applied to zeolites so far. These developments would allow quantifying most accurately rate constants, that could then be integrated in multi-scale kinetic models to quantify macroscopic parameters such as activities and selectivities as a function of operating parameters. Such an approach is a very relevant tool to validate the

mechanisms proposed by *ab initio* calculations and to propose predictive models. Several promising examples of this kind of approaches have been reported in the case of reactions catalyzed by Brønsted acidic zeolites,[346,350,534,632,665,666,820] but either with deviations from experimental observations, or with the need to adjust some of the DFT-predicted barriers to better fit to experiments. Finally, although significant progress has been made, the determination of diffusion coefficients for slowly diffusing molecules by computational methods remains challenging. Additional progress, for instance by using more systematically combinations of molecular mechanisms (e.g. Monte Carlo simulations) and *ab initio* modeling may improve the description of such phenomena at the molecular scale. Likewise, such techniques may also be helpful in cases where a solvent is present in order to propose realistic models of the pore occupation by solvent and substrate before performing mechanistic studies.

Finally, for many zeolites catalyzed reactions, the zeolite catalyst operates in the presence of carbonaceous deposits or coke in the porosity. The coke modifies the diffusion and confinement properties *versus* the pristine zeolite and it has been shown that it can also intervene in the catalytic cycle.[441] Characterizing the behavior of the real, coked zeolite is challenging, both experimentally and computationally, but will be a necessary step to the optimization of catalysts and processes catalyzed by Brønsted acidic zeolites.

12. Acknowledgments

The authors thank the many colleagues, students and collaborators that have contributed to their research activities in the field in the last years.

13. Author information

Corresponding author

Céline Chizallet

IFP Energies Nouvelles – Rond-Point de l'Echangeur de Solaize – BP 3, 69360 Solaize, France.

ORCID: http://orcid.org/0000-0001-5140-8397

Email: celine.chizallet@ifpen.fr

Authors

Christophe Bouchy

IFP Energies Nouvelles – Rond-Point de l'Echangeur de Solaize – BP 3, 69360 Solaize, France.

ORCID: https://orcid.org/0000-0002-1414-0333

Kim Larmier

IFP Energies Nouvelles – Rond-Point de l'Echangeur de Solaize – BP 3, 69360 Solaize, France.

ORCID: https://orcid.org/0000-0002-5199-1516

Gerhard Pirngruber

IFP Energies Nouvelles – Rond-Point de l'Echangeur de Solaize – BP 3, 69360 Solaize, France.

ORCID: http://orcid.org/0000-0003-0688-425X

14.Biographies

Céline Chizallet. Céline Chizallet (born 1980) graduated from Ecole Normale Supérieure (Paris, MSc in 2002, “Agrégation de Chimie” in 2003). She obtained a PhD in Inorganic Chemistry in 2006 (Paris VI University, under the supervision of Prof. M. Che), and an HDR (Habilitation à Diriger des Recherches) from Ecole Normale Supérieure de Lyon in 2017. She currently holds a Project leader position in the Catalysis, Biocatalysis and Separation Division of IFP Energies nouvelles in Solaize, France. Her role is the implementation of quantum chemistry approaches within applied experimental research programs. Her research interest deals with computational heterogeneous catalysis, with the simulation of complex catalysts of industrial relevance, in particular reactions catalyzed by aluminosilicates and supported metals. She is co-author of 97 peer reviewed articles, 5 patents and one book chapter.

Christophe Bouchy. Christophe Bouchy (born 1971) received his master degree from Université Louis Pasteur de Strasbourg, France, in the field of Materials Sciences. He obtained a PhD in Materials Sciences at Université Louis Pasteur, in 1998, under the joint supervision of Prof. M.J. Ledoux and Dr. C. Pham-Huu. Between 1999 and 2000, he held a post doc position at the Leverhulme Centre For Innovative Catalysis, The University of Liverpool, United Kingdom, under the guidance of Prof. E.G. Derouane. In 2001 he joined IFP Energies nouvelles. He currently holds a Project leader position in the Catalysis, Biocatalysis and Separation Division in Solaize, France. His research interest currently deals with the use of zeolites in the fields of petrochemistry and biofuels production. He is author or co-author of 55 peer reviewed articles and 61 patents.

Kim Larmier. Kim Larmier (born 1987) earned his B.S. and M.S. degrees in chemistry at École Normale Supérieure in Paris, France, in 2010. He received his Ph.D. in materials chemistry and physics from Sorbonne Université (formerly UPMC) in 2015, where he studied the reactivity of alcohols on the surface of oxides by combined computational and experimental approaches under the joint supervision of Prof. H. Pernot and Dr. E. Marceau. He was a postdoctoral fellow in the laboratory of Prof. C. Copéret at ETH Zürich from 2015 to 2018, where he worked on molecular aspects of CO_2 conversion reactions. He is currently a researcher at IFP Energies nouvelles in Lyon, working mostly on biomass conversion reactions to fuels and chemicals and the upcycling of plastics. He is author of 26 peer reviewed articles and 14 patents.

Gerhard Pirngruber. Gerhard Pirngruber (born 1972) received his master degree from TU Wien, Austria, in 1995, in the field of Physical and Analytical Chemistry. He obtained a PhD in Heterogeneous Catalysis at UTwente, The Netherlands, in 1999, under the guidance of Prof. J. Lercher. From 2000 to 2005, he supervised a subgroup in the lab of Prof. R. Prins at ETH Zurich, working on zeolites and mesoporous silicas. In 2005 he joined IFP Energies nouvelles in Lyon, where has been working ever since on various aspects of heterogeneous catalysis and separation processes, with a focus on the use of zeolites in refining and petrochemistry. He is author of 115 peer reviewed articles, 20 patents and 3 book chapters.

15. REFERENCES

(1) Cundy, C. S.; Cox, P. A. The Hydrothermal Synthesis of Zeolites: History and Development from the Earliest Days to the Present Time. *Chem. Rev.* **2003**, *103*, 663–702. DOI: 10.1021/cr020060i.

(2) Li, J.; Corma, A.; Yu, J. Synthesis of New Zeolite Structures. *Chem. Soc. Rev.* **2015**, *44*, 7112–7127. DOI: 10.1039/C5CS00023H.

(3) Li, Y.; Yu, J. New Stories of Zeolite Structures: Their Descriptions, Determinations, Predictions, and Evaluations. *Chem. Rev.* **2014**, *114*, 7268–7316. DOI: 10.1021/cr500010r.

(4) Roth, W. J.; Nachtigall, P.; Morris, R. E.; Čejka, J. Two-Dimensional Zeolites: Current Status and Perspectives. *Chem. Rev.* **2014**, *114*, 4807–4837. DOI: 10.1021/cr400600f.

(5) Vermeiren, W.; Gilson, J.-P. Impact of Zeolites on the Petroleum and Petrochemical Industry. *Top. Catal.* **2009**, *52*, 1131–1161. DOI: 10.1007/s11244-009-9271-8.

(6) Marcilly, C. *Acido-Basic Catalysis*; Technip, 2005.

(7) Busca, G. Acid Catalysts in Industrial Hydrocarbon Chemistry. *Chem. Rev.* **2007**, *107*, 5366–5410. DOI: 10.1021/cr068042e.

(8) Primo, A.; Garcia, H. Zeolites as Catalysts in Oil Refining. *Chem. Soc. Rev.* **2014**, *43*, 7548–7561. DOI: 10.1039/C3CS60394F.

(9) Brønsted, J. N. Einige Bemerkungen Über Den Begriff Der Säuren Und Basen. *Recl. Trav. Chim. Pays-Bas* **1923**, *42*, 718–728. DOI: 10.1002/recl.19230420815.

(10) Corma, A. Inorganic Solid Acids and Their Use in Acid-Catalyzed Hydrocarbon Reactions. *Chem. Rev.* **1995**, *95*, 559–614. DOI: 10.1021/cr00035a006.

(11) Del Campo, P.; Martínez, C.; Corma, A. Activation and Conversion of Alkanes in the Confined Space of Zeolite-Type Materials. *Chem. Soc. Rev.* **2021**, *50*, 8511–8595. DOI: 10.1039/d0cs01459a.

(12) Ennaert, T.; van Aelst, J.; Dijkmans, J.; Clercq, R. de; Schutyser, W.; Dusselier, M.; Verboekend, D.; Sels, B. F. Potential and Challenges of Zeolite Chemistry in the Catalytic Conversion of Biomass. *Chem. Soc. Rev.* **2016**, *45*, 584–611. DOI: 10.1039/C5CS00859J.

(13) Mardiana, S.; Azhari, N. J.; Ilmi, T.; Kadja, G. T. Hierarchical Zeolite for Biomass Conversion to Biofuel: A Review. *Fuel* **2022**, *309*, 122119. DOI: 10.1016/j.fuel.2021.122119.

(14) Martín, A. J.; Mondelli, C.; Jaydev, S. D.; Pérez-Ramírez, J. Catalytic Processing of Plastic Waste on the Rise. *Chem* **2021**, *7*, 1487–1533. DOI: 10.1016/j.chempr.2020.12.006.

(15) Gallego, E. M.; Portilla, M. T.; Paris, C.; León-Escamilla, A.; Boronat, M.; Moliner, M.; Corma, A. "Ab Initio" Synthesis of Zeolites for Preestablished Catalytic Reactions. *Science* **2017**, *355*, 1051–1054. DOI: 10.1126/science.aal0121.

(16) Derouane, E. G.; Andre, J.-M.; Lucas, A. A. Surface Curvature Effects in Physisorption and Catalysis by Microporous Solids and Molecular Sieves. *J. Catal.* **1988**, *110*, 58–73. DOI: 10.1016/0021-9517(88)90297-7.

(17) Bhan, A.; Iglesia, E. A Link Between Reactivity and Local Structure in Acid Catalysis on Zeolites. *Acc. Chem. Res.* **2008**, *41*, 559–567. DOI: 10.1021/ar700181t.

(18) Sastre, G.; Katada, N.; Niwa, M. Computational Study of Brønsted Acidity of Mordenite. Effect of the Electric Field on the Infrared OH Stretching Frequencies. *J. Phys. Chem. C* **2010**, *114*, 15424–15431. DOI: 10.1021/jp104316e.

(19) Gounder, R.; Iglesia, E. The Roles of Entropy and Enthalpy in Stabilizing Ion-Pairs at Transition States in Zeolite Acid Catalysis. *Acc. Chem. Res.* **2012**, *45*, 229–238. DOI: 10.1021/ar200138n.

(20) Bañares, M. A. Operando Methodology: Combination of in Situ Spectroscopy and Simultaneous Activity Measurements Under Catalytic Reaction Conditions. *Catal. Today* **2005**, *100*, 71–77. DOI: 10.1016/j.cattod.2004.12.017.

(21) Ivanova, I. I.; Kolyagin, Y. G. Impact of in Situ MAS NMR Techniques to the Understanding of the Mechanisms of Zeolite Catalyzed Reactions. *Chem. Soc. Rev.* **2010**, *39*, 5018–5050. DOI: 10.1039/C0CS00011F.

(22) Bordiga, S.; Lamberti, C.; Bonino, F.; Travert, A.; Thibault-Starzyk, F. Probing Zeolites by Vibrational Spectroscopies. *Chem. Soc. Rev.* **2015**, *44*, 7262–7341. DOI: 10.1039/C5CS00396B.

(23) Stavitski, E.; Weckhuysen, B. M. Infrared and Raman Imaging of Heterogeneous Catalysts. *Chem. Soc. Rev.* **2010**, *39*, 4615–4625. DOI: 10.1039/C0CS00064G.

(24) Stepanov, A. G. Results of NMR Spectroscopic Studies of Hydrocarbon Conversions on Solid Acid Catalysts in the Last 25 Years. *Kinet. Catal.* **2010**, *51*, 854–872. DOI: 10.1134/S0023158410060121.

(25) Chen, W.; Yi, X.; Liu, Z.; Tang, X.; Zheng, A. Carbocation Chemistry Confined in Zeolites: Spectroscopic and Theoretical Characterizations. *Chem. Soc. Rev.* **2022**, *51*, 4337–4385. DOI: 10.1039/d1cs00966d.

(26) Urakawa, A.; Bürgi, T.; Baiker, A. Sensitivity Enhancement and Dynamic Behavior Analysis by Modulation Excitation Spectroscopy: Principle and Application in Heterogeneous Catalysis. *Chem. Eng. Sci.* **2008**, *63*, 4902–4909. DOI: 10.1016/j.ces.2007.06.009.

(27) Bürgi, T.; Baiker, A. In Situ Infrared Spectroscopy of Catalytic Solid−Liquid Interfaces Using Phase-Sensitive Detection: Enantioselective Hydrogenation of a Pyrone over Pd/TiO_2. *J. Phys. Chem. B* **2002**, *106*, 10649–10658. DOI: 10.1021/jp0255987.

(28) Chizallet, C. Toward the Atomic Scale Simulation of Intricate Acidic Aluminosilicate Catalysts. *ACS Catal.* **2020**, *10*, 5579–5601. DOI: 10.1021/acscatal.0c01136.

(29) van Speybroeck, V.; Wispelaere, K. de; van der Mynsbrugge, J.; Vandichel, M.; Hemelsoet, K.; Waroquier, M. First Principle Chemical Kinetics in Zeolites: The Methanol-to-

Olefin Process as a Case Study. *Chem. Soc. Rev.* **2014**, *43*, 7326–7357. DOI: 10.1039/C4CS00146J.

(30) van Speybroeck, V.; Hemelsoet, K.; Joos, L.; Waroquier, M.; Bell, R. G.; Catlow, C. R. A. Advances in Theory and Their Application Within the Field of Zeolite Chemistry. *Chem. Soc. Rev.* **2015**, *44*, 7044–7111. DOI: 10.1039/C5CS00029G.

(31) Sauer, J. Molecular Models in Ab Initio Studies of Solids and Surfaces: From Ionic Crystals and Semiconductors to Catalysts. *Chem. Rev.* **1989**, *89*, 199–255. DOI: 10.1021/cr00091a006.

(32) van Santen, R. A.; Kramer, G. J. Reactivity Theory of Zeolitic Broensted Acidic Sites. *Chem. Rev.* **1995**, *95*, 637–660. DOI: 10.1021/cr00035a008.

(33) Baerlocher, C.; McCusker, J. K. *Database of Zeolite Structures*. http://www.iza-structure.org/databases/ (accessed 2021-01-07).

(34) Dědeček, J.; Sobalík, Z.; Wichterlová, B. Siting and Distribution of Framework Aluminium Atoms in Silicon-Rich Zeolites and Impact on Catalysis. *Catal. Rev.* **2012**, *54*, 135–223. DOI: 10.1080/01614940.2012.632662.

(35) Derouane, E. G.; Védrine, J. C.; Pinto, R. R.; Borges, P. M.; Costa, L.; Lemos, M.; Lemos, F.; Ribeiro, F. R. The Acidity of Zeolites: Concepts, Measurements and Relation to Catalysis: A Review on Experimental and Theoretical Methods for the Study of Zeolite Acidity. *Catal. Rev.* **2013**, *55*, 454–515. DOI: 10.1080/01614940.2013.822266.

(36) Guisnet, M.; Pinard, L. Characterization of Acid-Base Catalysts Through Model Reactions. *Catal. Rev.* **2018**, *60*, 337–436. DOI: 10.1080/01614940.2018.1446683.

(37) Hunger, M. Brønsted Acid Sites in Zeolites Characterized by Multinuclear Solid-State NMR Spectroscopy. *Catal. Rev.* **1997**, *39*, 345–393. DOI: 10.1080/01614949708007100.

(38) Resasco, D. E.; Crossley, S. P.; Wang, B.; White, J. L. Interaction of Water with Zeolites: A Review. *Catal. Rev.* **2021**, *63*, 302–362. DOI: 10.1080/01614940.2021.1948301.

(39) Farneth, W. E.; Gorte, R. J. Methods for Characterizing Zeolite Acidity. *Chem. Rev.* **1995**, *95*, 615–635. DOI: 10.1021/cr00035a007.

(40) Lamberti, C.; Zecchina, A.; Groppo, E.; Bordiga, S. Probing the Surfaces of Heterogeneous Catalysts by in Situ IR Spectroscopy. *Chem. Soc. Rev.* **2010**, *39*, 4951–5001. DOI: 10.1039/C0CS00117A.

(41) Paul, G.; Bisio, C.; Braschi, I.; Cossi, M.; Gatti, G.; Gianotti, E.; Marchese, L. Combined Solid-State NMR, FT-IR and Computational Studies on Layered and Porous Materials. *Chem. Soc. Rev.* **2018**, *47*, 5684–5739. DOI: 10.1039/C7CS00358G.

(42) Zecchina, A.; Areán, C. O. Diatomic Molecular Probes for Mid-IR Studies of Zeolites. *Chem. Soc. Rev.* **1996**, *25*, 187–197. DOI: 10.1039/CS9962500187.

(43) Bhan, A.; Iglesia, E. A Link Between Reactivity and Local Structure in Acid Catalysis on Zeolites. *Acc. Chem. Res.* **2008**, *41*, 559–567. DOI: 10.1021/ar700181t.

(44) Hafner, J.; Benco, L.; Bučko, T. Acid-Based Catalysis in Zeolites Investigated by Density-Functional Methods. *Top. Catal.* **2006**, *37*, 41–54. DOI: 10.1007/s11244-006-0003-z.

(45) Akhmedov, V. M.; Al-Khowaiter, S. H. Recent Advances and Future Aspects in the Selective Isomerization of High N-Alkanes. *Catal. Rev.* **2007**, *49*, 33–139. DOI: 10.1080/01614940601128427.

(46) Al-Khattaf, S.; Ali, S. A.; Aitani, A. M.; Žilková, N.; Kubička, D.; Čejka, J. Recent Advances in Reactions of Alkylbenzenes over Novel Zeolites: The Effects of Zeolite Structure and Morphology. *Catal. Rev.* **2014**, *56*, 333–402. DOI: 10.1080/01614940.2014.946846.

(47) Bezoukhanova, C. P.; Kalvachev, Y. A. Alcohol Reactivity on Zeolites and Molecular Sieves. *Catal. Rev.* **1994**, *36*, 125–143. DOI: 10.1080/01614949408013922.

(48) Houzvicka, J.; Ponec, V. Skeletal Isomerization of N-Butene. *Catal. Rev.* **1997**, *39*, 319–344. DOI: 10.1080/01614949708007099.

(49) Kissin, Y. V. Chemical Mechanisms of Catalytic Cracking over Solid Acidic Catalysts: Alkanes and Alkenes. *Catal. Rev.* **2001**, *43*, 85–146. DOI: 10.1081/CR-100104387.

(50) Kubička, D.; Kubičková, I.; Čejka, J. Application of Molecular Sieves in Transformations of Biomass and Biomass-Derived Feedstocks. *Catal. Rev.* **2013**, *55*, 1–78. DOI: 10.1080/01614940.2012.685811.

(51) Serrano, D. P.; Melero, J. A.; Morales, G.; Iglesias, J.; Pizarro, P. Progress in the Design of Zeolite Catalysts for Biomass Conversion into Biofuels and Bio-Based Chemicals. *Catal. Rev.* **2018**, *60*, 1–70. DOI: 10.1080/01614940.2017.1389109.

(52) van Donk, S.; Janssen, A. H.; Bitter, J. H.; de Jong, K. P. Generation, Characterization, and Impact of Mesopores in Zeolite Catalysts. *Catal. Rev.* **2003**, *45*, 297–319. DOI: 10.1081/CR-120023908.

(53) Corma, A. From Microporous to Mesoporous Molecular Sieve Materials and Their Use in Catalysis. *Chem. Rev.* **1997**, *97*, 2373–2420. DOI: 10.1021/cr960406n.

(54) Kiricsi, I.; Förster, H.; Tasi, G.; Nagy, J. B. Generation, Characterization, and Transformations of Unsaturated Carbenium Ions in Zeolites. *Chem. Rev.* **1999**, *99*, 2085–2114. DOI: 10.1021/cr9600767.

(55) Shi, J.; Wang, Y.; Yang, W.; Tang, Y.; Xie, Z. Recent Advances of Pore System Construction in Zeolite-Catalyzed Chemical Industry Processes. *Chem. Soc. Rev.* **2015**, *44*, 8877–8903. DOI: 10.1039/C5CS00626K.

(56) Vogt, E. T. C.; Weckhuysen, B. M. Fluid Catalytic Cracking: Recent Developments on the Grand Old Lady of Zeolite Catalysis. *Chem. Soc. Rev.* **2015**, *44*, 7342–7370. DOI: 10.1039/C5CS00376H.

(57) Bickel, E. E.; Nimlos, C. T.; Gounder, R. Developing Quantitative Synthesis-Structure-Function Relations for Framework Aluminum Arrangement Effects in Zeolite Acid Catalysis. *J. Catal.* **2021**, *399*, 75–85. DOI: 10.1016/j.jcat.2021.04.027.

(58) Gong, X.; Çağlayan, M.; Ye, Y.; Liu, K.; Gascon, J.; Dutta Chowdhury, A. First-Generation Organic Reaction Intermediates in Zeolite Chemistry and Catalysis. *Chem. Rev.* **2022**, *122*, 14275–14345. DOI: 10.1021/acs.chemrev.2c00076.

(59) Gallego, E. M.; Paris, C.; Cantín, Á.; Moliner, M.; Corma, A. Conceptual Similarities Between Zeolites and Artificial Enzymes. *Chem. Sci.* **2019**, *10*, 8009–8015. DOI: 10.1039/C9SC02477H.

(60) Chizallet, C.; Raybaud, P. Acidity of Amorphous Silica–Alumina: From Coordination Promotion of Lewis Sites to Proton Transfer. *ChemPhysChem* **2010**, *11*, 105–108. DOI: 10.1002/cphc.200900797.

(61) Chuit, C.; Corriu, R. J. P.; Reye, C.; Young, J. C. Reactivity of Penta- and Hexacoordinate Silicon Compounds and Their Role as Reaction Intermediates. *Chem. Rev.* **1993**, *93*, 1371–1448. DOI: 10.1021/cr00020a003.

(62) Koller, H.; Wölker, A.; Villaescusa, L. A.; Díaz-Cabañas, M. J.; Valencia, S.; Camblor, M. A. Five-Coordinate Silicon in High-Silica Zeolites. *J. Am. Chem. Soc.* **1999**, *121*, 3368–3376. DOI: 10.1021/ja9840549.

(63) Koller, H.; Wölker, A.; Eckert, H.; Panz, C.; Behrens, P. Five-Coordinate Silicon in Zeolites: Probing $SiO_{4/2}F^-$ Sites in Nonasil and ZSM-5 with ^{29}Si Solid-State NMR Spectroscopy. *Angew. Chem. Int. Ed.* **1997**, *36*, 2823–2825. DOI: 10.1002/anie.199728231.

(64) Stebbins, J. F. NMR Evidence for Five-Coordinated Silicon in a Silicate Glass at Atmospheric Pressure. *Nature* **1991**, *351*, 638–639. DOI: 10.1038/351638a0.

(65) Sato, H. Acidity Control and Catalysis of Pentasil Zeolites. *Catal. Rev.* **1997**, *39*, 395–424. DOI: 10.1080/01614949708007101.

(66) Dahlhoff, G.; Niederer, J. P. M.; Hoelderich, W. F. E-Caprolactam: New by-Product Free Synthesis Routes. *Catal. Rev.* **2001**, *43*, 381–441. DOI: 10.1081/CR-120001808.

(67) Li, W.-C.; Lu, A.-H.; Palkovits, R.; Schmidt, W.; Spliethoff, B.; Schüth, F. Hierarchically Structured Monolithic Silicalite-1 Consisting of Crystallized Nanoparticles and Its Performance in the Beckmann Rearrangement of Cyclohexanone Oxime. *J. Am. Chem. Soc.* **2005**, *127*, 12595–12600. DOI: 10.1021/ja052693v.

(68) Medeiros-Costa, I. C.; Dib, E.; Nesterenko, N.; Dath, J.-P.; Gilson, J.-P.; Mintova, S. Silanol Defect Engineering and Healing in Zeolites: Opportunities to Fine-Tune Their Properties and Performances. *Chem. Soc. Rev.* **2021**, *50*, 11156–11179. DOI: 10.1039/D1CS00395J.

(69) Kim, J.; Park, W.; Ryoo, R. Surfactant-Directed Zeolite Nanosheets: A High-Performance Catalyst for Gas-Phase Beckmann Rearrangement. *ACS Catal.* **2011**, *1*, 337–341. DOI: 10.1021/cs100160g.

(70) Fernández, A.-B.; Marinas, A.; Blasco, T.; Fornés, V.; Corma, A. Insight into the Active Sites for the Beckmann Rearrangement on Porous Solids by in Situ Infrared Spectroscopy. *J. Catal.* **2006**, *243*, 270–277. DOI: 10.1016/j.jcat.2006.06.029.

(71) Bucko, T.; Hafner, J.; Benco, L. Active Sites for the Vapor Phase Beckmann Rearrangement over Mordenite: An Ab Initio Study. *J. Phys. Chem. A* **2004**, *108*, 11388–11397. DOI: 10.1021/jp0471103.

(72) Mortier, W. J.; Sauer, J.; Lercher, J. A.; Noller, H. Bridging and Terminal Hydroxyls. A Structural Chemical and Quantum Chemical Discussion. *J. Phys. Chem.* **1984**, *88*, 905–912. DOI: 10.1021/j150649a016.

(73) Uytterhoeven, J. B.; Christner, L. G.; Hall, W. K. Studies of the Hydrogen Held by Solids. VIII. The Decationated Zeolites. *J. Phys. Chem.* **1965**, *69*, 2117–2126. DOI: 10.1021/j100890a052.

(74) Haag, W. O.; Lago, R. M.; Weisz, P. B. The Active Site of Acidic Aluminosilicate Catalysts. *Nature* **1984**, *309*, 589–591. DOI: 10.1038/309589a0.

(75) Ravi, M.; Sushkevich, V. L.; van Bokhoven, J. A. Lewis Acidity Inherent to the Framework of Zeolite Mordenite. *J. Phys. Chem. C* **2019**, *123*, 15139–15144. DOI: 10.1021/acs.jpcc.9b03620.

(76) Yakimov, A. V.; Ravi, M.; Verel, R.; Sushkevich, V. L.; van Bokhoven, J. A.; Copéret, C. Structure and Framework Association of Lewis Acid Sites in MOR Zeolite. *J. Am. Chem. Soc.* **2022**, *144*, 10377–10385. DOI: 10.1021/jacs.2c02212.

(77) Phung, T. K.; Busca, G. On the Lewis Acidity of Protonic Zeolites. *Appl. Catal. A* **2015**, *504*, 151–157. DOI: 10.1016/j.apcata.2014.11.031.

(78) Bučko, T.; Benco, L.; Demuth, T.; Hafner, J. Ab Initio Density Functional Investigation of the (001) Surface of Mordenite. *J. Chem. Phys.* **2002**, *117*, 7295–7305. DOI: 10.1063/1.1507102.

(79) Hernandez-Tamargo, C. E.; Roldan, A.; Leeuw, N. H. de. A Density Functional Theory Study of the Structure of Pure-Silica and Aluminium-Substituted MFI Nanosheets. *J. Solid State Chem.* **2016**, *237*, 192–203. DOI: 10.1016/j.jssc.2016.02.006.

(80) Rey, J.; Raybaud, P.; Chizallet, C. Ab Initio Simulation of the Acid Sites at the External Surface of Zeolite Beta. *ChemCatChem* **2017**, *9*, 2176–2185. DOI: 10.1002/cctc.201700080.

(81) Treps, L.; Gomez, A.; Bruin, T. de; Chizallet, C. Environment, Stability and Acidity of External Surface Sites of Silicalite-1 and ZSM-5 Micro and Nano Slabs, Sheets, and Crystals. *ACS Catal.* **2020**, *10*, 3297–3312. DOI: 10.1021/acscatal.9b05103.

(82) Chizallet, C.; Raybaud, P. Pseudo-Bridging Silanols as Versatile Brønsted Acid Sites of Amorphous Aluminosilicate Surfaces. *Angew. Chem., Int. Ed.* **2009**, *48*, 2891–2893. DOI: 10.1002/anie.200804580.

(83) Leydier, F.; Chizallet, C.; Chaumonnot, A.; Digne, M.; Soyer, E.; Quoineaud, A.-A.; Costa, D.; Raybaud, P. Brønsted Acidity of Amorphous Silica–alumina: The Molecular Rules of Proton Transfer. *J. Catal.* **2011**, *284*, 215–229. DOI: 10.1016/j.jcat.2011.08.015.

(84) Valla, M.; Rossini, A. J.; Caillot, M.; Chizallet, C.; Raybaud, P.; Digne, M.; Chaumonnot, A.; Lesage, A.; Emsley, L.; van Bokhoven, J. A.*; et al.* Atomic Description of the Interface Between Silica and Alumina in Aluminosilicates Through Dynamic Nuclear Polarization Surface-Enhanced NMR Spectroscopy and First-Principles Calculations. *J. Am. Chem. Soc.* **2015**, *137*, 10710–10719. DOI: 10.1021/jacs.5b06134.

(85) Treps, L.; Demaret, C.; Wisser, D.; Harbuzaru, B.; Méthivier, A.; Guillon, E.; Benedis, D. V.; Gomez, A.; Bruin, T. de; Rivallan, M.*; et al.* Spectroscopic Expression of the External Surface Sites of H-ZSM-5. *J. Phys. Chem. C* **2021**, *125*, 2163–2181. DOI: 10.1021/acs.jpcc.0c10200.

(86) Hadjiivanov, K. Chapter Two - Identification and Characterization of Surface Hydroxyl Groups by Infrared Spectroscopy. *Adv. Catal.* **2014**, *57*, 99–318. DOI: 10.1016/B978-0-12-800127-1.00002-3.

(87) Mortier, W. J.; Geerlings, P. CNDO Study of the Site II and the Site III in Faujasite-Type Zeolites. *J. Phys. Chem.* **1980**, *84*, 1982–1986. DOI: 10.1021/j100452a022.

(88) Védrine, J. C.; Auroux, A.; Bolis, V.; Dejaifve, P.; Naccache, C.; Wierzchowski, P.; Derouane, E. G.; Nagy, J. B.; Gilson, J.-P.; van Hooff, J. H.*; et al.* Infrared, Microcalorimetric, and Electron Spin Resonance Investigations of the Acidic Properties of the H-ZSM-5 Zeolite. *J. Catal.* **1979**, *59*, 248–262. DOI: 10.1016/S0021-9517(79)80029-9.

(89) Topsøe, N.-Y.; Pedersen, K.; Derouane, E. G. Infrared and Temperature-Programmed Desorption Study of the Acidic Properties of ZSM-5-Type Zeolites. *J. Catal.* **1981**, *70*, 41–52. DOI: 10.1016/0021-9517(81)90315-8.

(90) Jacobs, P. A.; Ballmoos, R. von. Framework Hydroxyl Groups of H-ZSM-5 Zeolites. *J. Phys. Chem.* **1982**, *86*, 3050–3052. DOI: 10.1021/j100212a046.

(91) Losch, P.; Joshi, H. R.; Vozniuk, O.; Grünert, A.; Ochoa-Hernández, C.; Jabraoui, H.; Badawi, M.; Schmidt, W. Proton Mobility, Intrinsic Acid Strength, and Acid Site Location in

Zeolites Revealed by Varying Temperature Infrared Spectroscopy and Density Functional Theory Studies. *J. Am. Chem. Soc.* **2018**, *140*, 17790–17799. DOI: 10.1021/jacs.8b11588.

(92) Maache, M.; Janin, A.; Lavalley, J. C.; Benazzi, E. FT Infrared Study of Brønsted Acidity of H-Mordenites: Heterogeneity and Effect of Dealumination. *Zeolites* **1995**, *15*, 507–516. DOI: 10.1016/0144-2449(95)00019-3.

(93) Zholobenko, V. L.; Makarova, M. A.; Dwyer, J. Inhomogeneity of Broensted Acid Sites in H-Mordenite. *J. Phys. Chem.* **1993**, *97*, 5962–5964. DOI: 10.1021/j100124a030.

(94) Bordiga, S.; Lamberti, C.; Geobaldo, F.; Zecchina, A.; Palomino, G. T.; Areán, C. O. Fourier-Transform Infrared Study of CO Adsorbed at 77 K on H-Mordenite and Alkali-Metal-Exchanged Mordenites. *Langmuir* **1995**, *11*, 527–533. DOI: 10.1021/la00002a027.

(95) Wakabayashi, F.; Kondo, J.; Wada, A.; Domen, K.; Hirose, C. FT-IR Studies of the Interaction Between Zeolitic Hydroxyl Groups and Small Molecules. 1. Adsorption of Nitrogen on H-Mordenite at Low Temperature. *J. Phys. Chem.* **1993**, *97*, 10761–10768. DOI: 10.1021/j100143a040.

(96) Bučko, T.; Hafner, J. The Role of Spatial Constraints and Entropy in the Adsorption and Transformation of Hydrocarbons Catalyzed by Zeolites. *J. Catal.* **2015**, *329*, 32–48. DOI: 10.1016/j.jcat.2015.04.015.

(97) Demuth, T.; Hafner, J.; Benco, L.; Toulhoat, H. Structural and Acidic Properties of Mordenite. An Ab Initio Density-Functional Study. *J. Phys. Chem. B* **2000**, *104*, 4593–4607. DOI: 10.1021/jp993843p.

(98) Marie, O.; Massiani, P.; Thibault-Starzyk, F. Infrared Evidence of a Third Brønsted Site in Mordenites. *J. Phys. Chem. B* **2004**, *108*, 5073–5081. DOI: 10.1021/jp037915v.

(99) Jacobs, P. A.; Uytterhoeven, J. B. Assignment of the Hydroxyl Bands in the Infrared Spectra of Zeolites X and Y. Part 1.—Na—H Zeolites. *J. Chem. Soc. Faraday Trans. 1* **1973**, *69*, 359–372. DOI: 10.1039/F19736900359.

(100) Ward, J. W. The Nature of Active Sites on Zeolites: I. The Decationated Y Zeolite. *J. Catal.* **1967**, *9*, 225–236. DOI: 10.1016/0021-9517(67)90248-5.

(101) Liengme, B. V.; Hall, W. K. Studies of Hydrogen Held by Solids:Part 11. Interaction of Simple Olefins and Pyridine with Decationated Zeolites. *Trans. Faraday Soc.* **1966**, *62*, 3229–3243.

(102) Jacobs, P. A.; Mortier, W. J. An Attempt to Rationalize Stretching Frequencies of Lattice Hydroxyl Groups in Hydrogen-Zeolites. *Zeolites* **1982**, *2*, 226–230. DOI: 10.1016/S0144-2449(82)80056-0.

(103) Sastre, G.; Katada, N.; Suzuki, K.; Niwa, M. Computational Study of Brønsted Acidity of Faujasite. Effect of the Al Content on the Infrared OH Stretching Frequencies. *J. Phys. Chem. C* **2008**, *112*, 19293–19301. DOI: 10.1021/jp807623m.

(104) Chen, K.; Abdolrhamani, M.; Sheets, E.; Freeman, J.; Ward, G.; White, J. L. Direct Detection of Multiple Acidic Proton Sites in Zeolite HZSM-5. *J. Am. Chem. Soc.* **2017**, *139*, 18698–18704. DOI: 10.1021/jacs.7b10940.

(105) Huang, J.; Jiang, Y.; Marthala, V. R. R.; Thomas, B.; Romanova, E.; Hunger, M. Characterization and Acidic Properties of Aluminum-Exchanged Zeolites X and Y. *J. Phys. Chem. C* **2008**, *112*, 3811–3818. DOI: 10.1021/jp7103616.

(106) Eichler, U.; Brändle, M.; Sauer, J. Predicting Absolute and Site Specific Acidities for Zeolite Catalysts by a Combined Quantum Mechanics/Interatomic Potential Function Approach. *J. Phys. Chem. B* **1997**, *101*, 10035–10050. DOI: 10.1021/jp971779a.

(107) Wang, M.; Jaegers, N. R.; Lee, M.-S.; Wan, C.; Hu, J. Z.; Shi, H.; Mei, D.; Burton, S. D.; Camaioni, D. M.; Gutiérrez, O. Y.*; et al.* Genesis and Stability of Hydronium Ions in Zeolite Channels. *J. Am. Chem. Soc.* **2019**, *141*, 3444–3455. DOI: 10.1021/jacs.8b07969.

(108) Wang, S.; He, Y.; Jiao, W.; Wang, J.; Fan, W. Recent Experimental and Theoretical Studies on Al Siting/acid Site Distribution in Zeolite Framework. *Curr. Opin. Chem. Eng.* **2019**, *23*, 146–154. DOI: 10.1016/j.coche.2019.04.002.

(109) Muraoka, K.; Chaikittisilp, W.; Okubo, T. Energy Analysis of Aluminosilicate Zeolites with Comprehensive Ranges of Framework Topologies, Chemical Compositions, and Aluminum Distributions. *J. Am. Chem. Soc.* **2016**, *138*, 6184–6193. DOI: 10.1021/jacs.6b01341.

(110) Zhai, D.; Liu, Y.; Zheng, H.; Zhao, L.; Gao, J.; Xu, C.; Shen, B. A First-Principles Evaluation of the Stability, Accessibility, and Strength of Brønsted Acid Sites in Zeolites. *J. Catal.* **2017**, *352*, 627–637. DOI: 10.1016/j.jcat.2017.06.035.

(111) Schröder, K.-P.; Sauer, J.; Leslie, M.; A.Catlow, C. Siting of AI and Bridging Hydroxyl Groups in ZSM-5: A Computer Simulation Study. *Zeolites* **1992**, *12*, 20–23. DOI: 10.1016/0144-2449(92)90004-9.

(112) Li, C.; Vidal-Moya, A.; Miguel, P. J.; Dedecek, J.; Boronat, M.; Corma, A. Selective Introduction of Acid Sites in Different Confined Positions in ZSM-5 and Its Catalytic Implications. *ACS Catal.* **2018**, *8*, 7688–7697. DOI: 10.1021/acscatal.8b02112.

(113) Dib, E.; Mineva, T.; Gaveau, P.; Véron, E.; Sarou-Kanian, V.; Fayon, F.; Alonso, B. Probing Disorder in Al-ZSM-5 Zeolites by ^{14}N NMR Spectroscopy. *J. Phys. Chem. C* **2017**, *121*, 15831–15841. DOI: 10.1021/acs.jpcc.7b04861.

(114) Knott, B. C.; Nimlos, C. T.; Robichaud, D. J.; Nimlos, M. R.; Kim, S.; Gounder, R. Consideration of the Aluminum Distribution in Zeolites in Theoretical and Experimental Catalysis Research. *ACS Catal.* **2018**, *8*, 770–784. DOI: 10.1021/acscatal.7b03676.

(115) Gutierrez-Acebo, E.; Rey, J.; Bouchy, C.; Schuurman, Y.; Chizallet, C. Location of the Active Sites for Ethylcyclohexane Hydroisomerization by Ring Contraction and Expansion in

the EUO Zeolitic Framework. *ACS Catal.* **2019**, *9*, 1692–1704. DOI: 10.1021/acscatal.8b04462.

(116) El Hayek, E.; Harbuzaru, B.; Martens, J. A.; Chizallet, C. Ab Initio Investigation of the Relative Stability of Silicogermanates and Their (Alumino)Silicates Counterparts. *Microporous Mesoporous Mater.* **2020**, *306*, 110425. DOI: 10.1016/j.micromeso.2020.110425.

(117) Zhang, N.; Liu, C.; Ma, J.; Li, R.; Jiao, H. Determining the Structures, Acidity and Adsorption Properties of Al Substituted HZSM-5. *Phys. Chem. Chem. Phys.* **2019**, *21*, 18758–18768. DOI: 10.1039/c9cp04050a.

(118) Dědeček, J.; Tabor, E.; Sklenak, S. Tuning the Aluminum Distribution in Zeolites to Increase Their Performance in Acid-Catalyzed Reactions. *ChemSusChem* **2019**, *12*, 556–576. DOI: 10.1002/cssc.201801959.

(119) Nimlos, C. T.; Hoffman, A. J.; Hur, Y. G.; Lee, B. J.; Di Iorio, J. R.; Hibbitts, D. D.; Gounder, R. Experimental and Theoretical Assessments of Aluminum Proximity in MFI Zeolites and Its Alteration by Organic and Inorganic Structure-Directing Agents. *Chem. Mater.* **2020**, *32*, 9277–9298. DOI: 10.1021/acs.chemmater.0c03154.

(120) Holzinger, J.; Beato, P.; Lundegaard, L. F.; Skibsted, J. Distribution of Aluminum over the Tetrahedral Sites in ZSM-5 Zeolites and Their Evolution After Steam Treatment. *J. Phys. Chem. C* **2018**, *122*, 15595–15613. DOI: 10.1021/acs.jpcc.8b05277.

(121) Holzinger, J.; Nielsen, M.; Beato, P.; Brogaard, R. Y.; Buono, C.; Dyballa, M.; Falsig, H.; Skibsted, J.; Svelle, S. Identification of Distinct Framework Aluminum Sites in Zeolite ZSM-23: A Combined Computational and Experimental ^{27}Al NMR Study. *J. Phys. Chem. C* **2019**, *123*, 7831–7844. DOI: 10.1021/acs.jpcc.8b06891.

(122) Sklenak, S.; Dedecek, J.; Li, C.; Wichterlová, B.; Gábová, V.; Sierka, M.; Sauer, J. Aluminum Siting in Silicon-Rich Zeolite Frameworks: A Combined High-Resolution ^{27}Al

NMR Spectroscopy and Quantum Mechanics / Molecular Mechanics Study of ZSM-5. *Angew. Chem., Int. Ed.* **2007**, *46*, 7286–7289. DOI: 10.1002/anie.200702628.

(123) Sklenak, S.; Dedecek, J.; Li, C.; Wichterlová, B.; Gábová, V.; Sierka, M.; Sauer, J. Aluminium Siting in the ZSM-5 Framework by Combination of High Resolution ^{27}Al NMR and DFT/MM Calculations. *Phys. Chem. Chem. Phys.* **2009**, *11*, 1237–1247. DOI: 10.1039/b807755j.

(124) Dib, E.; Mineva, T.; Veron, E.; Sarou-Kanian, V.; Fayon, F.; Alonso, B. ZSM-5 Zeolite: Complete Al Bond Connectivity and Implications on Structure Formation from Solid-State NMR and Quantum Chemistry Calculations. *J. Phys. Chem. Lett.* **2018**, *9*, 19–24. DOI: 10.1021/acs.jpclett.7b03050.

(125) Souverijns, W.; Rombouts, L.; Martens, J. A.; Jacobs, P. A. Molecular Shape Selectivity of EUO Zeolites. *Micropor. Mat.* **1995**, *4*, 123–130. DOI: 10.1016/0927-6513(94)00091-9.

(126) Peral, I.; Jones, C. Y.; Varkey, S. P.; Lobo, R. F. Structural Comparison of Two EUO-Type Zeolites Investigated by Neutron Diffraction. *Microporous Mesoporous Mater.* **2004**, *71*, 125–133. DOI: 10.1016/j.micromeso.2004.03.024.

(127) van Bokhoven, J. A.; Lee, T.-L.; Drakopoulos, M.; Lamberti, C.; Thiess, S.; Zegenhagen, J. Determining the Aluminium Occupancy on the Active T-Sites in Zeolites Using X-Ray Standing Waves. *Nat. Mater.* **2008**, *7*, 551–555. DOI: 10.1038/nmat2220.

(128) Pinar, A. B.; Rzepka, P.; Knorpp, A. J.; McCusker, L. B.; Baerlocher, C.; Huthwelker, T.; van Bokhoven, J. A. Pinpointing and Quantifying the Aluminum Distribution in Zeolite Catalysts Using Anomalous Scattering at the Al Absorption Edge. *J. Am. Chem. Soc.* **2021**, *143*, 17926–17930. DOI: 10.1021/jacs.1c06925.

(129) Vjunov, A.; Fulton, J. L.; Huthwelker, T.; Pin, S.; Mei, D.; Schenter, G. K.; Govind, N.; Camaioni, D. M.; Hu, J. Z.; Lercher, J. A. Quantitatively Probing the Al Distribution in Zeolites. *J. Am. Chem. Soc.* **2014**, *136*, 8296–8306. DOI: 10.1021/ja501361v.

(130) Bellmann, A.; Rautenberg, C.; Bentrup, U.; Brückner, A. Determining the Location of Co2+ in Zeolites by UV-Vis Diffuse Reflection Spectroscopy: A Critical View. *Catalysts* **2020**, *10*, 123. DOI: 10.3390/catal10010123.

(131) Knözinger, H. Infrared Spectroscopy for the Characterization of Surface Acidity and Basicity. In *Handbook of Heterogeneous Catalysis*, 2008; pp 1135–1163. DOI: 10.1002/9783527610044.hetcat0059.

(132) Boronat, M.; Corma, A. Factors Controlling the Acidity of Zeolites. *Catal. Lett.* **2015**, *145*, 162–172. DOI: 10.1007/s10562-014-1438-7.

(133) Boronat, M.; Corma, A. What Is Measured When Measuring Acidity in Zeolites with Probe Molecules? *ACS Catal.* **2019**, *9*, 1539–1548. DOI: 10.1021/acscatal.8b04317.

(134) Redondo, A.; Hay, P. J. Quantum Chemical Studies of Acid Sites in Zeolite ZSM-5. *J. Phys. Chem.* **1993**, *97*, 11754–11761. DOI: 10.1021/j100147a031.

(135) Rybicki, M.; Sauer, J. Acid Strength of Zeolitic Brønsted Sites—Dependence on Dielectric Properties. *Catal. Today* **2019**, *323*, 86–93. DOI: 10.1016/j.cattod.2018.04.031.

(136) Jones, A. J.; Iglesia, E. The Strength of Bronsted Acid Sites in Microporous Aluminosilicates. *ACS Catal.* **2015**, *5*, 5741–5755. DOI: 10.1021/acscatal.5b01133.

(137) Trachta, M.; Bulánek, R.; Bludský, O.; Rubeš, M. Brønsted Acidity in Zeolites Measured by Deprotonation Energy. *Scientific reports* **2022**, *12*, 7301. DOI: 10.1038/s41598-022-11354-x.

(138) Rybicki, M.; Sauer, J. Acidity of Two-Dimensional Zeolites. *Phys. Chem. Chem. Phys.* **2015**, *17*, 27873–27882. DOI: 10.1039/C5CP05088J.

(139) Leydier, F.; Chizallet, C.; Costa, D.; Raybaud, P. CO Adsorption on Amorphous Silica–alumina: Electrostatic or Brønsted Acidity Probe? *Chem. Commun.* **2012**, *48*, 4076–4078. DOI: 10.1039/C2CC30655G.

(140) Liu, C.; Tranca, I.; van Santen, R. A.; Hensen, E. J. M.; Pidko, E. A. Scaling Relations for Acidity and Reactivity of Zeolites. *J. Phys. Chem. C* **2017**, *121*, 23520–23530. DOI: 10.1021/acs.jpcc.7b08176.

(141) Bornes, C.; Sardo, M.; Lin, Z.; Amelse, J. A.; Fernandes, A.; Ribeiro, M. F.; Geraldes, C.; Rocha, J.; Mafra, L. ^{1}H–^{31}P HETCOR NMR Elucidates the Nature of Acid Sites in Zeolite HZSM-5 Probed with Trimethylphosphine Oxide. *Chem. Commun.* **2019**, *55*, 12635–12638. DOI: 10.1039/C9CC06763A.

(142) Bornes, C.; Fischer, M.; Amelse, J. A.; Geraldes, Carlos F. G. C.; Rocha, J.; Mafra, L. What Is Being Measured with P-Bearing NMR Probe Molecules Adsorbed on Zeolites? *J. Am. Chem. Soc.* **2021**, *143*, 13616–13623. DOI: 10.1021/jacs.1c05014.

(143) Busca, G. The Surface of Transitional Aluminas: A Critical Review. *Catal. Today* **2014**, *226*, 2–13. DOI: 10.1016/j.cattod.2013.08.003.

(144) Busca, G. Catalytic Materials Based on Silica and Alumina: Structural Features and Generation of Surface Acidity. *Prog. Mater. Sci.* **2019**, *104*, 215–249. DOI: 10.1016/j.pmatsci.2019.04.003.

(145) Chandran, C. V.; Kirschhock, C. E. A.; Radhakrishnan, S.; Taulelle, F.; Martens, J. A.; Breynaert, E. Alumina: Discriminative Analysis Using 3D Correlation of Solid-State NMR Parameters. *Chem. Soc. Rev.* **2019**, *48*, 134–156. DOI: 10.1039/C8CS00321A.

(146) Bourgeat-Lami, E.; Massiani, P.; Di Renzo, F.; Espiau, P.; Fajula, F.; Des Courières, T. Study of the State of Aluminium in Zeolite-B. *Appl. Catal.* **1991**, *72*, 139–152. DOI: 10.1016/0166-9834(91)85034-S.

(147) Ravi, M.; Sushkevich, V. L.; van Bokhoven, J. A. Towards a Better Understanding of Lewis Acidic Aluminium in Zeolites. *Nat. Mater.* **2020**, *19*, 1047–1056. DOI: 10.1038/s41563-020-0751-3.

(148) van Bokhoven, J. A.; van der Eerden, A. M. J.; Koningsberger, D. C. Three-Coordinate Aluminum in Zeolites Observed with in Situ X-Ray Absorption Near-Edge Spectroscopy at the Al K-Edge: Flexibility of Aluminum Coordinations in Zeolites. *J. Am. Chem. Soc.* **2003**, *125*, 7435–7442. DOI: 10.1021/ja0292905.

(149) Brus, J.; Kobera, L.; Schoefberger, W.; Urbanová, M.; Klein, P.; Sazama, P.; Tabor, E.; Sklenak, S.; Fishchuk, A. V.; Dědeček, J. Structure of Framework Aluminum Lewis Sites and Perturbed Aluminum Atoms in Zeolites as Determined by ^{27}Al{^{1}H} REDOR (3Q) MAS NMR Spectroscopy and DFT/Molecular Mechanics. *Angew. Chem. Int. Ed.* **2015**, *54*, 541–545. DOI: 10.1002/anie.201409635.

(150) Xin, S.; Wang, Q.; Xu, J.; Chu, Y.; Wang, P.; Feng, N.; Qi, G.; Trébosc, J.; Lafon, O.; Fan, W.*; et al.* The Acidic Nature of "NMR-Invisible" Tri-Coordinated Framework Aluminum Species in Zeolites. *Chem. Sci.* **2019**, *10*, 10159–10169. DOI: 10.1039/C9SC02634G.

(151) Omegna, A.; van Bokhoven, J. A.; Prins, R. Flexible Aluminum Coordination in Alumino−Silicates. Structure of Zeolite H−USY and Amorphous Silica−Alumina. *J. Phys. Chem. B* **2003**, *107*, 8854–8860. DOI: 10.1021/jp030094+.

(152) Kunkeler, P. J.; Zuurdeeg, B. J.; van der Waal, J. C.; van Bokhoven, J. A.; Koningsberger, D. C.; van Bekkum, H. Zeolite Beta: The Relationship Between Calcination Procedure, Aluminum Configuration, and Lewis Acidity. *J. Catal.* **1998**, *180*, 234–244. DOI: 10.1006/jcat.1998.2273.

(153) Woolery, G. L.; Kuehl, G. H.; Timken, H. C.; Chester, A. W.; Vartuli, J. C. On the Nature of Framework Brønsted and Lewis Acid Sites in ZSM-5. *Zeolites* **1997**, *19*, 288–296. DOI: 10.1016/S0144-2449(97)00086-9.

(154) Wouters, B. H.; Chen, T.-H.; Grobet, P. J. Reversible Tetrahedral−Octahedral Framework Aluminum Transformation in Zeolite Y. *J. Am. Chem. Soc.* **1998**, *120*, 11419–11425. DOI: 10.1021/ja982082l.

(155) Jia, C.; Massiani, P.; Barthomeuf, D. Characterization by Infrared and Nuclear Magnetic Resonance Spectroscopies of Calcined Beta Zeolite. *J. Chem. Soc. Faraday Trans.* **1993**, *89*, 3659–3665. DOI: 10.1039/FT9938903659.

(156) Ravi, M.; Sushkevich, V. L.; van Bokhoven, J. A. On the Location of Lewis Acidic Aluminum in Zeolite Mordenite and the Role of Framework-Associated Aluminum in Mediating the Switch Between Brønsted and Lewis Acidity. *Chem. Sci.* **2021**, *12*, 4094–4103. DOI: 10.1039/D0SC06130A.

(157) Silaghi, M.-C.; Chizallet, C.; Petracovschi, E.; Kerber, T.; Sauer, J.; Raybaud, P. Regioselectivity of Al–O Bond Hydrolysis During Zeolites Dealumination Unified by Brønsted–Evans–Polanyi Relationship. *ACS Catal.* **2015**, *5*, 11–15. DOI: 10.1021/cs501474u.

(158) Silaghi, M.-C.; Chizallet, C.; Raybaud, P. Challenges on Molecular Aspects of Dealumination and Desilication of Zeolites. *Microporous Mesoporous Mater.* **2014**, *191*, 82–96. DOI: 10.1016/j.micromeso.2014.02.040.

(159) Chen, K.; Gan, Z.; Horstmeier, S.; White, J. L. Distribution of Aluminum Species in Zeolite Catalysts: ^{27}Al NMR of Framework, Partially-Coordinated Framework, and Non-Framework Moieties. *J. Am. Chem. Soc.* **2021**, *143*, 6669–6680. DOI: 10.1021/jacs.1c02361.

(160) Pérez-Ramírez, J.; Christensen, C. H.; Egeblad, K.; Christensen, C. H.; Groen, J. C. Hierarchical Zeolites: Enhanced Utilisation of Microporous Crystals in Catalysis by Advances in Materials Design. *Chem. Soc. Rev.* **2008**, *37*, 2530–2542. DOI: 10.1039/B809030K.

(161) Ruiz, J. M.; McAdon, M. H.; Garcés, J. M. Aluminum Complexes as Models for Broensted Acid Sites in Zeolites: Structure and Energetics of $[Al(OH)_4]^-$, $[Al(H_2O)_6]^{3+}$, and Intermediate Monomeric Species $[Al(OH)_X(H_2O)_{N-X}\cdot mH_2O]^{3-X}$ Obtained by Hydrolysis. *J. Phys. Chem. B* **1997**, *101*, 1733–1744. DOI: 10.1021/jp961987n.

(162) Benco, L.; Demuth, T.; Hafner, J.; Hutschka, F.; Toulhoat, H. Extraframework Aluminum Species in Zeolites: Ab Initio Molecular Dynamics Simulation of Gmelinite. *J. Catal.* **2002**, *209*, 480–488. DOI: 10.1006/jcat.2002.3631.

(163) Benco, L.; Bučko, T.; Hafner, J.; Toulhoat, H. Ab Initio Simulation of Lewis Sites in Mordenite and Comparative Study of the Strength of Active Sites via CO Adsorption. *J. Phys. Chem. B* **2004**, *108*, 13656–13666. DOI: 10.1021/jp048056t.

(164) Bhering, D. L.; Ramírez-Solís, A.; Mota, C. J. A. A Density Functional Theory Based Approach to Extraframework Aluminum Species in Zeolites. *J. Phys. Chem. B* **2003**, *107*, 4342–4347. DOI: 10.1021/jp022331z.

(165) Yi, X.; Liu, K.; Chen, W.; Li, J.; Xu, S.; Li, C.; Xiao, Y.; Liu, H.; Guo, X.; Liu, S.-B.*; et al.* Origin and Structural Characteristics of Tri-Coordinated Extra-Framework Aluminum Species in Dealuminated Zeolites. *J. Am. Chem. Soc.* **2018**, *140*, 10764–10774. DOI: 10.1021/jacs.8b04819.

(166) Liu, C.; Li, G.; Hensen, E. J. M.; Pidko, E. A. Nature and Catalytic Role of Extraframework Aluminum in Faujasite Zeolite: A Theoretical Perspective. *ACS Catal.* **2015**, *5*, 7024–7033. DOI: 10.1021/acscatal.5b02268.

(167) Liu, C.; Li, G.; Hensen, E. J.; Pidko, E. A. Relationship Between Acidity and Catalytic Reactivity of Faujasite Zeolite: A Periodic DFT Study. *J. Catal.* **2016**, *344*, 570–577. DOI: 10.1016/j.jcat.2016.10.027.

(168) Li, S.; Zheng, A.; Su, Y.; Zhang, H.; Chen, L.; Yang, J.; Ye, C.; Deng, F. Brønsted/Lewis Acid Synergy in Dealuminated HY Zeolite: A Combined Solid-State NMR and Theoretical Calculation Study. *J. Am. Chem. Soc.* **2007**, *129*, 11161–11171. DOI: 10.1021/ja072767y.

(169) Mota, C. J. A.; Bhering, D. L.; Rosenbach Jr., N. A DFT Study of the Acidity of Ultrastable Y Zeolite: Where Is the Brønsted/Lewis Acid Synergism? *Angew. Chem. Int. Ed.* **2004**, *43*, 3050–3053. DOI: 10.1002/anie.200353049.

(170) Rosenbach, N.; Mota, C. J. A DFT–ONIOM Study on the Effect of Extra-Framework Aluminum on USY Zeolite Acidity. *Appl. Catal. A* **2008**, *336*, 54–60. DOI: 10.1016/j.apcata.2007.09.048.

(171) Malola, S.; Svelle, S.; Bleken, F. L.; Swang, O. Detailed Reaction Paths for Zeolite Dealumination and Desilication from Density Functional Calculations. *Angew. Chem. Int. Ed.* **2012**, *51*, 652–655. DOI: 10.1002/anie.201104462.

(172) Silaghi, M.-C.; Chizallet, C.; Sauer, J.; Raybaud, P. Dealumination Mechanisms of Zeolites and Extra-Framework Aluminum Confinement. *J. Catal.* **2016**, *339*, 242–255. DOI: 10.1016/j.jcat.2016.04.021.

(173) Nielsen, M.; Brogaard, R. Y.; Falsig, H.; Beato, P.; Swang, O.; Svelle, S. Kinetics of Zeolite Dealumination: Insights from H-SSZ-13. *ACS Catal.* **2015**, *5*, 7131–7139. DOI: 10.1021/acscatal.5b01496.

(174) Valdiviés-Cruz, K.; Lam, A.; Zicovich-Wilson, C. M. Full Mechanism of Zeolite Dealumination in Aqueous Strong Acid Medium: Ab Initio Periodic Study on H-Clinoptilolite. *J. Phys. Chem. C* **2017**, *121*, 2652–2660. DOI: 10.1021/acs.jpcc.6b09794.

(175) Shi, L.; Yang, J.; Shen, G.; Zhao, Y.; Chen, R.; Shen, M.; Wen, Y.; Shan, B. The Influence of Adjacent Al Atoms on the Hydrothermal Stability of H-SSZ-13: A First-Principles Study. *Phys. Chem. Chem. Phys.* **2020**, *22*, 2930–2937. DOI: 10.1039/C9CP05141D.

(176) Sun, J.; Fang, H.; Ravikovitch, P. I.; Sholl, D. S. Understanding Dealumination Mechanisms in Protonic and Cationic Zeolites. *J. Phys. Chem. C* **2020**, *124*, 668–676. DOI: 10.1021/acs.jpcc.9b09693.

(177) Louwen, J. N.; Simko, S.; Stanciakova, K.; Bulo, R. E.; Weckhuysen, B. M.; Vogt, E. T. C. Role of Rare Earth Ions in the Prevention of Dealumination of Zeolite Y for Fluid Cracking Catalysts. *J. Phys. Chem. C* **2020**, *124*, 4626–4636. DOI: 10.1021/acs.jpcc.9b11956.

(178) Heard, C. J.; Grajciar, L.; Rice, C. M.; Pugh, S. M.; Nachtigall, P.; Ashbrook, S. E.; Morris, R. E. Fast Room Temperature Lability of Aluminosilicate Zeolites. *Nat. Commun.* **2019**, *10*, 4690. DOI: 10.1038/s41467-019-12752-y.

(179) Stanciakova, K.; Ensing, B.; Göltl, F.; Bulo, R. E.; Weckhuysen, B. M. Cooperative Role of Water Molecules During the Initial Stage of Water-Induced Zeolite Dealumination. *ACS Catal.* **2019**, *9*, 5119–5135. DOI: 10.1021/acscatal.9b00307.

(180) Nielsen, M.; Hafreager, A.; Brogaard, R. Y.; Wispelaere, K. de; Falsig, H.; Beato, P.; van Speybroeck, V.; Svelle, S. Collective Action of Water Molecules in Zeolite Dealumination. *Catal. Sci. Technol.* **2019**, *9*, 3721–3725. DOI: 10.1039/C9CY00624A.

(181) Stanciakova, K.; Louwen, J. N.; Weckhuysen, B. M.; Bulo, R. E.; Göltl, F. Understanding Water–Zeolite Interactions: On the Accuracy of Density Functionals. *J. Phys. Chem. C* **2021**, *125*, 20261–20274. DOI: 10.1021/acs.jpcc.1c04270.

(182) Mintova, S.; Jaber, M.; Valtchev, V. Nanosized Microporous Crystals: Emerging Applications. *Chem. Soc. Rev.* **2015**, *44*, 7207–7233. DOI: 10.1039/C5CS00210A.

(183) Haw, K.-G.; Gilson, J.-P.; Nesterenko, N.; Akouche, M.; El Siblani, H.; Goupil, J.-M.; Rigaud, B.; Minoux, D.; Dath, J.-P.; Valtchev, V. Supported Embryonic Zeolites and Their Use to Process Bulky Molecules. *ACS Catal.* **2018**, *8*, 8199–8212. DOI: 10.1021/acscatal.8b01936.

(184) Choi, M.; Na, K.; Kim, J.; Sakamoto, Y.; Terasaki, O.; Ryoo, R. Stable Single-Unit-Cell Nanosheets of Zeolite MFI as Active and Long-Lived Catalysts. *Nature* **2009**, *461*, 246–249. DOI: 10.1038/nature08288.

(185) Kirschhock, C. E. A.; Kremer, S. P. B.; Vermant, J.; van Tendeloo, G.; Jacobs, P. A.; Martens, J. A. Design and Synthesis of Hierarchical Materials from Ordered Zeolitic Building Units. *Chem. Eur. J.* **2005**, *11*, 4306–4313. DOI: 10.1002/chem.200401329.

(186) Büchner, C.; Lichtenstein, L.; Yu, X.; Boscoboinik, J. A.; Yang, B.; Kaden, W. E.; Heyde, M.; Shaikhutdinov, S. K.; Włodarczyk, R.; Sierka, M.*; et al.* Ultrathin Silica Films: The

Atomic Structure of Two-Dimensional Crystals and Glasses. *Chem. Eur. J.* **2014**, *20*, 9176–9183. DOI: 10.1002/chem.201402452.

(187) Hoffmann, P.; Lobo, J. A. Identification of Diverse Silanols on Protonated ZSM-5 Zeolites by Means of FTIR Spectroscopy. *Microporous Mesoporous Mater.* **2007**, *106*, 122–128. DOI: 10.1016/j.micromeso.2007.02.035.

(188) Vayssilov, G. N.; Aleksandrov, H. A.; Dib, E.; Costa, I. M.; Nesterenko, N.; Mintova, S. Superacidity and Spectral Signatures of Hydroxyl Groups in Zeolites. *Microporous Mesoporous Mater.* **2022**, *343*, 112144. DOI: 10.1016/j.micromeso.2022.112144.

(189) Hernandez-Tamargo, C. E.; Roldan, A.; Leeuw, N. H. de. DFT Modeling of the Adsorption of Trimethylphosphine Oxide at the Internal and External Surfaces of Zeolite MFI. *J. Phys. Chem. C* **2016**, *120*, 19097–19106. DOI: 10.1021/acs.jpcc.6b03448.

(190) Ferrante, F.; Rubino, T.; Duca, D. Butene Isomerization and Double-Bond Migration on the H-ZSM-5 Outer Surface: A Density Functional Theory Study. *J. Phys. Chem. C* **2011**, *115*, 14862–14868. DOI: 10.1021/jp203284f.

(191) Prestianni, A.; Cortese, R.; Duca, D. Propan-2-Ol Dehydration on H-ZSM-5 and H-Y Zeolite: A DFT Study. *React. Kinet. Mech. Catal.* **2013**, *108*, 565–582. DOI: 10.1007/s11144-012-0522-5.

(192) Thang, H. V.; Vaculík, J.; Přech, J.; Kubů, M.; Čejka, J.; Nachtigall, P.; Bulánek, R.; Grajciar, L. The Brønsted Acidity of Three- and Two-Dimensional Zeolites. *Microporous Mesoporous Mater.* **2019**, *282*, 121–132. DOI: 10.1016/j.micromeso.2019.03.033.

(193) Bučko, T.; Benco, L.; Hafner, J. Defect Sites at the (001) Surface of Mordenite: An Ab Initio Study. *J. Chem. Phys.* **2003**, *118*, 8437–8445. DOI: 10.1063/1.1565321.

(194) Stoyanov, S. R.; Gusarov, S.; Kuznicki, S. M.; Kovalenko, A. Theoretical Modeling of Zeolite Nanoparticle Surface Acidity for Heavy Oil Upgrading. *J. Phys. Chem. C* **2008**, *112*, 6794–6810. DOI: 10.1021/jp075688h.

(195) Jarrin, T.; Bruin, T. de; Chizallet, C. Stability and Acidity of Sites at the External Surface and at Point Defects of Faujasite. *ChemCatChem* **2023**, *15*. DOI: 10.1002/cctc.202201302.

(196) Drake, I. J.; Zhang, Y.; Gilles, M. K.; Teris Liu, C. N.; Nachimuthu, P.; Perera, R. C. C.; Wakita, H.; Bell, A. T. An in Situ Al K-Edge XAS Investigation of the Local Environment of H+- and Cu+-Exchanged USY and ZSM-5 Zeolites. *J. Phys. Chem. B* **2006**, *110*, 11665–11676. DOI: 10.1021/jp058244z.

(197) Bučko, T.; Hafner, J.; Benco, L. Adsorption and Vibrational Spectroscopy of CO on Mordenite: Ab Initio Density-Functional Study. *J. Phys. Chem. B* **2005**, *109*, 7345–7357. DOI: 10.1021/jp050151u.

(198) Khalil, I.; Celis-Cornejo, C. M.; Thomas, K.; Bazin, P.; Travert, A.; Pérez-Martínez, D. J.; Baldovino-Medrano, V. G.; Paul, J. F.; Maugé, F. In Situ IR-ATR Study of the Interaction of Nitrogen Heteroaromatic Compounds with HY Zeolites: Experimental and Theoretical Approaches. *ChemCatChem* **2020**, *12*, 1095–1108. DOI: 10.1002/cctc.201901560.

(199) Bučko, T.; Hafner, J.; Benco, L. Adsorption and Vibrational Spectroscopy of Ammonia at Mordenite: Ab Initio Study. *J. Chem. Phys.* **2004**, *120*, 10263–10277. DOI: 10.1063/1.1737302.

(200) Martens, J. A.; Vanbutsele, G.; Jacobs, P. A.; Denayer, J. F.; Ocakoglu, R.; Baron, G. V.; Muñoz Arroyo, J. A.; Thybaut, J.; Marin, G. B. Evidences for Pore Mouth and Key–lock Catalysis in Hydroisomerization of Long N-Alkanes over 10-Ring Tubular Pore Bifunctional Zeolites. *Catal. Today* **2001**, *65*, 111–116. DOI: 10.1016/S0920-5861(00)00577-0.

(201) Martens, J. A.; Souverijns, W.; Verrelst, W.; Parton, R.; Froment, G. F.; Jacobs, P. A. Selective Isomerization of Hydrocarbon Chains on External Surfaces of Zeolite Crystals. *Angew. Chem. Int. Ed.* **1995**, *34*, 2528–2530. DOI: 10.1002/anie.199525281.

(202) Smit, B.; Maesen, T. L. M. Towards a Molecular Understanding of Shape Selectivity. *Nature* **2008**, *451*, 671–678. DOI: 10.1038/nature06552.

(203) Schenk, M.; Smit, B.; Vlugt, T. J. H.; Maesen, T. L. M. Shape Selectivity in Hydrocarbon Conversion. *Angew. Chem. Int. Ed.* **2001**, *40*, 736–739. DOI: 10.1002/1521-3773(20010216)40:4<736:AID-ANIE7360>3.0.CO;2-T.

(204) Palomares, A. E.; Eder-Mirth, G.; Rep, M.; Lercher, J. A. Alkylation of Toluene over Basic Catalysts—Key Requirements for Side Chain Alkylation. *J. Catal.* **1998**, *180*, 56–65.

(205) Santilli, D. S.; Harris, T. V.; Zones, S. I. Inverse Shape Selectivity in Molecular Sieves: Observations, Modelling, and Predictions. *Micropor. Mat.* **1993**, *1*, 329–341.

(206) Kogelbauer, A.; Grundling, C.; Lercher, J. A. Influence of the Chemical Composition Upon Adsorption, Coadsorption, and Reactivity of Ammonia and Methanol on Alkali-Exchanged Zeolites. *J. Phys. Chem.* **1996**, *100*, 1852–1857.

(207) Eder-Mirth, G.; Wanzenbock, H. D.; Lercher, J. A. Zeolite Induced Chemical Selectivity During Toluene Alkylation. *Stud. Surf. Sci. Catal.* **1995**, *94*, 449–455.

(208) Eder, F.; Lercher, J. A. On the Role of the Pore Size and Tortuosity for Sorption of Alkanes in Molecular Sieves. *J. Phys. Chem. B* **1997**, *101*, 1273–1278. DOI: 10.1021/jp961816i.

(209) Bates, S. P.; van Well, W. J. M.; van Santen, R. A.; Smit, B. Energetics of N-Alkanes in Zeolites: A Configurational-Bais Monte Carlo Investigation into Pore Size Dependence. *J. Am. Chem. Soc.* **1996**, *118*, 6753–6759.

(210) Eder, F.; Lercher, J. A. Alkane Sorption in Molecular Sieves: The Contribution of Ordering, Intermolecular Interactions and Sorption on Bronsted Acid Sites. *Zeolites* **1997**, *18*, 75–81.

(211) Eder, F.; Stockenhuber, M.; Lercher, J. A. Brønsted Acid Site and Pore Controlled Siting of Alkane Sorption in Acidic Molecular Sieves. *J. Phys. Chem. B* **1997**, *101*, 5414–5419. DOI: 10.1021/jp9706487.

(212) Denayer, J. F.; Baron, G. V.; Martens, J. A.; Jacobs, P. A. Chromatographic Study of Adsorption of N-Alkanes on Zeolites at High Temperatures. *J. Phys. Chem.* **1998**, *102*, 3077–3081. DOI: 10.1021/jp972328t.

(213) Denayer, J. F.; Ocakoglu, A. R.; Jonckheere, B. A. de; Martens, J. A.; Thybaut, J. W.; Marin, G. B.; Baron, G. V. Adsorption Competition Effects in Hydroconversion of Alkane Mixtures on Zeolites. *Int. J. Chem. React.* **2003**, *1*, A36.

(214) Talbot, J. Analysis of Adsorption Selectivity in a One-dimensional Model System. *AIChE J.* **1997**, *43*, 2471–2478.

(215) Krishna, R.; Calero, S.; Smit, B. Investigation of Entropy Effects During Sorption of Mixtures of Alkanes in MFI Zeolites. *Chem. Eng. J.* **2002**, *88*, 81–94.

(216) Krishna, R.; Smit, B.; Calero, S. Entropy Effects During Sorption of Alkanes in Zeolites. *Chem. Soc. Rev.* **2002**, *31*, 185–194. DOI: 10.1039/B101267N.

(217) Weitkamp, J.; Ernst, S. Catalytic Test Reactions for Probing the Pore Width of Large and Super-Large Molecular Sieves. *Catal. Today* **1994**, *19*, 107–150.

(218) van de Runstraat, A.; Kamp, J. A.; Stobbelaar, P. J.; van Grondelle, J.; Krijnen, S.; van Santen, R. A. Kinetics of Hydro-Isomerization of N-Hexane over Platinum Containing Zeolites. *J. Catal.* **1997**, *171*, 77–84. DOI: 10.1006/jcat.1997.1779.

(219) Gueudré, L.; Jolimaître, E.; Bats, N.; Dong, W. Diffusion in Zeolites: Is Surface Resistance a Critical Parameter? *Adsorption* **2010**, *16*, 17–27. DOI: 10.1007/s10450-010-9213-6.

(220) Gobin, O. C.; Reitmeier, S. J.; Jentys, A.; Lercher, J. A. Comparison of the Transport of Aromatic Compounds in Small and Large MFI Particles. *J. Phys. Chem. C* **2009**, *113*, 20435–20444. DOI: 10.1021/jp907444c.

(221) Zhang, L.; Chmelik, C.; van Laak, A. N. C.; Kärger, J.; de Jongh, P. E.; de Jong, K. P. Direct Assessment of Molecular Transport in Mordenite: Dominance of Surface Resistances. *Chem. Commun.* **2009**, 6424–6426. DOI: 10.1039/b914391b.

(222) Kärger, J.; Ruthven, D. M. On the Comparison Between Macroscopic and NMR Measurements of Intracrystalline Diffusion in Zeolites. *Zeolites* **1989**, *9*, 267–281.

(223) Kärger, J. Measurement of Diffusion in Zeolites - a Never Ending Challenge? *Adsorption* **2003**, *9*, 29–35.

(224) Vandegehuchte, B. D.; Thybaut, J. W.; Marin, G. B. Unraveling Diffusion and Other Shape Selectivity Effects in ZSM5 Using N -Hexane Hydroconversion Single-Event Microkinetics. *Ind. Eng. Chem. Res.* **2014**, *53*, 15333–15347. DOI: 10.1021/ie500164q.

(225) Klemm, E.; Emig, G. A Method for the Determination of Diffusion Coefficients in Product-Shape-Selective Catalysis on Zeolites Under Reaction Conditions. *Chem. Eng. Sci.* **1997**, *52*, 4239–4344.

(226) Noh, G.; Shi, Z.; Zones, S. I.; Iglesia, E. Isomerization and B-Scission Reactions of Alkanes on Bifunctional Metal-Acid Catalysts: Consequences of Confinement and Diffusional Constraints on Reactivity and Selectivity. *J. Catal.* **2018**, *368*, 389–410. DOI: 10.1016/j.jcat.2018.03.033.

(227) Galarneau, A.; Guenneau, F.; Gedeon, A.; Mereib, D.; Rodriguez, J.; Fajula, F.; Coasne, B. Probing Interconnectivity in Hierarchical Microporous/Mesoporous Materials Using Adsorption and Nuclear Magnetic Resonance Diffusion. *J. Phys. Chem. C* **2016**, *120*, 1562–1569. DOI: 10.1021/acs.jpcc.5b10129.

(228) Kortunov, P.; Vasenkov, S.; Kärger, J.; Valiullin, R.; Gottschalk, P.; Elía, M. F.; Perez, M.; Stöcker, M.; Drescher, B.; McElhiney, G.*; et al.* The Role of Mesopores in Intracrystalline Transport in USY Zeolite: PFG NMR Diffusion Study on Various Length Scales. *J. Am. Chem. Soc.* **2005**, *127*, 13055–13059. DOI: 10.1021/ja053134r.

(229) Zečević, J.; Vanbutsele, G.; de Jong, K. P.; Martens, J. A. Nanoscale Intimacy in Bifunctional Catalysts for Selective Conversion of Hydrocarbons. *Nature* **2015**, *528*, 245–248. DOI: 10.1038/nature16173.

(230) Herrmann, C.; Haas, J.; Fetting, F. Effect of the Crystal Size on the Activity of ZSM-5 Catalysts in Various Reactions. *Appl. Catal.* **1987**, *35*, 299–310.

(231) Shiralkar, V. P.; Joshi, P. N.; Eapen, M. J.; Rao, B. S. Synthesis of ZSM-5 with Variable Crystallite Size and Its Influence on Physicochemical Properties. *Zeolites* **1991**, *11*, 511–516.

(232) Mochizuki, H.; Yokoi, T.; Imai, H.; Watanabe, R.; Namba, S.; Kondo, J. N.; Tatsumi, T. Facile Control of Crystallite Size of ZSM-5 Catalyst for Cracking of Hexane. *Microporous and Mesoporous Materials* **2011**, *145*, 165–171. DOI: 10.1016/j.micromeso.2011.05.011.

(233) Wang, X.; Yu, Z.; Sun, J.; Wei, Q.; Liu, H.; Huang, W.; Zhao, L.; Si, M.; Zhou, Y. Synthesis of Small Crystal Size Y Zeolite Catalysts with High Hydrocracking Performance on N-Hexadecane. *Energy Fuels* **2022**, *36*, 13817–13832. DOI: 10.1021/acs.energyfuels.2c02851.

(234) Konno, H.; Okamura, T.; Kawahara, T.; Nakasaka, Y.; Tago, T.; Masuda, T. Kinetics of N-Hexane Cracking over ZSM-5 Zeolites – Effect of Crystal Size on Effectiveness Factor and Catalyst Lifetime. *Chem. Eng. J.* **2012**, *207-208*, 490–496. DOI: 10.1016/j.cej.2012.06.157.

(235) Gutierrez-Acebo, E.; Leroux, C.; Chizallet, C.; Schuurman, Y.; Bouchy, C. Metal/Acid Bifunctional Catalysis and Intimacy Criterion for Ethylcyclohexane Hydroconversion: When Proximity Does Not Matter. *ACS Catal.* **2018**, *8*, 6035–6046. DOI: 10.1021/acscatal.8b00633.

(236) Niwa, M.; Katada, N. New Method for the Temperature-Programmed Desorption (TPD) Of Ammonia Experiment for Characterization of Zeolite Acidity: A Review. *Chem. Rec.* **2013**, *13*, 432–455. DOI: 10.1002/tcr.201300009.

(237) Katada, N.; Suzuki, K.; Noda, T.; Park, M. B.; Min, H.-K.; Hong, S. B.; Niwa, M. Ammonia IRMS-TPD Characterization of Brønsted Acid Sites in Medium-Pore Zeolites with

Different Framework Topologies. *Top. Catal.* **2010**, *53*, 664–671. DOI: 10.1007/s11244-010-9503-y.

(238) Hunger, B.; Heuchel, M.; Clark, L. A.; Snurr, R. Q. Characterization of Acidic OH Groups in Zeolites of Different Types: An Interpretation of NH 3 -TPD Results in the Light of Confinement Effects. *J. Phys. Chem. B* **2002**, *106*, 3882–3889. DOI: 10.1021/jp012688n.

(239) Zholobenko, V.; Freitas, C.; Jendrlin, M.; Bazin, P.; Travert, A.; Thibault-Starzyk, F. Probing the Acid Sites of Zeolites with Pyridine: Quantitative AGIR Measurements of the Molar Absorption Coefficients. *J. Catal.* **2020**, *385*, 52–60. DOI: 10.1016/j.jcat.2020.03.003.

(240) Palkhiwala, A. G.; Gorte, R. J. *Catal. Lett.* **1999**, *57*, 19–23. DOI: 10.1023/A:1019010624157.

(241) Remy, M. J.; Stanica, D.; Poncelet, G.; Feijen, E. J. P.; Grobet, P. J.; Martens, J. A.; Jacobs, P. A. Dealuminated H-Y Zeolites: Relation Between Physicochemical Properties and Catalytic Activity in Heptane and Decane Isomerization. *J. Phys. Chem.* **1996**, *100*, 12440–12447.

(242) Katada, N. Analysis and Interpretation of Acidic Nature of Aluminosilicates. *Mol. Catal.* **2018**, *458*, 116–126. DOI: 10.1016/j.mcat.2017.12.024.

(243) Astafan, A.; Pouilloux, Y.; Patarin, J.; Bats, N.; Bouchy, C.; Jean Daou, T.; Pinard, L. Impact of Extreme Downsizing of *BEA-Type Zeolite Crystals on N-Hexadecane Hydroisomerization. *New J. Chem.* **2016**, *40*, 4335–4343. DOI: 10.1039/C5NJ02837J.

(244) Demaret, C. Mise En Forme De Zéolithes : Contrôle Des Propriétés Acides Des Zéolithes Et Description De L'interface Zéolithe / Liant, Université Claude Bernard Lyon, Lyon, 2019. https://www.theses.fr/2019LYSE1042 (accessed 2022-01-07).

(245) Eyring, H. The Activated Complex in Chemical Reactions. *J. Chem. Phys.* **1935**, *3*, 107–115. DOI: 10.1063/1.1749604.

(246) Lombardo, E. A.; Dereppe, J. M.; Marcelin, G.; Hall, W. NMR Study of Reactions of Alcohols on Solid Acids. *J. Catal.* **1988**, *114*, 167–175. DOI: 10.1016/0021-9517(88)90018-8.

(247) Olah, G. A. Stable Carbocations. CXVIII. General Concept and Structure of Carbocations Based on Differentiation of Trivalent (Classical) Carbenium Ions from Three-Center Bound Penta- of Tetracoordinated (Nonclassical) Carbonium Ions. Role of Carbocations in Electrophilic Reactions. *J. Am. Chem. Soc.* **1972**, *94*, 808–820. DOI: 10.1021/ja00758a020.

(248) Xu, T.; Haw, J. F. NMR Observation of Indanyl Carbenium Ion Intermediates in the Reactions of Hydrocarbons on Acidic Zeolites. *J. Am. Chem. Soc.* **1994**, *116*, 10188–10195. DOI: 10.1021/ja00101a044.

(249) Buurmans, I. L. C.; Pidko, E. A.; Groot, J. M. de; Stavitski, E.; van Santen, R. A.; Weckhuysen, B. M. Styrene Oligomerization as a Molecular Probe Reaction for Zeolite Acidity: A UV-Vis Spectroscopy and DFT Study. *Phys. Chem. Chem. Phys.* **2010**, *12*, 7032–7040. DOI: 10.1039/C002442B.

(250) Ristanović, Z.; Kubarev, A. V.; Hofkens, J.; Roeffaers, M. B. J.; Weckhuysen, B. M. Single Molecule Nanospectroscopy Visualizes Proton-Transfer Processes Within a Zeolite Crystal. *J. Am. Chem. Soc.* **2016**, *138*, 13586–13596. DOI: 10.1021/jacs.6b06083.

(251) Kennes, K.; Demaret, C.; van Loon, J.; Kubarev, A. V.; Fleury, G.; Sliwa, M.; Delpoux, O.; Maury, S.; Harbuzaru, B.; Roeffaers, M. B. J. Assessing Inter and Intra-Particle Heterogeneity in Alumina-Poor H-ZSM-5 Zeolites. *ChemCatChem* **2017**, *9*, 3440–3445. DOI: 10.1002/cctc.201700696.

(252) Janssen, K. P. F.; Cremer, G. de; Neely, R. K.; Kubarev, A. V.; van Loon, J.; Martens, J. A.; Vos, D. E. de; Roeffaers, M. B. J.; Hofkens, J. Single Molecule Methods for the Study of Catalysis: From Enzymes to Heterogeneous Catalysts. *Chem. Soc. Rev.* **2014**, *43*, 990–1006. DOI: 10.1039/C3CS60245A.

(253) Cabrero-Antonino, J. R.; Leyva-Pérez, A.; Corma, A. Beyond Acid Strength in Zeolites: Soft Framework Counteranions for Stabilization of Carbocations on Zeolites and Its Implication in Organic Synthesis. *Angew. Chem. Int. Ed.* **2015**, *54*, 5658–5661. DOI: 10.1002/anie.201500864.

(254) Xiao, D.; Xu, S.; Brownbill, N. J.; Paul, S.; Chen, L.-H.; Pawsey, S.; Aussenac, F.; Su, B.-L.; Han, X.; Bao, X.*; et al.* Fast Detection and Structural Identification of Carbocations on Zeolites by Dynamic Nuclear Polarization Enhanced Solid-State NMR. *Chem. Sci.* **2018**, *9*, 8184–8193. DOI: 10.1039/C8SC03848A.

(255) Wulfers, M. J.; Jentoft, F. C. The Role of Cyclopentadienium Ions in Methanol-to-Hydrocarbons Chemistry. *ACS Catal.* **2014**, *4*, 3521–3532. DOI: 10.1021/cs500722m.

(256) Xiao, D.; Xu, S.; Han, X.; Bao, X.; Liu, Z.; Blanc, F. Direct Structural Identification of Carbenium Ions and Investigation of Host–guest Interaction in the Methanol to Olefins Reaction Obtained by Multinuclear NMR Correlations. *Chem. Sci.* **2017**, *8*, 8309–8314. DOI: 10.1039/C7SC03657D.

(257) Haw, J. F.; Richardson, B. R.; Oshiro, I. S.; Lazo, N. D.; Speed, J. A. Reactions of Propene on Zeolite HY Catalyst Studied by in Situ Variable Temperature Solid-State Nuclear Magnetic Resonance Spectroscopy. *J. Am. Chem. Soc.* **1989**, *111*, 2052–2058. DOI: 10.1021/ja00188a016.

(258) Stepanov, A. G.; Sidelnikov, V. N.; Zamaraev, K. I. In Situ ^{13}C Solid-State NMR and Ex Situ GC–MS Analysis of the Products of Tert-Butyl Alcohol Dehydration on H-ZSM-5 Zeolite Catalyst. *Chem. Eur. J.* **1996**, *2*, 157–167. DOI: 10.1002/chem.19960020207.

(259) Song, W.; Nicholas, J. B.; Haw, J. F. Acid−Base Chemistry of a Carbenium Ion in a Zeolite Under Equilibrium Conditions: Verification of a Theoretical Explanation of Carbenium Ion Stability. *J. Am. Chem. Soc.* **2001**, *123*, 121–129. DOI: 10.1021/ja002775d.

(260) Xu, S.; Zheng, A.; Wei, Y.; Chen, J.; Li, J.; Chu, Y.; Zhang, M.; Wang, Q.; Zhou, Y.; Wang, J.*; et al.* Direct Observation of Cyclic Carbenium Ions and Their Role in the Catalytic Cycle of the Methanol-to-Olefin Reaction over Chabazite Zeolites. *Angew. Chem. Int. Ed.* **2013**, *52*, 11564–11568. DOI: 10.1002/anie.201303586.

(261) Wang, C.; Chu, Y.; Zheng, A.; Xu, J.; Wang, Q.; Gao, P.; Qi, G.; Gong, Y.; Deng, F. New Insight into the Hydrocarbon-Pool Chemistry of the Methanol-to-Olefins Conversion over Zeolite H-ZSM-5 from GC-MS, Solid-State NMR Spectroscopy, and DFT Calculations. *Chem. Eur. J.* **2014**, *20*, 12432–12443. DOI: 10.1002/chem.201403972.

(262) Wang, C.; Yi, X.; Xu, J.; Qi, G.; Gao, P.; Wang, W.; Chu, Y.; Wang, Q.; Feng, N.; Liu, X.*; et al.* Experimental Evidence on the Formation of Ethene Through Carbocations in Methanol Conversion over H-ZSM-5 Zeolite. *Chem. Eur. J.* **2015**, *21*, 12061–12068. DOI: 10.1002/chem.201501355.

(263) Yang, S.; Kondo, J. N.; Domen, K. Formation of Alkenyl Carbenium Ions by Adsorption of Cyclic Precursors on Zeolites. *Catal. Today* **2002**, *73*, 113–125. DOI: 10.1016/S0920-5861(01)00504-1.

(264) Long, J.; Wang, X.; Ding, Z.; Xie, L.; Zhang, Z.; Dong, J.; Lin, H.; Fu, X. Cyclopentadiene Transformation over H-Form Zeolites: TPD and IR Studies of the Formation of a Monomeric Cyclopentenyl Carbenium Ion Intermediate and Its Role in Acid-Catalyzed Conversions. *J. Catal.* **2008**, *255*, 48–58. DOI: 10.1016/j.jcat.2008.01.023.

(265) Haw, J. F.; Nicholas, J. B.; Song, W.; Deng, F.; Wang, Z.; Xu, T.; Heneghan, C. S. Roles for Cyclopentenyl Cations in the Synthesis of Hydrocarbons from Methanol on Zeolite Catalyst HZSM-5. *J. Am. Chem. Soc.* **2000**, *122*, 4763–4775. DOI: 10.1021/ja994103x.

(266) Lazo, N. D.; Richardson, B. R.; Schettler, P. D.; White, J. L.; Munson, E. J.; Haw, J. F. In Situ Variable-Temperature MAS Carbon-13 NMR Study of the Reactions of Isobutylene in Zeolites HY and HZSM-5. *J. Phys. Chem.* **1991**, *95*, 9420–9425. DOI: 10.1021/j100176a071.

(267) Stepanov, A. G.; Zamaraev, K. I.; Thomas, J. M. ^{13}C CP/MAS and ^{2}H NMR Study of Tert-Butyl Alcohol Dehydration on H-ZSM-5 Zeolite. Evidence for the Formation of Tert-Butyl Cation and Tert-Butyl Silyl Ether Intermediates. *Catal. Lett.* **1992**, *13*, 407–422. DOI: 10.1007/BF00765044.

(268) Haw, J. F.; Nicholas, J. B.; Xu, T.; Beck, L. W.; Ferguson, D. B. Physical Organic Chemistry of Solid Acids: Lessons from in Situ NMR and Theoretical Chemistry. *Acc. Chem. Res.* **1996**, *29*, 259–267. DOI: 10.1021/ar950105k.

(269) Dai, W.; Wang, C.; Yi, X.; Zheng, A.; Li, L.; Wu, G.; Guan, N.; Xie, Z.; Dyballa, M.; Hunger, M. Identification of Tert-Butyl Cations in Zeolite H-ZSM-5: Evidence from NMR Spectroscopy and DFT Calculations. *Angew. Chem. Int. Ed.* **2015**, *54*, 8783–8786. DOI: 10.1002/anie.201502748.

(270) Huang, M.; Wang, Q.; Yi, X.; Chu, Y.; Dai, W.; Li, L.; Zheng, A.; Deng, F. Insight into the Formation of the Tert-Butyl Cation Confined Inside H-ZSM-5 Zeolite from NMR Spectroscopy and DFT Calculations. *Chem. Commun.* **2016**, *52*, 10606–10608. DOI: 10.1039/C6CC04943E.

(271) Wang, W.; Hunger, M. Reactivity of Surface Alkoxy Species on Acidic Zeolite Catalysts. *Acc. Chem. Res.* **2008**, *41*, 895–904. DOI: 10.1021/ar700210f.

(272) Kondo, J. N.; Ishikawa, H.; Yoda, E.; Wakabayashi, F.; Domen, K. Structure of Dimerized Alkoxy Species of 2-Methylpropene on Zeolites and Silica−Alumina Studied by FT-IR. *J. Phys. Chem. B* **1999**, *103*, 8538–8543. DOI: 10.1021/jp991395f.

(273) Ishikawa, H.; Yoda, E.; Kondo, J. N.; Wakabayashi, F.; Domen, K. Stable Dimerized Alkoxy Species of 2-Methylpropene on Mordenite Zeolite Studied by FT-IR. *J. Phys. Chem. B* **1999**, *103*, 5681–5686. DOI: 10.1021/jp990444l.

(274) Stepanov, A. G.; Romannikov, V. N.; Zamaraev, K. I. ^{13}C CP/MAS NMR Study of Isobutyl Alcohol Dehydration on H-ZSM-5 Zeolite. Evidence for the Formation of Stable Isobutyl Silyl Ether Intermediate. *Catal. Lett.* **1992**, *13*, 395–405. DOI: 10.1007/BF00765043.

(275) Wang, W.; Jiao, J.; Jiang, Y.; Ray, S. S.; Hunger, M. Formation and Decomposition of Surface Ethoxy Species on Acidic Zeolite Y. *ChemPhysChem* **2005**, *6*, 1467–1469. DOI: 10.1002/cphc.200500262.

(276) Stepanov, A. G. In Situ NMR Identification of the Intermediates and the Reaction Products in Alcohols and Hydrocarbons Conversion on Zeolites. *Catal. Today* **1995**, *24*, 341–348. DOI: 10.1016/0920-5861(95)00056-L.

(277) Tang, X.; Chen, W.; Yi, X.; Liu, Z.; Xiao, Y.; Chen, Z.; Zheng, A. In Situ Observation of Non-Classical 2-Norbornyl Cation in Confined Zeolites at Ambient Temperature. *Angew. Chem. Int. Ed.* **2021**, *60*, 4581–4587. DOI: 10.1002/anie.202013384.

(278) Kazansky, V. B.; Senchenya, I. N. Quantum Chemical Study of the Electronic Structure and Geometry of Surface Alkoxy Groups as Probable Active Intermediates of Heterogeneous Acidic Catalysts: What Are the Adsorbed Carbenium Ions? *J. Catal.* **1989**, *119*, 108–120. DOI: 10.1016/0021-9517(89)90139-5.

(279) Viruela-Martin, P.; Zicovich-Wilson, C. M.; Corma, A. Ab Initio Molecular Orbital Calculations of the Protonation of Propylene and Isobutene by Acidic Hydroxyl Groups of Isomorphously Substituted Zeolites. *J. Phys. Chem.* **1993**, *97*, 13713–13719. DOI: 10.1021/j100153a047.

(280) Senchenya, I. N.; Kazansky, V. B. Quantum Chemical Studies of Ethylene Interaction with Zeolite OH-Groups. *Catal. Lett.* **1991**, *8*, 317–325. DOI: 10.1007/BF00764193.

(281) Kazansky, V. B.; Frash, M. V.; van Santen, R. A. Quantumchemical Study of the Isobutane Cracking on Zeolites. *Appl. Catal. A* **1996**, *146*, 225–247. DOI: 10.1016/0926-860X(96)00060-9.

(282) Rigby, A. M.; Kramer, G. J.; van Santen, R. A. Mechanisms of Hydrocarbon Conversion in Zeolites: A Quantum Mechanical Study. *J. Catal.* **1997**, *170*, 1–10. DOI: 10.1006/jcat.1997.1574.

(283) Frash, M. V.; Kazansky, V. B.; Rigby, A. M.; van Santen, R. A. Cracking of Hydrocarbons on Zeolite Catalysts: Density Functional and Hartree−Fock Calculations on the Mechanism of the B-Scission Reaction. *J. Phys. Chem. B* **1998**, *102*, 2232–2238. DOI: 10.1021/jp973203r.

(284) Hay, J. P.; Redondo, A.; Guo, Y. Theoretical Studies of Pentene Cracking on Zeolites: C–C B-Scission Processes. *Catal. Today* **1999**, *50*, 517–523. DOI: 10.1016/S0920-5861(98)00486-6.

(285) Boronat, M.; Zicovich-Wilson, C. M.; Viruela, P.; Corma, A. Influence of the Local Geometry of Zeolite Active Sites and Olefin Size on the Stability of Alkoxide Intermediates. *J. Phys. Chem. B* **2001**, *105*, 11169–11177. DOI: 10.1021/jp011481r.

(286) Boronat, M.; Viruela, P. M.; Corma, A. Reaction Intermediates in Acid Catalysis by Zeolites: Prediction of the Relative Tendency to Form Alkoxides or Carbocations as a Function of Hydrocarbon Nature and Active Site Structure. *J. Am. Chem. Soc.* **2004**, *126*, 3300–3309. DOI: 10.1021/ja039432a.

(287) Fang, H.; Zheng, A.; Li, S.; Xu, J.; Chen, L.; Deng, F. New Insights into the Effects of Acid Strength on the Solid Acid-Catalyzed Reaction: Theoretical Calculation Study of Olefinic Hydrocarbon Protonation Reaction. *J. Phys. Chem. C* **2010**, *114*, 10254–10264. DOI: 10.1021/jp103247f.

(288) Boronat, M.; Zicovich-Wilson, C. M.; Viruela, P.; Corma, A. Cluster and Periodic Calculations of the Ethene Protonation Reaction Catalyzed by Theta-1 Zeolite: Influence of Method, Model Size, and Structural Constraints. *Chem. Eur. J.* **2001**, *7*, 1295–1303. DOI: 10.1002/1521-3765(20010316)7:6<1295:AID-CHEM1295>3.0.CO;2-S.

(289) Liu, J.; Yin, Y.; Fu, X.-Z.; Luo, J.-L. Stability of C3-C6 Carbonium Ions Inside Zeolites: A First Principles Study. *Appl. Surf. Sci.* **2020**, *503*, 144148. DOI: 10.1016/j.apsusc.2019.144148.

(290) Boronat, M.; M. Zicovich-Wilson, C.; Corma, A.; Viruela, P. Cluster and Periodic Abinitio Study of the Ethane-Ethene Hydride Transfer Reaction Catalyzed by Acid Chabazite. Is the Cluster Model Able to Describe Accurately the Host–guest Interactions? *Phys. Chem. Chem. Phys.* **1999**, *1*, 537–543. DOI: 10.1039/A808037B.

(291) Rozanska, X.; van Santen, R. A.; Hutschka, F.; Hafner, J. A Periodic DFT Study of Intramolecular Isomerization Reactions of Toluene and Xylenes Catalyzed by Acidic Mordenite. *J. Am. Chem. Soc.* **2001**, *123*, 7655–7667. DOI: 10.1021/ja0103795.

(292) Rozanska, X.; van Santen, R. A.; Demuth, T.; Hutschka, F.; Hafner, J. A Periodic DFT Study of Isobutene Chemisorption in Proton-Exchanged Zeolites: Dependence of Reactivity on the Zeolite Framework Structure. *J. Phys. Chem. B* **2003**, *107*, 1309–1315. DOI: 10.1021/jp021646b.

(293) Benco, L.; Hafner, J.; Hutschka, F.; Toulhoat, H. Physisorption and Chemisorption of Some N-Hydrocarbons at the Brønsted Acid Site in Zeolites 12-Membered Ring Main Channels: Ab Initio Study of the Gmelinite Structure. *J. Phys. Chem. B* **2003**, *107*, 9756–9762. DOI: 10.1021/jp027625z.

(294) Guo, Y.-H.; Pu, M.; Chen, B.-H.; Cao, F. Theoretical Study on the Cracking Reaction Catalyzed by a Solid Acid with Zeolitic Structure: The Catalytic Cracking of 1-Hexene on the Surface of H-ZSM-5. *Appl. Catal. A* **2013**, *455*, 65–70. DOI: 10.1016/j.apcata.2013.01.013.

(295) Leydier, F.; Chizallet, C.; Costa, D.; Raybaud, P. Revisiting Carbenium Chemistry on Amorphous Silica-Alumina: Unraveling Their Milder Acidity as Compared to Zeolites. *J. Catal.* **2015**, *325*, 35–47. DOI: 10.1016/j.jcat.2015.02.012.

(296) Teraishi, K. Computational Study on the Product Selectivity of FCC Zeolitic Catalyst. *J. Mol. Catal. A* **1998**, *132*, 73–85. DOI: 10.1016/S1381-1169(97)00232-X.

(297) Ferguson, G. A.; Cheng, L.; Bu, L.; Kim, S.; Robichaud, D. J.; Nimlos, M. R.; Curtiss, L. A.; Beckham, G. T. Carbocation Stability in H-ZSM5 at High Temperature. *J. Phys. Chem. A* **2015**, *119*, 11397–11405. DOI: 10.1021/acs.jpca.5b07025.

(298) Boronat, M.; Corma, A. Are Carbenium and Carbonium Ions Reaction Intermediates in Zeolite-Catalyzed Reactions? *Appl. Catal. A* **2008**, *336*, 2–10. DOI: 10.1016/j.apcata.2007.09.050.

(299) Fang, H.; Zheng, A.; Xu, J.; Li, S.; Chu, Y.; Chen, L.; Deng, F. Theoretical Investigation of the Effects of the Zeolite Framework on the Stability of Carbenium Ions. *J. Phys. Chem. C* **2011**, *115*, 7429–7439. DOI: 10.1021/jp1097316.

(300) Tuma, C.; Sauer, J. Treating Dispersion Effects in Extended Systems by Hybrid MP2:DFT Calculations—Protonation of Isobutene in Zeolite Ferrierite. *Phys. Chem. Chem. Phys.* **2006**, *8*, 3955–3965. DOI: 10.1039/B608262A.

(301) Tuma, C.; Kerber, T.; Sauer, J. The Tert-Butyl Cation in H-Zeolites: Deprotonation to Isobutene and Conversion into Surface Alkoxides. *Angew. Chem. Int. Ed.* **2010**, *49*, 4678–4680. DOI: 10.1002/anie.200907015.

(302) Wispelaere, K. de; Plessow, P. N.; Studt, F. Toward Computing Accurate Free Energies in Heterogeneous Catalysis: A Case Study for Adsorbed Isobutene in H-ZSM-5. *ACS Phys. Chem. Au* **2022**, *2*, 399–406. DOI: 10.1021/acsphyschemau.2c00020.

(303) Tuma, C.; Sauer, J. Protonated Isobutene in Zeolites: Tert-Butyl Cation or Alkoxide? *Angew. Chem. Int. Ed.* **2005**, *44*, 4769–4771. DOI: 10.1002/anie.200501002.

(304) Nguyen, C. M.; Moor, B. A. de; Reyniers, M.-F.; Marin, G. B. Isobutene Protonation in H-FAU, H-MOR, H-ZSM-5, and H-ZSM-22. *J. Phys. Chem. C* **2012**, *116*, 18236–18249. DOI: 10.1021/jp304081k.

(305) Benco, L.; Demuth, T.; Hafner, J.; Hutschka, F.; Toulhoat, H. Linear Hydrocarbons Adsorbed in the Acid Zeolite Gmelinite at 700 K Ab Initio Molecular Dynamics Simulation of Hexane and Hexene. *J. Catal.* **2002**, *205*, 147–156. DOI: 10.1006/jcat.2001.3408.

(306) Rey, J.; Bignaud, C.; Raybaud, P.; Bučko, T.; Chizallet, C. Dynamic Features of Transition States for B-Scission Reactions of Alkenes over Acid Zeolites Revealed by AIMD Simulations. *Angew. Chem., Int. Ed.* **2020**, *59*, 18938–18942. DOI: 10.1002/anie.202006065.

(307) Hajek, J.; van der Mynsbrugge, J.; Wispelaere, K. de; Cnudde, P.; Vanduyfhuys, L.; Waroquier, M.; van Speybroeck, V. On the Stability and Nature of Adsorbed Pentene in Brønsted Acid Zeolite H-ZSM-5 at 323K. *J. Catal.* **2016**, *340*, 227–235. DOI: 10.1016/j.jcat.2016.05.018.

(308) Cnudde, P.; Wispelaere, K. de; van der Mynsbrugge, J.; Waroquier, M.; van Speybroeck, V. Effect of Temperature and Branching on the Nature and Stability of Alkene Cracking Intermediates in H-ZSM-5. *J. Catal.* **2017**, *345*, 53–69. DOI: 10.1016/j.jcat.2016.11.010.

(309) Cnudde, P.; Wispelaere, K. de; Vanduyfhuys, L.; Demuynck, R.; van der Mynsbrugge, J.; Waroquier, M.; van Speybroeck, V. How Chain Length and Branching Influence the Alkene Cracking Reactivity on H-ZSM-5. *ACS Catal.* **2018**, *8*, 9579–9595. DOI: 10.1021/acscatal.8b01779.

(310) Rey, J.; Raybaud, P.; Chizallet, C.; Bučko, T. Competition of Secondary Versus Tertiary Carbenium Routes for the Type B Isomerization of Alkenes over Acid Zeolites Quantified by Ab Initio Molecular Dynamics Simulations. *ACS Catal.* **2019**, *9*, 9813–9828. DOI: 10.1021/acscatal.9b02856.

(311) Bjørgen, M.; Bonino, F.; Kolboe, S.; Lillerud, K.-P.; Zecchina, A.; Bordiga, S. Spectroscopic Evidence for a Persistent Benzenium Cation in Zeolite H-Beta. *J. Am. Chem. Soc.* **2003**, *125*, 15863–15868. DOI: 10.1021/ja037073d.

(312) Chowdhury, A. D.; Houben, K.; Whiting, G. T.; Chung, S.-H.; Baldus, M.; Weckhuysen, B. M. Electrophilic Aromatic Substitution over Zeolites Generates Wheland-Type Reaction Intermediates. *Nat. Catal.* **2018**, *1*, 23–31. DOI: 10.1038/s41929-017-0002-4.

(313) Zhang, W.; Chen, J.; Xu, S.; Chu, Y.; Wei, Y.; Zhi, Y.; Huang, J.; Zheng, A.; Wu, X.; Meng, X.*; et al.* Methanol to Olefins Reaction over Cavity-Type Zeolite: Cavity Controls the Critical Intermediates and Product Selectivity. *ACS Catal.* **2018**, *8*, 10950–10963. DOI: 10.1021/acscatal.8b02164.

(314) Arstad, B.; Kolboe, S.; Swang, O. Theoretical Study of the Heptamethylbenzenium Ion. Intramolecular Isomerizations and C2, C3, C4 Alkene Elimination. *J. Phys. Chem. A* **2005**, *109*, 8914–8922. DOI: 10.1021/jp058166f.

(315) Ferri, P.; Li, C.; Paris, C.; Vidal-Moya, A.; Moliner, M.; Boronat, M.; Corma, A. Chemical and Structural Parameter Connecting Cavity Architecture, Confined Hydrocarbon Pool Species, and MTO Product Selectivity in Small-Pore Cage-Based Zeolites. *ACS Catal.* **2019**, *9*, 11542–11551. DOI: 10.1021/acscatal.9b04588.

(316) Ma, H.; Chen, Y. Y.; Wang, S.; Wei, Z. H.; Qin, Z. F.; Dong, M.; Li, J. F.; Fan, W. B.; Wang, J. G. Reaction Mechanism for the Conversion of Methanol to Olefins over H-ITQ-13 Zeolite: A Density Functional Theory Study. *Catal. Sci. Technol.* **2018**, *8*, 521–533. DOI: 10.1039/c7cy02047c.

(317) Hansen, N.; Brüggemann, T.; Bell, A. T.; Keil, F. J. Theoretical Investigation of Benzene Alkylation with Ethene over H-ZSM-5. *J. Phys. Chem. C* **2008**, *112*, 15402–15411. DOI: 10.1021/jp8036022.

(318) Clark, L. A.; Sierka, M.; Sauer, J. Stable Mechanistically-Relevant Aromatic-Based Carbenium Ions in Zeolite Catalysts. *J. Am. Chem. Soc.* **2003**, *125*, 2136–2141. DOI: 10.1021/ja0283302.

(319) Demuth, T.; Raybaud, P.; Lacombe, S.; Toulhoat, H. Effects of Zeolite Pore Sizes on the Mechanism and Selectivity of Xylene Disproportionation—A DFT Study. *J. Catal.* **2004**, *222*, 323–337. DOI: 10.1016/j.jcat.2003.10.017.

(320) Margarit, V. J.; Osman, M.; Al-Khattaf, S.; Martínez, C.; Boronat, M.; Corma, A. Control of the Reaction Mechanism of Alkylaromatics Transalkylation by Means of Molecular Confinement Effects Associated to Zeolite Channel Architecture. *ACS Catal.* **2019**, *9*, 5935–5946. DOI: 10.1021/acscatal.9b00763.

(321) Li, C.; Ferri, P.; Paris, C.; Moliner, M.; Boronat, M.; Corma, A. Design and Synthesis of the Active Site Environment in Zeolite Catalysts for Selectively Manipulating Mechanistic Pathways. *J. Am. Chem. Soc.* **2021**, *143*, 10718–10726. DOI: 10.1021/jacs.1c04818.

(322) Fečík, M.; Plessow, P. N.; Studt, F. A Systematic Study of Methylation from Benzene to Hexamethylbenzene in H-SSZ-13 Using Density Functional Theory and Ab Initio Calculations. *ACS Catal.* **2020**, *10*, 8916–8925. DOI: 10.1021/acscatal.0c02037.

(323) Fečík, M.; Plessow, P. N.; Studt, F. Theoretical Investigation of the Side-Chain Mechanism of the MTO Process over H-SSZ-13 Using DFT and Ab Initio Calculations. *Catal. Sci. Technol.* **2021**, *11*, 3826–3833. DOI: 10.1039/D1CY00433F.

(324) Bocus, M.; Vanduyfhuys, L.; Proft, F. de; Weckhuysen, B. M.; van Speybroeck, V. Mechanistic Characterization of Zeolite-Catalyzed Aromatic Electrophilic Substitution at Realistic Operating Conditions. *JACS Au* **2022**, *2*, 502–514. DOI: 10.1021/jacsau.1c00544.

(325) Bocus, M.; van Speybroeck, V. Insights into the Mechanism and Reactivity of Zeolite-Catalyzed Alkylphenol Dealkylation. *ACS Catal.* **2022**, 14227–14242. DOI: 10.1021/acscatal.2c03844.

(326) Moors, S. L. C.; Wispelaere, K. de; van der Mynsbrugge, J.; Waroquier, M.; van Speybroeck, V. Molecular Dynamics Kinetic Study on the Zeolite-Catalyzed Benzene Methylation in ZSM-5. *ACS Catal.* **2013**, *3*, 2556–2567. DOI: 10.1021/cs400706e.

(327) Ristanović, Z.; Chowdhury, A. D.; Brogaard, R. Y.; Houben, K.; Baldus, M.; Hofkens, J.; Roeffaers, M. B. J.; Weckhuysen, B. M. Reversible and Site-Dependent Proton-Transfer in Zeolites Uncovered at the Single-Molecule Level. *J. Am. Chem. Soc.* **2018**, *140*, 14195–14205. DOI: 10.1021/jacs.8b08041.

(328) Walspurger, S.; Sun, Y.; Souna Sido, A. S.; Sommer, J. Neopentane and Solid Acids: Direct Hydron Exchange Before Cracking. *J. Phys. Chem. B* **2006**, *110*, 18368–18373. DOI: 10.1021/jp0621676.

(329) Kazansky, V. B.; Frash, M. V.; van Santen, R. A. A Quantum-Chemical Study of Hydride Transfer in Catalytic Transformations of Paraffins on Zeolites. Pathways Through Adsorbed Nonclassical Carbonium Ions. *Catal. Lett.* **1997**, *48*, 61–67. DOI: 10.1023/A:1019066718512.

(330) Zygmunt, S. A.; Curtiss, L. A.; Zapol, P.; Iton, L. E. Ab Initio and Density Functional Study of the Activation Barrier for Ethane Cracking in Cluster Models of Zeolite H-ZSM-5. *J. Phys. Chem. B* **2000**, *104*, 1944–1949. DOI: 10.1021/jp993194h.

(331) Boronat, M.; Viruela, P.; Corma, A. Ab Initio and Density-Functional Theory Study of Zeolite-Catalyzed Hydrocarbon Reactions: Hydride Transfer, Alkylation and Disproportionation. *Phys. Chem. Chem. Phys.* **2000**, *2*, 3327–3333. DOI: 10.1039/B002013N.

(332) Zimmerman, P. M.; Tranca, D. C.; Gomes, J.; Lambrecht, D. S.; Head-Gordon, M.; Bell, A. T. Ab Initio Simulations Reveal That Reaction Dynamics Strongly Affect Product Selectivity for the Cracking of Alkanes over H-MFI. *J. Am. Chem. Soc.* **2012**, *134*, 19468–19476. DOI: 10.1021/ja3089372.

(333) Maihom, T.; Pantu, P.; Tachakritikul, C.; Probst, M.; Limtrakul, J. Effect of the Zeolite Nanocavity on the Reaction Mechanism of N-Hexane Cracking: A Density Functional Theory Study. *J. Phys. Chem. C* **2010**, *114*, 7850–7856. DOI: 10.1021/jp911732p.

(334) Tranca, D. C.; Zimmerman, P. M.; Gomes, J.; Lambrecht, D.; Keil, F. J.; Head-Gordon, M.; Bell, A. T. Hexane Cracking on ZSM-5 and Faujasite Zeolites: A QM/MM/QCT Study. *J. Phys. Chem. C* **2015**, *119*, 28836–28853. DOI: 10.1021/acs.jpcc.5b07457.

(335) Berger, F.; Rybicki, M.; Sauer, J. Adsorption and Cracking of Propane by Zeolites of Different Pore Size. *J. Catal.* **2021**, *395*, 117–128. DOI: 10.1016/j.jcat.2020.12.008.

(336) Collins, S. J.; O'Malley, P. J. The Mechanism of Alkane Activation over Zeolite Brønsted Acid Sites. A Density-Functional Study. *Chem. Phys. Lett.* **1995**, *246*, 555–561. DOI: 10.1016/0009-2614(95)01149-3.

(337) Brouwer, D. M.; Hogeveen, H. Electrophilic Substitutions at Alkanes and in Alkylcarbonium Ions. *Prog. Phys. Org. Chem.* **1972**, *9*, 179–240.

(338) Saunders, M.; Vogel, P.; Hagen, E. L.; Rosenfeld, J. Evidence for Protonated Cyclopropane Intermediates from Studies of Stable Solutions of Carbonium Ions. *Acc. Chem. Res.* **1973**, *6*, 53–59. DOI: 10.1021/ar50062a003.

(339) Martens, J. A.; Tielen, M.; Jacobs, P. A.; Weitkamp, J. Estimation of the Void Structure and Pore Dimensions of Molecular Sieve Zeolites Using the Hydroconversion of N-Decane. *Zeolites* **1984**, *4*, 98–107. DOI: 10.1016/0144-2449(84)90044-7.

(340) Sandbeck, D. J. S.; Markewich, D. J.; East, A. L. L. The Carbocation Rearrangement Mechanism, Clarified. *J. Org. Chem.* **2016**, *81*, 1410–1415. DOI: 10.1021/acs.joc.5b02553.

(341) Hoffmann, R. Extended Hückel Theory. IV. Carbonium Ions. *J. Chem. Phys.* **1964**, *40*, 2480–2488. DOI: 10.1063/1.1725551.

(342) Fischer, H.; Kollmar, H.; Smith, H. O.; Miller, K. Semiempirical Mo Calculations in the C3H7+series. *Tetrahedron Lett.* **1968**, *9*, 5821–5824. DOI: 10.1016/S0040-4039(00)76361-1.

(343) Sustmann, R.; Williams, J. E.; Dewar, M. J. S.; Allen, L. C.; Schleyer, P. v. R. Molecular Orbital Calculations on Carbonium Ions. II. Methyl, Ethyl, and Vinyl Cations. The Series C3H7+. *J. Am. Chem. Soc.* **1969**, *91*, 5350–5357. DOI: 10.1021/ja01047a026.

(344) Pople, J. A.; Radom, L.; Buss, V.; Schleyer, P. v. R. Structures and Relative Stabilities of C3H7+ Cations. *J. Am. Chem. Soc.* **1971**, *93*, 1813–1815. DOI: 10.1021/ja00736a059.

(345) Rey, J.; Gomez, A.; Raybaud, P.; Chizallet, C.; Bučko, T. On the Origin of the Difference Between Type a and Type B Skeletal Isomerization of Alkenes Catalyzed by Zeolites: The Crucial Input of Ab Initio Molecular Dynamics. *J. Catal.* **2019**, *373*, 361–373. DOI: 10.1016/j.jcat.2019.04.014.

(346) Gutierrez-Acebo, E.; Rey, J.; Bouchy, C.; Schuurman, Y.; Chizallet, C. Ethylcyclohexane Hydroconversion in EU-1 Zeolite: DFT-based Microkinetic Modeling Reveals the Nature of the Kinetically Relevant Intermediates. *ChemCatChem* **2021**, *13*, 3434–3442. DOI: 10.1002/cctc.202100421.

(347) East, A. L. L.; Bučko, T.; Hafner, J. Carbocation Branching Observed in a Simulation. *J. Phys. Chem. A* **2007**, *111*, 5945–5947. DOI: 10.1021/jp072327t.

(348) Natal-Santiago, M. A.; Alcalá, R.; Dumesic, J. A. DFT Study of the Isomerization of Hexyl Species Involved in the Acid-Catalyzed Conversion of 2-Methyl-Pentene-2. *J. Catal.* **1999**, *181*, 124–144. DOI: 10.1006/jcat.1998.2293.

(349) Frash, M. V.; Kazansky, V. B.; Rigby, A. M.; van Santen, R. A. Density Functional and Hartree−Fock Calculations on the Cyclopropane Ring Intermediates Involved in the Zeolite-Catalyzed Skeletal Isomerization of Hydrocarbons and in the Carbon Isotope Scrambling in 2-Propyl Cation. *J. Phys. Chem. B* **1997**, *101*, 5346–5351. DOI: 10.1021/jp964055s.

(350) Schweitzer, J.-M.; Rey, J.; Bignaud, C.; Bučko, T.; Raybaud, P.; Moscovici-Mirande, M.; Portejoie, F.; James, C.; Bouchy, C.; Chizallet, C. Multiscale Modeling as a Tool for the Prediction of Catalytic Performances: The Case of N-Heptane Hydroconversion in a Large-Pore Zeolite. *ACS Catal.* **2022**, *12*, 1068–1081. DOI: 10.1021/acscatal.1c04707.

(351) Gomes, J.; Head-Gordon, M.; Bell, A. T. Reaction Dynamics of Zeolite-Catalyzed Alkene Methylation by Methanol. *J. Phys. Chem. C* **2014**, *118*, 21409–21419. DOI: 10.1021/jp502804q.

(352) Denayer, J. F.; Baron, G. V.; Vanbutsele, G.; Jacobs, P. A.; Martens, J. A. Evidence for Alkylcarbenium Ion Reaction Intermediates from Intrinsic Reaction Kinetics of C6–C9 N-Alkane Hydroisomerization and Hydrocracking on Pt/H–Y and Pt/USY Zeolites. *J. Catal.* **2000**, *190*, 469–473. DOI: 10.1006/jcat.1999.2756.

(353) Thybaut, J.; Marin, G.; Baron, G. V.; Jacobs, P.; Martens, J. A. Alkene Protonation Enthalpy Determination from Fundamental Kinetic Modeling of Alkane Hydroconversion on Pt/H–(US)Y-Zeolite. *J. Catal.* **2001**, *202*, 324–339. DOI: 10.1006/jcat.2001.3292.

(354) Thybaut, J. W.; Narasimhan, C. L.; Marin, G. B.; Denayer, J. F.; Baron, G. V.; Jacobs, P. A.; Martens, J. A. Alkylcarbenium Ion Concentrations in Zeolite Pores During Octane Hydrocracking on Pt/H-USY Zeolite. *Catal. Lett.* **2004**, *94*, 81–88. DOI: 10.1023/B:CATL.0000019335.48350.24.

(355) Guisnet, M. "Ideal" Bifunctional Catalysis over Pt-Acid Zeolites. *Catal. Today* **2013**, *218-219*, 123–134. DOI: 10.1016/j.cattod.2013.04.028.

(356) Weitkamp, J. Catalytic Hydrocracking—Mechanisms and Versatility of the Process. *ChemCatChem* **2012**, *4*, 292–306. DOI: 10.1002/cctc.201100315.

(357) Bouchy, C.; Hastoy, G.; Guillon, E.; Martens, J. A. Fischer-Tropsch Waxes Upgrading via Hydrocracking and Selective Hydroisomerization. *Oil & Gas Science Technol. - Rev. IFP* **2009**, *64*, 91–112. DOI: 10.2516/ogst/2008047.

(358) Thybaut, J. W.; Laxmi Narasimhan, C. S.; Denayer, J. F.; Baron, G. V.; Jacobs, P. A.; Martens, J. A.; Marin, G. B. Acid−Metal Balance of a Hydrocracking Catalyst: Ideal Versus Nonideal Behavior. *Ind. Eng. Chem. Res.* **2004**, *44*, 5159–5169. DOI: 10.1021/ie049375.

(359) Blomsma, E.; Martens, J. A.; Jacobs, P. A. Mechanisms of Heptane Isomerization on Bifunctional Pd/H-Beta Zeolites. *J. Catal.* **1996**, *159*, 323–331. DOI: 10.1006/jcat.1996.0094.

(360) Martens, J. A.; Jacobs, P. A. *Theoretical Aspects of Heterogeneous Catalysis: Conceptual Background for the Conversion of Hydrocarbons on Heterogeneous Acid Catalysts*; Springer Netherlands, 1990. DOI: 10.1007/978-94-010-9882-3.

(361) Noh, G.; Zones, S. I.; Iglesia, E. Consequences of Acid Strength and Diffusional Constraints for Alkane Isomerization and B-Scission Turnover Rates and Selectivities on Bifunctional Metal-Acid Catalysts. *J. Phys. Chem. C* **2018**, *122*, 25475–25497. DOI: 10.1021/acs.jpcc.8b08460.

(362) Jones, A. J.; Carr, R. T.; Zones, S. I.; Iglesia, E. Acid Strength and Solvation in Catalysis by MFI Zeolites and Effects of the Identity, Concentration and Location of Framework Heteroatoms. *J. Catal.* **2014**, *312*, 58–68. DOI: 10.1016/j.jcat.2014.01.007.

(363) Ren, Q.; Rybicki, M.; Sauer, J. Interaction of C3 –C5 Alkenes with Zeolitic Brønsted Sites: Π-Complexes, Alkoxides, and Carbenium Ions in H-FER. *J. Phys. Chem. C* **2020**, *124*, 10067–10078. DOI: 10.1021/acs.jpcc.0c03061.

(364) Weitkamp, J.; Ernst, S.; Karge, H. G. Peculiarities in the Conversion of Naphthenes on Bifunctional Catalysts. *Erdol & Kohle Erdgas Petrochemie* **1984**, *37*, 457–462.

(365) Greensfelder, B. S.; Voge, H. H.; Good, G. M. Catalytic and Thermal Cracking of Pure Hydrocarbons: Mechanisms of Reaction. *Ind. Eng. Chem.* **1949**, *41*, 2573-2484.

(366) Thomas, C. L. Chemistry of Cracking Catalysts. *Ind. Eng. Chem.* **1949**, *41*, 2564–2573. DOI: 10.1021/ie50479a042.

(367) Sie, S. T. Acid-Catalyzed Cracking of Paraffinic Hydrocarbons. 1. Discussion of Existing Mechanisms and Proposal of a New Mechanism. *Ind. Eng. Chem. Res.* **1992**, *31*, 1881–1889. DOI: 10.1021/ie00008a008.

(368) Sie, S. T. Acid-Catalyzed Cracking of Paraffinic Hydrocarbons. 3. Evidence for the Protonated Cyclopropane Mechanism from Hydrocracking/hydroisomerization Experiments. *Ind. Eng. Chem. Res.* **1993**, *32*, 403–408. DOI: 10.1021/ie00015a002.

(369) Svoboda, G. D.; Vynckier, E.; Debrabandere, B.; Froment, G. F. Single-Event Rate Parameters for Paraffin Hydrocracking on a Pt/US-Y Zeolite. *Ind. Eng. Chem. Res.* **1995**, *34*, 3793–3800. DOI: 10.1021/ie00038a016.

(370) Alvarez, F.; Ribeiro, F. R.; Perot, G.; Thomazeau, C.; Guisnet, M. Hydroisomerization and Hydrocracking of Alkanes. *J. Catal.* **1996**, *162*, 179–189. DOI: 10.1006/jcat.1996.0275.

(371) Maesen, T. L.; Calero, S.; Schenk, M.; Smit, B. Alkane Hydrocracking: Shape Selectivity or Kinetics? *J. Catal.* **2004**, *221*, 241–251. DOI: 10.1016/j.jcat.2003.07.003.

(372) Burnens, G.; Bouchy, C.; Guillon, E.; Martens, J. A. Hydrocracking Reaction Pathways of 2,6,10,14-Tetramethylpentadecane Model Molecule on Bifunctional Silica–alumina and Ultrastable Y Zeolite Catalysts. *J. Catal.* **2011**, *282*, 145–154. DOI: 10.1016/j.jcat.2011.06.007.

(373) Thybaut, J. W.; Choudhury, I. R.; Denayer, J. F.; Baron, G. V.; Jacobs, P. A.; Martens, J. A.; Marin, G. B. Design of Optimum Zeolite Pore System for Central Hydrocracking of Long-Chain N-Alkanes Based on a Single-Event Microkinetic Model. *Top. Catal.* **2009**, *52*, 1251–1260. DOI: 10.1007/s11244-009-9274-5.

(374) Martens, J. A.; Tielen, M.; Jacobs, P. A. Attempts to Rationalize the Distribution of Hydrocracked Products. III. Mechanistic Aspects of Isomerization and Hydrocracking of Branched Alkanes on Ideal Bifunctional Large-Pore Zeolite Catalysts. *Catal. Today* **1987**, *1*, 435–453. DOI: 10.1016/0920-5861(87)80008-1.

(375) Mazar, M. N.; Al-Hashimi, S.; Cococcioni, M.; Bhan, A. B-Scission of Olefins on Acidic Zeolites: A Periodic PBE-D Study in H-ZSM-5. *J. Phys. Chem. C* **2013**, *117*, 23609–23620. DOI: 10.1021/jp403504n.

(376) Sun, Y.-X.; Yang, J.; Zhao, L.-F.; Dai, J.-X.; Sun, H. A Two-Layer ONIOM Study on Initial Reactions of Catalytic Cracking of 1-Butene to Produce Propene and Ethene over HZSM-5 and HFAU Zeolites. *J. Phys. Chem. C* **2010**, *114*, 5975–5984. DOI: 10.1021/jp910617m.

(377) Namuangruk, S.; Pantu, P.; Limtrakul, J. Investigation of Ethylene Dimerization over Faujasite Zeolite by the ONIOM Method. *ChemPhysChem* **2005**, *6*, 1333–1339. DOI: 10.1002/cphc.200500023.

(378) Chu, Y.; Han, B.; Zheng, A.; Deng, F. Influence of Acid Strength and Confinement Effect on the Ethylene Dimerization Reaction over Solid Acid Catalysts: A Theoretical Calculation Study. *J. Phys. Chem. C* **2012**, *116*, 12687–12695. DOI: 10.1021/jp302960w.

(379) Huang, B.; Bai, P.; Neurock, M.; Davis, R. J. Conversion of N-Hexane and N-Dodecane over H-ZSM-5, H-Y and Al-MCM-41 at Supercritical Conditions. *Appl. Catal. A* **2017**, *546*, 149–158. DOI: 10.1016/j.apcata.2017.07.027.

(380) Brouwer, D. M.; Hogeveen, H. The Importance of Orbital Orientation as a Rate-Controlling Factor in Intramolecular Reactions of Carbonium Ions. *Recl. Trav. Chim. Pays-Bas* **1970**, *89*, 211–224. DOI: 10.1002/recl.19700890213.

(381) Egan, C. J.; Langlois, G. E.; White, R. J. Selective Hydrocracking of C_9- to C_{12}-Alkylcyclohexanes on Acidic Catalysts. Evidence for the Paring Reaction. *J. Am. Chem. Soc.* **1962**, *84*, 1204–1212. DOI: 10.1021/ja00866a028.

(382) Brito, L.; Pirngruber, G. D.; Guillon, E.; Albrieux, F.; Martens, J. A. Hydroconversion of Octylcyclohexane over a Bifunctional Pt/USY Zeolite Catalyst. *Energy Fuels* **2021**, *35*, 13955–13966. DOI: 10.1021/acs.energyfuels.1c01977.

(383) Souverijns, W.; Parton, R.; Martens, J. A.; Froment, G. F.; Jacobs, P. A. Mechanism of the Paring Reaction of Naphtenes. *Catal. Lett.* **1996**, *37*, 207–212. DOI: 10.1007/BF00807755.

(384) Souverijns, W.; Houvenaghel, A.; Feijen, E.; Martens, J. A.; Jacobs, P. A. Isomerization of 1-Cyclohexyloctane on Pt/H-ZSM-22 Bifunctional Zeolite Catalyst. *J. Catal.* **1998**, *174*, 201–209. DOI: 10.1006/jcat.1998.1968.

(385) Martens, J. A.; Jacobs, P. A.; Weitkamp, J. Attempts to Rationalize the Distribution of Hydrocracked Products. I Qualitative Description of the Primary Hydrocracking Modes of Long Chain Paraffins in Open Zeolites. *Appl. Catal.* **1986**, *20*, 239–281. DOI: 10.1016/0166-9834(86)80020-3.

(386) Martens, J. A.; Jacobs, P. A.; Weitkamp, J. Attempts to Rationalize the Distribution of Hydrocracked Products. II. Relative Rates of Primary Hydrocracking Modes of Long Chain Paraffins in Open Zeolites. *Appl. Catal.* **1986**, *20*, 283–303. DOI: 10.1016/0166-9834(86)80021-5.

(387) Webb, E. B.; Grest, G. S.; Mondello, M. Intracrystalline Diffusion of Linear and Branched Alkanes in the Zeolites TON, EUO, and MFI. *J. Phys. Chem. B* **1999**, *103*, 4949–4959. DOI: 10.1021/jp9845266.

(388) Bai, P.; Jeon, M. Y.; Ren, L.; Knight, C.; Deem, M. W.; Tsapatsis, M.; Siepmann, J. I. Discovery of Optimal Zeolites for Challenging Separations and Chemical Transformations Using Predictive Materials Modeling. *Nat. Commun.* **2015**, *6*, 5912. DOI: 10.1038/ncomms6912.

(389) Benazzi, E.; Leite, L.; Marchal-George, N.; Toulhoat, H.; Raybaud, P. New Insights into Parameters Controlling the Selectivity in Hydrocracking Reactions. *J. Catal.* **2003**, *217*, 376–387. DOI: 10.1016/S0021-9517(03)00041-1.

(390) Mendes, P. S. F.; Chizallet, C.; Pérez-Pellitero, J.; Raybaud, P.; Silva, J. M.; Ribeiro, M. F.; Daudin, A.; Bouchy, C. Interplay of the Adsorption of Light and Heavy Paraffins in Hydroisomerization over H-Beta Zeolite. *Catal. Sci. Technol.* **2019**, *9*, 5368–5382. DOI: 10.1039/C9CY00788A.

(391) Lee, S.-W.; Ihm, S.-K. Characteristics of Magnesium-Promoted Pt/ZSM-23 Catalyst for the Hydroisomerization of N -Hexadecane. *Ind. Eng. Chem. Res.* **2013**, *52*, 15359–15365. DOI: 10.1021/ie400628q.

(392) Miller, S. J. New Molecular Sieve Process for Lube Dewaxing by Wax Isomerization. *Micropor. Mat.* **1994**, *2*, 439–449. DOI: 10.1016/0927-6513(94)00016-6.

(393) Huybrechts, W.; Vanbutsele, G.; Houthoofd, K. J.; Bertinchamps, F.; Laxmi Narasimhan, C. S.; Gaigneaux, E. M.; Thybaut, J. W.; Marin, G. B.; Denayer, J. F. M.; Baron, G. V.*; et al.* Skeletal Isomerization of Octadecane on Bifunctional ZSM-23 Zeolite Catalyst. *Catal. Lett.* **2005**, *100*, 235–242. DOI: 10.1007/s10562-004-3461-6.

(394) Souverijns, W.; Martens, J. A.; Froment, G. F.; Jacobs, P. A. Hydrocracking of Isoheptadecanes on Pt/H–ZSM-22: An Example of Pore Mouth Catalysis. *J. Catal.* **1998**, *174*, 177–184. DOI: 10.1006/jcat.1998.1959.

(395) Claude, M. C.; Vanbutsele, G.; Martens, J. A. Dimethyl Branching of Long N-Alkanes in the Range from Decane to Tetracosane on Pt/H–ZSM-22 Bifunctional Catalyst. *J. Catal.* **2001**, *203*, 213–231. DOI: 10.1006/jcat.2001.3325.

(396) Claude, M. C.; Martens, J. A. Monomethyl-Branching of Long N-Alkanes in the Range from Decane to Tetracosane on Pt/H-ZSM-22 Bifunctional Catalyst. *J. Catal.* **2000**, *190*, 39–48. DOI: 10.1006/jcat.1999.2714.

(397) Shubin, A. A.; Zilberberg, I. L. Entropy Driven Preference for Alkene Adsorption at the Pore Mouth as the Origin of Pore-Mouth Catalysis for Alkane Hydroisomerization in 1D Zeolites. *Catal. Sci. Technol.* **2021**, *11*, 563–574. DOI: 10.1039/D0CY01485K.

(398) Radhakrishnan, S.; Goossens, P.-J.; Magusin, Pieter C. M. M.; Sree, S. P.; Detavernier, C.; Breynaert, E.; Martineau, C.; Taulelle, F.; Martens, J. A. In Situ Solid-State (13)C NMR Observation of Pore Mouth Catalysis in Etherification of B-Citronellene with Ethanol on

Zeolite Beta. *Journal of the American Chemical Society* **2016**, *138*, 2802–2808. DOI: 10.1021/jacs.5b13282.

(399) Webb III, E. B.; Grest, G. S. Influence of Intracrystalline Diffusion in Shape Selective Catalytic Test Reactions. *Catal. Lett.* **1998**, *56*, 95–104. DOI: 10.1023/A:1019061113254.

(400) Raybaud, P.; Patrigeon, A.; Toulhoat, H. The Origin of the C7-Hydroconversion Selectivities on Y, B, ZSM-22, ZSM-23, and EU-1 Zeolites. *J. Catal.* **2001**, *197*, 98–112. DOI: 10.1006/jcat.2000.3064.

(401) Noh, G.; Zones, S. I.; Iglesia, E. Isomer Sieving and the Selective Formation of Terminal Methyl Isomers in Reactions of Linear Alkanes on One-Dimensional Zeolites. *J. Catal.* **2019**, *377*, 255–270. DOI: 10.1016/j.jcat.2019.07.022.

(402) Deldari, H. Suitable Catalysts for Hydroisomerization of Long-Chain Normal Paraffins. *Appl. Catal. A* **2005**, *293*, 1–10. DOI: 10.1016/j.apcata.2005.07.008.

(403) Nicholas, C. P. Applications of Light Olefin Oligomerization to the Production of Fuels and Chemicals. *Appl. Catal. A* **2017**, *543*, 82–97. DOI: 10.1016/j.apcata.2017.06.011.

(404) Wang, W.-C.; Tao, L. Bio-Jet Fuel Conversion Technologies. *Renew. Sustain. Energy Rev.* **2016**, *53*, 801–822. DOI: 10.1016/j.rser.2015.09.016.

(405) Eagan, N. M.; Kumbhalkar, M. D.; Buchanan, J. S.; Dumesic, J. A.; Huber, G. W. Chemistries and Processes for the Conversion of Ethanol into Middle-Distillate Fuels. *Nat. Rev. Chem.* **2019**, *3*, 223–249. DOI: 10.1038/s41570-019-0084-4.

(406) Pines, H. *The Chemistry of Catalytic Hydrocarbon Conversions*; Elsevier Science, 2014.

(407) Kim, Y. T.; Chada, J. P.; Xu, Z.; Pagan-Torres, Y. J.; Rosenfeld, D. C.; Winniford, W. L.; Schmidt, E.; Huber, G. W. Low-Temperature Oligomerization of 1-Butene with H-Ferrierite. *J. Catal.* **2015**, *323*, 33–44. DOI: 10.1016/j.jcat.2014.12.025.

(408) Quann, R. J.; Green, L. A.; Tabak, S. A.; Krambeck, F. J. Chemistry of Olefin Oligomerization over ZSM-5 Catalyst. *Ind. Eng. Chem. Res.* **1988**, *27*, 565–570. DOI: 10.1021/ie00076a006.

(409) Bellussi, G.; Mizia, F.; Calemma, V.; Pollesel, P.; Millini, R. Oligomerization of Olefins from Light Cracking Naphtha over Zeolite-Based Catalyst for the Production of High Quality Diesel Fuel. *Microporous Mesoporous Mater.* **2012**, *164*, 127–134. DOI: 10.1016/j.micromeso.2012.07.020.

(410) Sarazen, M. L.; Doskocil, E.; Iglesia, E. Effects of Void Environment and Acid Strength on Alkene Oligomerization Selectivity. *ACS Catal.* **2016**, *6*, 7059–7070. DOI: 10.1021/acscatal.6b02128.

(411) Datema, K. P.; Nowak, A. K.; van Braam Houckgeest, J.; Wielers, A. F. H. In-Situ13C Magic-Angle-Spinning NMR Measurements of the Conversion of Ethene to Aliphatic Hydrocarbons over Structurally Different Zeolites. *Catal. Lett.* **1991**, *11*, 267–276. DOI: 10.1007/BF00764317.

(412) Martens, J. A.; Verrelst, W. H.; Mathys, G. M.; Brown, S. H.; Jacobs, P. A. Tailored Catalytic Propene Trimerization over Acidic Zeolites with Tubular Pores. *Angew. Chem., Int. Ed.* **2005**, *44*, 5687–5690. DOI: 10.1002/anie.200463045.

(413) Martens, J. A.; Ravishankar, R.; Mishin, I. E.; Jacobs, P. A. Tailored Alkene Oligomerization with H-ZSM-57 Zeolite. *Angew. Chem. Int. Ed.* **2000**, *39*, 4376–4379. DOI: 10.1002/1521-3773(20001201)39:23<4376:AID-ANIE4376>3.0.CO;2-2.

(414) Chen, C. S.; Bridger, R. F. Shape-Selective Oligomerization of Alkenes to Near-Linear Hydrocarbons by Zeolite Catalysis. *J. Catal.* **1996**, *161*, 687–693. DOI: 10.1006/jcat.1996.0230.

(415) Popov, A. G.; Pavlov, V. S.; Ivanova, I. I. Effect of Crystal Size on Butenes Oligomerization over MFI Catalysts. *J. Catal.* **2016**, *335*, 155–164. DOI: 10.1016/j.jcat.2015.12.008.

(416) Wulfers, M. J.; Lobo, R. F. Assessment of Mass Transfer Limitations in Oligomerization of Butene at High Pressure on H-Beta. *Appl. Catal. A* **2015**, *505*, 394–401. DOI: 10.1016/j.apcata.2015.08.016.

(417) Díaz-Rey, M. R.; Paris, C.; Martínez-Franco, R.; Moliner, M.; Martínez, C.; Corma, A. Efficient Oligomerization of Pentene into Liquid Fuels on Nanocrystalline Beta Zeolites. *ACS Catal.* **2017**, *7*, 6170–6178. DOI: 10.1021/acscatal.7b00817.

(418) Moon, S.; Chae, H.-J.; Park, M. B. Oligomerization of Light Olefins over ZSM-5 and Beta Zeolite Catalysts by Modifying Textural Properties. *Appl. Catal. A* **2018**, *553*, 15–23. DOI: 10.1016/j.apcata.2018.01.015.

(419) Martínez, C.; Doskocil, E. J.; Corma, A. Improved THETA-1 for Light Olefins Oligomerization to Diesel: Influence of Textural and Acidic Properties. *Top. Catal.* **2014**, *57*, 668–682. DOI: 10.1007/s11244-013-0224-x.

(420) Sarazen, M. L.; Doskocil, E.; Iglesia, E. Catalysis on Solid Acids: Mechanism and Catalyst Descriptors in Oligomerization Reactions of Light Alkenes. *J. Catal.* **2016**, *344*, 553–569. DOI: 10.1016/j.jcat.2016.10.010.

(421) Mlinar, A. N.; Zimmerman, P. M.; Celik, F. E.; Head-Gordon, M.; Bell, A. T. Effects of Brønsted-Acid Site Proximity on the Oligomerization of Propene in H-MFI. *J. Catal.* **2012**, *288*, 65–73. DOI: 10.1016/j.jcat.2012.01.002.

(422) Bernauer, M.; Tabor, E.; Pashkova, V.; Kaucký, D.; Sobalík, Z.; Wichterlová, B.; Dedecek, J. Proton Proximity – New Key Parameter Controlling Adsorption, Desorption and Activity in Propene Oligomerization over H-ZSM-5 Zeolites. *J. Catal.* **2016**, *344*, 157–172. DOI: 10.1016/j.jcat.2016.09.025.

(423) Vernuccio, S.; Bickel, E. E.; Gounder, R.; Broadbelt, L. J. Microkinetic Model of Propylene Oligomerization on Brønsted Acidic Zeolites at Low Conversion. *ACS Catal.* **2019**, *9*, 8996–9008. DOI: 10.1021/acscatal.9b02066.

(424) Vernuccio, S.; Bickel, E. E.; Gounder, R.; Broadbelt, L. J. Propene Oligomerization on Beta Zeolites: Development of a Microkinetic Model and Experimental Validation. *J. Catal.* **2021**, *395*, 302–314. DOI: 10.1016/j.jcat.2021.01.018.

(425) Svelle, S.; Kolboe, S.; Swang, O. Theoretical Investigation of the Dimerization of Linear Alkenes Catalyzed by Acidic Zeolites. *J. Phys. Chem. B* **2004**, *108*, 2953–2962. DOI: 10.1021/jp0371985.

(426) Schallmoser, S.; Haller, G. L.; Sanchez-Sanchez, M.; Lercher, J. A. Role of Spatial Constraints of Brønsted Acid Sites for Adsorption and Surface Reactions of Linear Pentenes. *J. Am. Chem. Soc.* **2017**, *139*, 8646–8652. DOI: 10.1021/jacs.7b03690.

(427) Li, S.; Cao, J.; Feng, X.; Du, Y.; de Chen; Yang, C.; Wang, W.; Ren, W. Insights into the Confinement Effect on Isobutane Alkylation with C4 Olefin Catalyzed by Zeolite Catalyst: A Combined Theoretical and Experimental Study. *Chin. J. Chem. Eng.* **2022**, *47*, 174–184. DOI: 10.1016/j.cjche.2021.08.005.

(428) Berger, F.; Sauer, J. Dimerization of Linear Butenes and Pentenes in an Acidic Zeolite (H-MFI). *Angew. Chem. Int. Ed.* **2021**, *60*, 3529–3533. DOI: 10.1002/anie.202013671.

(429) Kondo, J. N.; Liqun, S.; Wakabayashi, F.; Domen, K. IR Study of Adsorption and Reaction of 1-Butene on H-ZSM-5. *Catal. Lett.* **1997**, *47*, 129–133. DOI: 10.1023/A:1019096703066.

(430) Ivanov, P.; Papp, H. FT-IR Study of the Isomerization of N-Butene over Different Zeolites. *Langmuir* **2000**, *16*, 7769–7772. DOI: 10.1021/la000583q.

(431) Coelho, A.; Caeiro, G.; Lemos, M.; Lemos, F.; Ribeiro, F. R. 1-Butene Oligomerization over ZSM-5 Zeolite: Part 1 – Effect of Reaction Conditions. *Fuel* **2013**, *111*, 449–460. DOI: 10.1016/j.fuel.2013.03.066.

(432) Henry, M.; Bulut, M.; Vermandel, W.; Sels, B.; Jacobs, P.; Minoux, D.; Nesterenko, N.; van Donk, S.; Dath, J. P. Low Temperature Conversion of Linear C4 Olefins with Acid ZSM-5 Zeolites of Homogeneous Composition. *Appl. Catal. A* **2012**, *413-414*, 62–77. DOI: 10.1016/j.apcata.2011.10.043.

(433) Silva, A. F.; Fernandes, A.; Antunes, M. M.; Ribeiro, M. F.; Silva, C. M.; Valente, A. A. Olefin Oligomerisation over Nanocrystalline MFI-Based Micro/mesoporous Zeotypes Synthesised via Bottom-up Approaches. *Renew. Energy* **2019**, *138*, 820–832. DOI: 10.1016/j.renene.2019.02.019.

(434) Brouwer, D. M.; Oelderik, J. M. HF-SbF_5 Catalysed Isomerization of 2-Methylpentane: Kinetics and Mechanism of Rearrangement and Hydride-Ion Transfer Steps in Alkylcarbonium Ion Reactions. *Recl. Trav. Chim. Pays-Bas* **1968**, *87*, 721–736. DOI: 10.1002/recl.19680870614.

(435) Mériaudeau, P.; Anh, T. V.; Le Ngoc, H.; Naccache, C. Reaction of N-Butene over H-ZSM-5 Zeolite. Influence of the Acid Strength on the Isobutene Selectivity. *Stud. Surf. Sci. Catal.* **1997**, *105*, 1373–1379. DOI: 10.1016/S0167-2991(97)80779-3.

(436) Mooiweer, H. H.; de Jong, K. P.; Kraushaar-Czarnetzki, B.; Stork, W.; Krutzen, B. Skeletal Isomerisation of Olefins with the Zeolite Ferrierite as Catalyst. *Stud. Surf. Sci. Catal.* **1994**, *84*, 2327–2334. DOI: 10.1016/S0167-2991(08)63797-0.

(437) Gleeson, D. Skeletal Isomerization of Butene in Ferrierite: Assessing the Energetic and Structural Differences Between Carbenium and Alkoxide Based Pathways. *J. Phys. Chem. A* **2011**, *115*, 14629–14636. DOI: 10.1021/jp207683p.

(438) Boronat, M.; Viruela, P.; Corma, A. Theoretical Study of the Mechanism of Zeolite-Catalyzed Isomerization Reactions of Linear Butenes. *J. Phys. Chem. A* **1998**, *102*, 982–989. DOI: 10.1021/jp972672q.

(439) Boronat, M.; Viruela, P.; Corma, A. The Skeletal Isomerization of but-1-Ene Catalyzed by Theta-1 Zeolite. *Phys. Chem. Chem. Phys.* **2001**, *3*, 3235–3239. DOI: 10.1039/B103429B.

(440) Meriaudeau, P., et al. Selective Isomerization of N-Butene into Isobutene over Deactivated H–Ferrierite Catalyst: Further Investigations. *J. Catal.* **1997**, *169*, 397–399.

(441) Guisnet, M.; Andy, P.; Boucheff, Y.; Gnep, N. S.; Travers, C.; Benazzi, E. Selective Isomerization of N-Butenes into Isobutene over Aged H-Ferrierite Catalyst: Nature of the Active Species. *Catal. Lett.* **1998**, *50*, 159–164. DOI: 10.1023/A:1019052026632.

(442) Domokos, L.; Lefferts, L.; Seshan, K.; Lercher, J. Isomerization of Linear Butenes to Iso-Butene over Medium Pore Zeolites. *J. Catal.* **2001**, *197*, 68–80. DOI: 10.1006/jcat.2000.3056.

(443) Wulfers, M. J.; Jentoft, F. C. Mechanism of N-Butane Skeletal Isomerization on H-Mordenite and Pt/H-Mordenite. *J. Catal.* **2015**, *330*, 507–519. DOI: 10.1016/j.jcat.2014.12.035.

(444) Wattanakit, C.; Nokbin, S.; Boekfa, B.; Pantu, P.; Limtrakul, J. Skeletal Isomerization of 1-Butene over Ferrierite Zeolite: A Quantum Chemical Analysis of Structures and Reaction Mechanisms. *J. Phys. Chem. C* **2012**, *116*, 5654–5663. DOI: 10.1021/jp209991y.

(445) Gleeson, D. The Skeletal Isomerization in Ferrierite: A Theoretical Assessment of the Bi-Molecular Conversion of Cis-Butene to Iso-Butene. *J. Mol. Catal. A* **2013**, *368-369*, 107–111. DOI: 10.1016/j.molcata.2012.11.010.

(446) He, M.; Zhang, J.; Liu, R.; Sun, X.-L.; Chen, B.-H.; Wang, Y.-G. Density Functional Theory Studies on the Skeletal Isomerization of 1-Butene Catalyzed by HZSM-23 and HZSM-48 Zeolites. *RSC Adv.* **2017**, *7*, 9251–9257. DOI: 10.1039/C6RA26894C.

(447) Guisnet, M.; Andy, P.; Gnep, N.; Benazzi, E.; Travers, C. Skeletal Isomerization of N-Butenes. *J. Catal.* **1996**, *158*, 551–560.

(448) Meriaudeau, P.; Bacaud, R.; Hung, L.; Vu, A. Isomerisation of Butene in Isobutene on Ferrierite Catalyst: A Mono- or a Bimolecular Process? *J. Mol. Catal. A* **1996**, *110*, L177-L179. DOI: 10.1016/1381-1169(96)00156-2.

(449) Jo, D.; Hong, S. B.; Camblor, M. A. Monomolecular Skeletal Isomerization of 1-Butene over Selective Zeolite Catalysts. *ACS Catal.* **2015**, *5*, 2270–2274. DOI: 10.1021/acscatal.5b00195.

(450) de Jong, K. P.; Mooiweer, H. H.; Buglass, J. G.; Maarsen, P. K. Activation and Deactivation of the Zeolite Ferrierite for Olefin Conversions. *Stud. Surf. Sci. Catal.* **1997**, *111*, 127–138. DOI: 10.1016/S0167-2991(97)80147-4.

(451) Andy, P.; Gnep, N. S.; Guisnet, M.; Benazzi, E.; Travers, C. Skeletal Isomerization Ofn-Butenes: II. Composition, Mode of Formation, and Influence of Coke Deposits on the Reaction Mechanism. *J. Catal.* **1998**, *173*, 322–332. DOI: 10.1006/jcat.1997.1945.

(452) van Donk, S.; Bus, E.; Broersma, A.; Bitter, J. H.; de Jong, K. P. Butene Skeletal Isomerization over H-Ferrierite: A TEOM and in Situ IR Study on the Role of Carbonaceous Deposits and the Location of Brønsted Acid Sites. *Appl. Catal. A* **2002**, *237*, 149–159. DOI: 10.1016/S0926-860X(02)00326-5.

(453) van Donk, S.; Groot, F. M. F. de; Stéphan, O.; Bitter, J. H.; de Jong, K. P. Monitoring the Location, Amount, and Nature of Carbonaceous Deposits on Aged Zeolite Ferrierite Crystals by Using STEM-EELS. *Chem. Eur. J.* **2003**, *9*, 3106–3111. DOI: 10.1002/chem.200204685.

(454) Khitev, Y.; Ivanova, I. I.; Kolyagin, Y.; Ponomareva, O. A. Skeletal Isomerization of 1-Butene over Micro/mesoporous Materials Based on FER Zeolite. *Appl. Catal. A* **2012**, *441-442*, 124–135. DOI: 10.1016/j.apcata.2012.07.010.

(455) Weisz, P. B.; Frilette, V. J.; Maatman, R. W.; Mower, E. B. Catalysis by Crystalline Aluminosilicates II. Molecular-Shape Selective Reactions. *J. Catal.* **1962**, *1*, 307–312. DOI: 10.1016/0021-9517(62)90058-1.

(456) Galadima, A.; Muraza, O. Catalytic Upgrading of Vegetable Oils into Jet Fuels Range Hydrocarbons Using Heterogeneous Catalysts: A Review. *J. Ind. Eng. Chem.* **2015**, *29*, 12–23. DOI: 10.1016/j.jiec.2015.03.030.

(457) Inayat, A.; Inayat, A.; Schwieger, W.; Sokolova, B.; Lestinsky, P. Enhancing Aromatics and Olefins Yields in Thermo-Catalytic Pyrolysis of LDPE over Zeolites: Role of Staged Catalysis and Acid Site Density of HZSM-5. *Fuel* **2022**, *314*, 123071. DOI: 10.1016/j.fuel.2021.123071.

(458) Liu, S.; Kots, P. A.; Vance, B. C.; Danielson, A.; Vlachos, D. G. Plastic Waste to Fuels by Hydrocracking at Mild Conditions. *Sci. Adv.* **2021**, *7*. DOI: 10.1126/sciadv.abf8283.

(459) Jumah, A. b.; Tedstone, A. A.; Garforth, A. A. Hydrocracking of Virgin and Post-Consumer Polymers. *Microporous Mesoporous Mater.* **2021**, *315*, 110912. DOI: 10.1016/j.micromeso.2021.110912.

(460) Frash, M. V.; van Santen, R. A. Quantum-Chemical Modeling of the Hydrocarbon Transformations in Acid Zeolite Catalysts. *Top. Catal.* **1999**, *9*, 191–205. DOI: 10.1023/A:1019183110705.

(461) van der Mynsbrugge, J.; Janda, A.; Lin, L.-C.; van Speybroeck, V.; Head-Gordon, M.; Bell, A. T. Understanding Brønsted-Acid Catalyzed Monomolecular Reactions of Alkanes in Zeolite Pores by Combining Insights from Experiment and Theory. *ChemPhysChem* **2018**, *19*, 341–358. DOI: 10.1002/cphc.201701084.

(462) Kotrel, S.; Knözinger, H.; Gates, B. C. The Haag–Dessau Mechanism of Protolytic Cracking of Alkanes. *Microporous Mesoporous Mater.* **2000**, *35-36*, 11–20. DOI: 10.1016/S1387-1811(99)00204-8.

(463) Li, S.-C.; Lin, Y.-C.; Li, Y.-P. Understanding the Catalytic Activity of Microporous and Mesoporous Zeolites in Cracking by Experiments and Simulations. *Catalysts* **2021**, *11*, 1114. DOI: 10.3390/catal11091114.

(464) Haag, W. O.; Dessau, R. M. *Proc. 8th Int. Congress on Catalysis* **1984**, *2*, 305.

(465) McVicker, G. B.; Kramer, G. M.; Ziemiak, J. J. Conversion of Isobutane over Solid Acids—A Sensitive Mechanistic Probe Reaction. *J. Catal.* **1983**, *83*, 286–300. DOI: 10.1016/0021-9517(83)90055-6.

(466) Krannila, H.; Haag, W. O.; Gates, B. C. Monomolecular and Bimolecular Mechanisms of Paraffin Cracking: N-Butane Cracking Catalyzed by HZSM-5. *J. Catal.* **1992**, *135*, 115–124. DOI: 10.1016/0021-9517(92)90273-K.

(467) Narbeshuber, T. F.; Vinek, H.; Lercher, J. A. Monomolecular Conversion of Light Alkanes over H-ZSM-5. *J. Catal.* **1995**, *157*, 388–395.

(468) Gounder, R.; Iglesia, E. Effects of Partial Confinement on the Specificity of Monomolecular Alkane Reactions for Acid Sites in Side Pockets of Mordenite. *Angew. Chem. Int. Ed.* **2010**, *49*, 808–811. DOI: 10.1002/anie.200905869.

(469) Engelhardt, J.; Hall, W. K. Contribution to the Understanding of the Reaction Chemistry of Isobutane and Neopentane over Acid Catalysts. *J. Catal.* **1990**, *125*, 472–487.

(470) Gounder, R.; Iglesia, E. Catalytic Consequences of Spatial Constraints and Acid Site Location for Monomolecular Alkane Activation on Zeolites. *J. Am. Chem. Soc.* **2009**, *131*, 1958–1971. DOI: 10.1021/ja808292c.

(471) Xu, B.; Sievers, C.; Hong, S. B.; Prins, R.; van Bokhoven, J. A. Catalytic Activity of Brønsted Acid Sites in Zeolites: Intrinsic Activity, Rate-Limiting Step, and Influence of the Local Structure of the Acid Sites. *J. Catal.* **2006**, *244*, 163–168. DOI: 10.1016/j.jcat.2006.08.022.

(472) Janda, A.; Bell, A. T. Effects of Si/Al Ratio on the Distribution of Framework Al and on the Rates of Alkane Monomolecular Cracking and Dehydrogenation in H-MFI. *J. Am. Chem. Soc.* **2013**, *135*, 19193–19207. DOI: 10.1021/ja4081937.

(473) Narbeshuber, T. F.; Brait, A.; Seshan, K.; Lercher, J. A. The Influence of Extraframework Aluminum on H-FAU Catalyzed Cracking of Light Alkanes. *Appl. Catal. A* **1996**, *146*, 119–129.

(474) Li, H.; Kadam, S. A.; Vimont, A.; Wormsbecher, R. F.; Travert, A. Monomolecular Cracking Rates of Light Alkanes over Zeolites Determined by IR Operando Spectroscopy. *ACS Catal.* **2016**, *6*, 4536–4548. DOI: 10.1021/acscatal.6b01025.

(475) Pereira, M. M.; Santos, F. M.; Silva, A. V.; Batalha, N.; Ferreira da Silva, H. F. J.; Esteves, P. M.; Louis, B. Insights into the Role of Framework and Nonframework Aluminum in the Protolytic Reaction of Carbon–Carbon and Tertiary Carbon–Hydrogen Bonds of Isobutane. *J. Phys. Chem. C* **2021**, *125*, 11636–11647.

(476) Almutairi, S. M. T.; Mezari, B.; Filonenko, G. A.; Magusin, Pieter C. M. M.; Rigutto, M. S.; Pidko, E. A.; Hensen, E. J. M. Influence of Extraframework Aluminum on the Brønsted Acidity and Catalytic Reactivity of Faujasite Zeolite. *ChemCatChem* **2013**, *5*, 452–466. DOI: 10.1002/cctc.201200612.

(477) Kester, P. M.; Iglesia, E.; Gounder, R. Parallel Alkane Dehydrogenation Routes on Bronsted Acid and Reaction-Derived Carbonaceous Active Sites in Zeolites. *J. Phys. Chem. C* **2020**, *124*, 15839–15855. DOI: 10.1021/acs.jpcc.0c01808.

(478) Janda, A.; Vlaisavljevich, B.; Lin, L.-C.; Smit, B.; Bell, A. T. Effects of Zeolite Structural Confinement on Adsorption Thermodynamics and Reaction Kinetics for Monomolecular Cracking and Dehydrogenation of N-Butane. *J. Am. Chem. Soc.* **2016**, *138*, 4739–4756. DOI: 10.1021/jacs.5b11355.

(479) Mallikarjun Sharada, S.; Zimmerman, P. M.; Bell, A. T.; Head-Gordon, M. Insights into the Kinetics of Cracking and Dehydrogenation Reactions of Light Alkanes in H-MFI. *J. Phys. Chem. C* **2013**, *117*, 12600–12611. DOI: 10.1021/jp402506m.

(480) Zheng, X.; Blowers, P. Reactivity of Alkanes on Zeolites: A Computational Study of Propane Conversion Reactions. *J. Phys. Chem. A* **2005**, *109*, 10734–10741. DOI: 10.1021/jp054605z.

(481) Ding, B.-J.; Huang, S.-P.; Wang, W.-C. N-Butane Monomolecular Cracking on Acidic Zeolites: A Density Functional Study. *Chin. J. Chem.* **2008**, *26*, 1173–1180. DOI: 10.1002/cjoc.200890215.

(482) Furtado, E. A.; Milas, I.; Milam de Albuquerque Lins, J.O.; Chaer Nascimento, M. A. The Dehydrogenation Reaction of Light Alkanes Catalyzed by Zeolites. *Phys. Stat. Sol. (a)* **2001**, *187*, 275–288. DOI: 10.1002/1521-396X(200109)187:1<275:AID-PSSA275>3.0.CO;2-9.

(483) Bučko, T.; Benco, L.; Dubay, O.; Dellago, C.; Hafner, J. Mechanism of Alkane Dehydrogenation Catalyzed by Acidic Zeolites: Ab Initio Transition Path Sampling. *J. Chem. Phys.* **2009**, *131*, 214508. DOI: 10.1063/1.3265715.

(484) van der Mynsbrugge, J.; Janda, A.; Mallikarjun Sharada, S.; Lin, L.-C.; van Speybroeck, V.; Head-Gordon, M.; Bell, A. T. Theoretical Analysis of the Influence of Pore Geometry on Monomolecular Cracking and Dehydrogenation of N-Butane in Brønsted Acidic Zeolites. *ACS Catal.* **2017**, *7*, 2685–2697. DOI: 10.1021/acscatal.6b03646.

(485) Ivanova, I. I.; Pomakhina, E. B.; Rebrov, A. I.; Derouane, E. G. ^{13}C MAS NMR Mechanistic Study of the Initial Stages of Propane Activation over H-ZSM-5 Zeolite. *Top. Catal.* **1998**, *6*, 49–59.

(486) Swisher, J. A.; Hansen, N.; Maesen, T.; Keil, F. J.; Smit, B.; Bell, A. T. Theoretical Simulation of N-Alkane Cracking on Zeolites. *J. Phys. Chem. C* **2010**, *114*, 10229–10239. DOI: 10.1021/jp101262y.

(487) Bučko, T.; Benco, L.; Hafner, J.; Ángyán, J. G. Monomolecular Cracking of Propane over Acidic Chabazite: An Ab Initio Molecular Dynamics and Transition Path Sampling Study. *J. Catal.* **2011**, *279*, 220–228. DOI: 10.1016/j.jcat.2011.01.022.

(488) Collins, S. J.; Omalley, P. J. A Theoretical Description for the Monomolecular Cracking of C-C Bonds over Acidic Zeolites. *J. Catal.* **1995**, *153*, 94–99. DOI: 10.1006/jcat.1995.1111.

(489) Yang, C.-T.; Deng, X.; Lin, L.-C. In Silico Screening of Zeolites for the Highly Selective Adsorption of Central C–C Bonds Toward More Effective Alkane Cracking. *Ind. Eng. Chem. Res.* **2021**, *60*, 15174–15183. DOI: 10.1021/acs.iecr.1c03213.

(490) Narbeshuber, T. F.; Brait, A.; Seshan, K.; Lercher, J. A. Dehydrogenation of Light Alkanes over Zeolites. *J. Catal.* **1997**, *172*, 127–136. DOI: 10.1006/jcat.1997.1860.

(491) Babitz, S. M.; Williams, B. A.; Miller, J. T.; Snurr, R. Q.; Haag, W. O.; Kung, H. H. Monomolecular Cracking of N-Hexane on Y, MOR, and ZSM-5 Zeolites. *Appl. Catal. A* **1999**, *179*, 71–86.

(492) Williams, B.; Ji, W.; Miller, J.; Snurr, R.; Kung, H. Evidence of Different Reaction Mechanisms During the Cracking of N-Hexane on H-USY Zeolite. *Appl. Catal. A* **2000**, *203*, 179–190. DOI: 10.1016/S0926-860X(00)00495-6.

(493) Ramachandran, C.; Williams, B.; Van Bokhoven, J.; Miller, J. Observation of a Compensation Relation for N-Hexane Adsorption in Zeolites with Different Structures: Implications for Catalytic Activity. *J. Catal.* **2005**, *233*, 100–108. DOI: 10.1016/j.jcat.2005.04.017.

(494) van Bokhoven, J. A.; Williams, B. A.; Ji, W.; Koningsberger, D. C.; Kung, H. H.; Miller, J. T. Observation of a Compensation Relation for Monomolecular Alkane Cracking by Zeolites:

The Dominant Role of Reactant Sorption. *J. Catal.* **2004**, *224*, 50–59. DOI: 10.1016/j.jcat.2004.02.003.

(495) van Bokhoven, J.; Tromp, M.; Koningsberger, D.; Miller, J.; Pieterse, J.; Lercher, J. A.; Williams, B.; Kung, H. An Explanation for the Enhanced Activity for Light Alkane Conversion in Mildly Steam Dealuminated Mordenite: The Dominant Role of Adsorption. *J. Catal.* **2001**, *202*, 129–140. DOI: 10.1006/jcat.2001.3265.

(496) Xu, B.; Sievers, C.; Lercher, J. A.; van Veen, J. A. R.; Giltay, P.; Prins, R.; van Bokhoven, J. A. Strong Brønsted Acidity in Amorphous Silica−Aluminas. *J. Phys. Chem. C* **2007**, *111*, 12075–12079. DOI: 10.1021/jp073677i.

(497) Kadam, S. A.; Li, H.; Wormsbecher, R. F.; Travert, A. Impact of Zeolite Structure on Entropic-Enthalpic Contributions to Alkane Monomolecular Cracking: An IR Operando Study. *Chem. Eur. J.* **2018**, *24*, 5489–5492. DOI: 10.1002/chem.201800793.

(498) Bhan, A.; Gounder, R.; Macht, J.; Iglesia, E. Entropy Considerations in Monomolecular Cracking of Alkanes on Acidic Zeolites. *J. Catal.* **2008**, *253*, 221–224. DOI: 10.1016/j.jcat.2007.11.003.

(499) Fritz, P. O.; Lunsford, J. H. The Effect of Sodium Poisoning on Dealuminated Y-Type Zeolites. *J. Catal.* **1989**, *118*, 85–98.

(500) Miyaji, A.; Iwase, Y.; Nishitoba, T.; Long, N. Q.; Motokura, K.; Baba, T. Influence of Zeolite Pore Structure on Product Selectivities for Protolysis and Hydride Transfer Reactions in the Cracking of N-Pentane. *Phys. Chem. Chem. Phys.* **2015**, *17*, 5014–5032. DOI: 10.1039/c4cp04438j.

(501) Kester, P. M.; Crum, J. T.; Li, S.; Schneider, W. F.; Gounder, R. Effects of Brønsted Acid Site Proximity in Chabazite Zeolites on OH Infrared Spectra and Protolytic Propane Cracking Kinetics. *J. Catal.* **2021**, *395*, 210–226. DOI: 10.1016/j.jcat.2020.12.038.

(502) Song, C.; Chu, Y.; Wang, M.; Shi, H.; Li Zhao; Guo, X.; Yang, W.; Shen, J.; Xue, N.; Peng, L.*; et al.* Cooperativity of Adjacent Brønsted Acid Sites in MFI Zeolite Channel Leads to Enhanced Polarization and Cracking of Alkanes. *J. Catal.* **2017**, *349*, 163–174. DOI: 10.1016/j.jcat.2016.12.024.

(503) Chen, K.; Horstmeier, S.; Nguyen, V. T.; Wang, B.; Crossley, S. P.; Pham, T.; Gan, Z.; Hung, I.; White, J. L. Structure and Catalytic Characterization of a Second Framework Al(IV) Site in Zeolite Catalysts Revealed by NMR at 35.2 T. *J. Am. Chem. Soc.* **2020**, *142*, 7514–7523. DOI: 10.1021/jacs.0c00590.

(504) Tranca, D. C.; Hansen, N.; Swisher, J. A.; Smit, B.; Keil, F. J. Combined Density Functional Theory and Monte Carlo Analysis of Monomolecular Cracking of Light Alkanes over H-ZSM-5. *J. Phys. Chem. C* **2012**, *116*, 23408–23417. DOI: 10.1021/jp307558u.

(505) Janda, A.; Vlaisavljevich, B.; Lin, L.-C.; Mallikarjun Sharada, S.; Smit, B.; Head-Gordon, M.; Bell, A. T. Adsorption Thermodynamics and Intrinsic Activation Parameters for Monomolecular Cracking of N-Alkanes on Brønsted Acid Sites in Zeolites. *J. Phys. Chem. C* **2015**, *119*, 10427–10438. DOI: 10.1021/acs.jpcc.5b01715.

(506) Göltl, F.; Hafner, J. Modelling the Adsorption of Short Alkanes in Protonated Chabazite: The Impact of Dispersion Forces and Temperature. *Microporous Mesoporous Mater.* **2013**, *166*, 176–184. DOI: 10.1016/j.micromeso.2012.04.052.

(507) Piccini, G.; Alessio, M.; Sauer, J.; Zhi, Y.; Liu, Y.; Kolvenbach, R.; Jentys, A.; Lercher, J. A. Accurate Adsorption Thermodynamics of Small Alkanes in Zeolites. Ab Initio Theory and Experiment for H-Chabazite. *J. Phys. Chem. C* **2015**, *119*, 6128–6137. DOI: 10.1021/acs.jpcc.5b01739.

(508) Rocca, D.; Dixit, A.; Badawi, M.; Lebègue, S.; Gould, T.; Bučko, T. Bridging Molecular Dynamics and Correlated Wave-Function Methods for Accurate Finite-Temperature Properties. *Phys. Rev. Materials* **2019**, *3*. DOI: 10.1103/PhysRevMaterials.3.040801.

(509) Rehak, F. R.; Piccini, G.; Alessio, M.; Sauer, J. Including Dispersion in Density Functional Theory for Adsorption on Flat Oxide Surfaces, in Metal-Organic Frameworks and in Acidic Zeolites. *Phys. Chem. Chem. Phys.* **2020**, *22*, 7577–7585. DOI: 10.1039/d0cp00394h.

(510) Galimberti, D. R.; Sauer, J. Chemically Accurate Vibrational Free Energies of Adsorption from Density Functional Theory Molecular Dynamics: Alkanes in Zeolites. *J. Chem. Theory Comput.* **2021**, *17*, 5849–5862.

(511) Moor, B. A. de; Reyniers, M.-F.; Gobin, O. C.; Lercher, J. A.; Marin, G. B. Adsorption of C2−C8 N-Alkanes in Zeolites. *J. Phys. Chem. C* **2011**, *115*, 1204–1219. DOI: 10.1021/jp106536m.

(512) Li, Y.-P.; Gomes, J.; Mallikarjun Sharada, S.; Bell, A. T.; Head-Gordon, M. Improved Force-Field Parameters for QM/MM Simulations of the Energies of Adsorption for Molecules in Zeolites and a Free Rotor Correction to the Rigid Rotor Harmonic Oscillator Model for Adsorption Enthalpies. *J. Phys. Chem. C* **2015**, *119*, 1840–1850. DOI: 10.1021/jp509921r.

(513) Janda, A.; Lin, L.-C.; Vlaisavljevich, B.; van der Mynsbrugge, J.; Bell, A. T. Response to "Impact of Zeolite Structure on Entropic-Enthalpic Contributions to Alkane Monomolecular Cracking: An IR Operando Study". *Chem. Eur. J.* **2019**, *25*, 7225–7226. DOI: 10.1002/chem.201801785.

(514) Kadam, S. A. IR Operando Study of Alkane Monomolecular Cracking over Zeolites. PhD thesis, Université de Caen Normandie, 2016.

(515) Alaithan, Z. A.; Mallia, G.; Harrison, N. M. Monomolecular Cracking of Propane: Effect of Zeolite Confinement and Acidity. *ACS Omega* **2022**, *7*, 7531–7540. DOI: 10.1021/acsomega.1c05532.

(516) Savitz, S.; Siperstein, F.; Gorte, R. J.; Myers, A. L. Calorimetric Study of Adsorption of Alkanes in High-Silica Zeolites. *J. Phys. Chem. B* **1998**, *102*, 6865–6872. DOI: 10.1021/jp981836f.

(517) Yeh, Y.-H.; Gorte, R. J.; Rangarajan, S.; Mavrikakis, M. Adsorption of Small Alkanes on ZSM-5 Zeolites: Influence of Brønsted Sites. *J. Phys. Chem. C* **2016**, *120*, 12132–12138. DOI: 10.1021/acs.jpcc.6b03855.

(518) Katada, N.; Sota, S.; Morishita, N.; Okumura, K.; Niwa, M. Relationship Between Activation Energy and Pre-Exponential Factor Normalized by the Number of Brønsted Acid Sites in Cracking of Short Chain Alkanes on Zeolites. *Catal. Sci. Technol.* **2015**, *5*, 1864–1869. DOI: 10.1039/C4CY01483A.

(519) Yun, J. H.; Lobo, R. F. Effects of Temperature Pretreatment on Propane Cracking over H-SSZ-13 Zeolites. *Catal. Sci. Technol.* **2015**, *5*, 264–273. DOI: 10.1039/C4CY00731J.

(520) Xu, B.; Bordiga, S.; Prins, R.; van Bokhoven, J. A. Effect of Framework Si/Al Ratio and Extra-Framework Aluminum on the Catalytic Activity of Y Zeolite. *Appl. Catal. A* **2007**, *333*, 245–253. DOI: 10.1016/j.apcata.2007.09.018.

(521) Miale, J. N.; Chen, N. Y.; Weisz, P. B. Catalysis by Crystalline Aluminosilicates IV. Attainable Catalytic Cracking Rate Constants and Superactivity. *J. Catal.* **1966**, *6*, 278–287.

(522) Abbot, J.; Wojchiechowski, B. W. The Mechanism of Catalytic Cracking of N-alkenes on ZSM-5 Zeolite. *Can. J. Chem. Eng.* **1985**, *63*.

(523) Iwase, Y.; Sakamoto, Y.; Shiga, A.; Miyaji, A.; Motokura, K.; Koyama, T.; Baba, T. Shape-Selective Catalysis Determined by the Volume of a Zeolite Cavity and the Reaction Mechanism for Propylene Production by the Conversion of Butene Using a Proton-Exchanged Zeolite. *J. Phys. Chem. C* **2012**, *116*, 5182–5196. DOI: 10.1021/jp212549j.

(524) Corma, A.; Orchilles, A. V. Current Views on the Mechanism of Catalytic Cracking. *Microporous Mesoporous Mater.* **2000**, *35-36*, 21–30.

(525) Lonyi, F.; Lunsford, J. H. The Development of Strong Acidity in the Hexafluorosilicate-Modified Y-Type Zeolites. *J. Catal.* **1992**, *136*, 566–577.

(526) Lago, R. M.; Haag, W. O.; Mikovsky, R. J.; Olson, D. H.; Hellring, S. D.; Schmitt, K. D.; Kerr, G. T. The Nature of the Catalytic Sites in HZSM-5- Activity Enhancement. *Stud. Surf. Sci. Catal.* **1986**, *28*, 677–684. DOI: 10.1016/S0167-2991(09)60934-4.

(527) Wang, Q. L.; Giannetto, G.; Guisnet, M. Dealumination of Zeolites III. Effect of Extra-Framework Aluminum Species on the Activity, Selectivity, and Stability of Y Zeolites in N-Heptane Cracking. *J. Catal.* **1991**, *130*, 471–482. DOI: 10.1016/0021-9517(91)90129-R.

(528) Mullen, G. M.; Janik, M. J. Density Functional Theory Study of Alkane-Alkoxide Hydride Transfer in Zeolites. *ACS Catal.* **2011**, *1*, 105–115. DOI: 10.1021/cs1000619.

(529) Fu, J.; Feng, X.; Liu, Y.; Shan, H.; Yang, C. Mechanistic Insights into the Pore Confinement Effect on Bimolecular and Monomolecular Cracking Mechanisms of N -Octane over HY and HZSM-5 Zeolites: A DFT Study. *J. Phys. Chem. C* **2018**, *122*, 12222–12230. DOI: 10.1021/acs.jpcc.8b00995.

(530) Li, S.; Cao, J.; Dang, Y.; Feng, X.; Liu, Y.; Chen, X.; Yang, C. Understanding the Effect of Acid Strength on the Alkane-Alkoxide Hydride Transfer Reaction over Solid Acid Catalysts: Insights from Density Functional Theory. *Ind. Eng. Chem. Res.* **2019**, *58*, 9314–9321. DOI: 10.1021/acs.iecr.9b01125.

(531) Li, S.; Cao, J.; Liu, Y.; Feng, X.; Chen, X.; Yang, C. Effect of Acid Strength on the Formation Mechanism of Tertiary Butyl Carbocation in Initial C4 Alkylation Reaction over H-BEA Zeolite: A Density Functional Theory Study. *Catal. Today* **2020**, *355*, 171–179. DOI: 10.1016/j.cattod.2019.05.060.

(532) Boronat, M.; Viruela, P.; Corma, A. A Theoretical Study of the Mechanism of the Hydride Transfer Reaction Between Alkanes and Alkenes Catalyzed by an Acidic Zeolite. *J. Phys. Chem. A* **1998**, *102*, 9863–9868. DOI: 10.1021/jp981484c.

(533) Lukyanov, D. B. Reactivity of Propene, N-Butene, and Isobutene in the Hydrogen Transfer Steps of N-Hexane Cracking over Zeolites of Different Structure. *J. Catal.* **1994**, *147*, 494–499.

(534) Liu, C.; van Santen, R. A.; Poursaeidesfahani, A.; Vlugt, T. J. H.; Pidko, E. A.; Hensen, E. J. M. Hydride Transfer Versus Deprotonation Kinetics in the Isobutane-Propene Alkylation Reaction: A Computational Study. *ACS Catal.* **2017**, *7*, 8613–8627. DOI: 10.1021/acscatal.7b02877.

(535) Shertukde, P. V.; Marcelin, G.; Sill, G. A.; Hall, W. K. Study of the Mechanism of Cracking of Small Alkane Molecules on HY Zeolites. *J. Catal.* **1992**, *136*, 446–462.

(536) Corma, A.; Miguel, P. J.; Orchilles, A. V. The Role of Reaction Temperature and Cracking Catalyst Characteristics in Determining the Relative Rates of Protolytic Cracking, Chain Propagation and Hydrogen Transfer. *J. Catal.* **1994**, *145*, 171–180.

(537) Wielers, A. F. H.; Vaarkamp, M.; Post, M. F. M. Relation Between Properties and Performance of Zeolites in Paraffin Cracking. *J. Catal.* **1991**, *127*, 51–66.

(538) Corma, A.; Miguel, P. J.; Orchilles, A. V. Can Macroscopic Parameters, Such as Conversion and Selectivity, Distinguish Between Different Cracking Mechanisms on Acid Catalysts? *J. Catal.* **1997**, *172*, 355–369.

(539) Corma, A.; Orchilles, A. V. Formation of Products Responsible for Motor and Research Octane of Gasolines Produced by Cracking. *J. Catal.* **1989**, *115*, 551–566.

(540) Wang, P.; Wang, S.; Yue, Y.; Wang, T.; Bao, X. Effects of Acidity and Topology of Zeolites on the N-Alkane Conversion at Low Reaction Temperatures. *Microporous Mesoporous Mater.* **2020**, *292*, 109748. DOI: 10.1016/j.micromeso.2019.109748.

(541) Corma, A.; Faraldos, M.; Mifsud, A. Influence of the Level of Dealumination on the Selective Adsorption of Olefins and Paraffins and Its Implication on Hydrogen Transfer Reactions During Catalytic Cracking on USY Zeolites. *Appl. Catal.* **1989**, *47*, 125–133.

(542) Altwasser, S.; Welker, C.; Traa, Y.; Weitkamp, J. Catalytic Cracking of N-Octane on Small-Pore Zeolites. *Microporous Mesoporous Mater.* **2005**, *83*, 345–356. DOI: 10.1016/j.micromeso.2005.04.028.

(543) Koyama, T.; Hayashi, Y.; Horie, H.; Kawauchi, S.; Matsumoto, A.; Iwase, Y.; Sakamoto, Y.; Miyaji, A.; Motokura, K.; Baba, T. Key Role of the Pore Volume of Zeolite for Selective Production of Propylene from Olefins. *Phys. Chem. Chem. Phys.* **2010**, *12*, 2541–2554. DOI: 10.1039/b921927g.

(544) Gounder, R.; Jones, A. J.; Carr, R. T.; Iglesia, E. Solvation and Acid Strength Effects on Catalysis by Faujasite Zeolites. *J. Catal.* **2012**, *286*, 214–223. DOI: 10.1016/j.jcat.2011.11.002.

(545) Katada, N.; Kageyama, Y.; Takahara, K.; Kanai, T.; Ara Begum, H.; Niwa, M. Acidic Property of Modified Ultra Stable Y Zeolite: Increase in Catalytic Activity for Alkane Cracking by Treatment with Ethylenediaminetetraacetic Acid Salt. *J. Mol. Catal. A* **2004**, *211*, 119–130. DOI: 10.1016/j.molcata.2003.10.001.

(546) Niwa, M.; Suzuki, K.; Morishita, N.; Sastre, G.; Okumura, K.; Katada, N. Dependence of Cracking Activity on the Brønsted Acidity of Y Zeolite: DFT Study and Experimental Confirmation. *Catal. Sci. Technol.* **2013**, *3*, 1919–1927. DOI: 10.1039/C3CY00195D.

(547) Chapellière, Y.; Daniel, C.; Tuel, A.; Farrusseng, D.; Schuurman, Y. Kinetics of N-Hexane Cracking over Mesoporous HY Zeolites Based on Catalyst Descriptors. *Catalysts* **2021**, *11*, 652. DOI: 10.3390/catal11060652.

(548) Mirodatos, C.; Barthomeuf, D. Superacid Sites in Zeolites. *J. Chem. Soc., Chem. Commun.* **1981**, 39–40. DOI: 10.1039/C39810000039.

(549) Shertukde, P. V.; Hall, W. K.; Dereppe, J. M.; Marcelin, G. Acidity of H-Y Zeolites: Role of Extralattice Aluminum. *J. Catal.* **1993**, *139*, 468–481. DOI: 10.1006/jcat.1993.1041.

(550) Pham, T. N.; Nguyen, V.; Wang, B.; White, J. L.; Crossley, S. Quantifying the Influence of Water on the Mobility of Aluminum Species and Their Effects on Alkane Cracking in Zeolites. *ACS Catal.* **2021**, *11*, 6982–6994. DOI: 10.1021/acscatal.1c01138.

(551) Zhang, Y.; Zhao, R.; Sanchez-Sanchez, M.; Haller, G. L.; Hu, J.; Bermejo-Deval, R.; Liu, Y.; Lercher, J. A. Promotion of Protolytic Pentane Conversion on H-MFI Zeolite by Proximity of Extra-Framework Aluminum Oxide and Brønsted Acid Sites. *J. Catal.* **2019**, *370*, 424–433. DOI: 10.1016/j.jcat.2019.01.006.

(552) Schallmoser, S.; Ikuno, T.; Wagenhofer, M. F.; Kolvenbach, R.; Haller, G. L.; Sanchez-Sanchez, M.; Lercher, J. A. Impact of the Local Environment of Brønsted Acid Sites in ZSM-5 on the Catalytic Activity in N-Pentane Cracking. *J. Catal.* **2014**, *316*, 93–102. DOI: 10.1016/j.jcat.2014.05.004.

(553) Perego, C.; Pollesel, P. Advances in Aromatics Processing Using Zeolite Catalysts. In *Advances in nanoporous materials*; Ernst, S., Ed.; Advances in Nanoporous Materials; Elsevier, 2010; pp 97–149. DOI: 10.1016/S1878-7959(09)00102-9.

(554) Pitts, P. M.; Connor, J. E.; Leum, L. N. Isomerization of Alkyl Aromatic Hydrocarbons. *Ind. Eng. Chem.* **1955**, *47*, 770–773. DOI: 10.1021/ie50544a035.

(555) Gnep, N. S.; Guisnet, M. Ethylbenzene Isomerization over Platinum Deposited on Fluorinated Alumina Catalysts .1. Influence of Acidic and Metallic Function Upon Activity and Selectivity. *Bull. Soc. Chim. Fr.* **1977**, *5-6*, 429–434.

(556) Gnep, N. S.; Guisnet, M. Ethylbenzene Isomerization over Platinum Deposited on Fluorinated Alumina Catalysts .2. Kinetic Study. *Bull. Soc. Chim. Fr.* **1977**, *5-6*, 435–440.

(557) Moreau, F.; Bernard, S.; Gnep, N.; Lacombe, S.; Merlen, E.; Guisnet, M. Ethylbenzene Isomerization on Bifunctional Platinum Alumina–Mordenite Catalysts. *J. Catal.* **2001**, *202*, 402–412. DOI: 10.1006/jcat.2001.3294.

(558) Moreau, F.; Gnep, N. S.; Lacombe, S.; Merlen, E.; Guisnet, M. Ethylbenzene Isomerization on Bifunctional Platinum Alumina−Mordenite Catalysts. 2. Influence of the Pt Content and of the Relative Amounts of Platinum Alumina and Mordenite Components. *Ind. Eng. Chem. Res.* **2002**, *41*, 1469–1476. DOI: 10.1021/ie010505d.

(559) Guillon, E.; Lacombe, S.; Sozinho, T.; Magnoux, P.; Gnep, S.; Moreau, P.; Guisnet, M. How to Improve the Selectivity of Zeolitic Catalysts in C 8 Aromatic Cut Isomerization. *Oil & Gas Science Technol. - Rev. IFP* **2009**, *64*, 731–744. DOI: 10.2516/ogst/2009030.

(560) Fernandes, L. D.; Monteiro, J.; Sousa-Aguiar, E. F.; Martinez, A.; Corma, A. Ethylbenzene Hydroisomerization over Bifunctional Zeolite Based Catalysts: The Influence of Framework and Extraframework Composition and Zeolite Structure. *J. Catal.* **1998**, *177*, 363–377. DOI: 10.1006/jcat.1998.2111.

(561) Moreau, P. Isomérisation De L'ethylbenzène Sur Catalyseurs Bifonctionnels Pt/Zéolithe À Taille De Pores Intermédiaire. PhD thesis, University of Poitiers, 2005.

(562) Moreau, F.; Moreau, P.; Gnep, N. S.; Magnoux, P.; Lacombe, S.; Guisnet, M. Ethylbenzene Isomerization over Bifunctional Platinum Alumina–EUO Catalysts: Location of the Active Sites. *Microporous Mesoporous Mater.* **2006**, *90*, 327–338. DOI: 10.1016/j.micromeso.2005.08.032.

(563) Mota, F. M.; Eliášová, P.; Jung, J.; Ryoo, R. Mesoporous EU-1 Zeolite as a Highly Active Catalyst for Ethylbenzene Hydroisomerization. *Catal. Sci. Technol.* **2016**, *6*, 2735–2741. DOI: 10.1039/C5CY02027A.

(564) Guisnet, M.; Gnep, N. S.; Morin, S. Mechanisms of Xylene Isomerization over Acidic Solid Catalysts. *Microporous Mesoporous Mater.* **2000**, *35-36*, 47–59. DOI: 10.1016/S1387-1811(99)00207-3.

(565) Cortes, A.; Corma, A. The Mechanism of Catalytic Isomerization of Xylenes: Kinetic and Isotopic Studies. *J. Catal.* **1978**, *51*, 338–344. DOI: 10.1016/0021-9517(78)90271-3.

(566) Corma, A.; Sastre, E. Evidence for the Presence of a Bimolecular Pathway in the Isomerization of Xylene on Some Large-Pore Zeolites. *J. Catal.* **1991**, *129*, 177–185. DOI: 10.1016/0021-9517(91)90021-U.

(567) Morin, S.; Ayrault, P.; El Mouahid, S.; Gnep, N. S.; Guisnet, M. Particular Selectivity of M-Xylene Isomerization over MCM-41 Mesoporous Aluminosilicates. *Appl. Catal. A* **1997**, *159*, 317–331. DOI: 10.1016/S0926-860X(97)00057-4.

(568) Gnep, N. S.; Guisnet, M. Effect of Alkanes on the O-Xylene Transformation on Y Zeolite. *React. Kinet. Catal. Lett.* **1983**, *22*, 237–239. DOI: 10.1007/BF02064839.

(569) Morin, S.; Gnep, N. S.; Guisnet, M. A Simple Method for Determining the Relative Significance of the Unimolecular and Bimolecular Pathways of Xylene Isomerization over HY Zeolites. *J. Catal.* **1996**, *159*, 296–304. DOI: 10.1006/jcat.1996.0091.

(570) Min, H.-K.; Cha, S. H.; Hong, S. B. Mechanistic Insights into the Zeolite-Catalyzed Isomerization and Disproportionation of M -Xylene. *ACS Catal.* **2012**, *2*, 971–981. DOI: 10.1021/cs300127w.

(571) Gonçalves, J. C.; Ferreira, A. F. P.; Rodrigues, A. E. Minimum Cross Diameter for C 6 –C 10 Aromatic Compounds. *Chem. Eng. Technol.* **2019**, *42*, 1169–1173. DOI: 10.1002/ceat.201800406.

(572) Bauer, F.; Chen, W.-H.; Ernst, H.; Huang, S.-J.; Freyer, A.; Liu, S.-B. Selectivity Improvement in Xylene Isomerization. *Microporous Mesoporous Mater.* **2004**, *72*, 81–89. DOI: 10.1016/j.micromeso.2004.04.007.

(573) Silva, J. M.; Ribeiro, M. F.; Ramôa Ribeiro, F.; Benazzi, E.; Gnep, N. S.; Guisnet, M. Influence of the Treatment of Mordenite by Ammonium Hexafluorosilicate on Physicochemical and Catalytic Properties. *Zeolites* **1996**, *16*, 275–280. DOI: 10.1016/0144-2449(95)00138-7.

(574) Martens, J. A.; Perez-Pariente, J.; Sastre, E.; Corma, A.; Jacobs, P. A. Isomerization and Disproportionation of M-Xylene. *Appl. Catal.* **1988**, *45*, 85–101. DOI: 10.1016/S0166-9834(00)82395-7.

(575) Jones, C. W.; Zones, S. I.; Davis, M. E. M-Xylene Reactions over Zeolites with Unidimensional Pore Systems. *Appl. Catal. A* **1999**, *181*, 289–303. DOI: 10.1016/S0926-860X(98)00401-3.

(576) Byun, Y.; Jo, D.; Shin, D. N.; Hong, S. B. Theoretical Investigation of the Isomerization and Disproportionation of M-Xylene over Medium-Pore Zeolites with Different Framework Topologies. *ACS Catal.* **2014**, *4*, 1764–1776. DOI: 10.1021/cs500186y.

(577) Čejka, J.; Wichterlová, B. Acid-Catalyzed Synthesis of Mono- and Dialkyl Benzenes over Zeolites: Active Sites, Zeolite Topology, and Reaction Mechanisms. *Catal. Rev.* **2002**, *44*, 375–421. DOI: 10.1081/CR-120005741.

(578) Min, H.-K.; Chidambaram, V.; Hong, S. B. Diethylated Diphenylethane Species: Main Reaction Intermediates of Ethylbenzene Disproportionation over Large-Pore Zeolites. *J. Phys. Chem. C* **2010**, *114*, 1190–1193. DOI: 10.1021/jp9094408.

(579) Min, H.-K.; Hong, S. B. Mechanistic Investigations of Ethylbenzene Disproportionation over Medium-Pore Zeolites with Different Framework Topologies. *J. Phys. Chem. C* **2011**, *115*, 16124–16133. DOI: 10.1021/jp204945c.

(580) Cha, S. H.; Hong, S. B. Reaction Intermediates and Mechanism of the Zeolite-Catalyzed Transalkylation of 1,2,4-Trimethylbenzene with Toluene. *J. Catal.* **2018**, *357*, 1–11. DOI: 10.1016/j.jcat.2017.10.015.

(581) Huang, J.; Jiang, Y.; Marthala, V. R. R.; Ooi, Y. S.; Hunger, M. Regioselective H/D Exchange at the Side-Chain of Ethylbenzene on Dealuminated Zeolite H-Y Studied by in Situ MAS NMR-UV/Vis Spectroscopy. *ChemPhysChem* **2008**, *9*, 1107–1109. DOI: 10.1002/cphc.200800065.

(582) Rozanska, X.; van Santen, R. A.; Hutschka, F. A Periodic Density Functional Theory Study of Intermolecular Isomerization of Toluene and Benzene Catalyzed by Acidic Mordenite Zeolite: Effect of the Zeolite Steric Constraints. *J. Phys. Chem. B* **2002**, *106*, 4652–4657. DOI: 10.1021/jp014125h.

(583) Xiong, Y.; Rodewald, P. G.; Chang, C. D. On the Mechanism of Toluene Disproportionation in a Zeolite Environment. *J. Am. Chem. Soc.* **1995**, *117*, 9427–9431. DOI: 10.1021/ja00142a007.

(584) Svelle, S.; Olsbye, U.; Lillerud, K.-P.; Kolboe, S.; Bjørgen, M. Diphenylmethane-Mediated Transmethylation of Methylbenzenes over H-Zeolites. *J. Am. Chem. Soc.* **2006**, *128*, 5618–5619. DOI: 10.1021/ja060931w.

(585) Huang, J.; Jiang, Y.; Marthala, V. R. R.; Hunger, M. Insight into the Mechanisms of the Ethylbenzene Disproportionation: Transition State Shape Selectivity on Zeolites. *J. Am. Chem. Soc.* **2008**, *130*, 12642–12644. DOI: 10.1021/ja8042849.

(586) Foster, M. D.; Rivin, I.; Treacy, M.; Delgado Friedrichs, O. A Geometric Solution to the Largest-Free-Sphere Problem in Zeolite Frameworks. *Microporous Mesoporous Mater.* **2006**, *90*, 32–38. DOI: 10.1016/j.micromeso.2005.08.025.

(587) Willems, T. F.; Rycroft, C. H.; Kazi, M.; Meza, J. C.; Haranczyk, M. Algorithms and Tools for High-Throughput Geometry-Based Analysis of Crystalline Porous Materials. *Microporous Mesoporous Mater.* **2012**, *149*, 134–141. DOI: 10.1016/j.micromeso.2011.08.020.

(588) Clark, L. A.; Sierka, M.; Sauer, J. Computational Elucidation of the Transition State Shape Selectivity Phenomenon. *J. Am. Chem. Soc.* **2004**, *126*, 936–947. DOI: 10.1021/ja0381712.

(589) Degnan, T. F. The Implications of the Fundamentals of Shape Selectivity for the Development of Catalysts for the Petroleum and Petrochemical Industries. *J. Catal.* **2003**, *216*, 32–46. DOI: 10.1016/S0021-9517(02)00105-7.

(590) Venuto, P. B. Organic Catalysis over Zeolites: A Perspective on Reaction Paths Within Micropores. *Micropor. Mat.* **1994**, *2*, 297–411. DOI: 10.1016/0927-6513(94)00002-6.

(591) Moliner, M.; Martínez, C.; Corma, A. Multipore Zeolites: Synthesis and Catalytic Applications. *Angew. Chem., Int. Ed.* **2015**, *54*, 3560–3579. DOI: 10.1002/anie.201406344.

(592) Toda, J.; Corma, A.; Sastre, G. Diffusion of Trimethylbenzenes and Xylenes in Zeolites with 12- and 10-Ring Channels as Catalyst for Toluene-Trimethylbenzene Transalkylation. *J. Phys. Chem. C* **2016**, *120*, 16668–16680. DOI: 10.1021/acs.jpcc.6b03806.

(593) Toda, J.; Sastre, G. Diffusion of Trimethylbenzenes, Toluene, and Xylenes in UWY Zeolite as a Catalyst for Transalkylation of Trimethylbenzenes with Toluene. *J. Phys. Chem. C* **2018**, *122*, 7885–7897. DOI: 10.1021/acs.jpcc.7b10407.

(594) Dorset, D. L.; Kennedy, G. J.; Strohmaier, K. G.; Diaz-Cabañas, M. J.; Rey, F.; Corma, A. P-Derived Organic Cations as Structure-Directing Agents: Synthesis of a High-Silica Zeolite (ITQ-27) With a Two-Dimensional 12-Ring Channel System. *J. Am. Chem. Soc.* **2006**, *128*, 8862–8867. DOI: 10.1021/ja061206o.

(595) Tsai, T.-C.; Wang, I. Disproportionation Mechanism Study of Probing by N-Propylbenzene. *J. Catal.* **1992**, *133*, 136–145. DOI: 10.1016/0021-9517(92)90191-J.

(596) Corma, A.; Wojciechowski, B. W. The Chemistry of Catalytic Cracking. *Catal. Rev.* **1985**, *27*, 29–150. DOI: 10.1080/01614948509342358.

(597) Csicsery, S. The Reactions of 1-Methyl-2-Ethylbenzene II. A Test for Bifunctional Catalysts. *J. Catal.* **1988**, *110*, 348–353. DOI: 10.1016/0021-9517(88)90325-9.

(598) Al-Khattaf, S.; Tukur, N. M.; Rabiu, S. Ethylbenzene Transformation over a ZSM-5-Based Catalyst in a Riser Simulator. *Ind. Eng. Chem. Res.* **2009**, *48*, 2836–2843. DOI: 10.1021/ie801609x.

(599) Toch, K.; Thybaut, J. W.; Vandegehuchte, B. D.; Narasimhan, C.; Domokos, L.; Marin, G. B. A Single-Event MicroKinetic Model for "Ethylbenzene Dealkylation/xylene Isomerization" on Pt/H-ZSM-5 Zeolite Catalyst. *Appl. Catal. A* **2012**, *425-426*, 130–144. DOI: 10.1016/j.apcata.2012.03.011.

(600) Amelse, J. A. On the Mechanism for Ethyl Transfer and Removal from Ethylbenzene During Commercial Xylene Isomerization. *Microporous Mesoporous Mater.* **2019**, *278*, 275–279. DOI: 10.1016/j.micromeso.2018.12.005.

(601) Amelse, J. A. A Shape Selective Shift in the Mechanism of Transethylation and Its Effect on the Ability to Hydrodeethylate Ethylbenzene. *Stud. Surf. Sci. Catal.* **1987**, *38*, 165–176.

(602) Silva, J. M.; Ribeiro, M. F.; Ribeiro, F. R.; Benazzi, E.; Guisnet, M. Influence of Platinum on the Transformation of an Ethylbenzene-O-Xylene Mixture on H-ZSM-5. *Appl. Catal. A* **1995**, *125*, 1–14. DOI: 10.1016/0926-860X(94)00261-4.

(603) Silva, J. M.; Ribeiro, M. F.; Ribeiro, F. R.; Benazzi, E.; Guisnet, M. Transformation of an Ethylbenzene-O-Xylene Mixture on HMOR and Pt-HMOR Catalysts. Comparison with ZSM-5 Catalysts. *Appl. Catal. A* **1995**, *125*, 15–27. DOI: 10.1016/0926-860X(94)00259-2.

(604) Meyers, B. L.; Ely, S. R.; Kutz, N. A.; Kaduk, J. A.; van den Bossche, E. Determination of Structural Boron in Borosilicate Molecular Sieves via X-Ray Diffraction. *J. Catal.* **1985**, *91*, 352–355. DOI: 10.1016/0021-9517(85)90348-3.

(605) Serra, J. M.; Guillon, E.; Corma, A. A Rational Design of Alkyl-Aromatics Dealkylation–transalkylation Catalysts Using C8 and C9 Alkyl-Aromatics as Reactants. *J. Catal.* **2004**, *227*, 459–469. DOI: 10.1016/j.jcat.2004.08.006.

(606) Marques Mota, F.; Eliášová, P.; Jung, J.; Ryoo, R. Impact of Pore Topology and Crystal Thickness of Nanosponge Zeolites on the Hydroconversion of Ethylbenzene. *Catal. Sci. Technol.* **2016**, *6*, 2653–2662. DOI: 10.1039/C5CY02029H.

(607) Seo, Y.; Cho, K.; Jung, Y.; Ryoo, R. Characterization of the Surface Acidity of MFI Zeolite Nanosheets by ^{31}P NMR of Adsorbed Phosphine Oxides and Catalytic Cracking of Decalin. *ACS Catal.* **2013**, *3*, 713–720. DOI: 10.1021/cs300824e.

(608) Sullivan, R. F.; Egan, C. J.; Langlois, G. E.; Sieg, R. P. A New Reaction That Occurs in the Hydrocracking of Certain Aromatic Hydrocarbons. *J. Am. Chem. Soc.* **1961**, *83*, 1156–1160.

(609) Knözinger, H.; Bühl, H.; Kochloefl, K. The Dehydration of Alcohols on Alumina: XIV. Reactivity and Mechanism. *J. Catal.* **1972**, *24*, 57–68. DOI: 10.1016/0021-9517(72)90007-3.

(610) Knözinger, H. Dehydration of Alcohols on Aluminum Oxide. *Angew. Chem. Int. Ed.* **1968**, *7*, 791–805. DOI: 10.1002/anie.196807911.

(611) Phung, T. K.; Busca, G. Diethyl Ether Cracking and Ethanol Dehydration: Acid Catalysis and Reaction Paths. *Chem. Eng. J.* **2015**, *272*, 92–101. DOI: 10.1016/j.cej.2015.03.008.

(612) Phung, T. K.; Proietti Hernández, L.; Lagazzo, A.; Busca, G. Dehydration of Ethanol over Zeolites, Silica Alumina and Alumina: Lewis Acidity, Brønsted Acidity and Confinement Effects. *Appl. Catal. A* **2015**, *493*, 77–89. DOI: 10.1016/j.apcata.2014.12.047.

(613) Zhang, M.; Yu, Y. Dehydration of Ethanol to Ethylene. *Ind. Eng. Chem. Res.* **2013**, *52*, 9505–9514. DOI: 10.1021/ie401157c.

(614) Jamil, F.; Aslam, M.; Al-Muhtaseb, A. H.; Bokhari, A.; Rafiq, S.; Khan, Z.; Inayat, A.; Ahmed, A.; Hossain, S.; Khurram, M. S.*; et al.* Greener and Sustainable Production of Bioethylene from Bioethanol: Current Status, Opportunities and Perspectives. *Rev. Chem. Eng.* **2022**, *38*, 185–207. DOI: 10.1515/revce-2019-0026.

(615) Lauron-Pernot, H. Evaluation of Surface Acido-Basic Properties of Inorganic-Based Solids by Model Catalytic Alcohol Reaction Networks. *Catal. Rev.* **2006**, *48*, 315–361. DOI: 10.1080/01614940600816634.

(616) Weisz, P. B.; Frilette, V. J. Intracrystalline and Molecular-Shape Selective Catalysis by Zeolite Salts. *J. Phys. Chem.* **1960**, *64*, 382. DOI: 10.1021/j100832a513.

(617) Williams, C.; Makarova, M. A.; Malysheva, L. V.; Paukshtis, E. A.; Zamaraev, K. I.; Thomas, J. M. Mechanistic Studies of the Catalytic Dehydration of Isobutyl Alcohol on NaH-ZSM-5. *J. Chem. Soc. Faraday Trans.* **1990**, *86*, 3473–3485. DOI: 10.1039/FT9908603473.

(618) Xin, H.; Li, X.; Fang, Y.; Yi, X.; Hu, W.; Chu, Y.; Zhang, F.; Zheng, A.; Zhang, H.; Li, X. Catalytic Dehydration of Ethanol over Post-Treated ZSM-5 Zeolites. *J. Catal.* **2014**, *312*, 204–215. DOI: 10.1016/j.jcat.2014.02.003.

(619) Takahara, I.; Saito, M.; Inaba, M.; Murata, K. Dehydration of Ethanol into Ethylene over Solid Acid Catalysts. *Catal. Lett.* **2005**, *105*, 249–252. DOI: 10.1007/s10562-005-8698-1.

(620) Makarova, M. A.; Williams, C.; Romannikov, V. N.; Zamaraev, K. I.; Thomas, J. M. Influence of Pore Confinement on the Catalytic Dehydration of Isobutyl Alcohol on H-ZSM-5. *J. Chem. Soc. Faraday Trans.* **1990**, *86*, 581–584. DOI: 10.1039/FT9908600581.

(621) Wang, Z.; O'Dell, L. A.; Zeng, X.; Liu, C.; Zhao, S.; Zhang, W.; Gaborieau, M.; Jiang, Y.; Huang, J. Insight into Three-Coordinate Aluminum Species on Ethanol-to-Olefin Conversion over ZSM-5 Zeolites. *Angew. Chem., Int. Ed.* **2019**, *58*, 18061–18068. DOI: 10.1002/anie.201910987.

(622) Zhao, S.; Yang, W.; Kim, K. D.; Wang, L.; Wang, Z.; Ryoo, R.; Huang, J. Synergy of Extraframework Al 3+ Cations and Brønsted Acid Sites on Hierarchical ZSM-5 Zeolites for Butanol-to-Olefin Conversion. *J. Phys. Chem. C* **2021**, *125*, 11665–11676. DOI: 10.1021/acs.jpcc.1c02171.

(623) Larmier, K.; Chizallet, C.; Maury, S.; Cadran, N.; Abboud, J.; Lamic-Humblot, A.-F.; Marceau, E.; Lauron-Pernot, H. Isopropanol Dehydration on Amorphous Silica–Alumina: Synergy of Brønsted and Lewis Acidities at Pseudo-Bridging Silanols. *Angew. Chem., Int. Ed.* **2017**, *56*, 230–234. DOI: 10.1002/anie.201609494.

(624) van Daele, S.; Minoux, D.; Nesterenko, N.; Maury, S.; Coupard, V.; Valtchev, V.; Travert, A.; Gilson, J.-P. A Highly Selective FER-Based Catalyst to Produce N-Butenes from Isobutanol. *Appl. Catal. B* **2021**, *284*, 119699. DOI: 10.1016/j.apcatb.2020.119699.

(625) Buniazet, Z.; Cabiac, A.; Maury, S.; Bianchi, D.; Loridant, S. Unexpected Selectivity of Ferrierite for the Conversion of Isobutanol to Linear Butenes and Water Effects. *Appl. Catal. B* **2019**, *243*, 594–603. DOI: 10.1016/j.apcatb.2018.11.007.

(626) Huber, P.; Studt, F.; Plessow, P. N. Reactivity of Surface Lewis and Brønsted Acid Sites in Zeolite Catalysis: A Computational Case Study of DME Synthesis Using H-SSZ-13. *J. Phys. Chem. C* **2022**, *126*, 5896–5905. DOI: 10.1021/acs.jpcc.2c00668.

(627) Haase, F.; Sauer, J. Interaction of Methanol with Broensted Acid Sites of Zeolite Catalysts: An Ab Initio Study. *J. Am. Chem. Soc.* **1995**, *117*, 3780–3789. DOI: 10.1021/ja00118a014.

(628) Luz, Z.; Vega, A. J. Interaction of H-Rho Zeolite with Water and Methanol Studied by Multinuclear NMR Spectroscopy. *J. Phys. Chem.* **1987**, *91*, 374–382. DOI: 10.1021/j100286a026.

(629) Haase, F.; Sauer, J.; Hutter, J. Ab Initio Molecular Dynamics Simulation of Methanol Adsorbed in Chabazite. *Chem. Phys. Lett.* **1997**, *266*, 397–402. DOI: 10.1016/S0009-2614(97)00006-7.

(630) Haase, F.; Sauer, J. Ab Initio Molecular Dynamics Simulation of Methanol Interacting with Acidic Zeolites of Different Framework Structure. *Microporous Mesoporous Mater.* **2000**, *35-36*, 379–385. DOI: 10.1016/S1387-1811(99)00235-8.

(631) Costa, R. J.; Castro, E. A. S.; Politi, J. R. S.; Gargano, R.; Martins, J. B. L. Methanol, Ethanol, Propanol, and Butanol Adsorption on H-ZSM-5 Zeolite: An ONIOM Study. *J. Mol. Model.* **2019**, *25*, 34. DOI: 10.1007/s00894-018-3894-2.

(632) John, M.; Alexopoulos, K.; Reyniers, M.-F.; Marin, G. B. Reaction Path Analysis for 1-Butanol Dehydration in H-ZSM-5 Zeolite: Ab Initio and Microkinetic Modeling. *J. Catal.* **2015**, *330*, 28–45. DOI: 10.1016/j.jcat.2015.07.005.

(633) Stückenschneider, K.; Merz, J.; Schembecker, G. Molecular Interactions of Alcohols with Zeolite BEA and MOR Frameworks. *J. Mol. Model.* **2013**, *19*, 5611–5624. DOI: 10.1007/s00894-013-2048-9.

(634) Nguyen, C. M.; Reyniers, M.-F.; Marin, G. B. Theoretical Study of the Adsorption of C1–C4 Primary Alcohols in H-ZSM-5. *Phys. Chem. Chem. Phys.* **2010**, *12*, 9481. DOI: 10.1039/c000503g.

(635) Nguyen, C. M.; Reyniers, M.-F.; Marin, G. B. Theoretical Study of the Adsorption of the Butanol Isomers in H-ZSM-5. *J. Phys. Chem. C* **2011**, *115*, 8658–8669. DOI: 10.1021/jp111698b.

(636) Nguyen, C. M.; Reyniers, M.-F.; Marin, G. B. Adsorption Thermodynamics of C1–C4 Alcohols in H-FAU, H-MOR, H-ZSM-5, and H-ZSM-22. *J. Catal.* **2015**, *322*, 91–103. DOI: 10.1016/j.jcat.2014.11.013.

(637) Svelle, S.; Tuma, C.; Rozanska, X.; Kerber, T.; Sauer, J. Quantum Chemical Modeling of Zeolite-Catalyzed Methylation Reactions: Toward Chemical Accuracy for Barriers. *J. Am. Chem. Soc.* **2009**, *131*, 816–825. DOI: 10.1021/ja807695p.

(638) Shah, R.; Gale, J. D.; Payne, M. C. Methanol Adsorption in Zeolites: A First-Principles Study. *J. Phys. Chem.* **1996**, *100*, 11688–11697. DOI: 10.1021/jp960365z.

(639) Piccini, G.; Alessio, M.; Sauer, J. Ab Initio Study of Methanol and Ethanol Adsorption on Brønsted Sites in Zeolite H-MFI. *Phys. Chem. Chem. Phys.* **2018**, *20*, 19964–19970. DOI: 10.1039/c8cp03632b.

(640) van der Mynsbrugge, J.; Hemelsoet, K.; Vandichel, M.; Waroquier, M.; van Speybroeck, V. Efficient Approach for the Computational Study of Alcohol and Nitrile Adsorption in H-ZSM-5. *J. Phys. Chem. C* **2012**, *116*, 5499–5508. DOI: 10.1021/jp2123828.

(641) Stich, I.; Gale, J. D.; Terakura, K.; Payne, M. C. Dynamical Observation of the Catalytic Activation of Methanol in Zeolites. *Chem. Phys. Lett.* **1998**, *283*, 402–408. DOI: 10.1016/S0009-2614(97)01398-5.

(642) Alexopoulos, K.; Lee, M.-S.; Liu, Y.; Zhi, Y.; Liu, Y.; Reyniers, M.-F.; Marin, G. B.; Glezakou, V.-A.; Rousseau, R.; Lercher, J. A. Anharmonicity and Confinement in Zeolites: Structure, Spectroscopy, and Adsorption Free Energy of Ethanol in H-ZSM-5. *J. Phys. Chem. C* **2016**, *120*, 7172–7182.

(643) Zhi, Y.; Shi, H.; Mu, L.; Liu, Y.; Mei, D.; Camaioni, D. M.; Lercher, J. A. Dehydration Pathways of 1-Propanol on HZSM-5 in the Presence and Absence of Water. *J. Am. Chem. Soc.* **2015**, *137*, 15781–15794. DOI: 10.1021/jacs.5b09107.

(644) Di Iorio, J. R.; Hoffman, A. J.; Nimlos, C. T.; Nystrom, S.; Hibbitts, D.; Gounder, R. Mechanistic Origins of the High-Pressure Inhibition of Methanol Dehydration Rates in Small-Pore Acidic Zeolites. *J. Catal.* **2019**, *380*, 161–177. DOI: 10.1016/j.jcat.2019.10.012.

(645) Nastase, S. A. F.; Cnudde, P.; Vanduyfhuys, L.; Wispelaere, K. de; van Speybroeck, V.; Catlow, C. R. A.; Logsdail, A. J. Mechanistic Insight into the Framework Methylation of H-ZSM-5 for Varying Methanol Loadings and Si/Al Ratios Using First-Principles Molecular Dynamics Simulations. *ACS Catal.* **2020**, *10*, 8904–8915. DOI: 10.1021/acscatal.0c01454.

(646) Zecchina, A.; Bordiga, S.; Spoto, G.; Scarano, D.; Spanò, G.; Geobaldo, F. IR Spectroscopy of Neutral and Ionic Hydrogen-Bonded Complexes Formed Upon Interaction of

CH_3OH, C_2H_5OH, $(CH_3)_2O$, $(C_2H_5)_2O$ and C_4H_8O with H-Y, H-ZSM-5 and H-Mordenite: Comparison with Analogous Adducts Formed on the H-Nafion Superacidic Membrane. *J. Chem. Soc. Faraday Trans.* **1996**, *92*, 4863–4875. DOI: 10.1039/FT9969204863.

(647) Kadam, S. A.; Shamzhy, M. V. IR Operando Study of Ethanol Dehydration over MFI Zeolites: Structure–Activity Relationships. *J. Phys. Chem. C* **2018**, *122*, 24055–24067. DOI: 10.1021/acs.jpcc.8b05697.

(648) Carey F. A.; Sundberg R.J. *Advanced organic chemistry. Part. A, structure and mechanisms*, 3rd ed.; Plenum press, Cop. 1990.

(649) Aronson, M. T.; Gorte, R. J.; Farneth, W. E.; White, D. Carbon-13 NMR Identification of Intermediates Formed by 2-Methyl-2-Propanol Adsorption in H-ZSM-5. *J. Am. Chem. Soc.* **1989**, *111*, 840–846. DOI: 10.1021/ja00185a009.

(650) Wang, W.; Seiler, M.; Hunger, M. Role of Surface Methoxy Species in the Conversion of Methanol to Dimethyl Ether on Acidic Zeolites Investigated by in Situ Stopped-Flow MAS NMR Spectroscopy. *J. Phys. Chem. B* **2001**, *105*, 12553–12558. DOI: 10.1021/jp0129784.

(651) Wang, W.; Buchholz, A.; Seiler, M.; Hunger, M. Evidence for an Initiation of the Methanol-to-Olefin Process by Reactive Surface Methoxy Groups on Acidic Zeolite Catalysts. *J. Am. Chem. Soc.* **2003**, *125*, 15260–15267. DOI: 10.1021/ja0304244.

(652) Kondo, J. N.; Ito, K.; Yoda, E.; Wakabayashi, F.; Domen, K. An Ethoxy Intermediate in Ethanol Dehydration on Brønsted Acid Sites in Zeolite. *J. Phys. Chem. B* **2005**, *109*, 10969–10972. DOI: 10.1021/jp050721q.

(653) Makarova, M. A.; Paukshtis, E. A.; Thomas, J. M.; Williams, C.; Zamaraev, K. I. Dehydration of N-Butanol on Zeolite H-ZSM-5 and Amorphous Aluminosilicate: Detailed Mechanistic Study and the Effect of Pore Confinement. *J. Catal.* **1994**, *149*, 36–51. DOI: 10.1006/jcat.1994.1270.

(654) Kondo, J. N.; Nishioka, D.; Yamazaki, H.; Kubota, J.; Domen, K.; Tatsumi, T. Activation Energies for the Reaction of Ethoxy Species to Ethene over Zeolites. *J. Phys. Chem. C* **2010**, *114*, 20107–20113. DOI: 10.1021/jp107082t.

(655) Fečík, M.; Plessow, P. N.; Studt, F. Simple Scheme to Predict Transition-State Energies of Dehydration Reactions in Zeolites with Relevance to Biomass Conversion. *J. Phys. Chem. C* **2018**, *122*, 23062–23067. DOI: 10.1021/acs.jpcc.8b07659.

(656) Fečík, M.; Plessow, P. N.; Studt, F. Influence of Confinement on Barriers for Alkoxide Formation in Acidic Zeolites. *ChemCatChem* **2021**, *13*, 2451–2458. DOI: 10.1002/cctc.202100009.

(657) Konda, S. S. M.; Caratzoulas, S.; Vlachos, D. G. Computational Insights into the Role of Metal and Acid Sites in Bifunctional Metal/Zeolite Catalysts: A Case Study of Acetone Hydrogenation to 2-Propanol and Subsequent Dehydration to Propene. *ACS Catal.* **2016**, *6*, 123–133. DOI: 10.1021/acscatal.5b01686.

(658) Kunz, L. Y.; Bu, L.; Knott, B. C.; Liu, C.; Nimlos, M. R.; Assary, R. S.; Curtiss, L. A.; Robichaud, D. J.; Kim, S. Theoretical Determination of Size Effects in Zeolite-Catalyzed Alcohol Dehydration. *Catalysts* **2019**, *9*, 700. DOI: 10.3390/catal9090700.

(659) Kim, S.; Robichaud, D. J.; Beckham, G. T.; Paton, R. S.; Nimlos, M. R. Ethanol Dehydration in HZSM-5 Studied by Density Functional Theory: Evidence for a Concerted Process. *J. Phys. Chem. A* **2015**, *119*, 3604–3614. DOI: 10.1021/jp513024z.

(660) Alexopoulos, K.; John, M.; van der Borght, K.; Galvita, V.; Reyniers, M.-F.; Marin, G. B. DFT-Based Microkinetic Modeling of Ethanol Dehydration in H-ZSM-5. *J. Catal.* **2016**, *339*, 173–185. DOI: 10.1016/j.jcat.2016.04.020.

(661) Mei, D.; Lercher, J. A. Mechanistic Insights into Aqueous Phase Propanol Dehydration in H-ZSM-5 Zeolite. *AIChE J.* **2017**, *63*, 172–184. DOI: 10.1002/aic.15517.

(662) Maeboonruan, N.; Boekfa, B.; Maihom, T.; Treesukol, P.; Kongpatpanich, K.; Namuangruk, S.; Probst, M.; Limtrakul, J. Adsorption and Dehydration of Ethanol on Isomorphously B, Al, and Ga Substituted H-ZSM-5 Zeolite: An Embedded ONIOM Study. *J. Mol. Model.* **2021**, *27*, 354. DOI: 10.1007/s00894-021-04979-8.

(663) Xia, H. Monomolecular Dehydration of Ethanol into Ethylene over H-MOR Studied by Density Functional Theory. *ACS Omega* **2020**, *5*, 9707–9713. DOI: 10.1021/acsomega.9b03984.

(664) John, M.; Alexopoulos, K.; Reyniers, M.-F.; Marin, G. B. First-Principles Kinetic Study on the Effect of the Zeolite Framework on 1-Butanol Dehydration. *ACS Catal.* **2016**, *6*, 4081–4094. DOI: 10.1021/acscatal.6b00708.

(665) John, M.; Alexopoulos, K.; Reyniers, M.-F.; Marin, G. B. Effect of Zeolite Confinement on the Conversion of 1-Butanol to Butene Isomers: Mechanistic Insights from DFT Based Microkinetic Modelling. *Catal. Sci. Technol.* **2017**, *7*, 2978–2997. DOI: 10.1039/C7CY00536A.

(666) John, M.; Alexopoulos, K.; Reyniers, M.-F.; Marin, G. B. Mechanistic Insights into the Formation of Butene Isomers from 1-Butanol in H-ZSM-5: DFT Based Microkinetic Modelling. *Catal. Sci. Technol.* **2017**, *7*, 1055–1072. DOI: 10.1039/C6CY02474B.

(667) Gešvandtnerová, M.; Bučko T.; Raybaud, P.; Chizallet, C. Monomolecular Mechanisms of Isobutanol Conversion to Butenes Catalyzed by Acidic Zeolites: Alcohol Isomerization as a Key to the Production of Linear Butenes. *J. Catal.* **2022**, *413*, 786–802. DOI: 10.1016/j.jcat.2022.07.025.

(668) Milakovic, L.; Hintermeier, P. H.; Liu, Q.; Shi, H.; Liu, Y.; Baráth, E.; Lercher, J. A. Towards Understanding and Predicting the Hydronium Ion Catalyzed Dehydration of Cyclic-Primary, Secondary and Tertiary Alcohols. *J. Catal.* **2020**, *390*, 237–243. DOI: 10.1016/j.jcat.2020.08.009.

(669) Hintermeier, P. H.; Eckstein, S.; Mei, D.; Olarte, M. V.; Camaioni, D. M.; Baráth, E.; Lercher, J. A. Hydronium-Ion-Catalyzed Elimination Pathways of Substituted Cyclohexanols in Zeolite H-ZSM5. *ACS Catal.* **2017**, *7*, 7822–7829. DOI: 10.1021/acscatal.7b01582.

(670) Liu, Y.; Vjunov, A.; Shi, H.; Eckstein, S.; Camaioni, D. M.; Mei, D.; Baráth, E.; Lercher, J. A. Enhancing the Catalytic Activity of Hydronium Ions Through Constrained Environments. *Nat. Commun.* **2017**, *8*, 14113. DOI: 10.1038/ncomms14113.

(671) Vjunov, A.; Hu, M. Y.; Feng, J.; Camaioni, D. M.; Mei, D.; Hu, J. Z.; Zhao, C.; Lercher, J. A. Following Solid-Acid-Catalyzed Reactions by MAS NMR Spectroscopy in Liquid Phase--Zeolite-Catalyzed Conversion of Cyclohexanol in Water. *Angew. Chem., Int. Ed.* **2014**, *53*, 479–482. DOI: 10.1002/anie.201306673.

(672) Shi, H.; Eckstein, S.; Vjunov, A.; Camaioni, D. M.; Lercher, J. A. Tailoring Nanoscopic Confines to Maximize Catalytic Activity of Hydronium Ions. *Nat. Commun.* **2017**, *8*, 15442. DOI: 10.1038/ncomms15442.

(673) Chen, F.; Shetty, M.; Wang, M.; Shi, H.; Liu, Y.; Camaioni, D. M.; Gutiérrez, O. Y.; Lercher, J. A. Differences in Mechanism and Rate of Zeolite-Catalyzed Cyclohexanol Dehydration in Apolar and Aqueous Phase. *ACS Catal.* **2021**, *11*, 2879–2888. DOI: 10.1021/acscatal.0c05674.

(674) Chiang, H.; Bhan, A. Catalytic Consequences of Hydroxyl Group Location on the Rate and Mechanism of Parallel Dehydration Reactions of Ethanol over Acidic Zeolites. *J. Catal.* **2010**, *271*, 251–261. DOI: 10.1016/j.jcat.2010.01.021.

(675) las Pozas, C. de; Lopez-Cordero, R.; Gonzalez-Morales, J. A.; Travieso, N.; Roque-Malherbe, R. Effect of Pore Diameter and Acid Strength in Ethanol Dehydration on Molecular Sieves. *J. Mol. Catal.* **1993**, *83*, 145–156. DOI: 10.1016/0304-5102(93)87015-Z.

(676) Reviere, A. de; Gunst, D.; Sabbe, M. K.; Reyniers, M.-F.; an Verberckmoes. Dehydration of Butanol Towards Butenes over MFI, FAU and MOR: Influence of Zeolite Topology. *Catal. Sci. Technol.* **2021**, *11*, 2540–2559. DOI: 10.1039/D0CY02366C.

(677) Blaszkowski, S. R.; van Santen, R. A. The Mechanism of Dimethyl Ether Formation from Methanol Catalyzed by Zeolitic Protons. *J. Am. Chem. Soc.* **1996**, *118*, 5152–5153.

(678) Blaszkowski, S. R.; van Santen, R. A. Theoretical Study of the Mechanism of Surface Methoxy and Dimethyl Ether Formation from Methanol Catalyzed by Zeolitic Protons. *J. Phys. Chem. B* **1997**, *101*, 2292–2305. DOI: 10.1021/jp962006+.

(679) Botchway, C. H.; Tia, R.; Adei, E.; Dzade, N. Y.; Leeuw, N. H. de. H-FER-Catalyzed Conversion of Methanol to Ethanol and Dimethyl Ether: A First-Principles DFT Study. *S. Afr. J. Chem.* **2021**, *74*. DOI: 10.17159/0379-4350/2021/v74a6.

(680) Ghorbanpour, A.; Rimer, J. D.; Grabow, L. C. Computational Assessment of the Dominant Factors Governing the Mechanism of Methanol Dehydration over H-ZSM-5 with Heterogeneous Aluminum Distribution. *ACS Catal.* **2016**, *6*, 2287–2298. DOI: 10.1021/acscatal.5b02367.

(681) Moses, P. G.; Nørskov, J. K. Methanol to Dimethyl Ether over ZSM-22: A Periodic Density Functional Theory Study. *ACS Catal.* **2013**, *3*, 735–745. DOI: 10.1021/cs300722w.

(682) Carr, R. T.; Neurock, M.; Iglesia, E. Catalytic Consequences of Acid Strength in the Conversion of Methanol to Dimethyl Ether. *J. Catal.* **2011**, *278*, 78–93. DOI: 10.1016/j.jcat.2010.11.017.

(683) Jones, A. J.; Iglesia, E. Kinetic, Spectroscopic, and Theoretical Assessment of Associative and Dissociative Methanol Dehydration Routes in Zeolites. *Angew. Chem., Int. Ed.* **2014**, *53*, 12177–12181. DOI: 10.1002/anie.201406823.

(684) Batchu, R.; Galvita, V. V.; Alexopoulos, K.; Glazneva, T. S.; Poelman, H.; Reyniers, M.-F.; Marin, G. B. Ethanol Dehydration Pathways in H-ZSM-5: Insights from Temporal Analysis of Products. *Catal. Today* **2020**, *355*, 822–831. DOI: 10.1016/j.cattod.2019.04.018.

(685) Di Iorio, J. R.; Nimlos, C. T.; Gounder, R. Introducing Catalytic Diversity into Single-Site Chabazite Zeolites of Fixed Composition via Synthetic Control of Active Site Proximity. *ACS Catal.* **2017**, *7*, 6663–6674. DOI: 10.1021/acscatal.7b01273.

(686) Gołąbek, K.; Tabor, E.; Pashkova, V.; Dedecek, J.; Tarach, K.; Góra-Marek, K. The Proximity of Aluminium Atoms Influences the Reaction Pathway of Ethanol Transformation over Zeolite ZSM-5. *Commun. Chem.* **2020**, *3*. DOI: 10.1038/s42004-020-0268-3.

(687) Jones, A. J.; Zones, S. I.; Iglesia, E. Implications of Transition State Confinement Within Small Voids for Acid Catalysis. *J. Phys. Chem. C* **2014**, *118*, 17787–17800. DOI: 10.1021/jp5050095.

(688) Zhou, X.; Wang, C.; Chu, Y.; Xu, J.; Wang, Q.; Qi, G.; Zhao, X.; Feng, N.; Deng, F. Observation of an Oxonium Ion Intermediate in Ethanol Dehydration to Ethene on Zeolite. *Nat. Commun.* **2019**, *10*, 1961. DOI: 10.1038/s41467-019-09956-7.

(689) Munson, E. J.; Haw, J. F. NMR Observation of Trimethyloxonium Formation from Dimethyl Ether on Zeolite HZSM-5. *J. Am. Chem. Soc.* **1991**, *113*, 6303–6305. DOI: 10.1021/ja00016a075.

(690) Whitmore, F. C. The Common Basis of Intramolecular Rearrangements. *J. Am. Chem. Soc.* **1932**, *54*, 3274–3283. DOI: 10.1021/ja01347a037.

(691) Taylor, J. D.; Jenni, M. M.; Peters, M. W. Dehydration of Fermented Isobutanol for the Production of Renewable Chemicals and Fuels. *Top. Catal.* **2010**, *53*, 1224–1230. DOI: 10.1007/s11244-010-9567-8.

(692) Liu, W.; Hu, H.; Liu, Y.; Zhang, L.; Xia, C.; Wang, Q.; Ke, M. Distribution of Effective Ferrierite Active Sites for Skeletal Isomerization of N -Butene to Isobutene. *ChemistrySelect* **2019**, *4*, 7851–7857. DOI: 10.1002/slct.201901495.

(693) Meriaudeau, P.; Tuan, V. A.; Le, N. H.; Szabo, G. Selective Isomerization of N-Butene into Isobutene over Deactivated H–Ferrierite Catalyst: Further Investigations. *J. Catal.* **1997**, *169*, 397–399.

(694) Kotsarenko, N. S., Malysheva, L. V. Influence of the Chemical Composition of Oxide Catalysts on the Rate of Dehydration of Isobutanol and the Composition of the Products Formed. *Kinet. Katal.* **1983**, *24*, 877–882.

(695) Zhang, D.; Al-Hajri, R.; Barri, S. A. I.; Chadwick, D. One-Step Dehydration and Isomerisation of N-Butanol to Iso-Butene over Zeolite Catalysts. *Chem. Commun.* **2010**, *46*, 4088–4090. DOI: 10.1039/c002240c.

(696) Gunst, D.; Alexopoulos, K.; van der Borght, K.; John, M.; Galvita, V.; Reyniers, M.-F.; an Verberckmoes. Study of Butanol Conversion to Butenes over H-ZSM-5: Effect of Chemical Structure on Activity, Selectivity and Reaction Pathways. *Appl. Catal. A* **2017**, *539*, 1–12. DOI: 10.1016/j.apcata.2017.03.036.

(697) Moser, W. R.; Thompson, R. W.; Chiang, C.-C.; Tong, H. Silicon-Rich H-ZSM-5 Catalyzed Conversion of Aqueous Ethanol to Ethylene. *J. Catal.* **1989**, *117*, 19–32.

(698) Santacesaria, E.; Gelosa, D.; Giorgi, E.; Carra, S. Role of Basic and Acid Sites in the Bimolecular Dehydration of Alcohols Catalyzed by HY Zeolite. *J. Catal.* **1984**, *90*, 1–9.

(699) Xu, M.; Lunsford, J. H.; Goodman, D. W.; Bhattacharyya, A. Synthesis of Dimethyl Ether (DME) From Methanol over Solid-Acid Catalysts. *Appl. Catal. A* **1997**, *149*, 289–301.

(700) Phillips, C. B.; Datta, R. Production of Ethylene from Hydrous Ethanol on H-ZSM-5 Under Mild Conditions. *Ind. Eng. Chem.* **1997**, *36*, 4466–4475.

(701) Maury, S.; Coupard, V.; Heinz, T.; Duplan, G.; Lopez, J.; Nesterenko, N. Method for the Isomerisation Dehydration of Non-Linear Primary Alcohol Feedstock in the Presence of Water Injection and a Catalyst Comprising an FER or MFS Zeolite WO 2018/087033 A1.

(702) Bates, J. S.; Gounder, R. Kinetic Effects of Molecular Clustering and Solvation by Extended Networks in Zeolite Acid Catalysis. *Chem. Sci.* **2021**, *12*, 4699–4708. DOI: 10.1039/d1sc00151e.

(703) Aronson, M. T.; Gorte, R. J.; Farneth, W. E.; White, D. Stability of Adsorption Complexes Formed by Alcohols on H-ZSM-5. *Langmuir* **1988**, *4*, 702–706.

(704) Ison, A.; Gorte, R. J. The Adsorption of Methanol and Water on H-ZSM-5. *J. Catal.* **1984**, *89*, 150–158.

(705) Grifoni, E.; Piccini, G.; Lercher, J. A.; Glezakou, V.-A.; Rousseau, R.; Parrinello, M. Confinement Effects and Acid Strength in Zeolites. *Nat. Commun.* **2021**, *12*, 2630. DOI: 10.1038/s41467-021-22936-0.

(706) Li, Z.; Dittmann, D.; Rieg, C.; Benz, M.; Dyballa, M. Confinement and Surface Sites Control Methanol Adsorbate Stability on MFI Zeolites, SBA-15, and a Silica-Supported Heteropoly Acid. *Catal. Sci. Technol.* **2022**, *12*, 2265–2277. DOI: 10.1039/D1CY02330F.

(707) Li, Z.; Dittmann, D.; Rieg, C.; Benz, M.; Dyballa, M. Hydronium Ion and Water Complexes Vs. Methanol on Solid Catalyst Surfaces: How Confinement Influences Stability and Reactivity. *Catal. Sci. Technol.* **2022**, *12*, 5189–5202. DOI: 10.1039/D2CY00829G.

(708) Potts, D. S.; Bregante, D. T.; Adams, J. S.; Torres, C.; Flaherty, D. W. Influence of Solvent Structure and Hydrogen Bonding on Catalysis at Solid-Liquid Interfaces. *Chem. Soc. Rev.* **2021**, *50*, 12308–12337. DOI: 10.1039/d1cs00539a.

(709) Stanciakova, K.; Weckhuysen, B. M. Water–active Site Interactions in Zeolites and Their Relevance in Catalysis. *Trends Chem.* **2021**, *3*, 456–468. DOI: 10.1016/j.trechm.2021.03.004.

(710) Bates, J. S.; Bukowski, B. C.; Greeley, J.; Gounder, R. Structure and Solvation of Confined Water and Water-Ethanol Clusters Within Microporous Brønsted Acids and Their Effects on Ethanol Dehydration Catalysis. *Chem. Sci.* **2020**, *11*, 7102–7122. DOI: 10.1039/d0sc02589e.

(711) Eckstein, S.; Hintermeier, P. H.; Zhao, R.; Baráth, E.; Shi, H.; Liu, Y.; Lercher, J. A. Influence of Hydronium Ions in Zeolites on Sorption. *Angew. Chem. Int. Ed. Engl.* **2019**, *58*, 3450–3455. DOI: 10.1002/anie.201812184.

(712) Liu, P.; Hao, W.; Mei, D. Understanding the Effects of Water Molecules on Cyclohexanol Dehydration over Zeolitic Acid Sites. *J. Phys. Chem. C* **2021**, *125*, 15283–15291. DOI: 10.1021/acs.jpcc.1c03846.

(713) Abdullah, A.; Zuhairi Abdullah, A.; Ahmed, M.; Khan, J.; Shahadat, M.; Umar, K.; Alim, M. A. A Review on Recent Developments and Progress in Sustainable Acrolein Production Through Catalytic Dehydration of Bio-Renewable Glycerol. *J. Clean. Prod.* **2022**, *341*, 130876. DOI: 10.1016/j.jclepro.2022.130876.

(714) Katryniok, B.; Paul, S.; Capron, M.; Dumeignil, F. Towards the Sustainable Production of Acrolein by Glycerol Dehydration. *ChemSusChem* **2009**, *2*, 719–730. DOI: 10.1002/cssc.200900134.

(715) Katryniok, B.; Paul, S.; Bellière-Baca, V.; Rey, P.; Dumeignil, F. Glycerol Dehydration to Acrolein in the Context of New Uses of Glycerol. *Green Chem.* **2010**, *12*, 2079. DOI: 10.1039/c0gc00307g.

(716) Talebian-Kiakalaieh, A.; Amin, N. A. S.; Hezaveh, H. Glycerol for Renewable Acrolein Production by Catalytic Dehydration. *Renew. Sustain. Energy Rev.* **2014**, *40*, 28–59. DOI: 10.1016/j.rser.2014.07.168.

(717) Dubois, J.-L.; Duquenne, C.; Holderich, W. Process for Dehydrating Glycerol to Acrolein. US Patent US 7,396,962 B1.

(718) Dubois, J.-L.; Duquenne, C.; Holderich, W.; Kervennal, J. Process for Dehydrating Glycerol to Acrolein. US Patent US 2008/0214880 A1.

(719) Corma, A.; Huber, G. W.; Sauvanaud, L.; O'Connor, P. Biomass to Chemicals: Catalytic Conversion of Glycerol/water Mixtures into Acrolein, Reaction Network. *J. Catal.* **2008**, *257*, 163–171. DOI: 10.1016/j.jcat.2008.04.016.

(720) Chai, S.-H.; Wang, H.-P.; Liang, Y.; Xu, B.-Q. Sustainable Production of Acrolein: Investigation of Solid Acid–base Catalysts for Gas-Phase Dehydration of Glycerol. *Green Chem.* **2007**, *9*, 1130. DOI: 10.1039/b702200j.

(721) Catuzo, G. L.; Possato, L. G.; Sad, M. E.; Padró, C.; Martins, L. Progress of the Catalytic Deactivation of H-ZSM-5 Zeolite in Glycerol Dehydration. *ChemCatChem* **2021**, *13*, 4419–4430. DOI: 10.1002/cctc.202100576.

(722) Oliveira, A. S. de; Vasconcelos, S. J.; Sousa, J. R. de; Sousa, F. F. de; Filho, J. M.; Oliveira, A. C. Catalytic Conversion of Glycerol to Acrolein over Modified Molecular Sieves: Activity and Deactivation Studies. *Chem. Eng. J.* **2011**, *168*, 765–774. DOI: 10.1016/j.cej.2010.09.029.

(723) Hulteberg, C.; Leveau, A.; Brandin, J. G. M. Pore Condensation in Glycerol Dehydration. *Top. Catal.* **2013**, *56*, 813–821. DOI: 10.1007/s11244-013-0039-9.

(724) Pala-Rosas, I.; Contreras, J. L.; Salmones, J.; Zeifert, B.; López-Medina, R.; Navarrete-Bolaños, J.; Hernández-Ramírez, S.; Pérez-Cabrera, J.; Fragoso-Montes de Oca, A. A. Catalytic Deactivation of HY Zeolites in the Dehydration of Glycerol to Acrolein. *Catalysts* **2021**, *11*, 360. DOI: 10.3390/catal11030360.

(725) Yoda, E.; Ootawa, A. Dehydration of Glycerol on H-MFI Zeolite Investigated by FT-IR. *Appl. Catal. A* **2009**, *360*, 66–70. DOI: 10.1016/j.apcata.2009.03.009.

(726) Kongpatpanich, K.; Nanok, T.; Boekfa, B.; Probst, M.; Limtrakul, J. Structures and Reaction Mechanisms of Glycerol Dehydration over H-ZSM-5 Zeolite: A Density Functional Theory Study. *Phys. Chem. Chem. Phys.* **2011**, *13*, 6462–6470. DOI: 10.1039/c0cp01720e.

(727) Yun, D.; Yun, Y. S.; Kim, T. Y.; Park, H.; Lee, J. M.; Han, J. W.; Yi, J. Mechanistic Study of Glycerol Dehydration on Brønsted Acidic Amorphous Aluminosilicate. *J. Catal.* **2016**, *341*, 33–43. DOI: 10.1016/j.jcat.2016.06.010.

(728) Gu, Y.; Cui, N.; Yu, Q.; Li, C.; Cui, Q. Study on the Influence of Channel Structure Properties in the Dehydration of Glycerol to Acrolein over H-Zeolite Catalysts. *Appl. Catal. A* **2012**, *429-430*, 9–16. DOI: 10.1016/j.apcata.2012.03.030.

(729) Kim, Y. T.; Jung, K.-D.; Park, E. D. A Comparative Study for Gas-Phase Dehydration of Glycerol over H-Zeolites. *Appl. Catal. A* **2011**, *393*, 275–287. DOI: 10.1016/j.apcata.2010.12.007.

(730) Wang, Z.; Wang, L.; Jiang, Y.; Hunger, M.; Huang, J. Cooperativity of Brønsted and Lewis Acid Sites on Zeolite for Glycerol Dehydration. *ACS Catal.* **2014**, *4*, 1144–1147. DOI: 10.1021/cs401225k.

(731) Lin, X.; Lv, Y.; Qu, Y.; Zhang, G.; Xi, Y.; Phillips, D. L.; Liu, C. A Combined Experimental and Computational Study of the Catalytic Dehydration of Glycerol on Microporous Zeolites: An Investigation of the Reaction Mechanism and Acrolein Selectivity. *Phys. Chem. Chem. Phys.* **2013**, *15*, 20120–20133. DOI: 10.1039/c3cp53915f.

(732) Karinen, R.; Vilonen, K.; Niemelä, M. Biorefining: Heterogeneously Catalyzed Reactions of Carbohydrates for the Production of Furfural and Hydroxymethylfurfural. *ChemSusChem* **2011**, *4*, 1002–1016. DOI: 10.1002/cssc.201000375.

(733) van Putten, R.-J.; van der Waal, J. C.; Jong, E. de; Rasrendra, C. B.; Heeres, H. J.; Vries, J. G. de. Hydroxymethylfurfural, a Versatile Platform Chemical Made from Renewable Resources. *Chem. Rev.* **2013**, *113*, 1499–1597. DOI: 10.1021/cr300182k.

(734) Kruger, J. S.; Nikolakis, V.; Vlachos, D. G. Carbohydrate Dehydration Using Porous Catalysts. *Curr. Opin. Chem. Eng.* **2012**, *1*, 312–320. DOI: 10.1016/j.coche.2012.06.003.

(735) Di Menno Bucchianico, D.; Wang, Y.; Buvat, J.-C.; Pan, Y.; Casson Moreno, V.; Leveneur, S. Production of Levulinic Acid and Alkyl Levulinates: A Process Insight. *Green Chem.* **2022**, *24*, 614–646. DOI: 10.1039/D1GC02457D.

(736) Ricciardi, L.; Verboom, W.; Lange, J.-P.; Huskens, J. Production of Furans from C 5 and C 6 Sugars in the Presence of Polar Organic Solvents. *Sustainable Energy Fuels* **2021**, *6*, 11–28. DOI: 10.1039/D1SE01572A.

(737) van Zandvoort, I.; Wang, Y.; Rasrendra, C. B.; van Eck, E. R. H.; Bruijnincx, P. C. A.; Heeres, H. J.; Weckhuysen, B. M. Formation, Molecular Structure, and Morphology of Humins in Biomass Conversion: Influence of Feedstock and Processing Conditions. *ChemSusChem* **2013**, *6*, 1745–1758. DOI: 10.1002/cssc.201300332.

(738) Baccile, N.; Laurent, G.; Babonneau, F.; Fayon, F.; Titirici, M.-M.; Antonietti, M. Structural Characterization of Hydrothermal Carbon Spheres by Advanced Solid-State MAS 13C NMR Investigations. *J. Phys. Chem. C* **2009**, *113*, 9644–9654. DOI: 10.1021/jp901582x.

(739) Yao, C.; Shin, Y.; Wang, L.-Q.; Windisch, C. F.; Samuels, W. D.; Arey, B. W.; Wang, C.; Risen, W. M.; Exarhos, G. J. Hydrothermal Dehydration of Aqueous Fructose Solutions in a Closed System. *J. Phys. Chem. C* **2007**, *111*, 15141–15145. DOI: 10.1021/jp074188l.

(740) Istasse, T.; Richel, A. Mechanistic Aspects of Saccharide Dehydration to Furan Derivatives for Reaction Media Design. *RSC advances* **2020**, *10*, 23720–23742. DOI: 10.1039/d0ra03892j.

(741) Sajid, M.; Farooq, U.; Bary, G.; Azim, M. M.; Zhao, X. Sustainable Production of Levulinic Acid and Its Derivatives for Fuel Additives and Chemicals: Progress, Challenges, and Prospects. *Green Chem.* **2021**, *23*, 9198–9238. DOI: 10.1039/D1GC02919C.

(742) Victor, A.; Sharma, P.; Pulidindi, I. N.; Gedanken, A. Levulinic Acid Is a Key Strategic Chemical from Biomass. *Catalysts* **2022**, *12*, 909. DOI: 10.3390/catal12080909.

(743) Zhang, Z.; Huber, G. W. Catalytic Oxidation of Carbohydrates into Organic Acids and Furan Chemicals. *Chem. Soc. Rev.* **2018**, *47*, 1351–1390. DOI: 10.1039/c7cs00213k.

(744) Yang, G.; Pidko, E. A.; Hensen, E. J. Mechanism of Brønsted Acid-Catalyzed Conversion of Carbohydrates. *J. Catal.* **2012**, *295*, 122–132. DOI: 10.1016/j.jcat.2012.08.002.

(745) Caratzoulas, S.; Vlachos, D. G. Converting Fructose to 5-Hydroxymethylfurfural: A Quantum Mechanics/molecular Mechanics Study of the Mechanism and Energetics. *Carbohydr. Res.* **2011**, *346*, 664–672. DOI: 10.1016/j.carres.2011.01.029.

(746) Lin, X.; Qu, Y.; Lv, Y.; Xi, Y.; Phillips, D. L.; Liu, C. The First Dehydration and the Competing Reaction Pathways of Glucose Homogeneously and Heterogeneously Catalyzed by Acids. *Phys. Chem. Chem. Phys.* **2013**, *15*, 2967–2982. DOI: 10.1039/c2cp43644b.

(747) Kunnikuruvan, S.; Nair, N. N. Mechanistic Insights into the Brønsted Acid-Catalyzed Dehydration of B- D -Glucose to 5-Hydroxymethylfurfural Under Ambient and Subcritical Conditions. *ACS Catal.* **2019**, *9*, 7250–7263. DOI: 10.1021/acscatal.9b00678.

(748) Assary, R. S.; Kim, T.; Low, J. J.; Greeley, J.; Curtiss, L. A. Glucose and Fructose to Platform Chemicals: Understanding the Thermodynamic Landscapes of Acid-Catalysed Reactions Using High-Level Ab Initio Methods. *Phys. Chem. Chem. Phys.* **2012**, *14*, 16603–16611. DOI: 10.1039/c2cp41842h.

(749) Lin, L.; Han, X.; Han, B.; Yang, S. Emerging Heterogeneous Catalysts for Biomass Conversion: Studies of the Reaction Mechanism. *Chem. Soc. Rev.* **2021**, *50*, 11270–11292. DOI: 10.1039/d1cs00039j.

(750) Liu, Y.; Kerton, F. M. Mechanistic Studies on the Formation of 5-Hydroxymethylfurfural from the Sugars Fructose and Glucose. *Pure Appl. Chem.* **2021**, *93*, 463–478.

(751) Feather, M. S.; Harris, J. F. Dehydration Reactions of Carbohydrates. *Adv. Carbohydr. Chem.*, *28*, 161–224. DOI: 10.1016/S0065-2318(08)60383-2.

(752) Antal, M. J.; Mok, W. S. L. Mechanism of Formation of 5-(Hydroxymethyl)-2-Furaldehyde from D-Fructose and Sucrose. *Carbohydr. Res.* **1990**, *199*, 91–109.

(753) Anet, E. F. L. J. 3-Deoxyhexosones. *J. Am. Chem. Soc.* **1960**, *82*, 1502–1503.

(754) Anet, E. F. L. J. 3-Deoxyglycosuloses and the Degradation of Carbohydrates. *Adv. Carbohydr. Chem.* **1964**, *19*, 181–218.

(755) Newth, F. H. The Formation of Furan Compounds from Hexoses. *Adv. Carbohydr. Chem.* **1951**, *6*, 83–106.

(756) Wolfrom, M. L.; Schuetz, R. D.; Cavalieri, L. F. Chemical Interactions of Amino Compounds and Sugars. III. The Conversion of D-Glucose to 5-(Hydroxymethyl)-2-Furaldehyde. *J. Am. Chem. Soc.* **1948**, *70*, 514–517.

(757) Divya, P. S.; Nair, S.; Kunnikuruvan, S. Identification of Crucial Intermediates in the Formation of Humins from Cellulose-Derived Platform Chemicals Under Brønsted Acid Catalyzed Reaction Conditions. *ChemPhysChem* **2022**, *23*, e202200057. DOI: 10.1002/cphc.202200057.

(758) Kuster, B. F. M.; Temmink, H. M. G. The Influence of PH and Weak-Acid Anions on the Dehydration of D-Fructose. *Carbohydr. Res.* **1977**, *54*, 185–191.

(759) Gürbüz, E. I.; Gallo, J. M. R.; Alonso, D. M.; Wettstein, S. G.; Lim, W. Y.; Dumesic, J. A. Conversion of Hemicellulose into Furfural Using Solid Acid Catalysts in Γ-Valerolactone. *Angew. Chem. Int. Ed. Engl.* **2013**, *52*, 1270–1274. DOI: 10.1002/anie.201207334.

(760) Grin', S. A.; Tsimbalaev, S. R.; Gel'fand, S. Y. Kinetic Isotope Effect in the Reaction of Dehydration of Fructose into 5-Hydroxymethylfurfural. *Kinet. Catal.* **1993**, *34*, 482–483.

(761) Kimura, H.; Nakahara, M.; Matubayasi, N. Solvent Effect on Pathways and Mechanisms for D-Fructose Conversion to 5-Hydroxymethyl-2-Furaldehyde: In Situ ^{13}C NMR Study. *J. Phys. Chem. A* **2013**, *117*, 2102–2113. DOI: 10.1021/jp312002h.

(762) Akien, G. R.; Qi, L.; Horváth, I. T. Molecular Mapping of the Acid Catalysed Dehydration of Fructose. *Chem. Commun.* **2012**, *48*, 5850–5852. DOI: 10.1039/c2cc31689g.

(763) Amarasekara, A. S.; Williams, L. D.; Ebede, C. C. Mechanism of the Dehydration of D-Fructose to 5-Hydroxymethylfurfural in Dimethyl Sulfoxide at 150 Degrees C: An NMR Study. *Carbohydr. Res.* **2008**, *343*, 3021–3024. DOI: 10.1016/j.carres.2008.09.008.

(764) Yang, L.; Tsilomelekis, G.; Caratzoulas, S.; Vlachos, D. G. Mechanism of Brønsted Acid-Catalyzed Glucose Dehydration. *ChemSusChem* **2015**, *8*, 1334–1341. DOI: 10.1002/cssc.201403264.

(765) Song, W.; Liu, H.; Zhang, J.; Sun, Y.; Peng, L. Understanding Hβ Zeolite in 1,4-Dioxane Efficiently Converts Hemicellulose-Related Sugars to Furfural. *ACS Catal.* **2022**, *12*, 12833–12844. DOI: 10.1021/acscatal.2c03227.

(766) Danon, B.; Hongsiri, W.; van der Aa, L.; de Jong, W. Kinetic Study on Homogeneously Catalyzed Xylose Dehydration to Furfural in the Presence of Arabinose and Glucose. *Biomass Bioenergy* **2014**, *66*, 364–370. DOI: 10.1016/j.biombioe.2014.04.007.

(767) Gallo, J. M. R.; Alonso, D. M.; Mellmer, M. A.; Yeap, J. H.; Wong, H. C.; Dumesic, J. A. Production of Furfural from Lignocellulosic Biomass Using Beta Zeolite and Biomass-Derived Solvent. *Top. Catal.* **2013**, *56*, 1775–1781. DOI: 10.1007/s11244-013-0113-3.

(768) Filiciotto, L.; Balu, A. M.; van der Waal, J. C.; Luque, R. Catalytic Insights into the Production of Biomass-Derived Side Products Methyl Levulinate, Furfural and Humins. *Catal. Today* **2018**, *302*, 2–15. DOI: 10.1016/j.cattod.2017.03.008.

(769) Ennaert, T.; Schutyser, W.; Dijkmans, J.; Dusselier, M.; Sels, B. F. Conversion of Biomass to Chemicals : The Catalytic Role of Zeolites. In *Zeolites and Zeolite-Like Materials*; Elsevier, 2016; pp 371–431. DOI: 10.1016/B978-0-444-63506-8.00010-0.

(770) Li, H.; Yang, S.; Riisager, A.; Pandey, A.; Sangwan, R. S.; Saravanamurugan, S.; Luque, R. Zeolite and Zeotype-Catalysed Transformations of Biofuranic Compounds. *Green Chem.* **2016**, *18*, 5701–5735. DOI: 10.1039/C6GC02415G.

(771) Kim, S. B.; You, S. J.; Kim, Y. T.; Lee, S.; Lee, H.; Park, K.; Park, E. D. Dehydration of D-Xylose into Furfural over H-Zeolites. *Korean J. Chem. Eng.* **2011**, *28*, 710–716. DOI: 10.1007/s11814-010-0417-y.

(772) Ordomsky, V. V.; van der Schaaf, J.; Schouten, J. C.; Nijhuis, T. A. The Effect of Solvent Addition on Fructose Dehydration to 5-Hydroxymethylfurfural in Biphasic System over Zeolites. *J. Catal.* **2012**, *287*, 68–75. DOI: 10.1016/j.jcat.2011.12.002.

(773) Caratzoulas, S.; Davis, M. E.; Gorte, R. J.; Gounder, R.; Lobo, R. F.; Nikolakis, V.; Sandler, S. I.; Snyder, M. A.; Tsapatsis, M.; Vlachos, D. G. Challenges of and Insights into Acid-Catalyzed Transformations of Sugars. *J. Phys. Chem. C* **2014**, *118*, 22815–22833. DOI: 10.1021/jp504358d.

(774) Li, Y.; Lu, X.; Yuan, L.; Liu, X. Fructose Decomposition Kinetics in Organic Acids-Enriched High Temperature Liquid Water. *Biomass Bioenergy* **2009**, *33*, 1182–1187. DOI: 10.1016/j.biombioe.2009.05.003.

(775) Moreau, C.; Durand, R.; Razigade, S.; Duhamet, J.; Faugeras, P.; Rivalier, P.; Ros, P.; Avignon, G. Dehydration of Fructose to 5-Hydroxymethylfurfural over H-Mordenites. *Appl. Catal. A* **1996**, *145*, 211–224.

(776) Wang, M.; Xia, Y.; Li Zhao; Song, C.; Peng, L.; Guo, X.; Xue, N.; Ding, W. Remarkable Acceleration of the Fructose Dehydration over the Adjacent Brønsted Acid Sites Contained in an MFI-Type Zeolite Channel. *J. Catal.* **2014**, *319*, 150–154. DOI: 10.1016/j.jcat.2014.08.008.

(777) Lourvanij, K.; Rorrer, G. L. Reactions of Aqueous Glucose Solutions over Solid-Acid Y-Zeolite Catalyst at 110-160 °C. *Ind. Eng. Chem.* **1993**, *32*, 11–19.

(778) Lourvanij, K.; Rorrer, G. L. Reaction Rates for the Partial Dehydration of Glucose to Organic Acids in Solid-acid, Molecular-sieving Catalyst Powders. *J. Chem. Tech. Biotechnol.* **1997**, *69*, 35–44.

(779) Jow, J.; Rorrer, G. L.; Hawley, M. C. Dehydration of D-Fructose to Levulinc Acid over LZY Zeolite Catalyst. *Biomass* **1987**, *14*, 185–194.

(780) Qi, L.; Alamillo, R.; Elliott, W. A.; Andersen, A.; Hoyt, D. W.; Walter, E. D.; Han, K. S.; Washton, N. M.; Rioux, R. M.; Dumesic, J. A.*; et al.* Operando Solid-State NMR Observation of Solvent-Mediated Adsorption-Reaction of Carbohydrates in Zeolites. *ACS Catal.* **2017**, *7*, 3489–3500. DOI: 10.1021/acscatal.7b01045.

(781) Cheng, L.; Curtiss, L. A.; Assary, R. S.; Greeley, J.; Kerber, T.; Sauer, J. Adsorption and Diffusion of Fructose in Zeolite HZSM-5: Selection of Models and Methods for Computational Studies. *J. Phys. Chem. C* **2011**, *115*, 21785–21790. DOI: 10.1021/jp2062018.

(782) Kruger, J. S.; Choudhary, V.; Nikolakis, V.; Vlachos, D. G. Elucidating the Roles of Zeolite H-BEA in Aqueous-Phase Fructose Dehydration and HMF Rehydration. *ACS Catal.* **2013**, *3*, 1279–1291. DOI: 10.1021/cs4002157.

(783) León, M.; Swift, T. D.; Nikolakis, V.; Vlachos, D. G. Adsorption of the Compounds Encountered in Monosaccharide Dehydration in Zeolite Beta. *Langmuir* **2013**, *29*, 6597–6605. DOI: 10.1021/la401138g.

(784) Choudhary, V.; Mushrif, S. H.; Ho, C.; Anderko, A.; Nikolakis, V.; Marinkovic, N. S.; Frenkel, A. I.; Sandler, S. I.; Vlachos, D. G. Insights into the Interplay of Lewis and Brønsted Acid Catalysts in Glucose and Fructose Conversion to 5-(Hydroxymethyl)Furfural and Levulinic Acid in Aqueous Media. *J. Am. Chem. Soc.* **2013**, *135*, 3997–4006. DOI: 10.1021/ja3122763.

(785) Dallas Swift, T.; Nguyen, H.; Anderko, A.; Nikolakis, V.; Vlachos, D. G. Tandem Lewis/Brønsted Homogeneous Acid Catalysis: Conversion of Glucose to 5-Hydoxymethylfurfural in an Aqueous Chromium(III) Chloride and Hydrochloric Acid Solution. *Green Chem.* **2015**, *17*, 4725–4735. DOI: 10.1039/C5GC01257K.

(786) Román-Leshkov, Y.; Moliner, M.; Labinger, J. A.; Davis, M. E. Mechanism of Glucose Isomerization Using a Solid Lewis Acid Catalyst in Water. *Angew. Chem. Int. Ed. Engl.* **2010**, *49*, 8954–8957. DOI: 10.1002/anie.201004689.

(787) van der Graaff, W. N. P.; Tempelman, C. H. L.; Li, G.; Mezari, B.; Kosinov, N.; Pidko, E. A.; Hensen, E. J. M. Competitive Adsorption of Substrate and Solvent in Sn-Beta Zeolite During Sugar Isomerization. *ChemSusChem* **2016**, *9*, 3145–3149. DOI: 10.1002/cssc.201600800.

(788) Saravanamurugan, S.; Riisager, A.; Taarning, E.; Meier, S. Mechanism and Stereoselectivity of Zeolite-Catalysed Sugar Isomerisation in Alcohols. *Chem. Commun.* **2016**, *52*, 12773–12776. DOI: 10.1039/c6cc05592c.

(789) Elliot, S. G.; Tolborg, S.; Sádaba, I.; Taarning, E.; Meier, S. Quantitative NMR Approach to Optimize the Formation of Chemical Building Blocks from Abundant Carbohydrates. *ChemSusChem* **2017**, *10*, 2990–2996. DOI: 10.1002/cssc.201700587.

(790) Marianou, A. A.; Michailof, C. M.; Pineda, A.; Iliopoulou, E. F.; Triantafyllidis, K. S.; Lappas, A. A. Effect of Lewis and Brønsted Acidity on Glucose Conversion to 5-HMF and Lactic Acid in Aqueous and Organic Media. *Appl. Catal. A* **2018**, *555*, 75–87. DOI: 10.1016/j.apcata.2018.01.029.

(791) Pescarmona, P. P.; Janssen, K. P. F.; Delaet, C.; Stroobants, C.; Houthoofd, K.; an Philippaerts; Jonghe, C. de; Paul, J. S.; Jacobs, P. A.; Sels, B. F. Zeolite-Catalysed Conversion of C3 Sugars to Alkyl Lactates. *Green Chem.* **2010**, *12*, 1083. DOI: 10.1039/b921284a.

(792) Gardner, D. W.; Huo, J.; Hoff, T. C.; Johnson, R. L.; Shanks, B. H.; Tessonnier, J.-P. Insights into the Hydrothermal Stability of ZSM-5 Under Relevant Biomass Conversion Reaction Conditions. *ACS Catal.* **2015**, *5*, 4418–4422. DOI: 10.1021/acscatal.5b00888.

(793) Kruger, J. S.; Nikolakis, V.; Vlachos, D. G. Aqueous-Phase Fructose Dehydration Using Brønsted Acid Zeolites: Catalytic Activity of Dissolved Aluminosilicate Species. *Appl. Catal. A* **2014**, *469*, 116–123. DOI: 10.1016/j.apcata.2013.09.030.

(794) Lima, S.; Antunes, M. M.; Fernandes, A.; Pillinger, M.; Ribeiro, M. F.; Valente, A. A. Catalytic Cyclodehydration of Xylose to Furfural in the Presence of Zeolite H-Beta and a Micro/mesoporous Beta/TUD-1 Composite Material. *Appl. Catal. A* **2010**, *388*, 141–148. DOI: 10.1016/j.apcata.2010.08.040.

(795) Lima, S.; Antunes, M. M.; Fernandes, A.; Pillinger, M.; Ribeiro, M. F.; Valente, A. A. Acid-Catalysed Conversion of Saccharides into Furanic Aldehydes in the Presence of Three-Dimensional Mesoporous Al-TUD-1. *Molecules* **2010**, *15*, 3863–3877. DOI: 10.3390/molecules15063863.

(796) Rac, V.; Rakić, V.; Stošić, D.; Otman, O.; Auroux, A. Hierarchical ZSM-5, Beta and USY Zeolites: Acidity Assessment by Gas and Aqueous Phase Calorimetry and Catalytic Activity in Fructose Dehydration Reaction. *Microporous Mesoporous Mater.* **2014**, *194*, 126–134. DOI: 10.1016/j.micromeso.2014.04.003.

(797) Shi, Y.; Li, X.; Hu, J.; Lu, J.; Ma, Y.; Zhang, Y.; Tang, Y. Zeolite Microspheres with Hierarchical Structures: Formation, Mechanism and Catalytic Performance. *J. Mater. Chem.* **2011**, *21*, 16223. DOI: 10.1039/c1jm11669j.

(798) Wang, Y.; Yang, X.; Zheng, H.; Li, X.; Zhu, Y.; Li, Y. Mechanistic Insights on Catalytic Conversion Fructose to Furfural on Beta Zeolite via Selective Carbon-Carbon Bond Cleavage. *Mol. Catal.* **2019**, *463*, 130–139. DOI: 10.1016/j.mcat.2018.11.022.

(799) Weingarten, R.; Tompsett, G. A.; Conner, W. C.; Huber, G. W. Design of Solid Acid Catalysts for Aqueous-Phase Dehydration of Carbohydrates: The Role of Lewis and Brønsted Acid Sites. *J. Catal.* **2011**, *279*, 174–182. DOI: 10.1016/j.jcat.2011.01.013.

(800) Moreau, C.; Durand, R.; Pourcheron, C.; Razigade, S. Preparation of 5-Hydroxymethylfurfural from Fructose and Precursors over H-from Zeolites. *Ind. Crops Prod.* **1994**, *3*, 85–90.

(801) Ordomsky, V. V.; van der Schaaf, J.; Schouten, J. C.; Nijhuis, T. A. Fructose Dehydration to 5-Hydroxymethylfurfural over Solid Acid Catalysts in a Biphasic System. *ChemSusChem* **2012**, *5*, 1812–1819. DOI: 10.1002/cssc.201200072.

(802) Tan, J.; Wang, H.; Ma, L.; Wang, C.; Liu, Q.; Zhang, Q.; He, M. Selective Yields of Furfural and Hydroxymethylfurfural from Glucose in Tetrahydrofuran over Hβ Zeolite. *RSC Adv.* **2018**, *8*, 24534–24540. DOI: 10.1039/C8RA04060E.

(803) Wang, L.; Guo, H.; Wang, Q.; Hou, B.; Jia, L.; Cui, J.; Li, D. The Study of Active Sites for Producing Furfural and Soluble Oligomers in Fructose Conversion over HZSM-5 Zeolites. *Mol. Catal.* **2019**, *474*, 110411. DOI: 10.1016/j.mcat.2019.110411.

(804) Zhang, J.; Ding, G.; Wang, Y.; Wang, F.; Wang, H.; Liu, Y.; Zhu, Y.; Li, Y. Regulation of Brønsted Acid Sites to Enhance the Decarburization of Hexoses to Furfural. *Catal. Sci. Technol.* **2022**, *12*, 3506–3515. DOI: 10.1039/D1CY02342J.

(805) Cui, J.; Tan, J.; Deng, T.; Cui, X.; Zhu, Y.; Li, Y. Conversion of Carbohydrates to Furfural via Selective Cleavage of the Carbon–carbon Bond: The Cooperative Effects of Zeolite and Solvent. *Green Chem.* **2016**, *18*, 1619–1624. DOI: 10.1039/C5GC01948F.

(806) Howard, M. J.; Jones, M. D.; Roberts, M. S.; Taylor, S. A. C1 to Acetyls: Catalysis and Process. *Catal. Today* **1993**, *18*, 325–354. DOI: 10.1016/0920-5861(93)80060-E.

(807) Sunley, G. J.; Watson, D. J. High Productivity Methanol Carbonylation Catalysis Using Iridium: The Cativa™ Process for the Manufacture of Acetic Acid. *Catal. Today* **2000**, *58*, 293–307. DOI: 10.1016/S0920-5861(00)00263-7.

(808) Koch, H. *Carbonsäure-Synthese aus Olefinen, Kohlenoxyd und Wasser*; Brennstow-Chemie, 1955.

(809) Stepanov A.G., Luzgin M.V., Romannikov V.N., Zamaraev K.I. NMR Observation of the Koch Reaction in Zeolite H-ZSM-5 Under Mild Conditions. *J. Am. Chem. Soc.* **1995**, *117*, 3615–3616.

(810) Fujimoto, K.; Shikada, T.; Omata, K.; Tominaga, H. Vapor Phase Carbonylation of Methanol with Solid Acid Catalysts. *Chem. Lett.* **1984**, *13*, 2047–2050. DOI: 10.1246/cl.1984.2047.

(811) Xu, Q.; Inoue, S.; Tsumori, N.; Mori, H.; Kameda, M.; Tanaka, M.; Fujiwara, M.; Souma, Y. Carbonylation of Tert-Butyl Alcohol over H-Zeolites. *J. Mol. Catal. A* **2001**, *170*, 147–153. DOI: 10.1016/S1381-1169(01)00054-1.

(812) Cheung, P.; Bhan, A.; Sunley, G. J.; Iglesia, E. Selective Carbonylation of Dimethyl Ether to Methyl Acetate Catalyzed by Acidic Zeolites. *Angew. Chem., Int. Ed.* **2006**, *45*, 1617–1620. DOI: 10.1002/anie.200503898.

(813) Cheung, P.; Bhan, A.; Sunley, G. J.; Law, D.; Iglesia, E. Site Requirements and Elementary Steps in Dimethyl Ether Carbonylation Catalyzed by Acidic Zeolites. *J. Catal.* **2007**, *245*, 110–123. DOI: 10.1016/j.jcat.2006.09.020.

(814) Luzgin, M. V.; Romannikov, V. N.; Stepanov, A. G.; Zamaraev, K. I. Interaction of Olefins with Carbon Monoxide on Zeolite H-ZSM-5. NMR Observation of the Friedel−Crafts Acylation of Alkenes at Ambient Temperature. *J. Am. Chem. Soc.* **1996**, *118*, 10890–10891. DOI: 10.1021/ja9615381.

(815) Kipnis, M. A.; Volnina, E. A. Methyl Acetate Synthesis by Dimethyl Ether Carbonylation in the Presence of Zeolites: A Review. *Kinet. Catal.* **2022**, *63*, 129–140. DOI: 10.1134/S0023158422020033.

(816) Feng, X.; Yao, J.; Li, H.; Fang, Y.; Yoneyama, Y.; Yang, G.; Tsubaki, N. A Brand New Zeolite Catalyst for Carbonylation Reaction. *Chem. Commun.* **2019**, *55*, 1048–1051. DOI: 10.1039/c8cc08411d.

(817) Chowdhury, A. D.; Paioni, A. L.; Houben, K.; Whiting, G. T.; Baldus, M.; Weckhuysen, B. M. Bridging the Gap Between the Direct and Hydrocarbon Pool Mechanisms of the Methanol-to-Hydrocarbons Process. *Angew. Chem., Int. Ed.* **2018**, *57*, 8095–8099. DOI: 10.1002/anie.201803279.

(818) Chowdhury, A. D.; Houben, K.; Whiting, G. T.; Mokhtar, M.; Asiri, A. M.; Al-Thabaiti, S. A.; Basahel, S. N.; Baldus, M.; Weckhuysen, B. M. Initial Carbon–Carbon Bond Formation During the Early Stages of the Methanol-to-Olefin Process Proven by Zeolite-Trapped Acetate and Methyl Acetate. *Angew. Chem. Int. Ed.* **2016**, *55*, 15840–15845. DOI: 10.1002/anie.201608643.

(819) Liu, Y.; Müller, S.; Berger, D.; Jelic, J.; Reuter, K.; Tonigold, M.; Sanchez-Sanchez, M.; Lercher, J. A. Formation Mechanism of the First Carbon-Carbon Bond and the First Olefin in the Methanol Conversion into Hydrocarbons. *Angew. Chem., Int. Ed.* **2016**, *55*, 5723–5726. DOI: 10.1002/anie.201511678.

(820) Plessow, P. N.; Smith, A.; Tischer, S.; Studt, F. Identification of the Reaction Sequence of the MTO Initiation Mechanism Using Ab Initio-Based Kinetics. *J. Am. Chem. Soc.* **2019**, *141*, 5908–5915. DOI: 10.1021/jacs.9b00585.

(821) Plessow, P. N.; Studt, F. Unraveling the Mechanism of the Initiation Reaction of the Methanol to Olefins Process Using Ab Initio and DFT Calculations. *ACS Catal.* **2017**, *7*, 7987–7994. DOI: 10.1021/acscatal.7b03114.

(822) Plessow, P. N.; Studt, F. Theoretical Insights into the Effect of the Framework on the Initiation Mechanism of the MTO Process. *Catal. Lett.* **2018**, *148*, 1246–1253. DOI: 10.1007/s10562-018-2330-7.

(823) Falbe, J.; Bahrmann, H. *New Syntheses with Carbon Monoxide*; Reactivity and Structure: Concepts in Organic Chemistry; Springer Berlin Heidelberg, 1980.

(824) Zhou, H.; Zhu, W.; Shi, L.; Liu, H.; Liu, S.; Ni, Y.; Liu, Y.; He, Y.; Xu, S.; Li, L.*; et al.* In Situ DRIFT Study of Dimethyl Ether Carbonylation to Methyl Acetate on H-Mordenite. *J. Mol. Catal. A* **2016**, *417*, 1–9. DOI: 10.1016/j.molcata.2016.02.032.

(825) Jiang, Y.; Hunger, M.; Wang, W. On the Reactivity of Surface Methoxy Species in Acidic Zeolites. *J. Am. Chem. Soc.* **2006**, *128*, 11679–11692. DOI: 10.1021/ja061018y.

(826) Boronat, M.; Martínez, C.; Corma, A. Mechanistic Differences Between Methanol and Dimethyl Ether Carbonylation in Side Pockets and Large Channels of Mordenite. *Phys. Chem. Chem. Phys.* **2011**, *13*, 2603–2612. DOI: 10.1039/c0cp01996h.

(827) Boronat, M.; Martínez-Sánchez, C.; Law, D.; Corma, A. Enzyme-Like Specificity in Zeolites: A Unique Site Position in Mordenite for Selective Carbonylation of Methanol and Dimethyl Ether with CO. *J. Am. Chem. Soc.* **2008**, *130*, 16316–16323. DOI: 10.1021/ja805607m.

(828) Chu, Y.; Lo, A.-Y.; Wang, C.; Deng, F. Origin of High Selectivity of Dimethyl Ether Carbonylation in the 8-Membered Ring Channel of Mordenite Zeolite. *J. Phys. Chem. C* **2019**, *123*, 15503–15512. DOI: 10.1021/acs.jpcc.9b01874.

(829) Gešvandtnerová, M.; Rocca, D.; Bučko, T. Methanol Carbonylation over Acid Mordenite: Insights from Ab Initio Molecular Dynamics and Machine Learning Thermodynamic Perturbation Theory. *J. Catal.* **2021**, *396*, 166–178. DOI: 10.1016/j.jcat.2021.02.011.

(830) Rasmussen, D. B.; Christensen, J. M.; Temel, B.; Studt, F.; Moses, P. G.; Rossmeisl, J.; Riisager, A.; Jensen, A. D. Reaction Mechanism of Dimethyl Ether Carbonylation to Methyl Acetate over Mordenite – a Combined DFT/experimental Study. *Catal. Sci. Technol.* **2017**, *7*, 1141–1152. DOI: 10.1039/C6CY01904H.

(831) Feng, P.; Zhang, G.; Chen, X.; Zang, K.; Li, X.; Xu, L. Specific Zone Within 8-Membered Ring Channel as Catalytic Center for Carbonylation of Dimethyl Ether and Methanol over FER Zeolite. *Appl. Catal. A* **2018**, *557*, 119–124. DOI: 10.1016/j.apcata.2018.03.018.

(832) Chen, W.; Li, G.; Yi, X.; Day, S. J.; Tarach, K. A.; Liu, Z.; Liu, S.-B.; Edman Tsang, S. C.; Góra-Marek, K.; Zheng, A. Molecular Understanding of the Catalytic Consequence of Ketene Intermediates Under Confinement. *J. Am. Chem. Soc.* **2021**, *143*, 15440–15452. DOI: 10.1021/jacs.1c08036.

(833) Blasco, T.; Boronat, M.; Concepción, P.; Corma, A.; Law, D.; Vidal-Moya, J. A. Carbonylation of Methanol on Metal-Acid Zeolites: Evidence for a Mechanism Involving a Multisite Active Center. *Angew. Chem., Int. Ed.* **2007**, *46*, 3938–3941. DOI: 10.1002/anie.200700029.

(834) Rasmussen, D. B.; Christensen, J. M.; Temel, B.; Studt, F.; Moses, P. G.; Rossmeisl, J.; Riisager, A.; Jensen, A. D. Ketene as a Reaction Intermediate in the Carbonylation of Dimethyl Ether to Methyl Acetate over Mordenite. *Angew. Chem., Int. Ed.* **2015**, *54*, 7261–7264. DOI: 10.1002/anie.201410974.

(835) He, T.; Ren, P.; Liu, X.; Xu, S.; Han, X.; Bao, X. Direct Observation of DME Carbonylation in the Different Channels of H-MOR Zeolite by Continuous-Flow Solid-State NMR Spectroscopy. *Chem. Commun.* **2015**, *51*, 16868–16870. DOI: 10.1039/c5cc07201h.

(836) Lezcano-González, I.; Vidal-Moya, J. A.; Boronat, M.; Blasco, T.; Corma, A. Identification of Active Surface Species for Friedel-Crafts Acylation and Koch Carbonylation

Reactions by in Situ Solid-State NMR Spectroscopy. *Angew. Chem., Int. Ed.* **2013**, *52*, 5138–5141. DOI: 10.1002/anie.201209907.

(837) Bhan, A.; Allian, A. D.; Sunley, G. J.; Law, D. J.; Iglesia, E. Specificity of Sites Within Eight-Membered Ring Zeolite Channels for Carbonylation of Methyls to Acetyls. *J. Am. Chem. Soc.* **2007**, *129*, 4919–4924. DOI: 10.1021/ja070094d.

(838) Feng, X.-B.; Cao, J.-P.; Su, C.; He, Z.-M.; Zhao, X.-Y. Tailoring the Acid Distribution and Identifying the Active Center of Rod-Shaped HSUZ-4 Zeolite for Enhancing Dimethyl Ether Carbonylation Performance. *Fuel* **2022**, *315*, 123267. DOI: 10.1016/j.fuel.2022.123267.

(839) Xiong, Z.; Zhan, E.; Li, M.; Shen, W. DME Carbonylation over a HSUZ-4 Zeolite. *Chem. Commun.* **2020**, *56*, 3401–3404. DOI: 10.1039/d0cc00886a.

(840) Yao, J.; Wu, Q.; Fan, J.; Komiyama, S.; Yong, X.; Zhang, W.; Zhao, T.; Guo, Z.; Yang, G.; Tsubaki, N. A Carbonylation Zeolite with Specific Nanosheet Structure for Efficient Catalysis. *ACS Nano* **2021.** DOI: 10.1021/acsnano.1c04419.

(841) Lusardi, M.; Chen, T. T.; Kale, M.; Kang, J. H.; Neurock, M.; Davis, M. E. Carbonylation of Dimethyl Ether to Methyl Acetate over SSZ-13. *ACS Catal.* **2020**, *10*, 842–851. DOI: 10.1021/acscatal.9b04307.

(842) Román-Leshkov, Y.; Moliner, M.; Davis, M. E. Impact of Controlling the Site Distribution of Al Atoms on Catalytic Properties in Ferrierite-Type Zeolites. *J. Phys. Chem. C* **2011**, *115*, 1096–1102. DOI: 10.1021/jp106247g.

(843) Wang, S.; Li, S.; Li Zhang; Qin, Z.; Chen, Y.; Dong, M.; Li, J.; Fan, W.; Wang, J. Mechanistic Insights into the Catalytic Role of Various Acid Sites on ZSM-5 Zeolite in the Carbonylation of Methanol and Dimethyl Ether. *Catal. Sci. Technol.* **2018**, *8*, 3193–3204. DOI: 10.1039/C8CY00296G.

(844) Cheng, Z.; Huang, S.; Li, Y.; Cai, K.; Wang, Y.; Wang, M.; Lv, J.; Ma, X. Role of Brønsted Acid Sites Within 8-MR of Mordenite in the Deactivation Roadmap for Dimethyl Ether Carbonylation. *ACS Catal.* **2021**, *11*, 5647–5657. DOI: 10.1021/acscatal.1c00159.

(845) Liu, Z.; Yi, X.; Wang, G.; Tang, X.; Li, G.; Huang, L.; Zheng, A. Roles of 8-Ring and 12-Ring Channels in Mordenite for Carbonylation Reaction: From the Perspective of Molecular Adsorption and Diffusion. *J. Catal.* **2019**, *369*, 335–344. DOI: 10.1016/j.jcat.2018.11.024.

(846) Liu, R.; Zeng, S.; Sun, T.; Xu, S.; Yu, Z.; Wei, Y.; Liu, Z. Selective Removal of Acid Sites in Mordenite Zeolite by Trimethylchlorosilane Silylation to Improve Dimethyl Ether Carbonylation Stability. *ACS Catal.* **2022**, *12*, 4491–4500. DOI: 10.1021/acscatal.1c05896.

(847) Liu, R.; Fan, B.; Zhang, W.; Wang, L.; Qi, L.; Wang, Y.; Xu, S.; Yu, Z.; Wei, Y.; Liu, Z. Increasing the Number of Aluminum Atoms in T3 Sites of a Mordenite Zeolite by Low-Pressure SiCl4 Treatment to Catalyze Dimethyl Ether Carbonylation. *Angew. Chem. Int. Ed.* **2022**, *61*, e202116990. DOI: 10.1002/anie.202116990.

(848) Xu, F.; Lv, J.; Chen, C.; Hong, Z.; Zhao, G.; Miao, L.; Yang, W.; Zhu, Z. Effect of Steam Treatment on the Properties of Mordenite and Its Catalytic Performance in a DME Carbonylation Reaction. *Ind. Eng. Chem. Res.* **2022**, *61*, 1258–1266. DOI: 10.1021/acs.iecr.1c04184.

(849) Xue, H.; Huang, X.; Zhan, E.; Ma, M.; Shen, W. Selective Dealumination of Mordenite for Enhancing Its Stability in Dimethyl Ether Carbonylation. *Catalysis Communications* **2013**, *37*, 75–79. DOI: 10.1016/j.catcom.2013.03.033.

(850) Zhou, Z.; Liu, H.; Ni, Y.; Wen, F.; Chen, Z.; Zhu, W.; Liu, Z. Direct Conversion of Dimethyl Ether and CO to Acetone via Coupling Carbonylation and Ketonization. *J. Catal.* **2021**, *396*, 360–373. DOI: 10.1016/j.jcat.2021.03.006.

(851) Liu, R.; Fan, B.; Zhi, Y.; Liu, C.; Xu, S.; Yu, Z.; Liu, Z. Dynamic Evolution of Aluminum Coordination Environments in Mordenite Zeolite and Their Role in the Dimethyl Ether (DME)

Carbonylation Reaction. *Angew. Chem., Int. Ed.* **2022**, e202210658. DOI: 10.1002/anie.202210658.

(852) Kaipeng Cao; Dong Fan; Mingbin Gao; Benhan Fan; Nan Chen; Linying Wang; Peng Tian; and Zhongmin Liu. Recognizing the Important Role of Surface Barriers in MOR Zeolite Catalyzed DME Carbonylation Reaction. *ACS Catal.* **2022**, *12*, 1–7.

(853) Stepanov, A. G.; Luzgin, M. V.; Romannikov, V. N.; Sidelnikov, V. N.; Zamaraev, K. I. Formation of Carboxylic Acids from Alcohols and Olefins in Zeolite H-ZSM-5 Under Mild Conditions via Trapping of Alkyl Carbenium Ions with Carbon Monoxide: An in Situ ^{13}C Solid State NMR Study. *J. Catal.* **1996**, *164*, 411–421. DOI: 10.1006/jcat.1996.0397.

(854) Luzgin, M. V.; Stepanov, A. G.; Sassi, A.; Sommer, J. Formation of Carboxylic Acids from Small Alkanes in Zeolite H-ZSM-5. *Chem. Eur. J.* **2000**, *6*, 2368–2376. DOI: 10.1002/1521-3765(20000703)6:13<2368:AID-CHEM2368>3.0.CO;2-H.

(855) Sommer, J.; Habermacher, D.; Jost, R.; Sassi, A.; Stepanov, A. G.; Luzgin, M. V.; Freude, D.; Ernst, H.; Martens, J. Activation of Small Alkanes on Solid Acids. An H/D Exchange Study by Liquid and Solid-State NMR: The Activation Energy and the Inhibiting Effect of Carbon Monoxide. *J. Catal.* **1999**, *181*, 265–270. DOI: 10.1006/jcat.1998.2302.

(856) Chang, C. D.; Silvestri, A. J. The Conversion of Methanol and Other O-Compounds to Hydrocarbons over Zeolite Catalysts. *J. Catal.* **1977**, *47*, 249–259.

(857) Geoppert, A.; Czaun, M.; Jones, J. P.; Prakash, G.; Olah, G. A. *Chem. Soc. Rev.* **2014**, *43*, 7995–8048.

(858) Pan, X.; Jiao, F.; Miao, D.; Bao, X. Oxide-Zeolite-Based Composite Catalyst Concept That Enables Syngas Chemistry Beyond Fischer-Tropsch Synthesis. *Chem. Rev.* **2021**, *121*, 6588–6609. DOI: 10.1021/acs.chemrev.0c01012.

(859) Hadi, N.; Farzi, A. A Review on Reaction Mechanisms and Catalysts of Methanol to Olefins Process. *Chem. Eng. Commun.* **2021**, 1–47. DOI: 10.1080/00986445.2021.1983547.

(860) Zhong, J.; Han, J.; Wei, Y.; Liu, Z. Catalysts and Shape Selective Catalysis in the Methanol-to-Olefin (MTO) Reaction. *J. Catal.* **2021**, *396*, 23–31. DOI: 10.1016/j.jcat.2021.01.027.

(861) Wang, C.; Xu, J.; Deng, F. Mechanism of Methanol-to-hydrocarbon Reaction over Zeolites: A Solid-state NMR Perspective. *ChemCatChem* **2020**, *12*, 965–980. DOI: 10.1002/cctc.201901937.

(862) Yarulina, I.; Chowdhury, A. D.; Meirer, F.; Weckhuysen, B. M.; Gascon, J. Recent Trends and Fundamental Insights in the Methanol-to-Hydrocarbons Process. *Nat. Catal.* **2018**, *1*, 398–411. DOI: 10.1038/s41929-018-0078-5.

(863) Olsbye, U.; Svelle, S.; Bjørgen, M.; Beato, P.; Janssens, T. V. W.; Joensen, F.; Bordiga, S.; Lillerud, K. P. Conversion of Methanol to Hydrocarbons: How Zeolite Cavity and Pore Size Controls Product Selectivity. *Angew. Chem., Int. Ed.* **2012**, *51*, 5810–5831. DOI: 10.1002/anie.201103657.

(864) Haw, J. F.; Song, W.; Marcus, D. M.; Nicholas, J. B. The Mechanism of Methanol to Hydrocarbon Catalysis. *Acc. Chem. Res.* **2003**, *36*, 317–326. DOI: 10.1021/ar020006o.

(865) Dessau, R. M.; LaPierre, R. B. On the Mechanism of Methanol Conversion to Hydrocarbons over HZSM-5. *J. Catal.* **1982**, *78*, 136–141.

(866) Dessau, R. M. On the H-ZSM-5 Catalyzed Formation of Ethylene from Methanol or Higher Olefins. *J. Catal.* **1986**, *99*, 111–116.

(867) Dahl, I. M.; St. Kolboe. On the Reaction Mechanism of Hydrocarbon Formation from Methanol over SAPO-34:1. Isotopic Labling Studies of the Co-Reaction of Ethene and Methanol. *J. Catal.* **1994**, *149*, 458–464.

(868) Mole, T.; Whiteside, J. A. Aromatic Co-Catalysis of Methanol Conversion of Zeolite Catalysts. *J. Catal.* **1983**, *82*, 261–266.

(869) Mole, T.; Bett, G.; Seddon, D. Conversion of Methanol to Hydrocarbons over ZSM-5 Zeolite: An Examination of the Role of Aromatic Hydrocarbons Using 13Carbon and Deuterium-Labeled Feeds. *J. Catal.* **1983**, *84*, 435–445.

(870) Song, W.; Haw, J. F.; Nicholas, J. B.; Heneghan, C. S. Methylbenzenes Are the Organic Reaction Centers for Methanol-to-Olefin Catalysis on HSAPO-34. *J. Am. Chem. Soc.* **2000**, *122*, 10726–10727. DOI: 10.1021/ja002195g.

(871) Arstad, B.; Kolboe, S. The Reactivity of Molecules Trapped Within the SAPO-34 Cavities in the Methanol-to-Hydrocarbons Reaction. *J. Am. Chem. Soc.* **2001**, *123*, 8137–8138. DOI: 10.1021/ja010668t.

(872) Song, W.; Fu, H.; Haw, J. F. Supramolecular Origins of Product Selectivity for Methanol-to-Olefin Catalysis on HSAPO-34. *J. Am. Chem. Soc.* **2001**, *123*, 4749–4754. DOI: 10.1021/ja0041167.

(873) Svelle, S.; Joensen, F.; Nerlov, J.; Olsbye, U.; Lillerud, K.-P.; Kolboe, S.; Bjørgen, M. Conversion of Methanol into Hydrocarbons over Zeolite H-ZSM-5: Ethene Formation Is Mechanistically Separated from the Formation of Higher Alkenes. *J. Am. Chem. Soc.* **2006**, *128*, 14770–14771. DOI: 10.1021/ja065810a.

(874) Bjørgen, M.; Svelle, S.; Joesen, F.; Nerlov, J.; Kolboe, S.; Bonino, F.; Palumbo, L.; Bordiga, S.; Olsbye, U. Conversion of Methanol to Hydrocarbons over Zeolite H-ZSM-5: On the Origin of the Olefinic Species. *J. Catal.* **2007**, *249*, 195–207. DOI: 10.1016/j.jcat.2007.04.006.

(875) Svelle, S.; Rønning, P. O.; Olsbye, U.; Kolboe, S. Kinetic Studies of Zeolite-Catalyzed Methylation Reactions. Part 2. Co-Reaction of [^{12}C]Propene or [^{12}C]N-Butene and [^{13}C]Methanol. *J. Catal.* **2005**, *234*, 385–400. DOI: 10.1016/j.jcat.2005.06.028.

(876) Svelle, S.; Rønning, P. O.; Kolboe, S. Kinetic Studies of Zeolite-Catalyzed Methylation Reactions1. Coreaction of [^{12}C]Ethene and [^{13}C]Methanol. *J. Catal.* **2004**, *224*, 115–123. DOI: 10.1016/j.jcat.2004.02.022.

(877) Wu, W.; Guo, W.; Xiao, W.; Luo, M. Dominant Reaction Pathway for Methanol Conversion to Propene over High Silicon H-ZSM-5. *Chem. Eng. Sci.* **2011**, *66*, 4722–4732. DOI: 10.1016/j.ces.2011.06.036.

(878) Ilias, S.; Bhan, A. Tuning the Selectivity of Methanol-to-Hydrocarbons Conversion on H-ZSM-5 by Co-Processing Olefin or Aromatic Compounds. *J. Catal.* **2012**, *290*, 186–192. DOI: 10.1016/j.jcat.2012.03.016.

(879) Müller, S.; Liu, Y.; Vishnuvarthan, M.; Sun, X.; van Veen, A. C.; Haller, G. L.; Sanchez-Sanchez, M.; Lercher, J. A. Coke Formation and Deactivation Pathways on H-ZSM-5 in the Conversion of Methanol to Olefins. *J. Catal.* **2015**, *325*, 48–59. DOI: 10.1016/j.jcat.2015.02.013.

(880) Olsbye, U.; Svelle, S.; Lillerud, K. P.; Wei, Z. H.; Chen, Y. Y.; Li, J. F.; Wang, J. G.; Fan, W. B. The Formation and Degradation of Active Species During Methanol Conversion over Protonated Zeotype Catalysts. *Chem. Soc. Rev.* **2015**, *44*, 7155–7176. DOI: 10.1039/c5cs00304k.

(881) Jiang, Y.; Wang, W.; Reddymarthala, V.; Huang, J.; Sulikowski, B.; Hunger, M. Effect of Organic Impurities on the Hydrocarbon Formation via the Decomposition of Surface Methoxy Groups on Acidic Zeolite Catalysts. *J. Catal.* **2006**, *238*, 21–27. DOI: 10.1016/j.jcat.2005.11.029.

(882) Munson, E. J.; Lazo, N. D.; Moellenhoff, M. E.; Haw, J. F. Carbon Monoxide Is Neither an Intermediate nor a Catalyst in MTG Chemistry on Zeolite HZSM-5. *J. Am. Chem. Soc.* **1991**, *113*, 2783–2784.

(883) Hutchings, G. J.; Hunter, R.; Johnston, P.; van Rensburg, L. J. Methanol Conversion to Hydrocarbons over Zeolite H-ZSM-5: Investigation of the Role of CO and Ketene in the Formation of the Initial C-C Bond. *J. Catal.* **1993**, *142*, 602–616.

(884) Wang, C.; Chu, Y.; Xu, J.; Wang, Q.; Qi, G.; Gao, P.; Zhou, X.; Deng, F. Extra-Framework Aluminum-Assisted Initial C-C Bond Formation in Methanol-to-Olefins Conversion on Zeolite H-ZSM-5. *Angew. Chem., Int. Ed.* **2018**, *57*, 10197–10201. DOI: 10.1002/anie.201805609.

(885) Comas-Vives, A.; Valla, M.; Copéret, C.; Sautet, P. Cooperativity Between Al Sites Promotes Hydrogen Transfer and Carbon-Carbon Bond Formation Upon Dimethyl Ether Activation on Alumina. *ACS Cent. Sci.* **2015**, *1*, 313–319. DOI: 10.1021/acscentsci.5b00226.

(886) Cesarini, A.; Mitchell, S.; Zichittella, G.; Agrachev, M.; Schmid, S. P.; Jeschke, G.; Pan, Z.; Bodi, A.; Hemberger, P.; Pérez-Ramírez, J. Elucidation of Radical- and Oxygenate-Driven Paths in Zeolite-Catalysed Conversion of Methanol and Methyl Chloride to Hydrocarbons. *Nat. Catal.* **2022**, *5*, 605–614. DOI: 10.1038/s41929-022-00808-0.

(887) Zhang, N.; Chen, S.-L.; Zhu, R.; Sun, W. Evolution Pathway and Role of Intermediates Acetaldehyde and Acetone Formed During the Methanol-to-Olefins Reaction. *Energy Fuels* **2022**, *36*, 12708–12718. DOI: 10.1021/acs.energyfuels.2c01858.

(888) Yang, L.; Yan, T.; Wang, C.; Dai, W.; Wu, G.; Hunger, M.; Fan, W.; Xie, Z.; Guan, N.; Li, L. Role of Acetaldehyde in the Roadmap from Initial Carbon–Carbon Bonds to Hydrocarbons During Methanol Conversion. *ACS Catal.* **2019**, *9*, 6491–6501. DOI: 10.1021/acscatal.9b00641.

(889) Khare, R.; Arora, S. S.; Bhan, A. Implications of Cofeeding Acetaldehyde on Ethene Selectivity in Methanol-to-Hydrocarbons Conversion on MFI and Its Mechanistic Interpretation. *ACS Catal.* **2016**, *6*, 2314–2331. DOI: 10.1021/acscatal.5b02818.

(890) Wu, X.; Zhang, Z.; Pan, Z.; Zhou, X.; Bodi, A.; Hemberger, P. Ketenes in the Induction of the Methanol-to-Olefins Process. *Angew. Chem., Int. Ed.* **2022**, e202207777. DOI: 10.1002/anie.202207777.

(891) Hoang, T. Q.; Zhu, X.; Sooknoi, T.; Resasco, D. E.; Mallinson, R. G. A Comparison of the Reactivities of Propanal and Propylene on HZSM-5. *J. Catal.* **2010**, *271*, 201–208. DOI: 10.1016/j.jcat.2010.01.017.

(892) Wang, S.; Chen, Y. Y.; Qin, Z. F.; Zhao, T. S.; Fan, S. B.; Dong, M.; Li, J. F.; Fan, W. B.; Wang, J. G. Origin and Evolution of the Initial Hydrocarbon Pool Intermediates in the Transition Period for the Conversion of Methanol to Olefins over H-ZSM-5 Zeolite. *J. Catal.* **2019**, *369*, 382–395. DOI: 10.1016/j.jcat.2018.11.018.

(893) Westgård Erichsen, M.; Svelle, S.; Olsbye, U. H-SAPO-5 as Methanol-to-Olefins (MTO) Model Catalyst: Towards Elucidating the Effects of Acid Strength. *J. Catal.* **2013**, *298*, 94–101. DOI: 10.1016/j.jcat.2012.11.004.

(894) Ilias, S.; Bhan, A. The Mechanism of Aromatic Dealkylation in Methanol-to-Hydrocarbons Conversion on H-ZSM-5: What Are the Aromatic Precursors to Light Olefins? *J. Catal.* **2014**, *311*, 6–16. DOI: 10.1016/j.jcat.2013.11.003.

(895) Hwang, A.; Johnson, B.; Bhan, A. Mechanistic Study of Methylbenzene Dealkylation in Methanol-to-Olefins Catalysis on HSAPO-34. *J. Catal.* **2019**, *369*, 86–94.

(896) Wispelaere, K. de; Hemelsoet, K.; Waroquier, M.; van Speybroeck, V. Complete Low-Barrier Side-Chain Route for Olefin Formation During Methanol Conversion in H-SAPO-34. *J. Catal.* **2013**, *305*, 76–80. DOI: 10.1016/j.jcat.2013.04.015.

(897) Arstad, B.; Nicholas, J. B.; Haw, J. F. Theoretical Study of the Methylbenzene Side-Chain Hydrocarbon Pool Mechanism in Methanol to Olefin Catalysis. *J. Am. Chem. Soc.* **2004**, *126*, 2991–3001. DOI: 10.1021/ja035923j.

(898) Wang, C.-M.; Wang, Y.-D.; Xie, Z.-K. Verification of the Dual Cycle Mechanism for Methanol-to-Olefin Conversion in HSAPO-34: A Methylbenzene-Based Cycle from DFT Calculations. *Catal. Sci. Technol.* **2014**, *4*, 2631–2638. DOI: 10.1039/C4CY00262H.

(899) Wang, S.; Chen, Y.; Wei, Z.; Qin, Z.; Ma, H.; Dong, M.; Li, J.; Fan, W.; Wang, J. Polymethylbenzene or Alkene Cycle? Theoretical Study on Their Contribution to the Process of Methanol to Olefins over H-ZSM-5 Zeolite. *J. Phys. Chem. C* **2015**, *119*, 28482–28498. DOI: 10.1021/acs.jpcc.5b10299.

(900) McCann, D. M.; Lesthaeghe, D.; Kletnieks, P. W.; Guenther, D. R.; Hayman, M. J.; van Speybroeck, V.; Waroquier, M.; Haw, J. F. A Complete Catalytic Cycle for Supramolecular Methanol-to-Olefins Conversion by Linking Theory with Experiment. *Angew. Chem., Int. Ed.* **2008**, *47*, 5179–5182. DOI: 10.1002/anie.200705453.

(901) Wang, C.-M.; Wang, Y.-D.; Du, Y.-J.; Yang, G.; Xie, Z.-K. Computational Insights into the Reaction Mechanism of Methanol-to-Olefins Conversion in H-ZSM-5: Nature of Hydrocarbon Pool. *Catal. Sci. Technol.* **2016**, *6*, 3279–3288. DOI: 10.1039/C5CY01419K.

(902) Chen, Y.; Wang, S.; Wei, Z.; Li, J.; Dong, M.; Qin, Z.; Wang, J.; Fan, W. Unraveling the Relationship Between Zeolite Structure and MTO Product Distribution by Theoretical Study of the Reaction Mechanism. *J. Phys. Chem. C* **2021**, *125*, 26472–26483. DOI: 10.1021/acs.jpcc.1c07692.

(903) Plessow, P. N.; Enss, A. E.; Huber, P.; Studt, F. A New Mechanistic Proposal for the Aromatic Cycle of the MTO Process Based on a Computational Investigation for H-SSZ-13. *Catal. Sci. Technol.* **2022**, *12*, 3516–3523. DOI: 10.1039/D2CY00021K.

(904) Teketel, S.; Skistad, W.; Benard, S.; Olsbye, U.; Lillerud, K. P.; Beato, P.; Svelle, S. Shape Selectivity in the Conversion of Methanol to Hydrocarbons: The Catalytic Performance of One-Dimensional 10-Ring Zeolites: ZSM-22, ZSM-23, ZSM-48, and EU-1. *ACS Catal.* **2012**, *2*, 26–37. DOI: 10.1021/cs200517u.

(905) Deimund, M. A.; Schmidt, J. E.; Davis, M. E. Effect of Pore and Cage Size on the Formation of Aromatic Intermediates During the Methanol-to-Olefins Reaction. *Top. Catal.* **2015**, *58*, 416–423. DOI: 10.1007/s11244-015-0384-y.

(906) Li, J.; Wei, Y.; Chen, J.; Xu, S.; Tian, P.; Yang, X.; Li, B.; Wang, J.; Liu, Z. Cavity Controls the Selectivity: Insights of Confinement Effects on MTO Reaction. *ACS Catal.* **2015**, *5*, 661–665. DOI: 10.1021/cs501669k.

(907) Kang, J. H.; Alshafei, F. H.; Zones, S. I.; Davis, M. E. Cage-Defining Ring: A Molecular Sieve Structural Indicator for Light Olefin Product Distribution from the Methanol-to-Olefins Reaction. *ACS Catal.* **2019**, *9*, 6012–6019. DOI: 10.1021/acscatal.9b00746.

(908) Park, S.; Sato, G.; Osuga, R.; Wang, Y.; Kubota, Y.; Kondo, J. N.; Gies, H.; Tatsumi, T.; Yokoi, T. Methanol-to-Olefins Reaction over Large-Pore Zeolites: Impact of Pore Structure on Catalytic Performance. *Chem. Ing. Tech.* **2021**, *93*, 990–1000. DOI: 10.1002/cite.202000174.

(909) Ferri, P.; Li, C.; Paris, C.; Rodríguez-Fernández, A.; Moliner, M.; Boronat, M.; Corma, A. The Limits of the Confinement Effect Associated to Cage Topology on the Control of the MTO Selectivity. *ChemCatChem* **2021**, *13*, 1578–1586. DOI: 10.1002/cctc.202001760.

(910) Guo, S. J.; Wang, S.; Zhang, L.; Qin, Z. F.; Wang, P. F.; Dong, M.; Wang, J. G.; Fan, W. B. Regulating the Acid Sites Distribution in ZSM-5 Zeolite and Its Catalytic Performance in the Conversion of Methanol to Olefins. *Chem. J. Chin. Univ.* **2021**, *42*, 227–238. DOI: 10.7503/cjcu20200413.

(911) Wang, S.; Li, Z. K.; Qin, Z. F.; Dong, M.; Li, J. F.; Fan, W. B.; Wang, J. G. Catalytic Roles of the Acid Sites in Different Pore Channels of H-ZSM-5 Zeolite for Methanol-to-Olefins Conversion. *Chin. J. Catal.* **2021**, *42*, 1126–1136. DOI: 10.1016/S1872-2067(20)63732-9.

(912) Wang, S.; Zhang, L.; Li, S. Y.; Qin, Z. F.; Shi, D. Z.; He, S. P.; Yuan, K.; Wang, P. F.; Zhao, T. S.; Fan, S. B.*; et al.* Tuning the Siting of Aluminum in ZSM-11 Zeolite and Regulating

Its Catalytic Performance in the Conversion of Methanol to Olefins. *J. Catal.* **2019**, *377*, 81–97. DOI: 10.1016/j.jcat.2019.07.028.

(913) Haag, W. O.; Lago, R. M.; Weisz, P. B. Transport and Reactivity of Hydrocarbon Molecules in a Shape-Selective Zeolite. *Faraday Discuss. Chem. Soc.* **1981**, *72*, 317. DOI: 10.1039/DC9817200317.

(914) Pagis, C.; Bouchy, C.; Dodin, M.; Franco, R. M.; Farrusseng, D.; Tuel, A. Hollow Y Zeolite Single Crystals:Synthesis, Characterization and Activity in the Hydroisomerization of N-Hexadecane. *Oil Gas Sci. Tech.* **2019**, *74*. DOI: 10.2516/ogst/2019015.

(915) Herzog, B.; Da Chagas Silva, M.; Casier, B.; Badawi, M.; Pascale, F.; Bučko, T.; Lebègue, S.; Rocca, D. Assessing the Accuracy of Machine Learning Thermodynamic Perturbation Theory: Density Functional Theory and Beyond. *J. Chem. Theory Comput.* **2022**, *18*, 1382–1394. DOI: 10.1021/acs.jctc.1c01034.

(916) Chehaibou, B.; Badawi, M.; Bučko, T.; Bazhirov, T.; Rocca, D. Computing RPA Adsorption Enthalpies by Machine Learning Thermodynamic Perturbation Theory. *J. Chem. Theory Comput.* **2019**, *15*, 6333–6342. DOI: 10.1021/acs.jctc.9b00782.

(917) Bučko, T.; Gešvandtnerová, M.; Rocca, D. Ab Initio Calculations of Free Energy of Activation at Multiple Electronic Structure Levels Made Affordable: An Effective Combination of Perturbation Theory and Machine Learning. *J. Chem. Theory Comput.* **2020**, *16*, 6049–6060. DOI: 10.1021/acs.jctc.0c00486.

(918) Jinnouchi, R.; Lahnsteiner, J.; Karsai, F.; Kresse, G.; Bokdam, M. Phase Transitions of Hybrid Perovskites Simulated by Machine-Learning Force Fields Trained on the Fly with Bayesian Inference. *Phys. Rev. Lett.* **2019**, *122*, 225701. DOI: 10.1103/PhysRevLett.122.225701.

(919) Jinnouchi, R.; Miwa, K.; Karsai, F.; Kresse, G.; Asahi, R. On-the-Fly Active Learning of Interatomic Potentials for Large-Scale Atomistic Simulations. *J. Phys. Chem. Lett.* **2020**, *11*, 6946–6955. DOI: 10.1021/acs.jpclett.0c01061.

16.Table of Contents Graphic